

CONTRIBUTIONS TO UNDERSTANDING OLIGOMERIC SUGARS
DERIVED FROM BIOMASS PYROLYSIS

By

MELBA D. DENSON

A dissertation submitted in partial fulfillment of
the requirements for the degree of

DOCTOR OF PHILOSOPHY

WASHINGTON STATE UNIVERSITY
Department of Biological Systems Engineering

DECEMBER 2023

© Copyright by MELBA D. DENSON, 2023
All Rights Reserved

To the Faculty of Washington State University:

The members of the Committee appointed to examine the dissertation of MELBA D. DENSON find it satisfactory and recommend that it be accepted.

Manuel Garcia-Perez, Ph.D., Co-Chair

Mariefel V. Olarte, Ph.D., Co-Chair

Hanwu Lei, Ph.D.

Jean-Sabin McEwen, Ph.D.

ACKNOWLEDGMENT

This endeavor would not have been possible without the generous financial support provided by the Department of Science and Technology–Engineering Research and Development for Technology (DOST–ERDT) through Central Luzon State University (CLSU), Nueva Ecija, Philippines. I extend my heartfelt gratitude to the Department of Agricultural and Biosystems Engineering, College of Engineering, CLSU, for granting me the opportunity to take a study leave, with special acknowledgment to the former Dean, Dr. Ireneo C. Agulto.

I want to convey my deepest appreciation to the PNNL–WSU Distinguished Graduate Research Program (DGRP) through the U.S. Department of Energy (DOE) Bioenergy Technologies Office under contract number DEAC0576RL0-1830 for the invaluable financial assistance provided during the concluding year of my academic pursuits. My research endeavors were also partially funded by the National Science Foundation (CBET 1926412) of the United States of America, U.S. Department of Energy (DE-EE0008505), U.S. Department of Agriculture – National Institute of Food and Agriculture (USDA-NIFA) through Hatch Project WNP00701 and the U.S. Department of Agriculture – Agricultural Research Service (USDA-ARS).

Words cannot adequately convey my gratitude to my advisor, Dr. Manuel Garcia-Perez, and co-advisor, Dr. Mariefel V. Olarte, for their unwavering support and guidance. I am profoundly thankful for the learnings, skills, and expertise they shared during my stay at Washington State University (WSU) and the Pacific Northwest National Laboratory (PNNL). Their constant monitoring of my progress and invaluable feedback throughout my Ph.D. program have been instrumental in my growth and development. I am also indebted to the advisory committee members, Dr. Jean-Sabin McEwen and Dr. Hanwu Lei, for their invaluable assistance

and warm support. I recognize all of you for invariably providing me with a great deal about scientific research and life in general. Your vast wisdom, achievements, and wealth of experience have inspired me throughout my studies.

Special thanks are due to the administrative staff of the Biological Systems Engineering department at WSU, particularly Joanna Dreger and Jonathan Lomber, as well as the faculty and staff of CLSU-DABE, especially Ms. Precious Joan Sibulburo, for their generous assistance. I am grateful and honored to have had the opportunity to work with diverse research groups, including “Manuelito’s group with a special mention to Raiza Manrique,” Dr. McEwen’s research team, and the PNNL staff. My time spent studying and residing in the USA has been a gratifying experience.

I am grateful to my family members for their immense love, enduring inspiration, and moral support. I would be remiss if I did not mention my CBBC family, Cougar colleagues, the Filipino community in Pullman, and all my friends for their prayers and unwavering emotional and practical support.

Lastly, I offer my profound thanks to the Lord God Almighty, to whom I owe everything. All glory and honor belong to Him, for without Him, I can do nothing (John 15:5).

CONTRIBUTIONS TO UNDERSTANDING OLIGOMERIC SUGARS
DERIVED FROM BIOMASS PYROLYSIS

Abstract

by Melba D. Denson, Ph.D.
Washington State University
December 2023

Co-Chairs: Manuel Garcia-Perez and Mariefel V. Olarte

Bio-oil emerges as a potent green energy to halt planet warming. However, its direct utilization as a biofuel is impeded by substantial challenges resulting from its complex composition, leading to undesirable properties. This research delves into elucidating and proposing structures of the unknown sugar oligomers in bio-oil by integrating experimental and modeling approaches. Additionally, it aims to upgrade the heavy bio-oil fractions, containing both sugar and lignin oligomers, and investigate the mechanism of oxygen removal during hydrotreatment.

Experimental techniques and computational modeling were employed to achieve these goals. Density functional theory (DFT) was used to study the dehydration and fragmentation reactions to propose structures of the unknown oligomeric sugars and investigate their reaction mechanisms during upgrading. Chromatographic techniques were applied to fractionate sugar compounds in bio-oil, followed by comprehensive characterization to identify their specific

components. Bio-oil upgrading was conducted by co-hydrotreating the heavy bio-oil fractions with waste cooking oil in a batch-type reactor under defined operating conditions.

The results put forward potential structures for the unidentified sugar oligomers. DFT results showed that water, hydroxyacetaldehyde, and hydroxyacetone are most favorably formed from the non-reducing end of the sugar oligomers. These modeling yields were integrated with the experimental data acquired from chromatographic techniques to gain a deeper understanding of the oligomers. The proposed structures/formulas of the unknown sugar oligomers were detected experimentally by HESI-FT-Orbitrap MS. Moreover, the upgrading of the heavy bio-oil, containing both sugar and lignin oligomers, resulted in relatively low coke yield ranging from 0.7 to 2.4 wt. %. This result demonstrated a comparable coke yield to what is obtained when solely using a pyrolytic fraction. It implies that the formation of coke during bio-oil upgrading is not exclusively attributed to sugar oligomers; instead, both sugar and lignin oligomers are involved in the coke formation process. An in-depth understanding of the structure of the unknown compounds and their behavior during hydrotreatment will contribute toward the development and advancement of biomass pyrolysis techniques and product upgrading strategies.

TABLE OF CONTENTS

	Page
ACKNOWLEDGMENT.....	iii
ABSTRACT.....	v
LIST OF TABLES.....	x
CHAPTERS	
CHAPTER ONE: INTRODUCTION.....	1
1.1 Background.....	1
1.2 Dissertation Objectives.....	6
1.3 Dissertation Structure.....	7
1.4 Publications.....	9
1.5 Scientific Contributions.....	11
1.6 REFERENCES.....	13
CHAPTER TWO: REVIEW OF CELLULOSE PYROLYSIS AND RESULTING OIL HYDROTREATMENT REACTIONS.....	20
2.1. Introduction.....	20
2.2 Review of Cellulose Pyrolysis Reaction Mechanisms.....	22
2.3. Review of Bio-Oil Catalytic Hydrotreatment Reactions.....	42
2.4 Conclusion and Outlook.....	59
2.5 REFERENCES.....	61
CHAPTER THREE: ELUCIDATION OF STRUCTURE AND PHYSICAL PROPERTIES OF PYROLYTIC SUGAR OLIGOMERS DERIVED FROM CELLULOSE DEPOLYMERIZATION/DEHYDRATION REACTIONS: A DENSITY FUNCTIONAL THEORY STUDY.....	87
Abstract.....	88

3.1 Introduction.....	89
3.2 Methodology.....	92
3.3 Results and Discussion	101
3.4 Conclusion	119
3.5 REFERENCES	120
CHAPTER FOUR: THEORETICAL INSIGHTS ON THE FRAGMENTATION OF CELLULOSIC OLIGOMERS TO FORM HYDROXYACETONE AND HYDROXYACETALDHYDE.....	129
Abstract.....	130
4.1 Introduction.....	131
4.2 Methodology.....	133
4.3 Results and Discussion	137
4.4 Conclusion	147
4.5 REFERENCES	149
CHAPTER FIVE: TOWARDS A RATIONAL DESCRIPTION OF THE CHEMICAL COMPOSITION OF BIO-OIL WATER SOLUBLE FRACTIONS	155
Abstract.....	155
5.1 Introduction.....	156
5.2 Methodology.....	158
5.3 Results and Discussion	166
5.4 Conclusion	184
5.5 REFERENCES	186
CHAPTER SIX: CO-HYDROTREATMENT OF BIO-OIL AND WASTE COOKING OIL TO PRODUCE BIOFUEL.....	190
Abstract.....	190

6.1 Introduction.....	192
6.2 Methodology.....	195
6.3 Results and Discussion	201
6.4 Conclusion	212
6.5 REFERENCES	213
CHAPTER SEVEN: HYDRODEOXYGENATION OF HYDROXYACETONE OVER NiMo CATALYST FROM FIRST PRINCIPLES.....	219
7.1 Introduction.....	219
7.2 Methodology.....	223
7.3 Result and Discussion.....	225
7.5 REFERENCES	230
CHAPTER EIGHT: CONCLUSION AND RECOMMENDATION	242
8.1 Conclusions.....	242
8.2 Recommendations.....	244
APPENDICES	246
APPENDIX A: SUPPLEMENTAL INFORMATION FOR CHAPTER THREE.....	247
APPENDIX B: SUPPLEMENTAL INFORMATION FOR CHAPTER FOUR	292
APPENDIX C: SUPPLEMENTAL INFORMATION FOR CHAPTER SIX	300
APPENDIX D: SUPPLEMENTAL INFORMATION FOR CHAPTER SEVEN.....	305

LIST OF TABLES

	Page
Table 2.1. Reviews on the hydrotreatment of bio-oil for the last 5 years.....	45
Table 3.1. Most thermodynamically stable structures of the dehydrated sugars.....	103
Table 3.2. Estimated physical property values for each proposed structure of the anhydrosugars.....	116
Table 3.3. Estimated ideal gas property values for each proposed structure of the anhydrosugars.....	117
Table 3.4. Estimated condensed gas property values for each proposed structure of the anhydrosugars.....	118
Table 4.1. Proposed structures of the oligomeric sugar fragments where hydroxyacetaldehyde is removed. ^a	137
Table 4.2. Proposed structures of the oligomeric sugar fragments where hydroxyacetone is removed. ^b	138
Table 4.3. Estimated property values for each proposed structure of the oligomeric sugar fragments where hydroxyacetone is removed.....	143
Table 4.4. Estimated physical change property values for each proposed structure of the oligomeric sugar fragments where hydroxyacetaldehyde is removed.....	145
Table 5.1. Number of ions and mass distribution of pyrolytic sugar sub-fractions based on the (-)H-ESI-FT-Orbitrap MS spectra.....	175
Table 5.2. Number of ions and mass distribution of pyrolytic sugar sub-fractions based on the (+)H-ESI-FT-Orbitrap MS spectra.....	175
Table 6.1. Composition of the BTG bio-oil and WCO.....	201
Table 6.2. Elemental composition of the distillation cuts (wt.%).....	206
Table 6.3. Density (g/mL) of the distillation cuts.....	207
Table 6.4. Surface tension (mN/m) of the distillation cuts.....	207
Table 6.5. Viscosity (mm ² /s) of the distillation cuts.....	208

LIST OF FIGURES

	Page
Figure 1.1: Global CO ₂ emissions from energy combustion and industrial processes, 1900-2021. Reproduced from ref. 1	3
Figure 1.2: Sources of greenhouse gas emissions (a) global, (b) United States. Reprinted from refs. 2 and 3	3
Figure 1.3: Overview of the dissertation structure.....	9
Figure 2.1: Graphical representation of a cellulose unit with carbon positions labeled 1-6. Reproduced from ref. 4,50	23
Figure 2.2: Bio-oil components and yields from various feedstocks. Reproduced from ref. 61.	25
Figure 2.3: Lumped models of cellulose decomposition: (a) B-S model, ⁹⁵ (b) Diebold model, ⁹⁶ (c) Waterloo model. ⁹⁷	29
Figure 2.4: Kinetic model of cellulose decomposition by Lin et al. ³⁹	31
Figure 2.5: Mechanistic kinetic model of various C1 to C6 compounds from glucose by Vinu and Broadbelt ¹⁰⁰	32
Figure 2.6: Major volatile products of cellulose pyrolysis. Reproduced from ref. 101.....	32
Figure 2.7: Mechanism of cellulose depolymerization: (a) LG formation with H ⁺ cation; ¹⁹ (b) concerted mechanism of anhydrosugars formation. ⁴⁰	34
Figure 2.8: Two-chain (a) and three-chain (b) LG-end models of cellulose; and reaction model of LG formation from crystalline cellulose chains (c). Reproduced from ref. 108.	36
Figure 2.9: Water loss mechanisms from fast pyrolysis of cellulose ¹¹⁴	38
Figure 2.10: van Krevelen plot of the nonvolatile fraction of the BTG bio-oil. Distinctive line patterns can be associated with specific reactions: (A) removal of Levoglucosan, (B) removal of Furan, (C) removal of acetol, (D) removal of methane, (E) demethoxylation, dehydration (F) dehydration, (G) removal of glycoaldehyde, (H) deraboxylation, and (J) decarbonylation. ⁶⁵	38
Figure 2.11: Proposed structures of highly dehydrated cellulose oligomers from sequential Maccoll elimination method (up to 3x dehydration). ¹¹⁸	39
Figure 2.12: Reaction mechanisms of HA (a) and HAA (b) formation from sugar oligomers. Reproduced from ref. 127.	41

Figure 2.13: Main pathways in bio-oil HDO. Reproduced from ref. 128.	47
Figure 2.14: Reactivity scale of oxygenated compounds in bio-oil under hydrotreatment conditions. Reproduced from ref. 148.	47
Figure 2.15: Co-adsorbed hydroxyacetone and hydrogen on NiMo catalyst (a) and hydrogenated hydroxyacetone (b) (Color legend: violet sticks: nickel, green sticks: molybdenum, yellow sticks: sulfur, red sticks: oxygen, maroon sticks: carbon, and white sticks: hydrogen).	49
Figure 2.16: FTIR spectra of a spent catalyst at different reaction temperatures. Reproduced from ref. 176.	56
Figure 2.17: TEM image of a spent catalyst at different reaction temperatures. Reproduced from ref. 176.	56
Figure 2.18: Simplified reaction scheme of coke formation during bio-oil HDO. Reproduced from ref. 190.	57
Figure 2.19: Simplified reaction scheme of coke formation during bio-oil HDO. Reproduced from Ref. 192.	58
Figure 3.1: Optimized structures of the model compounds: (a) levoglucosan, (b) cellobiosan, (c) cellotriosan, and (d) celloquatrosan.	93
Figure 3.2: Sequential dehydration and numbering scheme for CBN. CBN stands for cellobiosan, <i>A</i> is for the LG-end, and <i>B</i> for the NR-end (in the case of cellotriosan, <i>B</i> is for the internal unit and <i>C</i> for the NR-end, the same pattern was followed for celloquatrosan).	95
Figure 3.3: Comparison between experimental and modeled FTIR spectra of selected sugars.	97
Figure 3.4: Comparison between experimental and modeled ¹³ C-NMR spectra of selected sugars (solvent peak: DMSO = 39.7 ppm).	99
Figure 3.5: Theoretical FTIR spectra of the identified dehydrated anhydrosugars.	111
Figure 3.6: Theoretical ¹ H-NMR spectra of the dehydrated anhydrosugars.	112
Figure 3.7: Theoretical ¹³ C-NMR spectra of the dehydrated anhydrosugars.	113
Figure 3.8: Experimental ¹³ C-NMR spectra of the WS BTG bio-oil fraction. Reproduced with permission from Ref.12. Copyright 2023. ACS Publications.	114
Figure 4.1: Proposed mechanism of hydroxyacetaldehyde fragmentation from oligomeric sugars. CBN: cellobiosan; a: ring <i>a</i> of the model compound; b: ring <i>b</i> of the model compound; 1,2-D: 1,2 dehydration reaction; RO: ring opening	

reaction; RDA: retro-Diels-Alder reaction; TR: tautomerization; HAA: hydroxyacetaldehyde; CBN-HAAb: final product.	135
Figure 4.2: Proposed mechanism of hydroxyacetone fragmentation from oligomeric sugars. CBN stands for cellobiosan; a: ring <i>a</i> of the model compound; b: ring <i>b</i> of the model compound; 1,2-D: 1,2 dehydration reaction; RO: ring opening reaction; H shift: proton transfer; TR: tautomerization reaction; RA: retro-aldol reaction; HA: hydroxyacetone; CBN-HAB: final product.	136
Figure 4.3: Theoretical ¹³ C-NMR (a) and ¹ H-NMR (b) of the proposed oligomeric sugar fragments where hydroxyacetaldehyde was removed (experimental sugar solvent peak: DMSO-d ₆ = 39.7 for ¹³ C-NMR and 2.5 ppm for ¹ H-NMR).	140
Figure 4.4: Theoretical ¹³ C-NMR (a) and ¹ H-NMR (b) of the proposed oligomeric sugar fragments where hydroxyacetone was removed (DMSO peak at 39.7 ppm for ¹³ C-NMR and 2.5 ppm for the ¹ H-NMR).	141
Figure 4.5: Theoretical FTIR spectra of the oligomeric sugar fragments where the hydroxyacetaldehyde (a) and hydroxyacetone (b) were removed.	142
Figure 5.1: Separation scheme of sugars from the bio-oil.	161
Figure 5.2: Yield of the sugar sub-fractions obtained from silica gel chromatography (left figure is the sugar sub-fractions dissolved in MeOH.	167
Figure 5.3: FTIR spectra of the sugar and its sub-fractions.	168
Figure 5.4: UV-Fluorescence analysis of the sugar and its sub-fractions.	169
Figure 5.5: ¹³ C-NMR (left) and ¹ H-NMR (right) of the sugar and its sub-fractions (solvent and impurity peaks: DMSO = 2.52 ppm for ¹ H, 39.75 ppm for ¹³ C; and H ₂ O = 3.29 ppm for ¹ H).	172
Figure 5.6: 2D HSQC NMR of the whole sugar and its sub-fractions.	173
Figure 5.7: Compositional characterization of pyrolytic sugar from BTG bio-oil and their subfractions by (-)H-ESI-FT Orbitrap MS. (Top) Diagrams of O/C ratio vs. Kendrick mass; (Middle) Diagrams of DBE vs. Carbon Number; and (Bottom) Diagrams of van Krevelen for H/C ratio vs. O/C ratio.	178
Figure 5.8: Compositional characterization of pyrolytic sugars from BTG bio-oil and their subfractions (+)H-ESI-FT Orbitrap MS. (Top) Diagrams of O/C ratio vs. Kendrick mass; (Middle) Diagrams of DBE vs. Carbon Number; and (Bottom) Diagrams of van Krevelen for H/C ratio vs. O/C ratio.	179
Figure 5.9: Semi-preparative HPLC chromatograms of the sugar sub-fractions obtained from: (a) THF-eluted sub-fractions, (b) MeOH-eluted sub-fractions, and (c) water-eluted sub-fractions.	182

Figure 6.1: Hydrotreated oil at different bio-oil concentrations (left) and representative distillation cuts (right).	202
Figure 6.2: Product yields of the co-hydrotreated bio-oil and WCO.....	202
Figure 6.3: Product yield (%) of the distillation cuts.....	203
Figure 6.4: FTIR spectra of the feedstocks and hydrotreated oils.	205
Figure 6.5: UV-Fluorescence spectra of the feedstocks and hydrotreated oils.....	205
Figure 6.6: Percentage distribution of carbon species identified in the fuel cuts.	210
Figure 6.7: Percentage distribution of each class of hydrocarbons identified in the fuel cuts (Note: Samples were insufficient for the analysis of gasoline cut with 40 wt.% bio-oil concentration).	211
Figure 7.1: NiMoS model (100 surface) used in the study: (a) perspective view showing both Mo and S edges, and (b) front view showing the Ni-promoted Mo-edge. Color legend: Mo – magenta, Ni – gray, S – yellow.....	225
Figure 7.2: Hydrodeoxygenation pathway of hydroxyacetone to propanediol.....	226
Figure 7.3: Adsorption sites and configurations of hydroxyacetone: (a) ketone on Ni-1 perpendicular, (b) ketone on Mo perpendicular, (c) ketone on Mo parallel, (d) ketone on Mo inclined, (e) ketone on Ni-1 parallel, (f) ketone on Mo perpendicular flat, (g) bidentate – ketone on Ni-1 and alcohol on Mo, and (g) ketone on Ni-2 parallel. Color legend: Mo magenta, Ni – gray, S – yellow, C – brown, O – red, and pinkish white – H.	227
Figure 7.4: Hydrogenation steps of hydroxyacetone to propanediol.....	228

Dedication

To You, my God, I dedicate this humble piece of work.

Surely, You have carried me through;

All the days of my life, You've been faithful;

Your love and mercy never end, they are new every morning.

Forever, I will sing the goodness of God!

CHAPTER ONE: INTRODUCTION

1.1 Background

The escalating worldwide energy demand and concerns over environmental pollution have ignited a quest for sustainable, renewable alternatives to traditional hydrocarbon-based energy sources. Fossil fuels, which have been the backbone of our energy supply, are finite resources, and their extraction and use contribute to greenhouse gas emissions (GHG). In 2021, the global CO₂ emissions rebounded to reach the highest-ever annual level, accounting for 36.3 gigatonnes.¹ The primary contributor to GHG is burning fossil fuels to produce electricity and heat, comprising 25% of total emissions, as shown in Figure 1.1a. This is trailed closely by emissions from the agriculture, forestry, and land use sectors (24%) and the transportation sector (14%).² Approximately 95% of the world's energy used for transportation is sourced from petroleum-based fuels, with gasoline and diesel being the primary constituents.² In the United States, the transportation sector stands as the foremost contributor to GHG emissions, making up 29% of the total (Figure 1.1b),³ with 10% of these emissions stemming from the aviation industry, a figure expected to rise over time. This heavy reliance on petroleum-based fuels necessitates a paradigm shift toward sustainable and environmentally friendly alternatives.

To bolster the green energy initiative, governments worldwide have instituted regulations mandating the inclusion of biofuels as a cleaner fuel option at the pump. Several policies and incentives have been introduced to champion the adoption of eco-friendly energy sources. The U.S. government, for example, has implemented a range of significant measures:

1. The Renewable Fuel Standard (RFS) is a pivotal regulation mandating the integration of specific biofuel volumes into commercial fuel supplies.⁴⁷

2. The Department of Energy (DOE) and the U.S. Department of Agriculture (USDA) allocate funding to support research and developments in the bioenergy field.
3. The Biomass Crop Assistance Program (BCAP) is designed to provide financial support to farmers and landowners involved in cultivating biomass for biofuel production.⁴⁸
4. Tax incentives and credits have been established to encourage both producers and consumers to adopt biofuels.
5. Government collaboration with educational institutions, industries, and research institutions is fostering partnerships to expedite R&D efforts related to biofuel technologies.

Harnessing the power of solar, water, wind, geothermal, and biomass resources provides a sustainable and clean path forward to reduce our dependence on fossil fuels and alleviate the environmental impact of our energy consumption. In 2022, biomass contributed 5% of the total U.S. energy consumption, primarily biofuels (49%) and wood and wood waste (43%).⁴ Biomass is attractive due to its abundance, carbon-neutral characteristics, and non-competition with food resources. Furthermore, biomass utilization facilitates the management of agricultural and forestry residues, promoting waste reduction and fostering a circular economy. Multiple routes exist to convert biomass into valuable energy sources, including direct combustion, thermochemical, chemical, and biological conversion. Among these, thermochemical conversion through fast pyrolysis emerged as a well-established technology to transform biomass into pyrolysis oil, commonly referred to as bio-oil. This conversion occurs under high-temperature conditions (typically between 400-600 °C) without oxygen.^{5,6,7,8,9} Fast pyrolysis can convert around 60 to 70% of lignocellulosic biomass into bio-oil, depending on feedstock types and

operating conditions.^{10,11,12,13,14,15,16,17} Bio-oil is a dark brown, free-flowing substance composed of a diverse range of low to high-molecular-weight compounds and various functional groups.

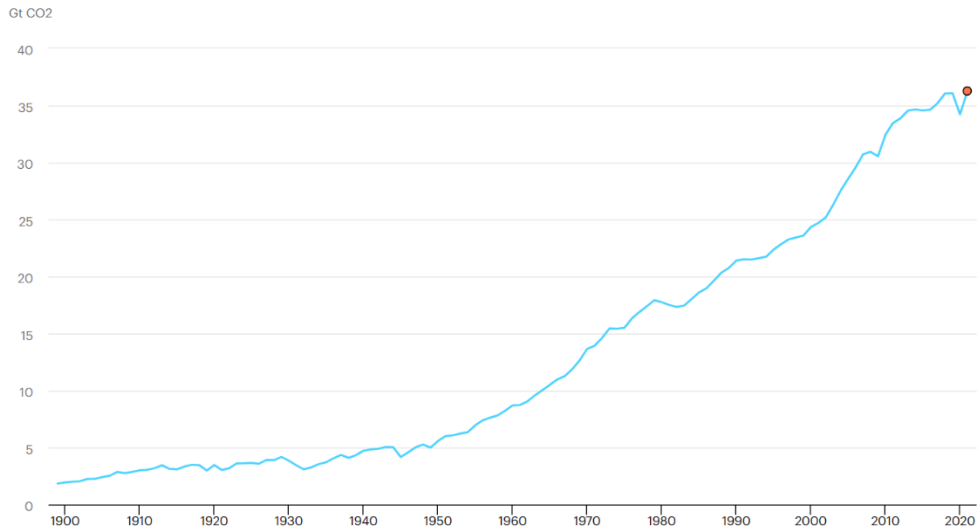


Figure 1.1: Global CO₂ emissions from energy combustion and industrial processes, 1900-2021. Reproduced from ref. 1

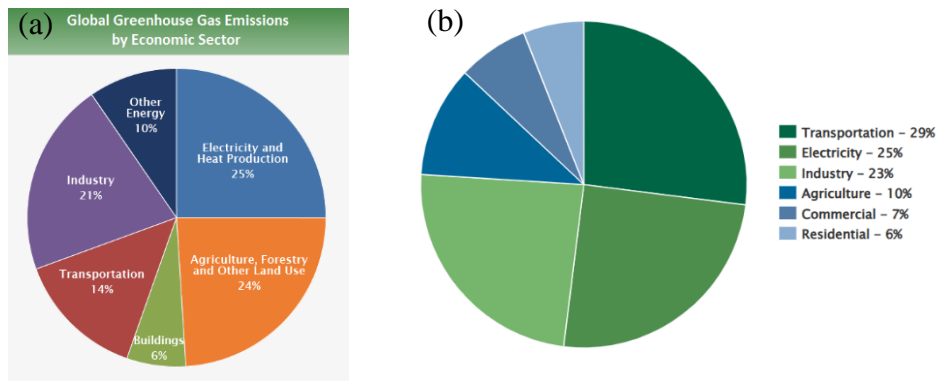


Figure 1.2: Sources of greenhouse gas emissions (a) global, (b) United States. Reprinted from refs. 2 and 3

The primary constituents of bio-oil include water (15-30 wt %), light oxygenates (8-26 wt %), monophenols (2-7 wt %), water-insoluble oligomers or pyrolytic lignin (15-25 wt %), and water-soluble molecules (10-30 wt %).¹⁸ Mainly, levoglucosan is the predominant product in bio-oil.^{13,19,20,21,22,23,24,25} Despite extensive studies, a fraction of the bio-oil remains relatively poorly studied. Lin et al.²⁰ identified 9.8 wt % of unidentified compounds in cellulose pyrolysis, and Garcia et al.¹⁸ reported nearly 20 wt % of unidentifiable compounds, likely originating from cellulose. Another study²⁶ focused on characterizing the water-soluble fraction, revealing 35 to 55 wt. % unknown compounds believed to be highly dehydrated sugars. Besides these unidentified bio-oil compounds, the high oxygen and water content in bio-oil present challenges. These factors influence the quality of bio-oil, rendering it highly acidic, with low thermal energy and poor stability, making it incompetent as a direct drop-in transportation fuel.^{27,28,29,30,31} Consequently, a refining process is necessary.

Several routes have been explored to upgrade bio-oil, with the primary ones being hydrotreatment and catalytic cracking.^{32,33} To some extents, several researchers have employed bio-oil fractionation to get rid of the sugar fraction, which is considered a significant contributor to coke formation, thus focusing on the upgrading of the lignin fraction.³⁴⁻³⁷ Hydrotreatment is a conventional method employed in the petroleum refining industry to eliminate impurities such as sulfur (hydrodesulfurization, HDS) and nitrogen (hydrodenitrogenation, HDN). This technology is now being applied to bio-oil for the purpose of oxygen removal (hydrodeoxygenation, HDO). HDO involves the treatment of bio-oil with hydrogen at elevated pressure and temperature conditions to saturate the highly reactive, oxygen-deficient bio-oil compounds.

However, in the absence of catalysts, severe coking is experienced, leading to catalyst encapsulation and subsequent reactor blockages, making coke formation a major concern during

bio-oil upgrading.^{38,39} Several strategies have been employed to mitigate coking, including reactor design, catalyst innovation, and process optimizations. A notable discovery from PNNL involves a two-stage hydrotreatment process comprising stabilization and deoxygenation.^{40,41} In the first stage, stabilization is carried out at a lower temperature (150 to 200 °C), facilitating the conversion of the reactive oxygen-containing compounds like carbonyls and carboxylic acids into alcohols. The second step, deoxygenation, is performed at a higher temperature (350 to 405 °C) under 140 bars of H₂ to crack large molecules and expel oxygen, often in the form of water. Various studies have also explored the addition of solvents (methanol, ethanol, decalin, tetralin, butanol) and other hydrogen-rich substances (waste cooking oil)^{36,42} to the bio-oil prior to hydrotreatment. Regarding catalyst designs for hydrodeoxygenation, noble metals (Pt, Pd, Ru, and Rh), transition metals (Ni, Mo, Co, and Fe), and bifunctional catalysts (NiMo and CoMo) have been investigated. While noble catalysts proved highly active for hydrodeoxygenation, they are expensive for commercial applications.⁴³⁻⁴⁵

Cooperative research, combining experimental and computational modeling, is instrumental in understanding the very complex chemistry underpinning the thermochemical conversion of biomass to hydrocarbons and other chemicals. Computational modeling, particularly through density functional theory (DFT), assumes a central role in this process. Its contributions span a wide range of applications, including unraveling reaction mechanisms, providing valuable information about thermodynamics and kinetics of chemical reactions, product analysis, assessing catalyst design, identifying active sites, and predicting properties such as vibrational frequencies, charge distribution, and heat of formation, among others. DFT facilitates a detailed investigation of these processes at the molecular level by employing functionals to describe intermolecular interactions. In general, the selection of functionals entails

a tradeoff between accuracy and computational cost. Employing high-level functionals yields more accurate results but is associated with increased computational expenses. Several studies have reported good agreement between experimental findings and DFT modeling yields.

1.2 Dissertation Objectives

Bio-oil compositions have long been studied and characterized; however, their high complexity has left a fraction unidentified and poorly understood. Experimental studies through FT-ICR MS analyses have proven the existence of high molecular weight compounds, which are believed to originate from highly dehydrated cellulose. These heavy, oxygenated sugars are linked with coke formation during upgrading. Therefore, this work aims to contribute to understanding the oligomeric sugar fractions formed during fast pyrolysis and their behavior during upgrading.

The specific objectives of the study include the following:

- 1.** Investigate the dehydration and fragmentation reactions of the unidentified heavy oligomeric sugars to elucidate and propose potential structures of these fractions,
- 2.** Utilize the group contribution method to estimate the physical and thermochemical properties of sugar oligomers,
- 3.** Employ column chromatography techniques to isolate the oligomeric sugars, conduct characterization, and match findings with the modeling yields,
- 4.** Perform co-hydrotreatment of the heavy bio-oil fractions, which include both sugar and lignin oligomers, with waste cooking oil to produce hydrocarbon-range biofuels,
- 5.** Evaluate the properties and potential coke formation of the resulting hydrocarbon-range biofuels, and

6. Examine the reaction mechanisms governing the interaction between bio-oil and catalyst during hydrotreatment to elucidate oxygen removal processes, utilizing density functional theory.

1.3 Dissertation Structure

This dissertation adopted a collaborative research approach integrating experimental and modeling techniques to understand the fundamentals of biomass thermochemical conversions to hydrocarbons and other chemicals. The dissertation is structured into eight chapters, as shown in Figure 1:3.

Chapter 1 serves as the introductory section, offering a concise overview of the study.

Chapter 2 is devoted to an in-depth literature review, primarily assessing the existing body of knowledge and pinpointing areas that demand further investigation.

Chapters 3 and 4 investigate the selected reaction mechanisms of biomass fast pyrolysis to propose structures of resulting products. Chapter 3 primarily centers on the study of dehydration reactions, while Chapter 4 investigates fragmentation reactions, both dedicated to elucidating the structures of the unidentified bio-oil fractions. These modeling endeavors were built upon prior experimental work employing FT-ICR MS analysis, which detected high molecular weight compounds in the water-soluble (sugar-rich) bio-oil fraction and unveiled a substantial portion of unidentified compounds, ranging from 35 to 55 wt %.²⁶ A follow-up study⁴⁶ was carried out to identify structures of these compounds by coupling FT-ICR MS results with combinatoric dehydration and fragmentation modeling, leading to proposed chemical structures for these unknown oligomers. Consequently, this work further extends the previous efforts to elucidate oligomers' structure using density functional theory. Chapters 3 and 4 have already been published in Energy & Fuels.

Chapter 5 comprises experimental works aimed at separating and characterizing oligomeric sugars in bio-oil. A combination of chromatographic techniques was utilized to isolate the sugar fractions, followed by a comprehensive characterization process to identify their specific components. These results were then synthesized with the previously obtained modeling yields to match the results.

Chapters 6 and 7 are geared towards understanding bio-oil refining to produce hydrocarbon-range biofuels. Chapter 6 emphasizes experimental work on bio-oil upgrading by co-hydrotreating the heavy bio-oil fraction (light oxygenates were removed) with waste cooking oil to mitigate coke formation. In the literature, coke formation is linked to pyrolytic sugars. Consequently, scholars tend to eliminate these fractions and prioritize the hydrotreatment of pyrolytic lignin fractions. In this study, both pyrolytic sugars and pyrolytic lignin were utilized.

Chapter 7 is committed to understanding the interaction between bio-oil and catalyst to reveal the mechanism of oxygen removal from bio-oil compounds during hydrotreatment using density functional theory. The mechanisms of hydrogenation and deoxygenation were examined. Due to the intricate nature of sugar oligomer structures, a fragment of sugar, hydroxyacetone, was modeled over an unsupported NiMo catalyst.

Finally, **Chapter 8** summarizes the significant outcomes obtained in Chapters 1 through 7. Based on these findings, several recommendations have been put forth for future research endeavors.

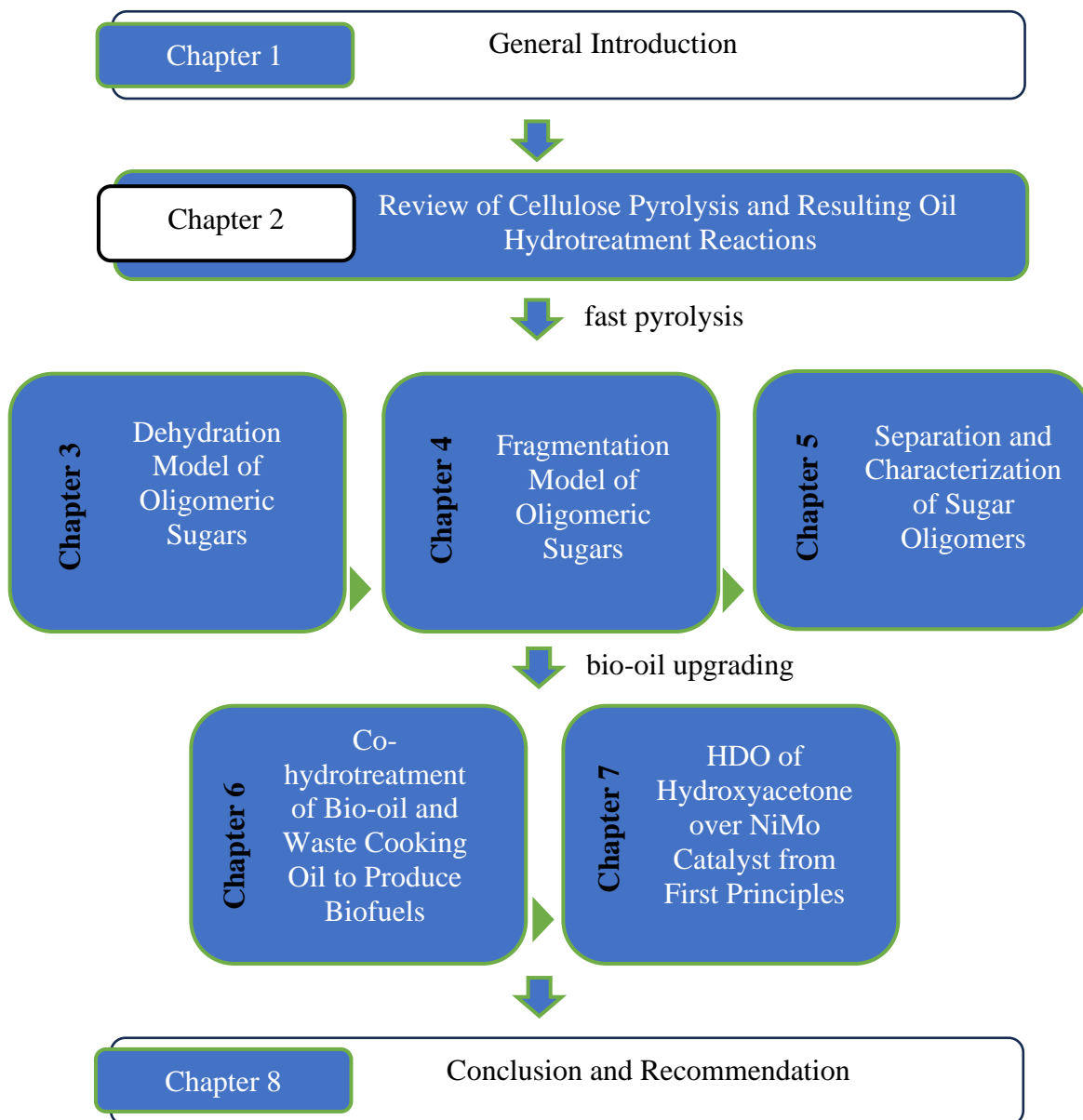


Figure 1.3: Overview of the dissertation structure.

1.4 Publications

The research presented in this dissertation has resulted in the publication of the following papers, with some currently in the preparation stage for publication.

As main author:

1. **Denson, M.**; Terrell, E.; Kostetsky, P.; Olarte, M.; Broadbelt, L.; Garcia-Perez, M.
Elucidation of Structure and Physical Properties of Pyrolytic Sugar Oligomers Derived from Cellulose Depolymerization/Dehydration Reactions: A Density Functional Theory Study. *Energy & Fuels* 37 (11), 7834–7847. <https://doi.org/10.1021/acs.energyfuels.3c00641>.
2. **Denson, M.**; Terrell, E.; Kostetsky, P.; Olarte, M.; Broadbelt, L.; Garcia-Perez, M.
Theoretical Insights on the Fragmentation of Cellulosic Oligomers to Form Hydroxyacetone and Hydroxyacetaldehyde. *Energy & Fuels* 37 (18), 13997–14005.
<https://doi.org/10.1021/acs.energyfuels.3c01924>.
3. **Denson, M.**; Olarte, M.; Garcia-Perez, M. Review of Cellulose Pyrolysis and Resulting Oil Hydrotreatment Reactions. Paper in preparation. To be submitted to *Energy & Fuels* 2024.
4. **Denson, M.**; Carvalho, J.; Alsbou, E.; Gagaa, M.; Afrin, A.; Wisniewski, A.; Olarte, M.; Garcia-Perez, M. Towards a Rational Description of the Chemical Composition of Bio-oil Water Soluble Fractions. Paper in preparation. To be submitted to *Energy & Fuels* 2023.
5. **Denson, M.**; Manrique, R.; Olarte, M.; Garcia-Perez, M. Co-hydrotreatment of Bio-oil and Waste Cooking Oil to Produce Biofuel. Paper in preparation. To be submitted to *Energy & Fuels* 2023.
6. **Denson, M.**; Olarte, M.; Garcia-Perez, M.; McEwen, J. Hydrodeoxygenation of Hydroxyacetone over NiMo Catalyst from First Principles. Paper in preparation. To be submitted to *Catalysis* 2024.

As co-author:

7. Paiva Pinheiro Pires, A.; Garcia-Perez, M.; Olarte, M.; Kew, W.; Schmidt, A.; Zemaitis, K.; **Denson, M.**; Terrell, E.; McDonald, A.; Han, Y. Comparison of the Chemical Composition of

Liquids from the Pyrolysis and Hydrothermal Liquefaction of Lignocellulosic Materials. *Energy & Fuels* 37 (10), 7221–7236. <https://doi.org/10.1021/acs.energyfuels.2c03239>.

8. Han, Y.; Pinheiro Pires, A. P.; **Denson, M.**; McDonald, A. G.; Garcia-Perez, M. Ternary Phase Diagram of Water/Bio-Oil/Organic Solvent for Bio-Oil Fractionation. *Energy and Fuels* 2020, 34 (12), 16250–16264. <https://doi.org/10.1021/acs.energyfuels.0c03100>.

1.5 Scientific Contributions

The execution of this research led to the following scientific contributions:

1. We proposed potential structures of the unknown sugar oligomeric fractions in bio-oil. These structures have allowed the prediction of FTIR and NMR peaks, offering valuable insights into the oligomers' functional groups and molecular mass. This data can be matched with experimental findings to aid in the characterization and understanding of the chemistry of oligomeric sugars. Moreover, the structural information paved the way to estimate their physical and thermochemical properties. This information holds significance for enhancing product selectivity, driving catalyst innovation, optimizing process parameters, and designing efficient reactors for processing and upgrading.
2. A new method was devised to isolate sugar oligomers from bio-oil, employing several chromatographic techniques, one of which is semi-preparative HPLC. Characterizing these sugars enriches our understanding of their properties, which are invaluable for optimizing both upstream and downstream processing. These findings are matched with the modeling yields to gain a deeper insight into the nature of oligomers. Notably, the proposed structures/formulas of the sugar oligomers from the modeling works in Chapters 3 and 4 were detected experimentally by (\pm)H-ESI-FT Orbitrap MS.

3. The experiment on bio-oil upgrading showed that the heavy bio-oil, stripped of light oxygenates but retaining both pyrolytic sugars and pyrolytic lignin, could be co-hydrotreated with waste cooking oil, resulting in remarkably low coke formation, ranging from 0.7 to 2.4 wt. %. Remarkably, this coke yield is on par with using solely the pyrolytic lignin fraction for hydrotreatment. This implies that coke formation is not exclusively linked to sugar oligomers; instead, both sugars and lignin play a role in the process. Moreover, the process of bio-oil fractionation to eliminate pyrolytic sugars prior to hydrotreatment can be obviated, saving resources and time. Additionally, the introduction of 1-butanol as a solvent helps alleviate coke formation.

4. The modeling of the hydroxyacetone hydrodeoxygenation gives more profound insights and a fundamental understanding of the chemistry behind bio-oil conversion to biofuels. Specifically, it sheds light on the interaction between a sugar fragment and NiMo catalysts during upgrading to expel oxygen. This insight can be extended to the heavy and highly oxygenated bio-oil compounds like oligomers responsible for coke formation. This simulation can also provide information about the active sites of the catalysts, leading to the development of more efficient and selective catalysts for HDO.

1.6 REFERENCES

- (1) *CO2 Emissions in 2022 – Analysis - IEA*. <https://www.iea.org/reports/co2-emissions-in-2022?ref=hackernoon.com> (accessed 2023-10-17).
- (2) *Global Greenhouse Gas Emissions Data | US EPA*.
<https://www.epa.gov/ghgemissions/global-greenhouse-gas-emissions-data> (accessed 2023-10-17).
- (3) *Fast Facts on Transportation Greenhouse Gas Emissions | US EPA*.
<https://www.epa.gov/greenvehicles/fast-facts-transportation-greenhouse-gas-emissions> (accessed 2023-10-17).
- (4) *Biomass explained - U.S. Energy Information Administration (EIA)*.
<https://www.eia.gov/energyexplained/biomass/> (accessed 2023-10-18).
- (5) Zhou, X.; Nolte, M. W.; Mayes, H. B.; Shanks, B. H.; Broadbelt, L. J. Experimental and Mechanistic Modeling of Fast Pyrolysis of Neat Glucose-Based Carbohydrates. 1. Experiments and Development of a Detailed Mechanistic Model. *Ind. Eng. Chem. Res.* **2014**, *53* (34), 13274–13289. <https://doi.org/10.1021/ie502259w>.
- (6) Abdilla-Santes, R. M.; Agarwal, S.; Xi, X.; Heeres, H.; Deuss, P. J.; Heeres, H. J. Valorization of Humins Type Byproducts from Pyrolytic Sugar Conversions to Biobased Chemicals. *J. Anal. Appl. Pyrolysis* **2020**, *152* (October).
<https://doi.org/10.1016/j.jaap.2020.104963>.
- (7) Boucher, M. E.; Chala, A.; Pakdel, H.; Roy, C. Bio-Oils Obtained by Vacuum Pyrolysis of Softwood Bark as a Liquid Fuel for Gas Turbines. Part II: Stability and Ageing of Bio-Oil and Its Blends with Methanol and a Pyrolytic Aqueous Phase. *Biomass and Bioenergy* **2000**, *19* (5), 351–361. [https://doi.org/10.1016/S0961-9534\(00\)00044-1](https://doi.org/10.1016/S0961-9534(00)00044-1).

- (8) Bridgwater, A. V. Production of High Grade Fuels and Chemicals from Catalytic Pyrolysis of Biomass. *Catal. Today* **1996**, *29* (1–4), 285–295.
[https://doi.org/10.1016/0920-5861\(95\)00294-4](https://doi.org/10.1016/0920-5861(95)00294-4).
- (9) Bridgwater, A. V. Catalysis in Thermal Biomass Conversion. *Appl. Catal. A, Gen.* **1994**, *116* (1–2), 5–47. [https://doi.org/10.1016/0926-860X\(94\)80278-5](https://doi.org/10.1016/0926-860X(94)80278-5).
- (10) Kan, T.; Strezov, V.; Evans, T. J. Lignocellulosic Biomass Pyrolysis: A Review of Product Properties and Effects of Pyrolysis Parameters. *Renew. Sustain. Energy Rev.* **2016**, *57*, 1126–1140. <https://doi.org/10.1016/j.rser.2015.12.185>.
- (11) Pinheiro Pires, A. P.; Arauzo, J.; Fonts, I.; Domine, M. E.; Fernández Arroyo, A.; Garcia-Perez, M. E.; Montoya, J.; Chejne, F.; Pfromm, P.; Garcia-Perez, M. Challenges and Opportunities for Bio-Oil Refining: A Review. *Energy and Fuels* **2019**, *33* (6), 4683–4720. <https://doi.org/10.1021/acs.energyfuels.9b00039>.
- (12) Venderbosch, R. H.; Prins, W. Fast Pyrolysis Technology Development. *Biofuels, Bioproducts and Biorefining*. 2010, pp 178–208. <https://doi.org/10.1002/bbb.205>.
- (13) Agarwal, V.; Dauenhauer, P. J.; Huber, G. W.; Auerbach, S. M. Ab Initio Dynamics of Cellulose Pyrolysis: Nascent Decomposition Pathways at 327 and 600 °C. *J. Am. Chem. Soc.* **2012**, *134* (36), 14958–14972. <https://doi.org/10.1021/ja305135u>.
- (14) Oasmaa, A.; Fonts, I.; Pelaez-Samaniego, M. R.; Garcia-Perez, M. E.; Garcia-Perez, M. Pyrolysis Oil Multiphase Behavior and Phase Stability: A Review. *Energy and Fuels* **2016**, *30* (8), 6179–6200. <https://doi.org/10.1021/acs.energyfuels.6b01287>.
- (15) Nachenius, R. W.; Ronsse, F.; Venderbosch, R. H.; Prins, W. *Biomass Pyrolysis*, 1st ed.; Elsevier Inc., 2013; Vol. 42. <https://doi.org/10.1016/B978-0-12-386505-2.00002-X>.
- (16) Patwardhan, P. R.; Satrio, J. A.; Brown, R. C.; Shanks, B. H. Product Distribution from

- Fast Pyrolysis of Glucose-Based Carbohydrates. *J. Anal. Appl. Pyrolysis* **2009**, *86* (2), 323–330. <https://doi.org/10.1016/j.jaap.2009.08.007>.
- (17) Mohan, D.; Pittman, C. U.; Steele, P. H. Pyrolysis of Wood /Biomass for Bio-Oil. *Prog. Energy Combust. Sci.* **2017**, *62* (4), 848–889.
- (18) Garcia-Perez, M.; Wang, S.; Shen, J.; Rhodes, M.; Lee, W. J.; Li, C. Z. Effects of Temperature on the Formation of Lignin-Derived Oligomers during the Fast Pyrolysis of Mallee Woody Biomass. *Energy and Fuels* **2008**, *22* (3), 2022–2032. <https://doi.org/10.1021/ef7007634>.
- (19) Gong, X.; Yu, Y.; Gao, X.; Qiao, Y.; Xu, M.; Wu, H. Formation of Anhydro-Sugars in the Primary Volatiles and Solid Residues from Cellulose Fast Pyrolysis in a Wire-Mesh Reactor. **2014**. <https://doi.org/10.1021/ef501112q>.
- (20) Lin, Y. C.; Cho, J.; Tompsett, G. A.; Westmoreland, P. R.; Huber, G. W. Kinetics and Mechanism of Cellulose Pyrolysis. *J. Phys. Chem. C* **2009**, *113* (46), 20097–20107. <https://doi.org/10.1021/jp906702p>.
- (21) Yu, Y.; Chua, Y. W.; Wu, H. Characterization of Pyrolytic Sugars in Bio-Oil Produced from Biomass Fast Pyrolysis. **2016**. <https://doi.org/10.1021/acs.energyfuels.6b00464>.
- (22) Sharifzadeh, M.; Sadeqzadeh, M.; Guo, M.; Borhani, T. N.; Murthy Konda, N. V. S. N.; Garcia, M. C.; Wang, L.; Hallett, J.; Shah, N. The Multi-Scale Challenges of Biomass Fast Pyrolysis and Bio-Oil Upgrading: Review of the State of Art and Future Research Directions. *Prog. Energy Combust. Sci.* **2019**, *71*, 1–80. <https://doi.org/10.1016/j.pecs.2018.10.006>.
- (23) Richards, G. N. Glycolaldehyde from Pyrolysis of Cellulose. *J. Anal. Appl. Pyrolysis* **1987**, *10* (3), 251–255. [https://doi.org/10.1016/0165-2370\(87\)80006-2](https://doi.org/10.1016/0165-2370(87)80006-2).

- (24) Shen, D. K.; Gu, S. The Mechanism for Thermal Decomposition of Cellulose and Its Main Products. *Bioresour. Technol.* **2009**, *100* (24), 6496–6504.
<https://doi.org/10.1016/j.biortech.2009.06.095>.
- (25) Piskorz, J.; Radlein, D.; Scott, D. S. On the Mechanism of the Rapid Pyrolysis of Cellulose. *J. Anal. Appl. Pyrolysis* **1986**, *9* (2), 121–137. [https://doi.org/10.1016/0165-2370\(86\)85003-3](https://doi.org/10.1016/0165-2370(86)85003-3).
- (26) Stankovikj, F.; McDonald, A. G.; Helms, G. L.; Olarte, M. V.; Garcia-Perez, M. Characterization of the Water-Soluble Fraction of Woody Biomass Pyrolysis Oils. *Energy and Fuels* **2017**, *31* (2), 1650–1664. <https://doi.org/10.1021/acs.energyfuels.6b02950>.
- (27) Kadarwati, S.; Hu, X.; Gunawan, R.; Westerhof, R.; Gholizadeh, M.; Hasan, M. D. M.; Li, C. Coke Formation during the Hydrotreatment of Bio-Oil Using NiMo and CoMo Catalysts. *Fuel Process. Technol.* **2017**, *155*, 261–268.
<https://doi.org/10.1016/j.fuproc.2016.08.021>.
- (28) Garcia-Perez, M.; Adams, T. T.; Goodrum, J. W.; Geller, D.; Das, K. C. Production and Fuel Properties of Pine Chip Bio-Oil/Biodiesel Blends. *Energy and Fuels* **2007**, *21* (4), 2363–2372. <https://doi.org/10.1021/ef060533e>.
- (29) Koike, N.; Hosokai, S.; Takagaki, A.; Nishimura, S.; Kikuchi, R.; Ebitani, K.; Suzuki, Y.; Oyama, S. T. Upgrading of Pyrolysis Bio-Oil Using Nickel Phosphide Catalysts. *J. Catal.* **2016**, *333*, 115–126. <https://doi.org/10.1016/j.jcat.2015.10.022>.
- (30) Kim, J. S. Production, Separation and Applications of Phenolic-Rich Bio-Oil - A Review. *Bioresour. Technol.* **2015**, *178*, 90–98. <https://doi.org/10.1016/j.biortech.2014.08.121>.
- (31) Pham, T. N.; Shi, D.; Resasco, D. E. Evaluating Strategies for Catalytic Upgrading of Pyrolysis Oil in Liquid Phase. *Appl. Catal. B Environ.* **2014**, *145*, 10–23.

- <https://doi.org/10.1016/j.apcatb.2013.01.002>.
- (32) Han, Y.; Gholizadeh, M.; Tran, C. C.; Kaliaguine, S.; Li, C. Z.; Olarte, M.; Garcia-Perez, M. Hydrotreatment of Pyrolysis Bio-Oil: A Review. *Fuel Process. Technol.* **2019**, *195* (June). <https://doi.org/10.1016/j.fuproc.2019.106140>.
- (33) Mortensen, P. M.; Grunwaldt, J. D.; Jensen, P. A.; Knudsen, K. G.; Jensen, A. D. A Review of Catalytic Upgrading of Bio-Oil to Engine Fuels. *Appl. Catal. A Gen.* **2011**, *407* (1–2), 1–19. <https://doi.org/10.1016/j.apcata.2011.08.046>.
- (34) Yin, W.; Venderbosch, R. H.; Alekseeva, M. V.; Figueirêdo, M. B.; Heeres, H.; Khromova, S. A.; Yakovlev, V. A.; Cannilla, C.; Bonura, G.; Frusteri, F.; Heeres, H. J. Hydrotreatment of the Carbohydrate-Rich Fraction of Pyrolysis Liquids Using Bimetallic Ni Based Catalyst: Catalyst Activity and Product Property Relations. *Fuel Process. Technol.* **2018**, *169* (October 2017), 258–268. <https://doi.org/10.1016/j.fuproc.2017.10.006>.
- (35) Han, Y.; Pires, A. P. P.; Garcia-Perez, M. Co-Hydrotreatment of the Bio-Oil Lignin-Rich Fraction and Vegetable Oil. *Energy and Fuels* **2020**, *34* (1), 516–529. <https://doi.org/10.1021/acs.energyfuels.9b03344>.
- (36) Paiva Pinheiro Pires, A.; Olarte, M.; Terrell, E.; Garcia-Perez, M.; Han, Y. Co-Hydrotreatment of Yellow Greases and the Water-Insoluble Fraction of Pyrolysis Oil. Part I: Experimental Design to Increase Kerosene Yield and Reduce Coke Formation. *Energy and Fuels* **2023**, *37* (3), 2100–2114. <https://doi.org/10.1021/acs.energyfuels.2c03250>.
- (37) Kloekhorst, A.; Wildschut, J.; Heeres, H. J. Catalytic Hydrotreatment of Pyrolytic Lignins to Give Alkylphenolics and Aromatics Using a Supported Ru Catalyst. *Catal. Sci. Technol.* **2014**, *4* (8), 2367–2377. <https://doi.org/10.1039/c4cy00242c>.

- (38) Wang, Y.; Mourant, D.; Hu, X.; Zhang, S.; Lievens, C.; Li, C. Z. Formation of Coke during the Pyrolysis of Bio-Oil. *Fuel* **2013**, *108*, 439–444.
<https://doi.org/10.1016/j.fuel.2012.11.052>.
- (39) Hu, X.; Zhang, Z.; Gholizadeh, M.; Zhang, S.; Lam, C. H.; Xiong, Z.; Wang, Y. Coke Formation during Thermal Treatment of Bio-Oil. *Energy and Fuels* **2020**, *34* (7), 7863–7914. <https://doi.org/10.1021/acs.energyfuels.0c01323>.
- (40) Elliott, D. C.; Baker, E. G. Method for Upgrading Biomass Pyrolyzates. **1989**, No. 19.
- (41) Elliott, D. C. Historical Developments in Hydroprocessing Bio-Oils. *Energy and Fuels* **2007**, *21* (3), 1792–1815. <https://doi.org/10.1021/ef070044u>.
- (42) Han, Y.; Stankovikj, F.; Garcia-Perez, M. Co-Hydrotreatment of Tire Pyrolysis Oil and Vegetable Oil for the Production of Transportation Fuels. *Fuel Process. Technol.* **2017**, *159*, 328–339. <https://doi.org/10.1016/j.fuproc.2017.01.048>.
- (43) Bridgwater, A. V. Review of Fast Pyrolysis of Biomass and Product Upgrading. *Biomass and Bioenergy* **2012**, *38*, 68–94. <https://doi.org/10.1016/j.biombioe.2011.01.048>.
- (44) Lee, C. R.; Yoon, J. S.; Suh, Y. W.; Choi, J. W.; Ha, J. M.; Suh, D. J.; Park, Y. K. Catalytic Roles of Metals and Supports on Hydrodeoxygenation of Lignin Monomer Guaiacol. *Catal. Commun.* **2012**, *17*, 54–58. <https://doi.org/10.1016/j.catcom.2011.10.011>.
- (45) Wan, H.; Chaudhari, R. V.; Subramaniam, B. Aqueous Phase Hydrogenation of Acetic Acid and Its Promotional Effect on P-Cresol Hydrodeoxygenation. *Energy and Fuels* **2013**, *27* (1), 487–493. <https://doi.org/10.1021/ef301400c>.
- (46) Terrell, E.; Garcia-Perez, M. Novel Strategy to Analyze Fourier Transform Ion Cyclotron Resonance Mass Spectrometry Data of Biomass Pyrolysis Oil for Oligomeric Structure Assignment. *Energy and Fuels* **2020**, *34* (7), 8466–8481.

<https://doi.org/10.1021/acs.energyfuels.0c01687>.

(47) *Final Renewable Fuels Standards Rule for 2023, 2024, and 2025 | US EPA.*

<https://www.epa.gov/renewable-fuel-standard-program/final-renewable-fuels-standards-rule-2023-2024-and-2025> (accessed 2023-10-22).

(48) *Alternative Fuels Data Center: Biodiesel Laws and Incentives in Federal.*

<https://afdc.energy.gov/fuels/laws/BIOD?state=US> (accessed 2023-10-22).

CHAPTER TWO: REVIEW OF CELLULOSE PYROLYSIS AND RESULTING OIL HYDROTREATMENT REACTIONS

2.1. Introduction

The continuous rise in global population growth, industrialization, and the depletion of fossil fuel reserves necessitates the exploration of an alternative renewable energy source. This has led to an increased interest in research and development activities focused on renewable resources. Lignocellulosic biomass, characterized by its widespread availability, affordability, and non-competition with food sources, emerges as an intriguing and high-potential energy reservoir.¹ This biomass serves as a direct carbon source for producing renewable fuels and equally significant hydrocarbons. Lignocellulosic biomass comprises approximately 40-50 % cellulose;^{2,3,4,5} hence the need to study cellulose fast pyrolysis to unveil mechanisms behind bio-oil formation. Cellulose consists of crystalline, repeating D-glucose units interconnected by β -1-4 glycosidic bonds^{3,4}. Fast pyrolysis is a mature technology that converts approximately 60-70 % of lignocellulosic biomass materials to bio-oil, contingent on the specific feedstocks and process parameters employed.^{5,6,7,8,9,10,11,12} The conversion process represents a compelling approach in which biomass undergoes exposure to moderately high temperatures (400-600 °C) in an oxygen-free environment.^{13,14,15,16,17} The process is complex in that it entails various reaction pathways and mechanisms;⁸ as a result, hundreds to thousands of compounds are found within the bio-oil product.¹⁸ Generally, the resulting bio-oil is a mixture of six significant fractions: water (15-30 wt %); light oxygenates (8-26 wt %); monophenols (2-7 wt %); water-insoluble oligomers or pyrolytic lignin (15-25 wt %); and water-soluble molecules (10-30 wt %).⁶

Bio-oil has the advantages of easy storage, transportation, and high energy density.^{19,20,21,22,23} However, it has poor fuel characteristics because of its chemical composition;

therefore, it is acidic, viscous, precarious, and reactive, among other unwanted properties.²⁴ It is of low heating value and cannot be treated as a ‘drop-in’ transportation fuel.^{21,25,26,27,28} Hence, the necessity to upgrade bio-oil to remove the unwanted high amount of oxygenates.

Hydrotreatment, a process that mimics that of fossil fuels, is a promising upgrading method currently used to valorize bio-oil into biofuels through hydrodeoxygenation catalysts²⁶.

Hydrodeoxygenation involves the reaction of organic compounds treated with high-pressure hydrogen to remove oxygen (deoxygenation) from the bio-oil, mainly in the form of water.²⁹

Experimental studies show significant deoxygenation, but larger molecules still require reacting with hydrogen under higher-pressure conditions to break them into lower-boiling-point molecules that can be readily upgraded to fuels.³⁰ This process is called hydrocracking.

While experimental results provide significant insights regarding molecular mass and elemental composition, a critical role is played by computer simulation in calculating and predicting fundamental properties that have not been examined experimentally.³¹ Computer simulations can also be used to complement experimental results. Computational simulations such as density functional theory (DFT) is a robust modeling tool used to study the details of complex reaction mechanisms at the molecular/atomic level and to project potential structures of pyrolysis products.² Hu et al.³² and Kostetsky and Broadbelt³³ discussed the application and recent developments of quantum chemistry (QC) modeling, such as DFT, in studying the mechanisms of biomass pyrolysis. Similarly, DFT has been used to investigate the interaction of bio-oil with catalyst surfaces during hydrotreatment. Banerjee et al.³⁴ studied the deoxygenation of bio-oil on a Ru catalyst using furfural as a model compound. Sun et al. investigated the mechanism of phenol deoxygenation on Fe and Pd catalysts,³⁵ as well as the vapor-phase hydrodeoxygenation (HDO) of guaiacol on carbon-supported bimetallic Pd-Fe catalysts.³⁶

Despite numerous investigations, which encompass either experimental, modeling or both approaches, aimed at comprehending cellulose pyrolysis, the intricate nature of the reactions and resulting products has rendered the true mechanism elusive. Therefore, this paper undertakes a comprehensive review of existing literature pertaining to the reaction mechanisms underlying the conversion of cellulose into hydrocarbons, specifically fast pyrolysis and hydrotreatment. A deep understanding of the mechanisms of fast pyrolysis and methods of upgrading bio-oil is a cornerstone to product selectivity,^{4,37} efficient design, and optimization of processing technologies^{38,39,40,41} to produce biofuels and biochemicals.

2.2 Review of Cellulose Pyrolysis Reaction Mechanisms

2.2.1 Cellulose Structure and Pyrolysis

Cellulose is the principal scaffolding of all plant cell walls, imparting strength to wood fibers.⁴² It constitutes a significant portion, approximately 40-50 % on a dry weight basis, of wood mass, making it the most abundant material in the biosphere.^{32,43,44,45,46,47} Cellulose possesses a robust crystalline structure and consists of a linear homopolymer composed of 1-4, D-glucopyranose units.^{4,48} These glucose units are linked through dehydration reactions at carbon 1 and carbon 4, resulting in an interconnected structure.⁴

The structure of a native cellulose has been discussed elsewhere.⁴⁶ Figure 2.1 provides an illustration of a cellulose unit with a generic chemical formula of $[C_6H_{10}O_5]_n$. The chain length of a cellulose molecule ranges from 300 to 1700 units for wood pulp and 800 to 10,000 units for cotton and other plant fibers.⁴⁹

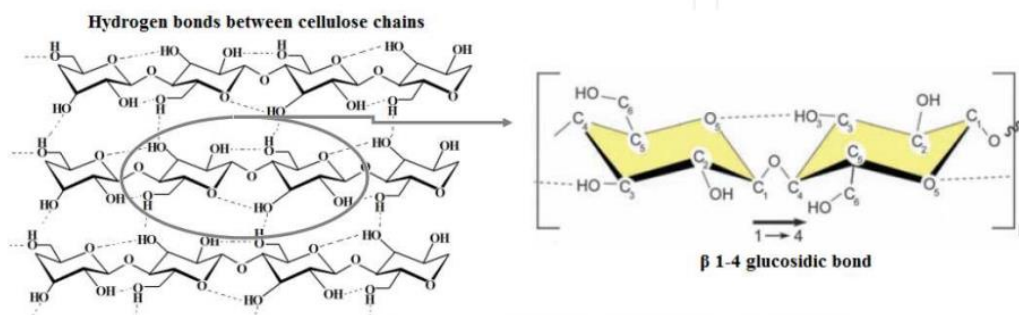


Figure 2.1: Graphical representation of a cellulose unit with carbon positions labeled 1-6. Reproduced from ref. 4,50

The first step to utilizing cellulosic biomass is to overcome its recalcitrant nature for energy conversion such as fast pyrolysis to produce liquid fuel.³⁹ Fast pyrolysis is a highly promising technique that involves the rapid heating of biomass particles (< 2 mm) under reactor operating conditions of 400 to 600°C in an oxygen-free environment.^{51,52} The resulting liquid product is a dark brown, freely flowing liquid formed through the rapid quenching and removal of condensable vapors generated during the reaction.⁵² This product is commonly referred to as pyrolysis oil or bio-oil. Bio-oil yield can range from 60 to 75 % on a dry weight basis of the biomass, with solid char constituting 15 to 25 wt % and non-condensable gases accounting for 10 to 20 wt %. These proportions can vary depending on factors such as the feedstock used, reactor design, and process parameters.^{13,12,53}

During pyrolysis, the primary products undergo further decomposition through secondary reactions. These primary products encompass anhydrosugars, predominantly levoglucosan, along with furan derivatives, carbonyls, carboxylic acids, and phenolics.⁵ These products continue to react to form low molecular weight compounds through secondary processes. Both primary and secondary reactions occur rapidly and without distinct boundaries. The products resulting from secondary processes include aldehydes or ketones and non-condensable gases, which originate

from the fragmentation of levoglucosan at elevated temperatures.⁵⁴ Patwardhan et al.⁵⁵ reported that secondary reactions involve the oligomerization of levoglucosan and the decomposition of the primary products into compounds such as 5-HMF, anhydroxylopyranose, and 2-furaldehyde.

2.2.2 Bio-oil Composition

Numerous papers^{6,13,22,52} have discussed the components and characteristics of bio-oil. Bio-oil is composed of mixtures of different molecular sizes and functional groups due to depolymerization, dehydration, and fragmentation reactions that occur during fast pyrolysis. The primary categories of compounds present in bio-oil include water, anhydrosugars, furan derivatives, phenolics, and light-oxygenated compounds.^{11,22} Levoglucosan is the most abundant anhydrosugar and organic liquid product found in bio-oil.^{8,20,39,53,56,57,58,59} When using pure cellulose, levoglucosan yield can be as high as 59 %.⁶⁰ Figure 2.2 depicts the major yields of bio-oils derived from several feedstocks.⁶¹

Bio-oil exhibits high viscosity and acidity and contains a significant concentration of oxygenated compounds, resulting in poor stability, low energy density, and immiscibility with hydrocarbon fuels.^{22,24,62} These undesirable properties limit its direct usability as a fuel source due to the risk of engine deterioration and low cetane number.⁷ A study conducted by Garcia-Perez et al.⁶³ revealed the conversion of biomass into various components on a dry basis. These components included the formation of 8 to 15 wt % of small organic compounds, primarily hydroxyacetaldehyde, hydroxyacetone, acetic acid, formic acid, and methanol. Additionally, 5 to 10 wt % of biomass was converted to monophenols and furans, while 6 to 15 wt % into hydrolyzable sugars. Lignin oligomers constituted 6 to 15 wt % and water content ranged from 10 to 15 wt %. Furthermore, nearly 20 wt % of the biomass was transformed into an unidentified water-soluble fraction, likely derived from cellulose. Lin et al.³⁹ reported 9.8 wt % of

unidentified compounds in cellulose pyrolysis. The study of Stankovikj et al.⁶⁴ on the characterization of water-soluble bio-oil fraction revealed an unknown fraction of compounds ranging from 35 to 50 wt %. Several studies^{64,65,66,67,68} have elucidated and proposed potential structures of these unknown sugar-derived oligomers by integrating both experimental and modeling works.

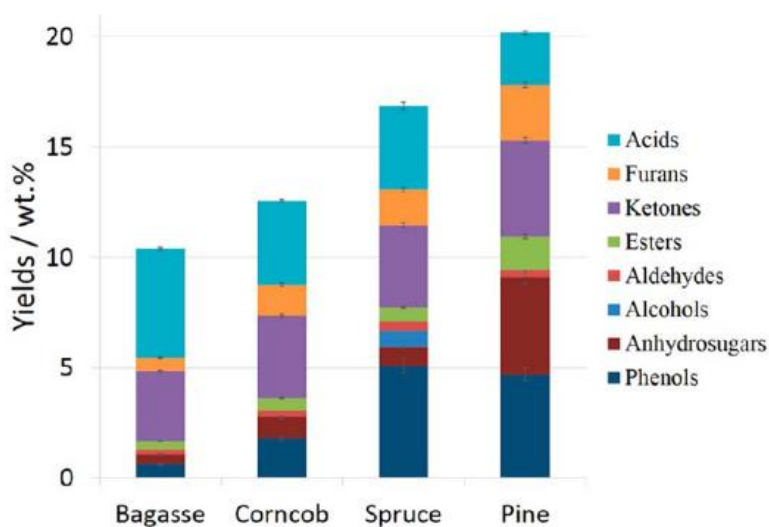


Figure 2.2: Bio-oil components and yields from various feedstocks. Reproduced from ref. 61.

Given the complex and diverse functional groups present in bio-oil, it is not feasible to characterize it using a single analytical technique comprehensively.⁵⁹ Several works have reported various analytical techniques for bio-oil analyses including total acid number, P-NMR, GC-MS, carbonyl titrations, among others.^{9,69,70,71} Similarly, Oasmaa et al.⁷² and Pires et al.⁷³ discussed the application of chromatographic spectroscopic techniques to analyze bio-oils and their upgraded products. Deep knowledge of the bio-oil properties is important for upgrading

purposes. Heavy compounds which cannot be detected by GC-MS are studied using FT-ICR MS,^{64, 65,74, 75} Orbitrap, and Quadruple time-of-flight (Q-TOF).^{70,76}

2.2.3 Cellulose Pyrolysis Reactions

Because cellulose is the primary component of lignocellulosic biomass, several reaction models have been put forth to comprehend the behavior of cellulose pyrolysis.

Thermogravimetric analysis (TGA) has been prevalent in studying the kinetic models for cellulose thermochemical conversion.^{11,39,45,77,78,79,80,81} Gas chromatography-mass spectrometry (GC/MS) has also found extensive application in examining pyrolysis reactions and their resulting products.^{4,82,83,84,85}

Moreover, employing theoretical methods based on first principles calculations proves to be a potent approach for delving into the intricacies of pyrolysis chemistry. Several research endeavors have leveraged DFT to complement experimental investigation of chemical reaction mechanisms in cellulose pyrolysis and to assign potential structures of bio-oil compounds. For instance, Zhao et al.⁸⁶ used DFT to investigate the initial degradation of cellulose under inert and oxidative atmospheres. Their findings revealed that the thermal cleavage of glycosidic bonds is an endothermic process. Importantly, their modeling results agree with experimental findings.

Similarly, Wang et al.⁸⁵ combined Py-GC/MS with DFT to study the mechanism of cellulose pyrolysis. Experimental results highlighted pyrans (such as LG and LGO), furans, and linear small molecular mass compounds as the primary pyrolysis products. DFT calculations demonstrated that the formation of 5-HMF and DGP is more favorable than LG, consistent with experimental observations. Further, DFT has been instrumental in examining the reaction pathways of other bio-oil fractions such as hemicellulose and lignin compounds. Huang et al.⁸⁷ employed DFT, utilizing xylopyranose as a model compound for hemicellulose, to explore the

reaction pathways of key products during pyrolysis. Remarkably, their modeling results demonstrated good agreement with experimental yields. The integration of experimental investigations and DFT studies will deduce cellulose pyrolysis chemistry to provide valuable assistance in the development of pyrolysis technology.

The cellulose pyrolysis global models have been reviewed elsewhere.^{10,88,89,90,91} The widely accepted and influential lumped models in the scientific community include Broido-Shafizadeh (B-S) model^{11,43,92,93,94,95} Diebold model,⁹⁶ and Waterloo model.⁹⁷ According to the B-S model (Figure 2.3a), cellulose initially undergoes a transformation into an undefined reaction intermediate referred to as “active cellulose” or “intermediate liquid cellulose”. Subsequently, it decomposes into two competitive products, anhydrosugars and the other char and gas.⁹⁵ In a study by Lede,⁹² the formation and characteristics of this intermediate active cellulose were discussed. It was reported that the composition of active cellulose varies depending on experimental conditions but consistently contains significant proportions of anhydrosugars. The formation of active cellulose is succeeded by competitive reactions, including glycosidic bond cleavage (depolymerization) and fragmentation reactions. Shafizadeh and Fu⁹⁸ similarly proposed a theoretical reaction pathway in which cellulose degradation occurs through the rivalrous actions of glycosidic bond cleavage, dehydration, and the breakdown of sugar compounds.

The Diebold global reaction model (Figure 2.3b) posited a non-reversible first-order reaction. According to this model, primary and active cellulose undergo dehydration and chain cleavage, producing char, water, and carbon oxides. Additionally, the vaporization of active cellulose initiates the formation of primary vapors. These primary vapors subsequently undergo competitive reactions involving cleavage, dehydration, decarboxylation, and decarbonylation.

These reactions yield secondary gases like CO, H₂, CO₂, CH₄, and higher olefins. Simultaneously, secondary tars are formed, possibly as phenolic or polycyclic aromatic tars.

The Waterloo model (Figure 2.3c) describes the three competitive main reactions such as dehydration, depolymerization, and fragmentation, which occur simultaneously. The fragmentation reaction yields hydroxyacetaldehyde, along with other carbonyls, acids, and alcohols. The depolymerization reaction primarily produces levoglucosan and some anhydrosugars, while the dehydration reaction forms char, gases, and water.⁹⁹

However, lumped models that categorize products into three or four phases (gases, tar, char, and active cellulose) fail to provide a comprehensive understanding of the intricate decomposition pathways and resulting chemical speciation. Consequently, they offer a limited perspective on pyrolysis.¹³ Therefore, more kinetic models of cellulose pyrolysis have emerged.

Lin et al.³⁹ proposed a kinetic model (Figure 2.4), which is based on the TGA and Py-GC-MS analyses of cellulose. According to this model, cellulose initially decomposes to active cellulose, and this process is reversible. Active cellulose further decomposes into anhydro-oligosaccharides and subsequently undergoes depolymerization to yield levoglucosan. The model suggests that levoglucosan can repolymerize to form larger oligomers or undergo dehydration and isomerization, resulting in its transformation into different sugar forms. These monosugars further undergo processes such as dehydration and fragmentation, resulting in the formation of furans and various lightweight oxygenated compounds, respectively. These products, together with the anhydro-monosugars, have the capacity to undergo repolymerization, ultimately leading to the formation of char and light gases. The CO and CO₂ gases are formed by decarbonylation and decarboxylation reactions. CO is the main gas generated from cellulose at high temperatures (above 550 °C), while CO₂ is mainly derived from hemicellulose.

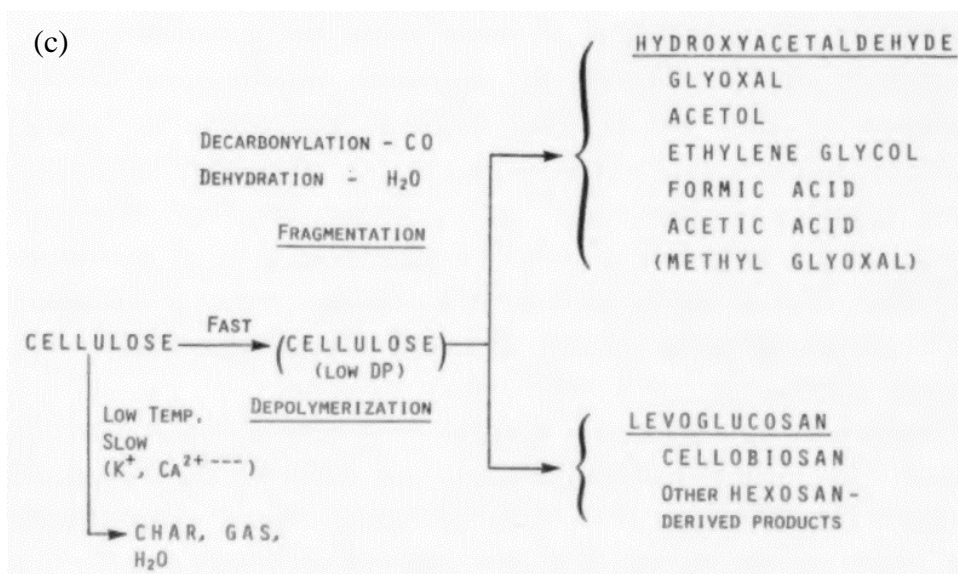
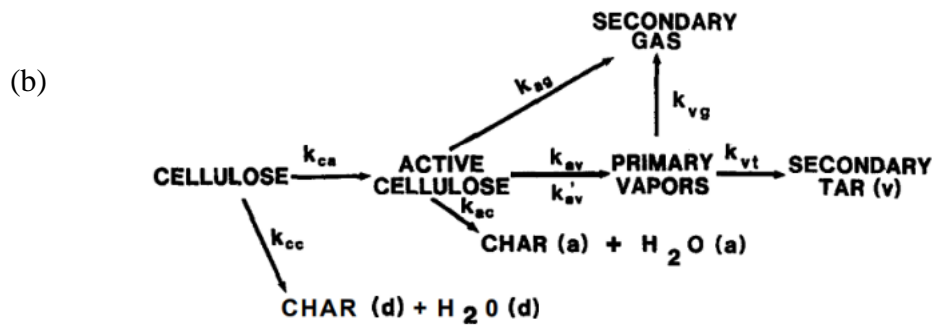
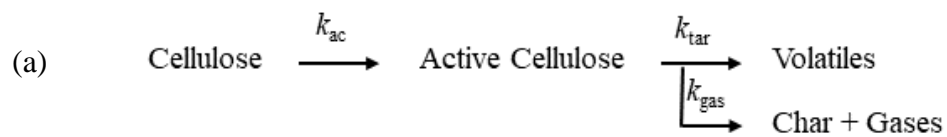


Figure 2.3: Lumped models of cellulose decomposition: (a) B-S model,⁹⁵ (b) Diebold model,⁹⁶ (c) Waterloo model.⁹⁷

Vinu and Broadbelt¹⁰⁰ introduced a predictive mechanistic kinetic model of cellulose pyrolysis (Figure 2.5), built on experimental works using a micropyrolyzer system. This model offers a detailed mechanistic description of pyrolysis product formation and has demonstrated a good match with experimental results, particularly for primary products, such as levoglucosan, 5-HMF, 2-furfural, formic acid, glycolaldehyde, and char.

Later, the Washington State Model introduced a hybridized model, which incorporated four main reactions: (1) depolymerization, (2) fragmentation, (3) dehydration, and (4) polycondensation.

Figure 2.6 shows the major volatile products from cellulose pyrolysis, which emerge from the diverse reactions occurring throughout the process.¹⁰¹ These include anhydrosugars and their derivatives, produced via transglycosylation or the concerted mechanism of breaking the glycosidic bond, furans generated through dehydration, and smaller oxygenated fragments originating from the fragmentation reaction.

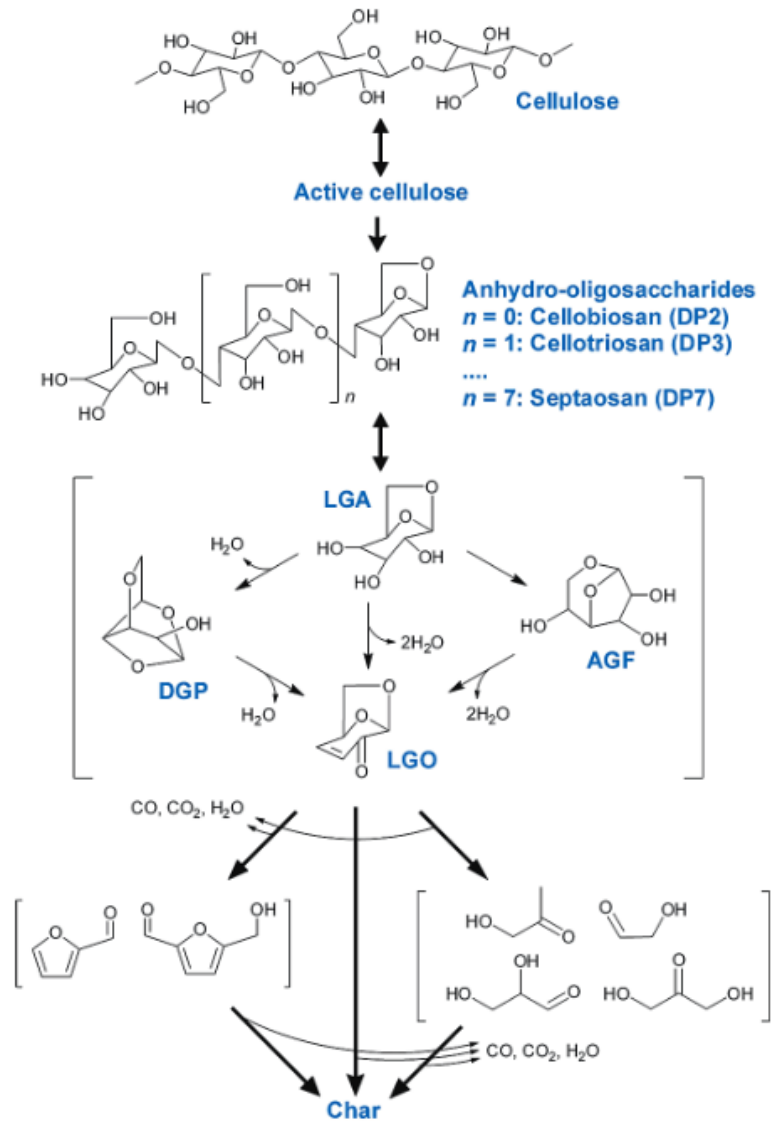


Figure 2.4: Kinetic model of cellulose decomposition by Lin et al.³⁹

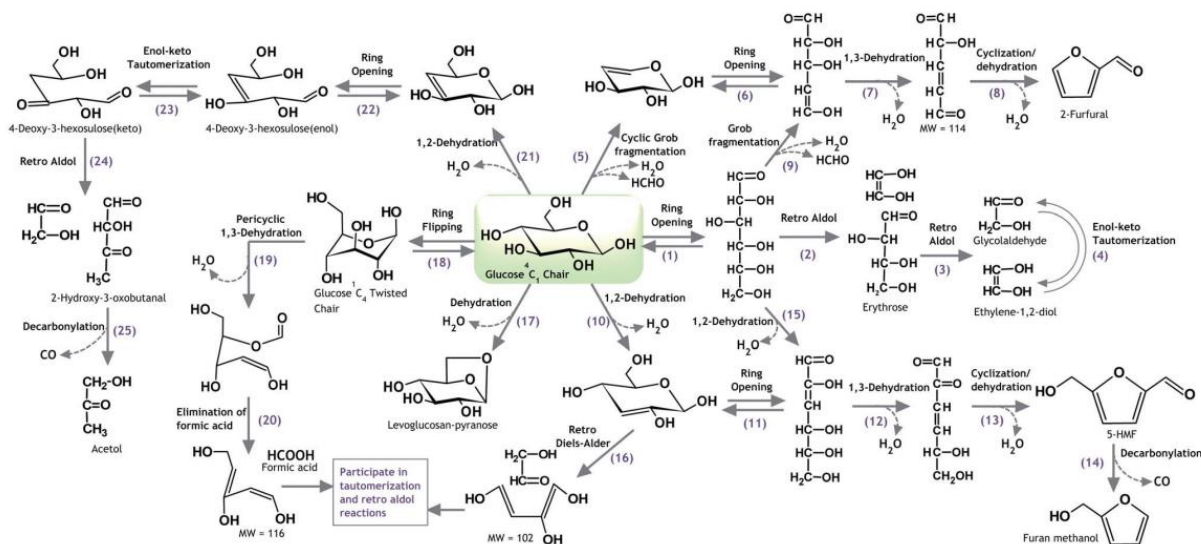


Figure 2.5: Mechanistic kinetic model of various C1 to C6 compounds from glucose by Vinu and Broadbelt¹⁰⁰

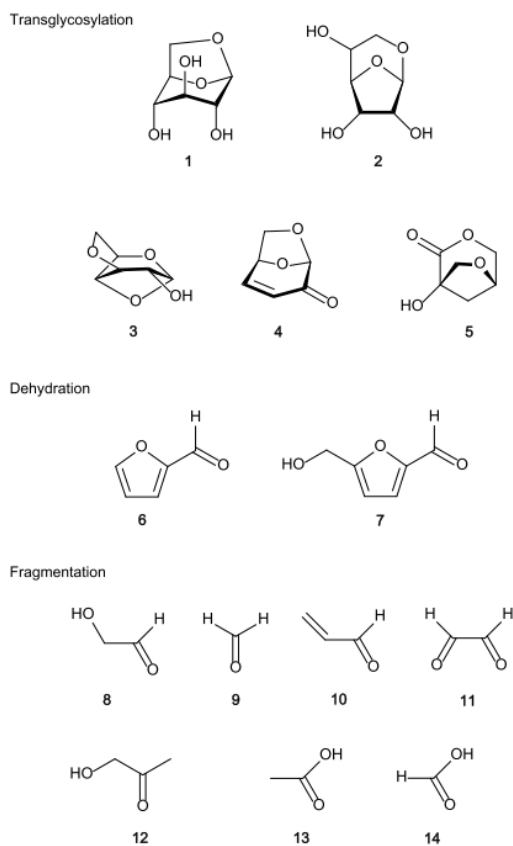


Figure 2.6: Major volatile products of cellulose pyrolysis. Reproduced from ref. 101

The main reactions during fast pyrolysis are further discussed as follows. Both experimental and modeling studies were reviewed. Several review papers have been done but no detailed discussions on the reaction mechanisms.

Depolymerization Reaction

Depolymerization is a chemical reaction characterized by the breakdown of glycosidic bonds between polymer units. This process leads to the formation of low DP anhydrocellulose, often called 'active cellulose.' This process generates two new chain ends that require stabilization.¹⁰² As depolymerization advances, it gradually reduces the degree of polymerization of cellulose chains, ultimately causing the molecules to become volatile. A comprehensive review by Molton¹⁰³ summarized that cellulose with a high DP degrades to a lower DP, reaching a constant DP of around 300, even after prolonged heating periods. This observation indicates cellulose undergoes depolymerization without experiencing significant weight loss until it reaches a stable plateau, typically at a DP of approximately 300. The initiation of cellulose depolymerization occurs at moderate temperatures ranging from 100 to 150 °C.³⁹ At higher temperatures, between 300 to 500 °C, depolymerization proceeds rapidly, forming anhydrosugar units.⁹⁵ These anhydrosugars, which have relatively lower molecular units, continue to complete chain breaks until they reach the sugar level. A noteworthy consequence of depolymerization is the significant abundance of levoglucosan.^{39,41,55} Additionally, this process generates furan compounds, including 5-HMF and furfural.¹⁰²

Zhang et al.¹⁹ employed DFT to study several pathways of cellulose depolymerization and fragmentation reactions. The chemical pathway in the presence of H⁺ cation (Figure 2.7a), especially with acid pretreatment, gave the lowest energy barrier. Another mechanism known as the concerted mechanism or transglycosylation, was reported by several authors^{84,104,105,106,107} as

the dominant and optimal pathway for the generation of levoglucosan over homolytic and heterolytic pathways. The concerted mechanism is explained by the transfer of the H atom from the C6-OH hydroxyl group to the glycosidic bond, resulting in the cooperative cleavage of the glycosidic bond. Figure 2.7b illustrates the concerted mechanism of cellulose depolymerization, ultimately yielding anhydrosugars and, eventually, levoglucosan. The long chain of cellulose is first depolymerized into levoglucosan end and nonreducing end, then broken down into smaller oligomers and levoglucosan.

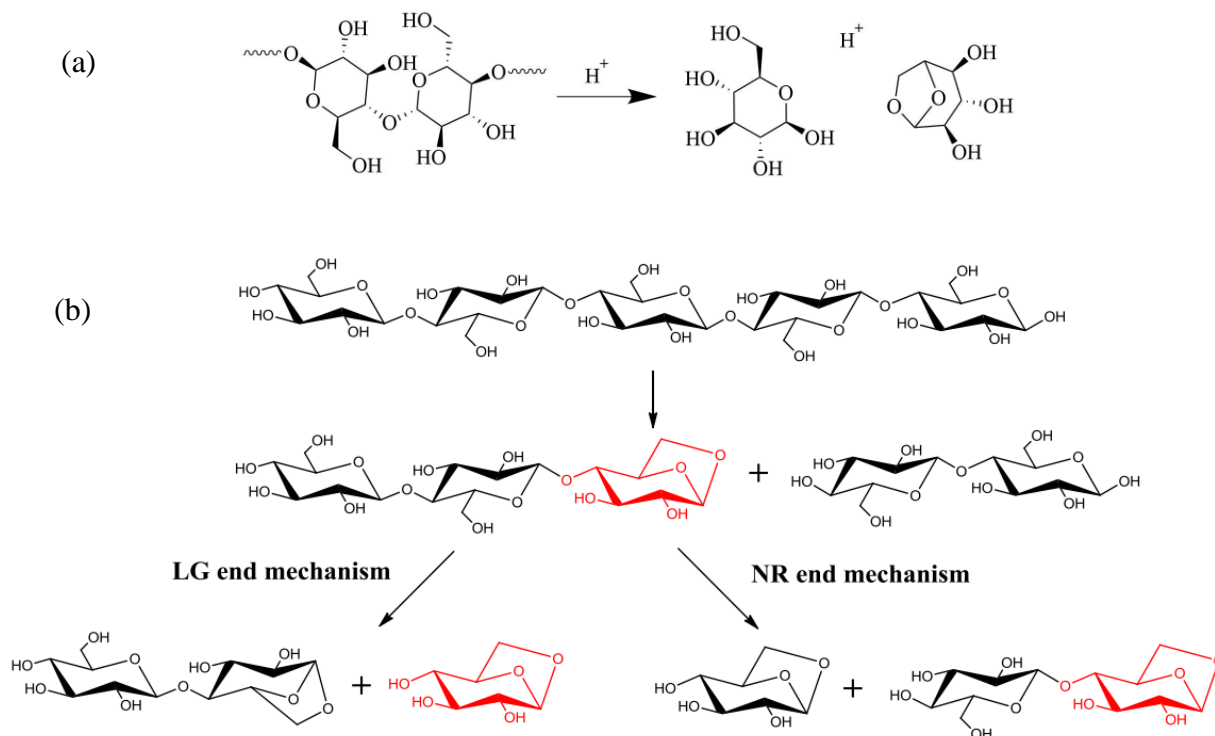


Figure 2.7: Mechanism of cellulose depolymerization: (a) LG formation with H^+ cation;¹⁹
 (b) concerted mechanism of anhydrosugars formation.⁴⁰

Hosoya et al.¹⁰⁸ further explored the formation of levoglucosan using various cellulose models, including dimer models and oligomeric models with one, two, and three chains. Their

investigation delved into the utilization of the two- and three-chain models to account for interchain hydrogen bonds (Figure 8a and b). In their findings, the dimer model notably adhered to the concerted mechanism. However, the one-chain model failed to demonstrate the formation of levoglucosan due to certain disparities, such as an activation enthalpy of 38 kcal mol^{-1} , which fell below the experimental range of 40 to 60 kcal mol^{-1} . The two-chain model effectively resolved this issue and shed light on the formation of levoglucosan precursor at the chain end. Subsequently, the production of levoglucosan selectively favors the levoglucosan-end. The three-chain model (Figure 2.8c) displayed a propensity for levoglucosan degradation occurring predominantly on the crystalline surface. This finding was reported to be consistent with experimental observations.¹⁰⁹ Initially, the LG-end forms at the crystal surface (Reaction A) through the depolymerization reaction, followed sequentially by the generation of LGs (Reaction C). The presence of high crystallinity, with interchain hydrogen bonds, promotes the formation of LG.

Dehydration Reaction

Dehydration reaction is the removal of water during pyrolysis due to heat application. It is reported as the main reaction happening during fast pyrolysis due to the massive amount of hydroxyl groups in cellulose. Scheirs et al.¹¹⁰ studied the mechanisms of water evolution during cellulose pyrolysis. Their findings demonstrated that about 10% of the total water evolved is physically desorbed at temperatures near $110 \text{ }^{\circ}\text{C}$, with the remaining 90% being released at a higher temperature, roughly $300 \text{ }^{\circ}\text{C}$. According to Chaiwat,⁷⁹ water primarily arises from the OH functional groups of the cellulose structure during pyrolysis at temperatures between 300 and

360 °C. Tang and Bacon¹¹¹ reported that dehydration reactions majorly occur in the temperature range of 200 to 280 °C. This is supported in other works^{112,113} where a significant amount of

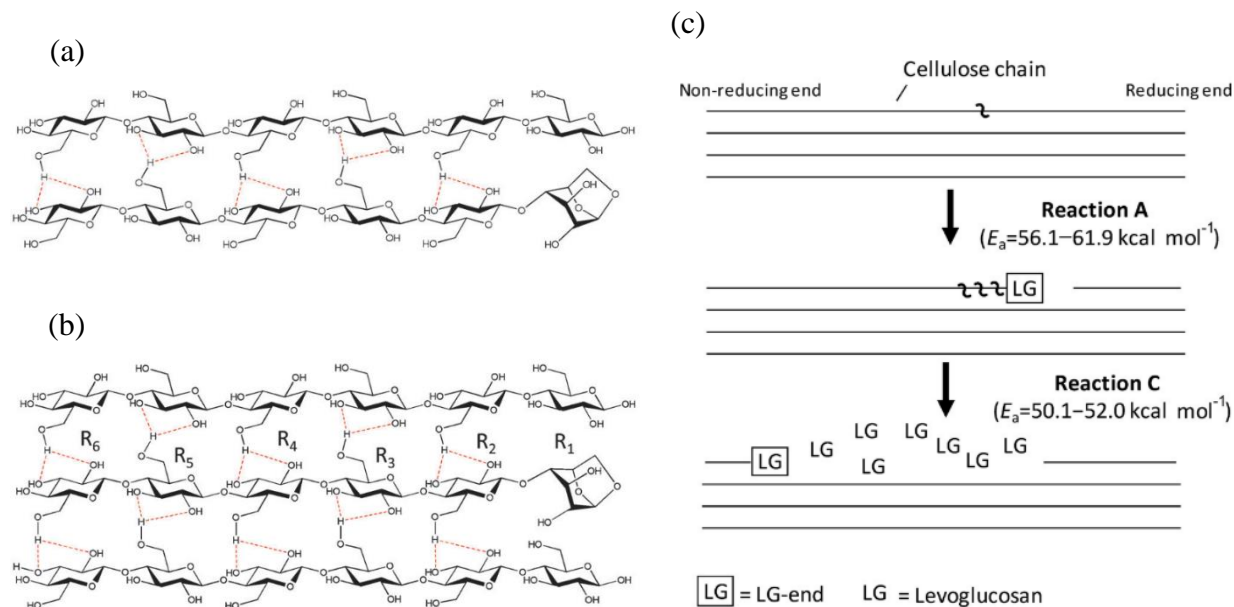


Figure 2.8: Two-chain (a) and three-chain (b) LG-end models of cellulose; and reaction model of LG formation from crystalline cellulose chains (c). Reproduced from ref. 108.

water was observed in this temperature range. Dehydration increased with low temperature and slow heating rate leading to the formation of char.

Several dehydration mechanisms were reported in the literature but dominated by the Maccoll elimination mechanism (or *1-2* dehydration). In this mechanism, a C-O bond is broken with a concerted proton loss from a beta position moving to the oxygen atom to form a double bond and eliminate water¹¹⁴. The *1-3* dehydration mechanism¹¹⁵ was also investigated; this is similar to *1-2* dehydration except that the proton is lost from a gamma carbon. Easton et al.¹¹⁴ theoretically investigated several pathways where dehydration can proceed from a cellulose unit.

These include the Maccoll elimination, Pinacol ring contraction, cyclic Grob fragmentation and the generalized retro aldol rearrangement mechanism, shown in Figure 2.9. The researchers computationally studied the four water loss mechanisms using glucose and cellobiose as model compounds during cellulose fast pyrolysis.¹¹⁴ Their results showed that the aldol condensation mechanism gave the lowest calculated free-energy barrier ($50.4 \text{ kcal mol}^{-1}$) for glucose dehydration. A similar trend was obtained for the cellobiose model compound. These results indicated that the reaction is applicable to other gluco-oligosaccharides with higher degree of polymerization. Zhang et al.¹¹⁶ studied cellulose dehydration using cellotriose as a model compound. They assessed three mechanisms: 1,2-dehydration, pinacol ring contraction, and cyclic grob fragmentation. Additionally, they examined different OH positions at -O2H, -O3H, and -O6H of the internal unit. Their findings reaffirmed the critical role of hydroxyl group position, with -O2H emerging as the most reactive, and pinacol ring contraction as the most favorable pathway.

Dehydration reaction is believed to be responsible for the formation of the molecular pool of oligomeric molecules.^{114,117} This outcome is evidenced in a study⁶⁴ of the functional groups in the volatile and the oligomeric fractions of pyrolysis oils, shown in the van Krevelen plot (Figure 2.10) derived from an FT-ICR MS analysis. This plot of the nonvolatile fraction shows for the first time the existence of heavy unknown water-soluble oligomers accounting for 30-55 wt.%.⁶⁴ These are produced by the gradual dehydration of the cellulose primary depolymerization products. Because these oligomeric fractions remain poorly understood,^{6,64} Terrell and Garcia-Perez⁶⁵ conducted a study to match experimentally detected bio-oil oligomers with hypothetical pathways for their formation during pyrolysis. They coupled results from high-resolution Fourier transform ion cyclotron resonance mass spectrometry (FT-ICR MS) with combinatoric

dehydration and fragmentation modeling and came up with pathway structures of the oligomeric sugars. Later, a DFT was employed to study the sequential dehydration (up to 3x) reactions and propose structures of the oligomeric sugars.¹¹⁸ All potential permutations from where water can be desorbed were evaluated. Results showed that water molecules are most favorably desorbed from the non-reducing end of the oligomers (Figure 2.11).

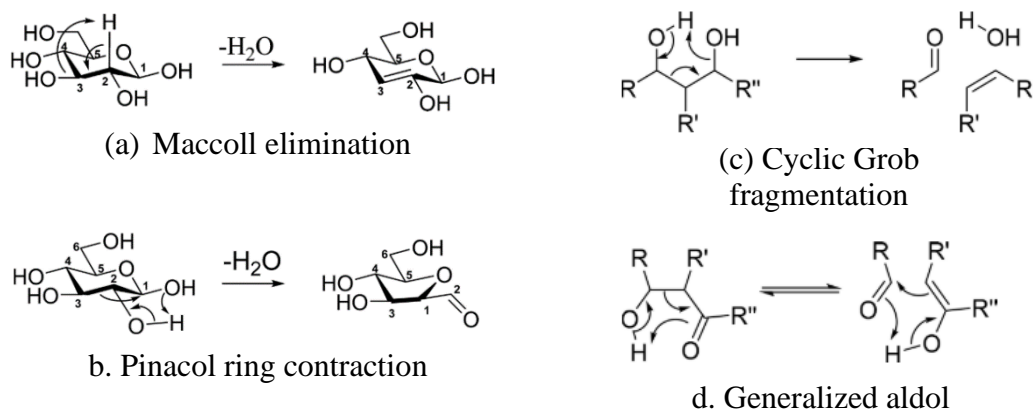


Figure 2.9: Water loss mechanisms from fast pyrolysis of cellulose¹¹⁴

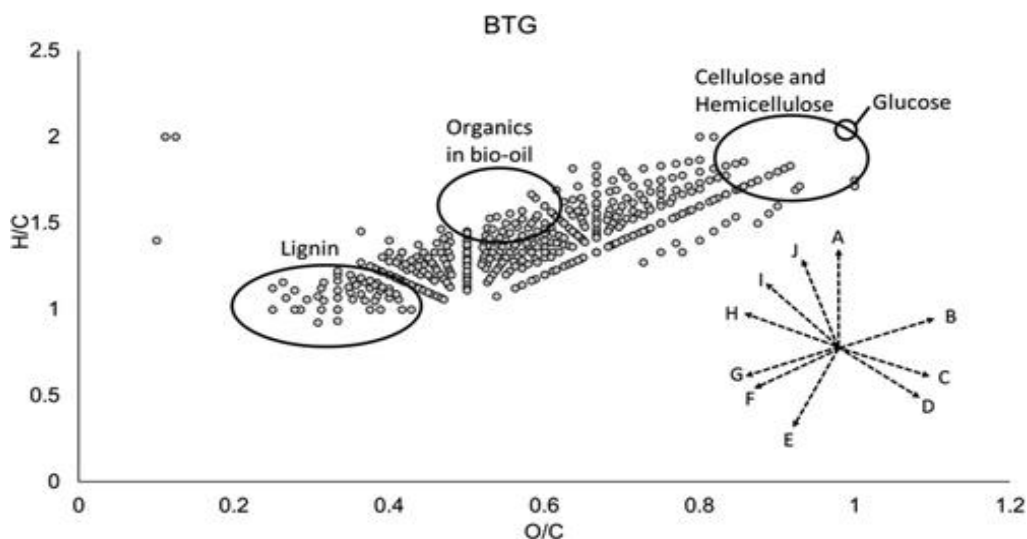


Figure 2.10: van Krevelen plot of the nonvolatile fraction of the BTG bio-oil. Distinctive line patterns can be associated with specific reactions: (A) removal of Levoglucosan, (B) removal of Furan, (C) removal of acetol, (D) removal of methane, (E) demethoxylation, dehydration (F) dehydration, (G) removal of glycoaldehyde, (H) deraboxylation, and (J) decarbonylation.⁶⁵

In a study that employed DFT to study the 1,2-dehydration of alcohols as a model for water loss during carbohydrate pyrolysis, Nimlos et al.¹¹⁹ calculated an energy barrier of 67 kcal/mol for the alcohols, a finding consistent with the experimental data. A separate study¹¹⁵ found that 1,2-dehydration of neutral glycerol displays a higher barrier than the barrier for pericyclic 1,3-dehydration, which is 65.2 kcal mol⁻¹. Zhang et al.¹²⁰ studied three levoglucosan dehydration mechanisms, including the free-radical mechanism, glucose intermediate mechanism, and levoglucosan chain-end mechanism, and found that the latter is the most favorable pathway due to its lowest barrier energy and better fit with experimental results. One more study¹²¹ modeled the mechanism of levoglucosan thermal decomposition during pyrolysis employing 1,2-dehydration and found that the removal of hydroxyl group from C2 and a hydrogen atom from C3 is the most favorable pathway, consistent with our previous work.¹¹⁸

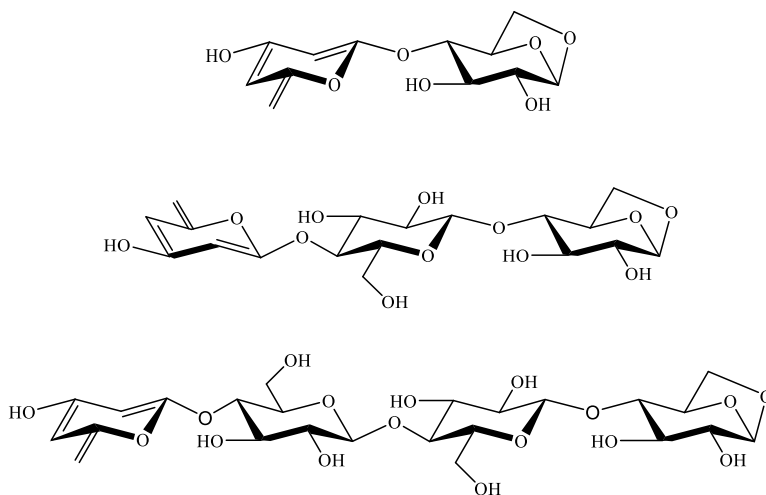


Figure 2.11: Proposed structures of highly dehydrated cellulose oligomers from sequential Maccoll elimination method (up to 3x dehydration).¹¹⁸

Fragmentation Reaction

Fragmentation means the breaking of covalent bonds in monomer units to form mostly C1 to C4 molecules and gases. The main products of fragmentation reaction include hydroxyacetaldehyde (HAA), hydroxyacetone (HA), formic acid, etc. Hydroxyacetone (1.0 to 13.7 wt.% yield) and hydroxyacetaldehyde (2.6 to 8.6 wt. % yield) are well-known and among the most abundant single compounds found in pyrolysis oils.^{6,74,122} Several works have been done to investigate the formation of these products during the biomass pyrolysis in the presence of alkaline compounds and mineral salts. While hydroxyacetaldehyde yield decreases dramatically in the presence of KOH even in small amounts, the yield of hydroxyacetone was not affected. The authors concluded that the action of KOH changes even with compounds of the same class. When using a Lewis acid such as ZnCl₂, the yields of both hydroxyacetone and hydroxyacetaldehyde decrease very fast because Lewis acids acted as a dehydrating and cross-linking agent promoting char and water formation.¹²³ In the presence of Ca (OH)₂, however, the yield of hydroxyacetone and hydroxyacetaldehyde increased very fast because mineral salts and higher temperature accelerated the formation of low molecular mass compounds compared to anhydrosugars.¹²⁴ The yields of hydroxyacetaldehyde and hydroxyacetone reach maximum yields in the presence of NaCl and KCl. Much lower impact was observed when MgCl₂ and CaCl₂ were used.¹²⁴ Further, Radelin et al.⁵⁹ studied the effect of temperature on the yield of hydroxyacetaldehyde and found that the maximum yield is achieved at 600 °C. Higher temperatures resulted in a dramatic reduction in yield.

Some modeling studies^{2,125,126} investigated the formation of hydroxyacetaldehyde and hydroxyacetone compounds but only from the glucose monomers. It was shown that these products are mostly generated from the C₁-C₂-C₃ and C₄-C₅-C₆ segments of the monomer.

Richards⁵⁷ also proposed a very preliminary mechanism to explain cellulose fragmentation. The van Krevelen plot presented in Figure 2.10 shows the different reactions occurring during pyrolysis including the removal of hydroxyacetaldehyde and hydroxyacetone. These reactions were theoretically studied by Terrell and Garcia to directly fragment these compounds from sugar oligomers. Later, the first principles calculation was applied to propose reaction mechanisms of how hydroxyacetaldehyde and hydroxyacetone compounds are fragmented from oligomeric sugars¹²⁷ (Figure 2.12). Di- up to tetra- states of the sugar oligomers were evaluated and results showed that HAA and HA are most favorably fragmented from the nonreducing end of sugar oligomers.

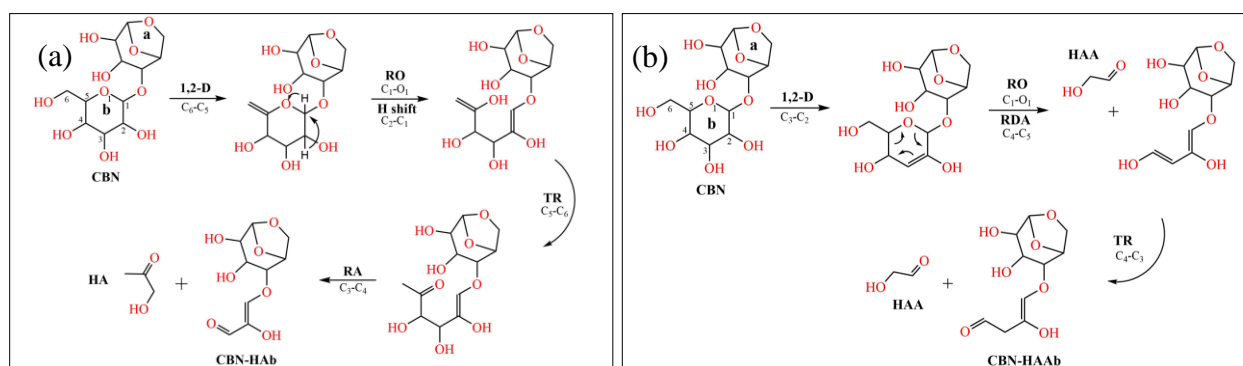


Figure 2.12: Reaction mechanisms of HA (a) and HAA (b) formation from sugar oligomers. Reproduced from ref. 127.

Polymerization and Cross-Linking

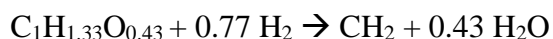
Polymerization is a reaction where small molecules are bonded together to create polymers. Lin et al.³⁹ proposed that the formations of active cellulose and levoglucosan are reversible reactions. Cross-linking reaction forms bonds between polymers or molecules to yield a bigger compound. After dehydration, cellulose is prone to crosslinking reactions, ultimately forming char. In one study,⁷⁹ cellulose pyrolysis at different heating rates was conducted to

investigate the cross-linking reaction. Results from FTIR and XRD analyses showed that water from dehydration and cross-linked precursors simultaneously occurred with the glycosidic reaction to form tar during pyrolysis. The study also reported that cross-linking at low heating rate may occur until approximately 360 °C and the cross-linked tars are released above this temperature. Chaiwat et al.⁷⁹ used a filter paper cellulose powder to study cross-linking reactions during pyrolysis. TGA results showed that the onset temperature exhibited a gradual shift towards lower temperatures, transitioning from 350 °C to 300 °C as the heating rate was reduced from 323 to 278 °C min⁻¹ (50 to 5 K min⁻¹). This means that lower heating rate requires more reaction time to decompose cellulose and therefore heightened dehydration reaction leading to the formation of water and cross-linked precursors. FTIR and XRD patterns confirmed that cross-linking and dehydration reactions occur simultaneously with glycosidic bond cleavage to form tar.

2.3. Review of Bio-Oil Catalytic Hydrotreatment Reactions

The high amounts of oxygenated compounds and oligomeric fractions found in bio-oil constitute a prominent challenge in utilizing bio-oils^{18,40}; hence, these oils must be chemically modified or upgraded to overcome these issues through oxygen removal and cracking. Typically, there are two methods used for bio-oil upgrading: zeolite cracking and hydrotreatment.^{18,128} Zeolite cracking involves the removal of oxygen gas in the form of CO₂ and H₂O under atmospheric pressure and elevated temperature (300-600 °C) in the presence of acidic zeolites. Hydrotreatment is done under high pressure and moderate temperature in the presence of an active catalyst to remove oxygen. After upgrading, the final product is usually evaluated based on its O/C and H/C ratio; lower O/C and higher H/C points to a liquid product of good quality.⁴²

Because of the complexity of real bio-oil, model compounds have been used instead to simplify reactants and focus on research interest.¹²⁹ Despite this, there is a big gap between model compounds and the real bio-oil due to actual properties and the interaction of these compounds were not accounted.¹³⁰ However, it may not give actual results, but it is a step-forward to understand reaction mechanisms and kinetics. The general equation of hydrodeoxygenation is depicted by the following conceptual reaction:⁵²



2.3.1 Processing Conditions

In their review paper, Zhang et al.¹³¹ tackled the processing conditions of HDO, including effects of temperature, pressure, H-donor solvents, and residence time. Briefly, higher temperatures lead to coke formation. High H₂ pressure favors hydrogenation reactions but poses expensive operation and safety concerns. Further, the use of H-donor solvents, such as methanol, butanol, ethanol, isopropanol, and tetralin, to stabilize the highly reactive bio-oil compounds and reduce polymerization reactions. Lastly, the interaction time between the feedstocks and catalysts could also affect HDO efficiency. Shorter residence time resulted in low HDO efficiency.

2.3.2 Selection of Catalysts

Catalysts are substances that speed up the rate of reactions by lowering the activation energy without altering results and remain unchanged after the reaction. An HDO catalyst should primarily consider price and performance (high activity, selectivity, and stability).^{132,133,134} An ideal catalyst should withstand/tolerate coke formation, poisoning, high water content of feed, and easy regeneration without losing too much activity.^{24,133}

Sulfidation is one method that increases the activity of catalysts. In this process, the catalyst is activated by reacting it with sulfiding agents (e.g., H₂S, DMDS) to convert the catalyst metal oxides to metal sulfides under low H₂ pressure and temperature conditions. During this stage, the formation of S-bridge or S-vacancy possibly occurs and becomes a favorable site for the adsorption of reactants (hydrogen atom and bio-oil compounds). It is reported that sulfided catalysts have higher activity over their reduced (oxide) form because of the difference in their structures. This is attributed to the significantly lower bond strength of SH groups which is 25 kcal mol⁻¹ weaker than OH groups.¹³⁵ A study on the co-hydrotreatment of bio-oil lignin fraction and vegetable oil using unsulfided CoMo/ γ -Al₂O₃ yielded remarkably high coke between 25 to 50 wt. % of the lignin fraction.¹³⁶

Conventional catalysts like CoMo and NiMo supported on alumina are extensively used for HDO.^{24,137,138,139} Metal-based catalysts such as Ru Pd, Pt were also reported^{52,140,141} to have high activity during HDO, however they are expensive. Cheah et al.¹⁴² studied the effect of transition metals such as Ni, Zn, Co, and Fe as MoS₂ promoters in the HDO of propylguaiaicol in a batch reactor and showed that Ni promoter has the highest yield of deoxygenated cycloalkanes. Similarly, Olivas et al.¹⁴³ investigated the promoter effect of Ni, Co, and Fe in the HDO of furfurlamine and dibenzothiophene and result showed that the Ni-promoted MoS₂ has the highest activity. Set et al.¹⁴⁴ studied the hydrotreatment of the carbohydrate-rich fraction using mono- and bimetallic Ni based catalysts and revealed that NiMo/SiO₂-Al₂O₃ was a very promising catalyst for the first mild hydrotreatment step of bio-oil to stabilize the products before the second deep hydrotreatment step. The review of Cordero-Lanzac et al.¹⁴⁵ specified that noble metals (Pt, Pd, Ru, Rh) have higher HDO activity over transition metals (Ni, Mo, Co, Fe, etc). However, they are expensive and thus hamper their use in commercial applications.

Different catalysts yield various products depending on the interaction between the catalyst and the feed. Results¹⁴⁶ on the hydrodeoxygenation of furfural using supported Cu, Pd and Ni catalysts yield several products. Furfural reaction over Cu mainly yielded furfural alcohol and lesser amounts of 2-methyl furan; Pd produced furan by means of decarbonylation reaction and few amounts of tetrahydrofuran and tetrahydrofurfuryl alcohol; Ni predominantly produced furan with few amounts of furfural alcohol, 2-methyl furan and interestingly, butanal, butanol and butane. Ru was evaluated using model compounds at elevated temperatures and resulted in excessive gas yield, especially methane.¹⁴⁷

2.3.3 Reaction Mechanisms of Cellulose and Catalyst during Hydrotreatment

Hydrotreatment is a well-established process used in the petroleum refinery and being adopted for crude oil upgrading. The major reactions involved during bio-oil upgrading by means of catalytic hydrotreatment include hydrogenation, hydrodeoxygenation, dehydration, polymerization, and coke formation. Elliot et al.¹⁴⁸ provided a concrete overview of the developments in bio-oil hydroprocessing prior to 2007. The recent reviews for the last 5 years regarding bio-oil hydrotreatment reactions are summarized in Table 2.1.

Table 2.1. Reviews on the hydrotreatment of bio-oil for the last 5 years

Year	Authors	Focus of the review	Ref.
2019	Han et al.	Research progress in bio-oil characterizations and heterogenous catalysis	149
2020	Hansen et al.	Critical challenges in bio-oil upgrading and potential research directions	150
2021	Zhang et al.	Progress in understanding reaction behaviors of bio-oil heavy organics	151
2021	Cordero-Lanzac et al.	HDO mechanisms and activated carbon-supported catalysts	130

2021	Pujro et al.	Reaction mechanisms in bio-oil upgrading	152
2021	Gea et al.	Experimental parameters to upgrade bio-oil	153
2021	Qu et al.	Model compounds and their basic reaction pathways, catalysts, and equipment for bio-oil HDO	139
2023	Gholizadeh et al.	Features of biofuels from bio-oil Hydrotreatment issues	154
2023	Yang et al.	Description of the main HDO processes and various catalytic systems	129

The multifaceted composition of bio-oil gives rise to diverse reaction pathways of hydrogenation and oxygen removal during hydrotreatment, some of which are shown in Figure 2.13. Elliot et al.¹⁴⁸ developed a reactivity scale of the oxygenated compounds found in bio-oil based on experimental results and information from literature. This reactivity scale is visualized in Figure 2.14. The scale reveals that olefins and alcohols are easily treated with hydrogen at temperatures up to 200 °C, while furanic compounds pose the greatest challenge to treat. Nolte et al.¹⁵⁵ studied the hydrodeoxygenation of cellulose model compounds over Mo oxide and low-pressure hydrogen and reported the reactivity of cellulose functional groups towards deoxygenation as follows: C-OH > C=O > C-O-C.

Hydrogenation

Hydrogenation is among the important processes during hydrotreatment, where high pressure hydrogen is introduced into the bio-oil compounds to saturate the highly reactive hydrogen-deficient functional groups. Gaseous hydrogen is aspirated from the reactor headspace to the liquid phase through bubbles.¹⁵⁶ Batch type reactors are equipped with a stirrer to increase gas-liquid mass transfer. Subsequently, the bio-oil compounds and hydrogen chemisorb onto the catalyst surface. The adsorption of bio-oil compounds proceeds on the active sites of the catalyst while the molecular hydrogen dissociatively binds to the metal surface of the catalyst. For example in a Ni-promoted MoS₂ catalyst with S-bridge (defect formed during the sulfidation process), the hydrogen chemisorbs onto the adjacent Ni (hydridic species) and S-bridge (protonic species).^{156,157,158} The dissociative adsorption of hydrogen on the catalyst surface and hydrogenation is modeled in Figure 2.15a and b, respectively, with hydroxyacetone as bio-oil model compound. In this particular example, the carbon of the aldehyde group is hydrogenated by the hydrogen atom from the Ni. Subsequently, the acidic hydrogen from the sulphhydryl group is attracted to the oxygen atom converting the aldehyde group to an alcohol group. The O or C=C groups of the bio-oil structures are adsorbed on the metal surface (active site), activating it toward hydrogen attack.¹⁴⁹ Hydrogenation of aldehyde and ketones proves more facile than that of acids, while oligomeric compounds present a significant hydrogenation challenge. The same oligomeric compounds contribute to polymerization reactions then subsequently coke formation. Oligomers have poor adsorption characteristics, potentially attributable to steric hindrances, resulting to diminished low hydrogenation rates. Furthermore, hydrogenation competes with cross linking and polymerization reactions. Increasing the hydrogenation operating pressure could potentially reduce coking issues, yet it introduces safety concerns and increased expenses.

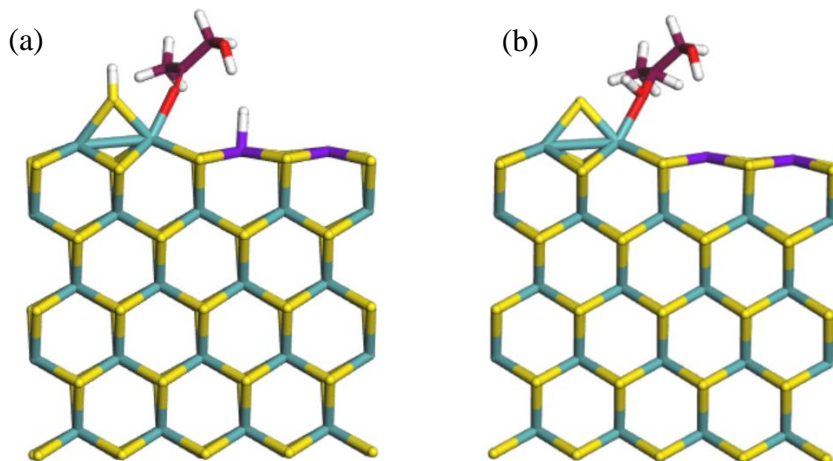


Figure 2.15: Co-adsorbed hydroxyacetone and hydrogen on NiMo catalyst (a) and hydrogenated hydroxyacetone (b) (Color legend: violet sticks: nickel, green sticks: molybdenum, yellow sticks: sulfur, red sticks: oxygen, maroon sticks: carbon, and white sticks: hydrogen).

A study¹⁵⁹ employed low temperature hydrogenation (LTH) of the aqueous phase fraction of bio-oil over Ru/C catalyst. This reaction mainly yielded diols and sorbitol, but undesired methane and light gases were also obtained. Another study¹⁶⁰ on the two-stage continuous hydrogenation of bio-oil aqueous phase using Ru/C and Pt/C catalysts showed that stabilization at lower temperature is necessary to saturate carbonyl groups to alcohols and thus mitigated coke formation. The main products of LTH are ethylene and propylene glycols and sorbitol with small amounts of acetic acid, levoglucosan, furanone, phenol and phenol substitutes. At higher temperature hydrogenation (HTH), sorbitol was hydrogenated to mono-alcohols and diols by hydrogenolysis and secondary hydrogenation reactions. The general chemistry of hydrogenation reaction showed four main pathways: (1) the hydrogenation of carbonyl groups at low temperature resulting to alcohols, (2) hydrolysis of levoglucosan C-O-C bonds to glucose in the presence of acid sites (C-O-C) cleavage, (3) hydrogenolysis of polyols with C-C bond cleavage, and (4) secondary hydrogenation reactions in the presence of metals. Hydrogenation improves

bio-oil stability through the conversion of acids, aldehydes, alcohols, and unsaturated compounds into their more.

Hydrogen should then be renewable and sustainable. It can be sourced from refineries, biomass gasification, steam reforming of bio-oil fractions or biomass, and water electrolysis.¹⁶¹ Production should also be feasible. The complete removal of oxygen during the process corresponds to high hydrogen consumption.⁶² Hydrogen consumption increases with high temperature and reaction time. In batch reactors, hydrogen consumption ranges from 100 to 300 NL kg⁻¹ of bio-oil while continuous type reactors consume about 600 NL kg⁻¹ bio-oil.¹⁶²

Hydrogenolysis

Hydrogenolysis is a catalytic reaction where C-C and C-O bonds are directly cleaved via interaction with a hydrogen atom.¹⁶³ It was reported that this reaction is typical for noble metals; the first studies were made on nickel catalysts.¹⁶⁴ Hydrogenolysis occurs when the newly formed bond between the bio-oil structure and the metal catalyst is stronger than the C-O or C-C bonds within the bio-oil structures.

To illustrate this reaction, using Figure 2.15b, the direct rupture of the middle C-O bond generates OH group bound to the Mo and a hydroxy-propyl (CH₃CH₂CHOH) intermediate bound to the adjacent Ni. This mechanism is explained by the S_N2 reaction when the hydrogen atom activated by the adjacent Ni metal attacks and breaks the C-O bond. A study evaluated such mechanism and resulted in a high barrier energy and therefore only considered under high temperature conditions.¹⁵⁶ Similar mechanisms have been reported for the hydrogenolysis of glycerol to propanediols.^{165,166}

Hydrodeoxygenation

Hydrodeoxygenation is the removal of oxygen (deoxygenation) in bio-oil compounds in the presence of hydrogen atoms. Bio-oil contains a remarkably high amount of oxygen ranging from 35 to 40 wt %, ¹⁶⁷ therefore, the need to expel oxygen usually in the form of water to produce a high-grade oil compatible with existing transportation fuels. Elliot et al. ^{168,169,148} developed and proposed two stages of bio-oil hydrotreatment: stabilization and deoxygenation. Stabilization is done under mild conditions with lower temperature (100-300 °C) to convert carbonyl and carboxyl groups into alcohols and thus minimizes the polymerization reaction and formation of heavy coke. ^{24, 168,170} The second stage is done at a higher temperature (350-400 °C) to achieve complete hydrodeoxygenation. The conventional catalysts (CoMo and NiMo supported on alumina) are reported to favor deoxygenation reaction. ¹⁵⁷ Senol et al. ¹⁷¹ used these catalysts, sulfided and supported on alumina, to deoxygenate methyl heptanoate, n-heptanoic acid and 1-heptanol and the NiMo catalyst showed a better performance over CoMo but consumed more hydrogen.

A separate study ¹⁷² investigated the HDO of sugars using carbohydrate model compounds such as D-glucose and D-cellobiose over Ru/C catalyst at 250 °C and 1450 psi H₂ pressure. Two parallel pathways were demonstrated; (1) thermal noncatalyzed pathway that led to the formation of solid products (char), and (2) hydrogenation pathway that yielded polyols and gases mainly methanol and ethane. The use of model compounds can contribute towards catalyst screening and design and provide initial knowledge on the reaction pathways of real bio-oil compounds. Studies from first principles calculations reported that the deoxygenation reaction over NiMo catalyst happens in the absence of the S-bridge. ^{156,157,158}

Polymerization

The polymerization reaction involves the linking of small molecular compounds like monomers to form polymers. This relates to the highly reactive nature of the oxygen-containing functionalities in bio-oil such as hydroxyl groups, carbonyl groups, acids, aldehydes/ketones, ether groups, etc.^{173,174} High temperature favors polymerization of these reactive functionalities found in bio-oil.^{175,176} Unfortunately, deoxygenation (hydrotreatment) involves heat application.¹⁷⁴

During HDO, polymerization reactions compete with hydrotreating reactions leading to the formation of unwanted product properties.^{177,178} Mercader et al.¹⁷⁷ studied these reactions using a batch type reactor and reported that the extent of polymerization reaction was decreased by choosing adequate reactor hydrotreating parameters such as stirring intensity, reaction temperature and heating time. Fast polymerization was observed above 200 °C, therefore operating conditions at low reaction temperature (stabilization) and enough hydrotreating time are favorable. The PNNL two-step hydrotreatment design; first, the low-temperature stage was especially designed to mitigate polymerization. Polymerization reactions lead to coke formation which encapsulates catalysts and plugs reactors. The second stage involves higher temperature for cracking and deoxygenation reactions to break large molecules and reject water, respectively. However, it was also reported that polymerization occurs even at mild temperatures¹⁷⁹ and even during bio-oil storage as evidenced by increase in viscosity over time.^{180,181,182,183}

Kadarwati et al.¹⁸⁴ studied the polymerization and cracking reactions in different bio-oil fractions such as whole bio-oil, heavy bio-oil (without water and light oxygenates, carbohydrate-rich), and pyrolytic lignin over Ru/C and unsulfided NiMo/Al₂O₃ catalyst. Results showed that the heavy oil exhibited polymerization reaction during both stabilization and the second step

hydrotreatment yielding the highest amount of large, heavy molecular products which were difficult to crack. Pyrolytic lignin yielded the least amount of large molecular products. It was reported that most of the coke and polymerization products came from the sugar-rich fractions. With these results, the authors further concluded that water and light oxygenates could suppress polymerization reactions. Similarly, Venderborsch et al.¹⁷⁸ reported that polymerization may have come from the polymerization of sugars to large molecules.

Another study¹⁷⁷ used model compounds (mixture of carbohydrates, light oxygenates, and aromatics) dissolved both in water and methanol solvent to investigate the polymerization reaction during bio-oil heating. Results showed that sugars, especially levoglucosan, played a vital role in polymerization because of their multiple and highly reactive oxygenated functional groups. Levoglucosan in the water medium mainly underwent hydrolysis at increased temperature and further degraded to furfural. Furfural has the highest tendency towards polymerization. Similarly, Gao et al.¹⁸⁵ used furfural and sugar monomers and oligomers as model compounds to investigate cross-polymerization reactions of major bio-oil components during hydrotreatment. The outcome of their study revealed that the reaction yielded a substantial amount of polymers, leading to notable modifications in polymer characteristics, including elemental composition, thermal stability, and morphology. Another study explored the cross-polymerization between biomass-derived phenols (specifically vanillin and guaiacol) and sugar derivatives (including furan, furfural, furfuryl alcohol), which substantiated the occurrence of cross-polymerization between sugar and lignin components. The opening of furan rings initiated this reaction hydration reactions, resulting in the cross-polymerization of these intermediates with phenolic compounds. Consequently, it led to a new compound characterized by high molecular weight and oxygen content.

Several works have reported the increased yield of heavy fractions in hydrotreated oils which is attributed to polymerization reaction. UV-fluorescence analysis has also have shown the formation of polycondensed/aromatic compounds after hydrotreatment. These compounds are believed to be precursors to coke formation.

Coke Formation

Continuous polymerization reactions lead to coke formation. Coke are carbonaceous residues produced after massive condensation/polymerization of the unstable and reactive bio-oil compounds during thermal treatment.¹³⁴ Coke formation is the primary challenge during bio-oil upgrading. Several studies^{37,64,170,186,187} have reported that sugar oligomers are responsible for repolymerization, and coke formation and these reactions may cause deactivation of catalysts and reactor plugging. The amount of coke is dependent on the feedstock properties and reaction conditions.¹⁸⁸

Kadarwati et al.²¹ studied coke formation by introducing additional levoglucosan to the bio-oil prior to hydrotreatment. Results showed that the addition of levoglucosan into bio-oil prior to hydrotreatment did not yield more coke compared to pure bio-oil under identical conditions. However, coke yield was increased in the absence of catalyst. The study of Cai et al.¹⁸⁹ on the influence of bio-oil aqueous fraction (BAF) and methanol mixing ratio confirmed the role and importance of methanol blending in the feed before hydrotreatment. That is, it acted as hydrogen donor to the bio-oil components to mitigate coke formation. This is evident when the BAF to methanol ratio is high (2:1) because the insufficient supply of hydrogen leads to accelerated deactivation of the catalyst.

Temperature dramatically affects coke formation on the catalysts. Li et al.¹⁷⁶ investigated coke deposition during bio-oil HDO over Ni/HZSM-5 catalyst in a batch reactor. Results showed

that reaction temperature is a critical factor contributing to coke formation. The authors reported three different coke species, soft, hard, and graphite-like, observed at different temperatures. Briefly, the cokes deposited in the catalyst at 250 °C are soft carbons soluble in organic solvents; the catalysts coked at 300 °C are hard cokes insoluble in organic solvents. The catalyst coked at 330 °C showed evidence of deposited graphite or amorphous graphite. FTIR analyses (Figure 2.16) showed that cokes formed at higher temperatures are mainly aromatic rings, while cokes formed at lower temperatures are mostly aliphatic. This result is evidenced in the peak strength at 1450 to 1630 cm^{-1} , corresponding to the vibration of aromatics increased with increasing temperature. Similarly, the strength of peaks at 2921 to 2963 cm^{-1} increased with increasing temperature, indicating the increased alkylation reaction as temperature increases.

Catalyst deactivation happens due to coke deposits on the catalyst surface. These carbonaceous deposits affect the physico-chemical properties of the catalyst including the decrease in surface area, pore volume, mesopore and micropore volumes. The TEM image (Figure 2.17) of a spent catalyst shows the evolution of colors from gray to black upon increased heating. Additionally, the formation of filament-like carbon is observed at 280 °C but disappeared at 330 °C. A flat plate of large carbon-rich molecules was also formed. These filamentous and carbon-rich flat plates possess incredibly low volatility and solubility and therefore slowly block the acid sites of the catalyst surface. With this, the active catalyst surface is getting low surface area and total pore volume which subsequently affects reactants to not reach the acid sites.

A separate work¹⁷⁵ investigated the effects of temperature on coke formation during bio-oil hydrotreatment over a pre-sulfided NiMo/ γ -Al₂O₃ catalyst in a continuous reactor. Result

showed that severe coke formation was observed at elevated temperature (450 °C) causing reactor plugging. UV-fluorescence analyses showed a much stronger intensity peaks of the residues left inside the reactor after hydrotreatment than the raw bio-oil. This indicates the formation of heavy polyaromatic and conjugated compounds after the hydrotreatment.

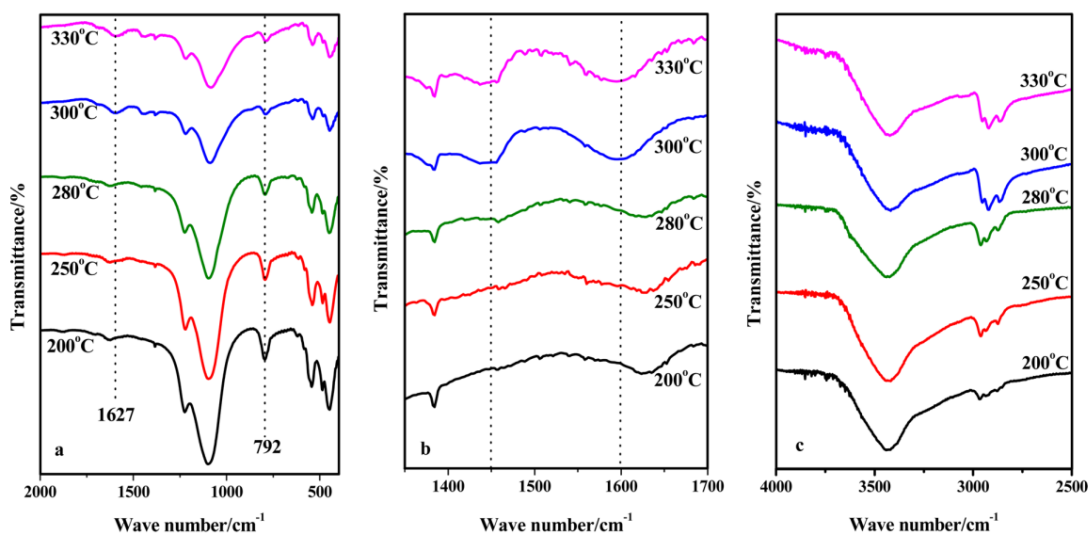


Figure 2.16: FTIR spectra of a spent catalyst at different reaction temperatures. Reproduced from ref. 176.

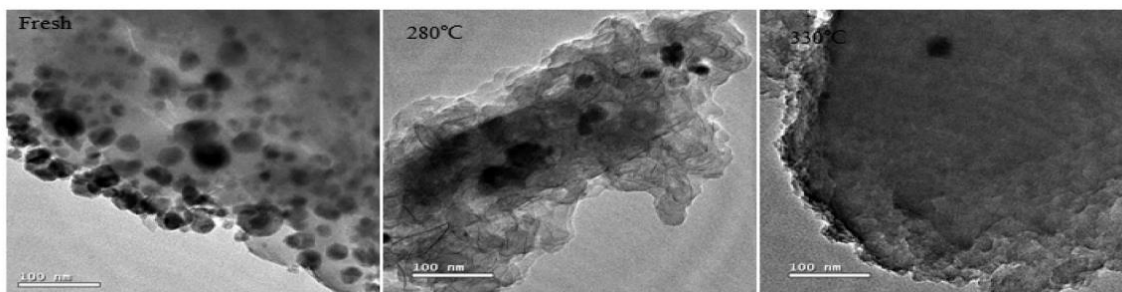


Figure 2.17: TEM image of a spent catalyst at different reaction temperatures. Reproduced from ref. 176.

Kadarwati¹⁹⁰ proposed a preliminary mechanism of coke formation (Figure 2.18). As the substrates are subjected to heating during the hydrotreatment process, bio-oil compounds may

break that results in the generation of radicals that require stabilization. Active hydrogen plays a pivotal role during this phase, stabilizing the extremely reactive functionalities, including the radicals and oxygenated compounds.^{137,191} During the breaking of bonds, smaller molecules are generated or undergo repolymerization to form larger molecules, especially when there is insufficient supply of hydrogen gas.¹⁹¹ Polymerization or the recombination of oxygenated compounds occurs more rapidly at lower temperatures. Simultaneously, bio-oil compounds adsorb to the catalyst's surface. However, due to steric hindrances, large molecules encounter greater challenges to access the acid sites compared to smaller molecules.

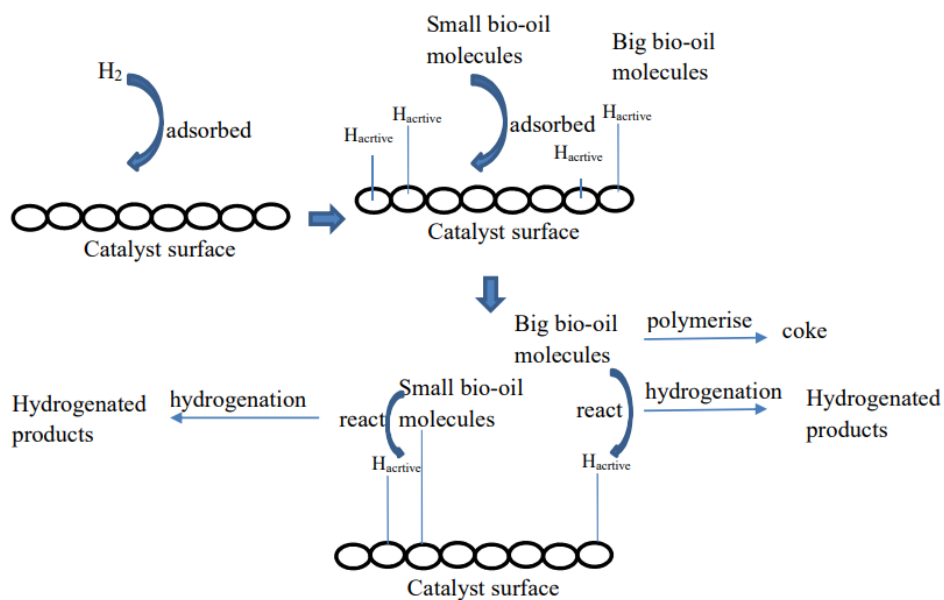


Figure 2.18: Simplified reaction scheme of coke formation during bio-oil HDO. Reproduced from ref. 190.

Cordero-Lanzac et al.¹⁹² investigated the phenomenon of coke during the HDO of raw bio-oil over noble metal nanoparticles supported on mildly acid supports. Briefly, the study unveiled two distinct pathways (Figure 2.19) responsible for catalyst deactivation: the first

pathway involves the polymerization reaction stemming from the oxygenated compounds. Notably, this pathway exhibits heightened reactivity at lower temperatures, particularly when there is a substantial concentration of highly reactive oxygenated compounds due to lower HDO conversion rates. Subsequently, lighter carbonaceous compounds containing oxygen functional groups are deposited onto the catalyst surfaces. The second pathway entails the formation of polyaromatic structures through the condensation of the alkyl aromatics into bigger aromatic compounds. The second pathway is initiated by higher temperatures, promoting the dehydrogenation of alkyl aromatics, leading to formation of larger aromatic compounds. For instance, an intermediate such as cyclohexene tends to interact with aromatics in the acidic sites, rather than forming cyclohexanes. This mechanism elucidates the formation of higher-yield and heavier coke structures at elevated temperatures.

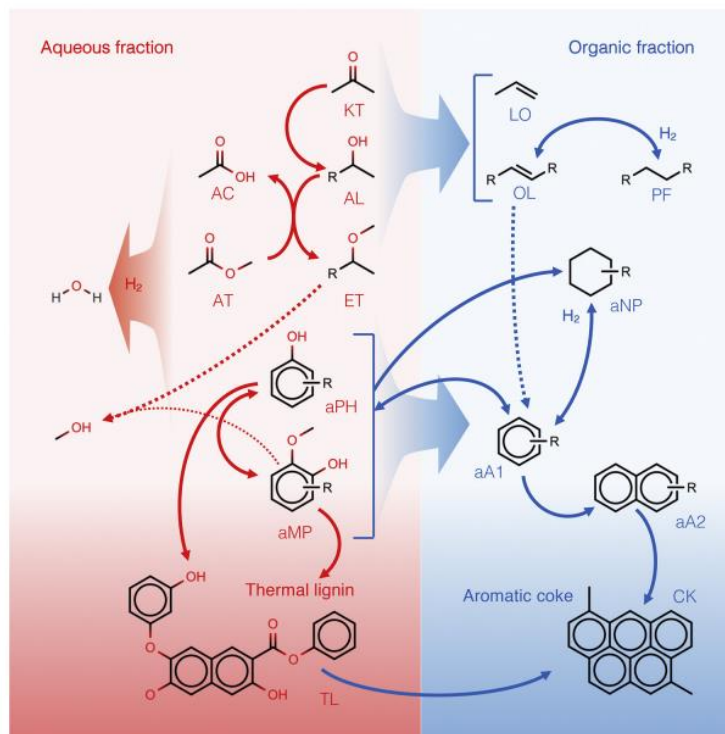


Figure 2.19: Simplified reaction scheme of coke formation during bio-oil HDO. Reproduced from Ref. 192.

Tang et al.¹⁹³ integrated hydrotreatment, esterification, and cracking processes to upgrade bio-oil while mitigating coke formation over a Pd/SO₄²⁻/ZrO₂/SBA-15 catalyst operating under supercritical conditions. Results showed the effectiveness of this upgrading approach, resulting in minimal coke formation and significant improvements in the properties of the upgraded oil.

A study¹⁹⁴ that characterized the deactivated Ru/C and CoMo/C catalysts during bio-oil HDO revealed that severe fouling was the leading cause of catalyst deactivation. Analyses using TGA and X-ray photoelectron spectroscopy (XPS) indicated that carbonaceous residues or coke formation originated from the condensation of sugars and their derivatives, including aldehydes and ketones.

2.4 Conclusion and Outlook

This review article provides insights into the reaction mechanisms involved in the thermochemical conversion of biomass into hydrocarbons. Despite extensive research on bio-oil, its highly complex composition has left an unknown fraction poorly understood at the moment. Few studies have experimentally detected these unknown compounds during the characterization of the water-soluble fraction, pinpointing them as highly dehydrated sugars resulting from deep dehydration reactions. Consequently, there is a paucity of research dedicated to understanding the reaction mechanisms responsible for the formation of these sugar oligomers and their behavior during upgrading.

The primary reaction mechanisms associated with fast pyrolysis have been examined, including depolymerization, dehydration, fragmentation, polymerization, and cross-linking. On the other hand, the key reactions occurring during bio-oil hydrotreatment, including hydrogenation, hydrogenolysis, hydrodeoxygenation, polymerization, and coking, have also been reviewed. Because of the complexity of bio-oil, most studies have focused on using model

compounds to study these reaction mechanisms. These model compounds used to study the mechanisms of bio-oil HDO include the basic units of lignin such as guaiacol and phenols, furans for sugars, and linear, low-molecular weight compounds. Density functional theory has also been instrumental in elucidating these reaction mechanisms.

Based on the literature review, several important considerations emerge:

- 1. Unraveling heavy oligomers:** The literature highlights a significant gap in understanding heavy oligomers, which remains poorly understood. Therefore, more studies should be conducted to unravel the fundamental chemistry and properties of sugar oligomers. This knowledge is an essential pre-requisite for developing catalysts, designing processing and upgrading equipment, and optimizing process parameters for effective conversion.
- 2. Tackling coke formation:** A substantial concern in bio-oil upgrading is the formation of coke, which can hinder the commercialization of this technology. Addressing this issue requires innovative approaches, such as developing low-cost, high-performance catalysts capable of withstanding the challenging properties of bio-oil. Moreover, optimizing the HDO process parameters such as temperature, pressure, and reaction time and exploring novel methods like introducing solvents and other hydrogen-rich chemicals to stabilize bio-oil compounds can alleviate coke formation.
- 3. Sustainable hydrogen sources:** The extensive use of hydrogen during bio-oil HDO raises concerns due to its safety risks and high costs. Researchers may find alternative sources of sustainable hydrogen, making the process more environmentally friendly and economically viable.

2.5 REFERENCES

- (1) Zhang, S.; Yan, Y.; Li, T.; Ren, Z. Upgrading of Liquid Fuel from the Pyrolysis of Biomass. *Bioresour. Technol.* **2005**, *96* (5), 545–550.
<https://doi.org/10.1016/j.biortech.2004.06.015>.
- (2) Lu, Q.; Hu, B.; Zhang, Z. xi; Wu, Y. ting; Cui, M. shu; Liu, D. jia; Dong, C. qing; Yang, Y. ping. Mechanism of Cellulose Fast Pyrolysis: The Role of Characteristic Chain Ends and Dehydrated Units. *Combust. Flame* **2018**, *198*, 267–277.
<https://doi.org/10.1016/j.combustflame.2018.09.025>.
- (3) Shen, D.; Jin, W.; Hu, J.; Xiao, R.; Luo, K. An Overview on Fast Pyrolysis of the Main Constituents in Lignocellulosic Biomass to Valued-Added Chemicals: Structures, Pathways and Interactions. *Renew. Sustain. Energy Rev.* **2015**, *51*, 761–774.
<https://doi.org/10.1016/j.rser.2015.06.054>.
- (4) Shen, D.; Xiao, R.; Gu, S.; Luo, K. The Pyrolytic Behavior of Cellulose in Lignocellulosic Biomass: A Review. *RSC Adv.* **2011**, *1* (9), 1641–1660.
<https://doi.org/10.1039/c1ra00534k>.
- (5) Kan, T.; Strezov, V.; Evans, T. J. Lignocellulosic Biomass Pyrolysis: A Review of Product Properties and Effects of Pyrolysis Parameters. *Renew. Sustain. Energy Rev.* **2016**, *57*, 1126–1140. <https://doi.org/10.1016/j.rser.2015.12.185>.
- (6) Pinheiro Pires, A. P.; Arauzo, J.; Fonts, I.; Domine, M. E.; Fernández Arroyo, A.; Garcia-Perez, M. E.; Montoya, J.; Chejne, F.; Pfromm, P.; Garcia-Perez, M. Challenges and Opportunities for Bio-Oil Refining: A Review. *Energy and Fuels* **2019**, *33* (6), 4683–4720. <https://doi.org/10.1021/acs.energyfuels.9b00039>.
- (7) Venderbosch, R. H.; Prins, W. Fast Pyrolysis Technology Development. *Biofuels*,

- Bioproducts and Biorefining*. 2010, pp 178–208. <https://doi.org/10.1002/bbb.205>.
- (8) Agarwal, V.; Dauenhauer, P. J.; Huber, G. W.; Auerbach, S. M. Ab Initio Dynamics of Cellulose Pyrolysis: Nascent Decomposition Pathways at 327 and 600 °C. *J. Am. Chem. Soc.* **2012**, *134* (36), 14958–14972. <https://doi.org/10.1021/ja305135u>.
- (9) Oasmaa, A.; Fonts, I.; Pelaez-Samaniego, M. R.; Garcia-Perez, M. E.; Garcia-Perez, M. Pyrolysis Oil Multiphase Behavior and Phase Stability: A Review. *Energy and Fuels* **2016**, *30* (8), 6179–6200. <https://doi.org/10.1021/acs.energyfuels.6b01287>.
- (10) Nachenius, R. W.; Ronsse, F.; Venderbosch, R. H.; Prins, W. *Biomass Pyrolysis*, 1st ed.; Elsevier Inc., 2013; Vol. 42. <https://doi.org/10.1016/B978-0-12-386505-2.00002-X>.
- (11) Patwardhan, P. R.; Satrio, J. A.; Brown, R. C.; Shanks, B. H. Product Distribution from Fast Pyrolysis of Glucose-Based Carbohydrates. *J. Anal. Appl. Pyrolysis* **2009**, *86* (2), 323–330. <https://doi.org/10.1016/j.jaap.2009.08.007>.
- (12) Mohan, D.; Pittman, C. U.; Steele, P. H. Pyrolysis of Wood /Biomass for Bio-Oil. *Prog. Energy Combust. Sci.* **2017**, *62* (4), 848–889.
- (13) Zhou, X.; Nolte, M. W.; Mayes, H. B.; Shanks, B. H.; Broadbelt, L. J. Experimental and Mechanistic Modeling of Fast Pyrolysis of Neat Glucose-Based Carbohydrates. 1. Experiments and Development of a Detailed Mechanistic Model. *Ind. Eng. Chem. Res.* **2014**, *53* (34), 13274–13289. <https://doi.org/10.1021/ie502259w>.
- (14) Abdilla-Santes, R. M.; Agarwal, S.; Xi, X.; Heeres, H.; Deuss, P. J.; Heeres, H. J. Valorization of Humins Type Byproducts from Pyrolytic Sugar Conversions to Biobased Chemicals. *J. Anal. Appl. Pyrolysis* **2020**, *152* (October). <https://doi.org/10.1016/j.jaap.2020.104963>.
- (15) Boucher, M. E.; Chala, A.; Pakdel, H.; Roy, C. Bio-Oils Obtained by Vacuum Pyrolysis

- of Softwood Bark as a Liquid Fuel for Gas Turbines. Part II: Stability and Ageing of Bio-Oil and Its Blends with Methanol and a Pyrolytic Aqueous Phase. *Biomass and Bioenergy* **2000**, *19* (5), 351–361. [https://doi.org/10.1016/S0961-9534\(00\)00044-1](https://doi.org/10.1016/S0961-9534(00)00044-1).
- (16) Bridgwater, A. V. Production of High Grade Fuels and Chemicals from Catalytic Pyrolysis of Biomass. *Catal. Today* **1996**, *29* (1–4), 285–295. [https://doi.org/10.1016/0920-5861\(95\)00294-4](https://doi.org/10.1016/0920-5861(95)00294-4).
- (17) Bridgwater, A. V. Catalysis in Thermal Biomass Conversion. *Appl. Catal. A, Gen.* **1994**, *116* (1–2), 5–47. [https://doi.org/10.1016/0926-860X\(94\)80278-5](https://doi.org/10.1016/0926-860X(94)80278-5).
- (18) Han, Y.; Gholizadeh, M.; Tran, C. C.; Kaliaguine, S.; Li, C. Z.; Olarte, M.; Garcia-Perez, M. Hydrotreatment of Pyrolysis Bio-Oil: A Review. *Fuel Process. Technol.* **2019**, *195* (June). <https://doi.org/10.1016/j.fuproc.2019.106140>.
- (19) Zhang, Y.; Liu, C.; Chen, X. Unveiling the Initial Pyrolytic Mechanisms of Cellulose by DFT Study. *J. Anal. Appl. Pyrolysis* **2015**, *113*, 621–629. <https://doi.org/10.1016/j.jaap.2015.04.010>.
- (20) Gong, X.; Yu, Y.; Gao, X.; Qiao, Y.; Xu, M.; Wu, H. Formation of Anhydro-Sugars in the Primary Volatiles and Solid Residues from Cellulose Fast Pyrolysis in a Wire-Mesh Reactor. **2014**. <https://doi.org/10.1021/ef501112q>.
- (21) Kadarwati, S.; Hu, X.; Gunawan, R.; Westerhof, R.; Gholizadeh, M.; Hasan, M. D. M.; Li, C. Coke Formation during the Hydrotreatment of Bio-Oil Using NiMo and CoMo Catalysts. *Fuel Process. Technol.* **2017**, *155*, 261–268. <https://doi.org/10.1016/j.fuproc.2016.08.021>.
- (22) Czernik, S.; Bridgwater, A. V. Overview of Applications of Biomass Fast Pyrolysis Oil. *Energy and Fuels* **2004**, *18* (2), 590–598. <https://doi.org/10.1021/ef034067u>.

- (23) Wang, Q.; Song, H.; Pan, S.; Dong, N.; Wang, X.; Sun, S. Initial Pyrolysis Mechanism and Product Formation of Cellulose: An Experimental and Density Functional Theory(DFT) Study. *Sci. Rep.* **2020**, *10* (1), 1–18. <https://doi.org/10.1038/s41598-020-60095-2>.
- (24) He, Z.; Wang, X. Hydrodeoxygenation of Model Compounds and Catalytic Systems for Pyrolysis Bio-Oils Upgrading. *Catal. Sustain. Energy* **2013**, *1*, 28–52. <https://doi.org/10.2478/cse-2012-0004>.
- (25) Garcia-Perez, M.; Adams, T. T.; Goodrum, J. W.; Geller, D.; Das, K. C. Production and Fuel Properties of Pine Chip Bio-Oil/Biodiesel Blends. *Energy and Fuels* **2007**, *21* (4), 2363–2372. <https://doi.org/10.1021/ef060533e>.
- (26) Koike, N.; Hosokai, S.; Takagaki, A.; Nishimura, S.; Kikuchi, R.; Ebitani, K.; Suzuki, Y.; Oyama, S. T. Upgrading of Pyrolysis Bio-Oil Using Nickel Phosphide Catalysts. *J. Catal.* **2016**, *333*, 115–126. <https://doi.org/10.1016/j.jcat.2015.10.022>.
- (27) Kim, J. S. Production, Separation and Applications of Phenolic-Rich Bio-Oil - A Review. *Bioresour. Technol.* **2015**, *178*, 90–98. <https://doi.org/10.1016/j.biortech.2014.08.121>.
- (28) Pham, T. N.; Shi, D.; Resasco, D. E. Evaluating Strategies for Catalytic Upgrading of Pyrolysis Oil in Liquid Phase. *Appl. Catal. B Environ.* **2014**, *145*, 10–23. <https://doi.org/10.1016/j.apcatb.2013.01.002>.
- (29) Brown, T. R. A Techno-Economic Review of Thermochemical Cellulosic Biofuel Pathways. *Bioresour. Technol.* **2015**, *178*, 166–176. <https://doi.org/10.1016/j.biortech.2014.09.053>.
- (30) Brown, R. C.; Brown, T. R. Thermochemical Processing of Lignocellulosic Biomass. *Biorenewable Resour.* **2014**, 195–236. <https://doi.org/10.1002/9781118524985.ch8>.

- (31) Kim, S. H.; Lee, C. M.; Kafle, K. Characterization of Crystalline Cellulose in Biomass: Basic Principles, Applications, and Limitations of XRD, NMR, IR, Raman, and SFG. *Korean J. Chem. Eng.* **2013**, *30* (12), 2127–2141. <https://doi.org/10.1007/s11814-013-0162-0>.
- (32) Hu, B.; Zhang, B.; Xie, W. L.; Jiang, X. Y.; Liu, J.; Lu, Q. Recent Progress in Quantum Chemistry Modeling on the Pyrolysis Mechanisms of Lignocellulosic Biomass. *Energy and Fuels* **2020**, *34* (9), 10384–10440. <https://doi.org/10.1021/acs.energyfuels.0c01948>.
- (33) Kostetskyy, P.; Broadbelt, L. J. Progress in Modeling of Biomass Fast Pyrolysis: A Review. *Energy and Fuels* **2020**, *34* (12), 15195–15216. <https://doi.org/10.1021/acs.energyfuels.0c02295>.
- (34) Banerjee, A.; Mushrif, S. H. Reaction Pathways for the Deoxygenation of Biomass-Pyrolysis-Derived Bio-Oil on Ru:ADFT Study Using Furfural as AM Odel Compound. <https://doi.org/10.1002/cctc.201700036>.
- (35) Hensley, A. J. R.; Wang, Y.; McEwen, J.-S. Supporting Information Phenol Deoxygenation Mechanisms on Fe (110) and Pd (111). **2014**, No. 110.
- (36) Sun, J.; Karim, A. M.; Zhang, H.; Kovarik, L.; Li, X. S.; Hensley, A. J.; McEwen, J. S.; Wang, Y. Carbon-Supported Bimetallic Pd-Fe Catalysts for Vapor-Phase Hydrodeoxygenation of Guaiacol. *J. Catal.* **2013**, *306*, 47–57. <https://doi.org/10.1016/j.jcat.2013.05.020>.
- (37) Hu, X.; Lievens, C.; Larcher, A.; Li, C. Z. Reaction Pathways of Glucose during Esterification: Effects of Reaction Parameters on the Formation of Humin Type Polymers. *Bioresour. Technol.* **2011**, *102* (21), 10104–10113. <https://doi.org/10.1016/j.biortech.2011.08.040>.

- (38) Gong, X.; Yu, Y.; Gao, X.; Qiao, Y.; Xu, M.; Wu, H. Formation of Anhydro-Sugars in the Primary Volatiles and Solid Residues from Cellulose Fast Pyrolysis in a Wire-Mesh Reactor. *Energy and Fuels* **2014**, *28* (8), 5204–5211. <https://doi.org/10.1021/ef501112q>.
- (39) Lin, Y. C.; Cho, J.; Tompsett, G. A.; Westmoreland, P. R.; Huber, G. W. Kinetics and Mechanism of Cellulose Pyrolysis. *J. Phys. Chem. C* **2009**, *113* (46), 20097–20107. <https://doi.org/10.1021/jp906702p>.
- (40) Wang, S.; Dai, G.; Yang, H.; Luo, Z. Lignocellulosic Biomass Pyrolysis Mechanism: A State-of-the-Art Review. *Prog. Energy Combust. Sci.* **2017**, *62*, 33–86. <https://doi.org/10.1016/j.pecs.2017.05.004>.
- (41) Mayes, H. B.; Broadbelt, L. J. Unraveling the Reactions That Unravel Cellulose. *J. Phys. Chem. A* **2012**, *116*. <https://doi.org/10.1021/jp300405x>.
- (42) Winandy, J. E.; Rowell, R. M. *The Chemistry of Wood Strength*; 1984. <https://doi.org/10.1021/ba-1984-0207.ch005>.
- (43) Mamleev, V.; Bourbigot, S.; Yvon, J. Kinetic Analysis of the Thermal Decomposition of Cellulose: The Main Step of Mass Loss. *J. Anal. Appl. Pyrolysis* **2007**, *80* (1), 151–165. <https://doi.org/10.1016/j.jaap.2007.01.013>.
- (44) Zhang, M.; Hu, Y.; Wang, H.; Li, H.; Han, X.; Zeng, Y.; Xu, C. C. A Review of Bio-Oil Upgrading by Catalytic Hydrotreatment: Advances, Challenges, and Prospects. *Mol. Catal.* **2021**, *504* (February), 111438. <https://doi.org/10.1016/j.mcat.2021.111438>.
- (45) Krumm, C.; Pfaendtner, J.; Dauenhauer, P. J. Millisecond Pulsed Films Unify the Mechanisms of Cellulose Fragmentation. *Chem. Mater.* **2016**, *28* (9), 3108–3114. <https://doi.org/10.1021/acs.chemmater.6b00580>.
- (46) O'sullivan, A. C. Cellulose: The Structure Slowly Unravels. *Cellulose* **1997**, *4* (3), 173–

- 207.
- (47) Simoneit, B. R. T.; Schauer, J. J.; Nolte, C. G.; Oros, D. R.; Elias, V. O.; Fraser, M. P.; Rogge, W. F.; Cass, G. R. <Simoneit Levoglucosan.Pdf>. *Atmos. Environ.* **1999**, *33* (2), 1–10.
- (48) Huber, G. W.; Corma, A. Synergies between Bio- and Oil Refineries for the Production of Fuels from Biomass. *Angew. Chemie - Int. Ed.* **2007**, *46* (38), 7184–7201.
<https://doi.org/10.1002/anie.200604504>.
- (49) Klemm, D.; Heublein, B.; Fink, H. P.; Bohn, A. Cellulose: Fascinating Biopolymer and Sustainable Raw Material. *Angew. Chemie - Int. Ed.* **2005**, *44* (22), 3358–3393.
<https://doi.org/10.1002/anie.200460587>.
- (50) Zhou, C. H.; Xia, X.; Lin, C. X.; Tong, D. S.; Beltramini, J. Catalytic Conversion of Lignocellulosic Biomass to Fine Chemicals and Fuels. *Chem. Soc. Rev.* **2011**, *40* (11), 5588–5617. <https://doi.org/10.1039/c1cs15124j>.
- (51) Jahirul, M. I.; Rasul, M. G.; Chowdhury, A. A.; Ashwath, N. Biofuels Production through Biomass Pyrolysis- A Technological Review. *Energies* **2012**, *5* (12), 4952–5001.
<https://doi.org/10.3390/en5124952>.
- (52) Bridgwater, A. V. Review of Fast Pyrolysis of Biomass and Product Upgrading. *Biomass and Bioenergy* **2012**, *38*, 68–94. <https://doi.org/10.1016/j.biombioe.2011.01.048>.
- (53) Yu, Y.; Chua, Y. W.; Wu, H. Characterization of Pyrolytic Sugars in Bio-Oil Produced from Biomass Fast Pyrolysis. **2016**. <https://doi.org/10.1021/acs.energyfuels.6b00464>.
- (54) Fukutome, A.; Kawamoto, H.; Saka, S. Kinetics and Molecular Mechanisms for the Gas-Phase Degradation of Levoglucosan as a Cellulose Gasification Intermediate. *J. Anal. Appl. Pyrolysis* **2017**, *124*, 666–676. <https://doi.org/10.1016/j.jaap.2016.12.010>.

- (55) Patwardhan, P. R.; Dalluge, D. L.; Shanks, B. H.; Brown, R. C. Distinguishing Primary and Secondary Reactions of Cellulose Pyrolysis. *Bioresour. Technol.* **2011**, *102* (8), 5265–5269. <https://doi.org/10.1016/j.biortech.2011.02.018>.
- (56) Sharifzadeh, M.; Sadeqzadeh, M.; Guo, M.; Borhani, T. N.; Murthy Konda, N. V. S. N.; Garcia, M. C.; Wang, L.; Hallett, J.; Shah, N. The Multi-Scale Challenges of Biomass Fast Pyrolysis and Bio-Oil Upgrading: Review of the State of Art and Future Research Directions. *Prog. Energy Combust. Sci.* **2019**, *71*, 1–80. <https://doi.org/10.1016/j.pecs.2018.10.006>.
- (57) Richards, G. N. Glycolaldehyde from Pyrolysis of Cellulose. *J. Anal. Appl. Pyrolysis* **1987**, *10* (3), 251–255. [https://doi.org/10.1016/0165-2370\(87\)80006-2](https://doi.org/10.1016/0165-2370(87)80006-2).
- (58) Shen, D. K.; Gu, S. The Mechanism for Thermal Decomposition of Cellulose and Its Main Products. *Bioresour. Technol.* **2009**, *100* (24), 6496–6504. <https://doi.org/10.1016/j.biortech.2009.06.095>.
- (59) Piskorz, J.; Radlein, D.; Scott, D. S. On the Mechanism of the Rapid Pyrolysis of Cellulose. *J. Anal. Appl. Pyrolysis* **1986**, *9* (2), 121–137. [https://doi.org/10.1016/0165-2370\(86\)85003-3](https://doi.org/10.1016/0165-2370(86)85003-3).
- (60) Kuzhiyil, N.; Dalluge, D.; Bai, X.; Kim, K. H.; Brown, R. C. Pyrolytic Sugars from Cellulosic Biomass. *ChemSusChem* **2012**, *5* (11), 2228–2236. <https://doi.org/10.1002/cssc.201200341>.
- (61) Lyu, G.; Wu, S.; Zhang, H. Estimation and Comparison of Bio-Oil Components from Different Pyrolysis Conditions. *Front. Energy Res.* **2015**, *3* (JUN), 1–11. <https://doi.org/10.3389/fenrg.2015.00028>.
- (62) Wildschut, J.; Mahfud, F. H.; Venderbosch, R. H.; Heeres, H. J. Hydrotreatment of Fast

- Pyrolysis Oil Using Heterogeneous Noble-Metal Catalysts. *Ind. Eng. Chem. Res.* **2009**, *48* (23), 10324–10334. <https://doi.org/10.1021/ie9006003>.
- (63) Garcia-Perez, M.; Wang, S.; Shen, J.; Rhodes, M.; Lee, W. J.; Li, C. Z. Effects of Temperature on the Formation of Lignin-Derived Oligomers during the Fast Pyrolysis of Mallee Woody Biomass. *Energy and Fuels* **2008**, *22* (3), 2022–2032. <https://doi.org/10.1021/ef7007634>.
- (64) Stankovikj, F.; McDonald, A. G.; Helms, G. L.; Olarte, M. V.; Garcia-Perez, M. Characterization of the Water-Soluble Fraction of Woody Biomass Pyrolysis Oils. *Energy and Fuels* **2017**, *31* (2), 1650–1664. <https://doi.org/10.1021/acs.energyfuels.6b02950>.
- (65) Terrell, E.; Garcia-Perez, M. Novel Strategy to Analyze Fourier Transform Ion Cyclotron Resonance Mass Spectrometry Data of Biomass Pyrolysis Oil for Oligomeric Structure Assignment. *Energy and Fuels* **2020**, *34* (7), 8466–8481. <https://doi.org/10.1021/acs.energyfuels.0c01687>.
- (66) Abdilla-Santes, R. M.; Agarwal, S.; Xi, X.; Heeres, H.; Deuss, P. J.; Heeres, H. J. Valorization of Humins Type Byproducts from Pyrolytic Sugar Conversions to Biobased Chemicals. *J. Anal. Appl. Pyrolysis* **2020**, *152* (January). <https://doi.org/10.1016/j.jaap.2020.104963>.
- (67) Denson, M.; Terrell, E.; Kostetskyy, P.; Olarte, M.; Broadbelt, L.; Garcia-Perez, M. Elucidation of Structure and Physical Properties of Pyrolytic Sugar Oligomers Derived from Cellulose Depolymerization/Dehydration Reactions: A Density Functional Theory Study. *Energy & Fuels* **37** (11), 7834–7847. <https://doi.org/10.1021/acs.energyfuels.3c00641>.
- (68) Denson, M.; Terrell, E.; Kostetskyy, P.; Olarte, M.; Broadbelt, L.; Garcia-Perez, M.

- Theoretical Insights on the Fragmentation of Cellulosic Oligomers to Form Hydroxyacetone and Hydroxyacetaldehyde. *Energy & Fuels* **37** (18), 13997–14005. <https://doi.org/10.1021/acs.energyfuels.3c01924>.
- (69) Ferrell, J. R.; Olarte, M. V.; Christensen, E. D.; Padmaperuma, A. B.; Connatser, R. M.; Stankovikj, F.; Meier, D.; Paasikallio, V. Standardization of Chemical Analytical Techniques for Pyrolysis Bio-Oil: History, Challenges, and Current Status of Methods. *Biofuels, Bioprod. Biorefining* **2016**, *10* (5), 496–507. <https://doi.org/10.1002/bbb.1661>.
- (70) Michailof, C. M.; Kalogiannis, K. G.; Sfetsas, T.; Patiaka, D. T.; Lappas, A. A. Advanced Analytical Techniques for Bio-Oil Characterization. *Wiley Interdiscip. Rev. Energy Environ.* **2016**, *5* (6), 614–639. <https://doi.org/10.1002/wene.208>.
- (71) Lu, Y.; Li, G. S.; Lu, Y. C.; Fan, X.; Wei, X. Y. Analytical Strategies Involved in the Detailed Componential Characterization of Biooil Produced from Lignocellulosic Biomass. *Int. J. Anal. Chem.* **2017**, *2017*. <https://doi.org/10.1155/2017/9298523>.
- (72) Oasmaa, A.; Kuoppala, E.; Elliott, D. C. Development of the Basis for an Analytical Protocol for Feeds and Products of Bio-Oil Hydrotreatment. *Energy and Fuels* **2012**, *26* (4), 2454–2460. <https://doi.org/10.1021/ef300252y>.
- (73) Pires, A. P. P.; Han, Y.; Kramlich, J.; Garcia-Perez, M. Alternative Jet Fuel Properties. *BioResources* **2018**, *13* (2), 2632–2657.
- (74) Stankovikj, F.; McDonald, A. G.; Helms, G. L.; Garcia-Perez, M. Quantification of Bio-Oil Functional Groups and Evidences of the Presence of Pyrolytic Humins. *Energy and Fuels* **2016**, *30* (8), 6505–6524. <https://doi.org/10.1021/acs.energyfuels.6b01242>.
- (75) Zhong, D.; Zeng, K.; Li, J.; Qiu, Y.; Flamant, G.; Nzihou, A.; Vladimirovich, V. S.; Yang, H.; Chen, H. Characteristics and Evolution of Heavy Components in Bio-Oil from the

- Pyrolysis of Cellulose, Hemicellulose and Lignin. *Renew. Sustain. Energy Rev.* **2022**, *157* (June 2021), 111989. <https://doi.org/10.1016/j.rser.2021.111989>.
- (76) Staš, M.; Chudoba, J.; Auersvald, M.; Kubička, D.; Conrad, S.; Schulzke, T.; Pospíšil, M. Application of Orbitrap Mass Spectrometry for Analysis of Model Bio-Oil Compounds and Fast Pyrolysis Bio-Oils from Different Biomass Sources. *J. Anal. Appl. Pyrolysis* **2017**, *124*, 230–238. <https://doi.org/10.1016/j.jaap.2017.02.002>.
- (77) Yang, H.; Yan, R.; Chen, H.; Lee, D. H.; Zheng, C. Characteristics of Hemicellulose, Cellulose and Lignin Pyrolysis. *Fuel* **2007**, *86* (12–13), 1781–1788. <https://doi.org/10.1016/j.fuel.2006.12.013>.
- (78) Liu, Q.; Zhong, Z.; Wang, S.; Luo, Z. Interactions of Biomass Components during Pyrolysis: A TG-FTIR Study. *J. Anal. Appl. Pyrolysis* **2011**, *90* (2), 213–218. <https://doi.org/10.1016/j.jaap.2010.12.009>.
- (79) Chaiwat, W.; Hasegawa, I.; Tani, T.; Sunagawa, K.; Mae, K. Analysis of Cross-Linking Behavior during Pyrolysis of Cellulose for Elucidating Reaction Pathway. *Energy and Fuels* **2009**, *23* (12), 5765–5772. <https://doi.org/10.1021/ef900674b>.
- (80) Yang, X.; Zhao, Y.; Li, R.; Wu, Y.; Yang, M. A Modified Kinetic Analysis Method of Cellulose Pyrolysis Based on TG–FTIR Technique. *Thermochim. Acta* **2018**, *665* (January), 20–27. <https://doi.org/10.1016/j.tca.2018.05.008>.
- (81) Antal, M. J.; Várhegyi, G.; Jakab, E. Cellulose Pyrolysis Kinetics: Revisited. *Ind. Eng. Chem. Res.* **1998**, *37* (4), 1267–1275. <https://doi.org/10.1021/ie970144v>.
- (82) Mészáros, E.; Jakab, E.; Várhegyi, G. TG/MS, Py-GC/MS and THM-GC/MS Study of the Composition and Thermal Behavior of Extractive Components of Robinia Pseudoacacia. *J. Anal. Appl. Pyrolysis* **2007**, *79* (1-2 SPEC. ISS.), 61–70.

- <https://doi.org/10.1016/j.jaap.2006.12.007>.
- (83) Qiang, L.; Wen-zhi, L.; Dong, Z.; Xi-feng, Z. Analytical Pyrolysis-Gas Chromatography/Mass Spectrometry (Py-GC/MS) of Sawdust with Al/SBA-15 Catalysts. *J. Anal. Appl. Pyrolysis* **2009**, *84* (2), 131–138. <https://doi.org/10.1016/j.jaap.2009.01.002>.
- (84) Wang, Q.; Song, H.; Pan, S.; Dong, N.; Wang, X.; Sun, S. Initial Pyrolysis Mechanism and Product Formation of Cellulose: An Experimental and Density Functional Theory(Dft) Study. <https://doi.org/10.1038/s41598-020-60095-2>.
- (85) Wang, S.; Guo, X.; Liang, T.; Zhou, Y.; Luo, Z. Mechanism Research on Cellulose Pyrolysis by Py-GC/MS and Subsequent Density Functional Theory Studies. *Bioresour. Technol.* **2012**, *104*, 722–728. <https://doi.org/10.1016/j.biortech.2011.10.078>.
- (86) Zhao, S.; Bi, X.; Sun, R.; Niu, M.; Pan, X. Density Functional Theory and Experimental Study of Cellulose Initial Degradation Stage under Inert and Oxidative Atmosphere. *J. Mol. Struct.* **2020**, *1204*, 127543. <https://doi.org/10.1016/j.molstruc.2019.127543>.
- (87) Huang, J.; Liu, C.; Tong, H.; Li, W.; Wu, D. Theoretical Studies on Pyrolysis Mechanism of Xylopyranose. *Comput. Theor. Chem.* **2012**, *1001*, 44–50. <https://doi.org/10.1016/j.comptc.2012.10.015>.
- (88) Stelt, M. J. C. Van Der. *Chemistry and Reaction Kinetics of Biowaste Torrefaction*; 2010; Vol. 1. <https://doi.org/10.6100/IR695294>.
- (89) White, J. E.; Catallo, W. J.; Legendre, B. L. Biomass Pyrolysis Kinetics: A Comparative Critical Review with Relevant Agricultural Residue Case Studies. *J. Anal. Appl. Pyrolysis* **2011**, *91* (1), 1–33. <https://doi.org/10.1016/j.jaap.2011.01.004>.
- (90) Milosavljevic, I.; Suuberg, E. M. Cellulose Thermal Decomposition Kinetics: Global Mass Loss Kinetics. *Ind. Eng. Chem. Res.* **1995**, *34* (4), 1081–1091.

<https://doi.org/10.1021/ie00043a009>.

- (91) Șerbănescu, C. Kinetic Analysis of Cellulose Pyrolysis: A Short Review. *Chem. Pap.* **2014**, *68* (7), 847–860. <https://doi.org/10.2478/s11696-013-0529-z>.
- (92) Lédé, J. Cellulose Pyrolysis Kinetics: An Historical Review on the Existence and Role of Intermediate Active Cellulose. *J. Anal. Appl. Pyrolysis* **2012**, *94*, 17–32. <https://doi.org/10.1016/j.jaap.2011.12.019>.
- (93) Bradbury, A. G. W.; Sakai, Y.; Shafizadeh, F. A Kinetic Model for Pyrolysis of Cellulose. *J. Appl. Polym. Sci.* **1979**, *23* (11), 3271–3280. <https://doi.org/10.1002/app.1979.070231112>.
- (94) Dai, G.; Wang, K.; Wang, G.; Wang, S. Initial Pyrolysis Mechanism of Cellulose Revealed by In-Situ DRIFT Analysis and Theoretical Calculation. *Combust. Flame* **2019**, *208*, 273–280. <https://doi.org/10.1016/j.combustflame.2019.07.009>.
- (95) Shafizadeh, F. Introduction to Pyrolysis of Biomass. *J. Anal. Appl. Pyrolysis* **1982**, *3* (4), 283–305. [https://doi.org/10.1016/0165-2370\(82\)80017-X](https://doi.org/10.1016/0165-2370(82)80017-X).
- (96) Diebold, J. P. A Unified, Global Model for the Pyrolysis of Cellulose. *Biomass and Bioenergy* **1994**, *7* (1–6), 75–85. [https://doi.org/10.1016/0961-9534\(94\)00039-V](https://doi.org/10.1016/0961-9534(94)00039-V).
- (97) Wooten, J. B.; Seeman, J. I.; Hajaligol, M. R. Observation and Characterization of Cellulose Pyrolysis Intermediates by ¹³C CPMAS NMR. A New Mechanistic Model. *Energy and Fuels* **2004**, *18* (1), 1–15. <https://doi.org/10.1021/ef0300601>.
- (98) Shafizadeh, F.; Fu, Y. Of Cellulose. *Carbohydr. Res.* **1973**, *29*, 113–122.
- (99) Van de Velden, M.; Baeyens, J.; Brems, A.; Janssens, B.; Dewil, R. Fundamentals, Kinetics and Endothermicity of the Biomass Pyrolysis Reaction. *Renew. Energy* **2010**, *35* (1), 232–242. <https://doi.org/10.1016/j.renene.2009.04.019>.

- (100) Vinu, R.; Broadbelt, L. J. A Mechanistic Model of Fast Pyrolysis of Glucose-Based Carbohydrates to Predict Bio-Oil Composition. *Energy Environ. Sci.* **2012**, *5* (12), 9808–9826. <https://doi.org/10.1039/c2ee22784c>.
- (101) Kawamoto, H. Review of Reactions and Molecular Mechanisms in Cellulose Pyrolysis. *Curr. Org. Chem.* **2016**, *20* (23), 2444–2457. <https://doi.org/10.2174/2213337203666160525102910>.
- (102) Collard, F. X.; Blin, J. A Review on Pyrolysis of Biomass Constituents: Mechanisms and Composition of the Products Obtained from the Conversion of Cellulose, Hemicelluloses and Lignin. *Renew. Sustain. Energy Rev.* **2014**, *38*, 594–608. <https://doi.org/10.1016/j.rser.2014.06.013>.
- (103) Molton, P. M. Reaction Mechanisms in Cellulose Pyrolysis. *Energy Res. Dev. Adm.* **1977**, 178.
- (104) Mayes, H. B.; Broadbelt, L. J. Unraveling the Reactions That Unravel Cellulose. *J. Phys. Chem. A* **2012**, *116*, 22. <https://doi.org/10.1021/jp300405x>.
- (105) Maliekkal, V.; Dauenhauer, P. J.; Neurock, M. Glycosidic C-O Bond Activation in Cellulose Pyrolysis: Alpha Versus Beta and Condensed Phase Hydroxyl-Catalytic Scission. *ACS Catal.* **2020**, *10* (15), 8454–8464. <https://doi.org/10.1021/acscatal.0c02133>.
- (106) Seshadri, V.; Westmoreland, P. R. Concerted Reactions and Mechanism of Glucose Pyrolysis and Implications for Cellulose Kinetics. *J. Phys. Chem. A* **2012**, *116* (49), 11997–12013. <https://doi.org/10.1021/jp3085099>.
- (107) Hosoya, T.; Nakao, Y.; Sato, H.; Kawamoto, H.; Sakaki, S. Thermal Degradation of Methyl β -D-Glucoside. A Theoretical Study of Plausible Reaction Mechanisms. *J. Org. Chem.* **2009**, *74* (17), 6891–6894. <https://doi.org/10.1021/jo900457k>.

- (108) Hosoya, T.; Sakaki, S. Levoglucosan Formation from Crystalline Cellulose: Importance of a Hydrogen Bonding Network in the Reaction. *ChemSusChem* **2013**, *6* (12), 2356–2368.
<https://doi.org/10.1002/cssc.201300338>.
- (109) Kawamoto, H.; Saito, S.; Hatanaka, W.; Saka, S. Catalytic Pyrolysis of Cellulose in Sulfolane with Some Acidic Catalysts. *J. Wood Sci.* **2007**, *53* (2), 127–133.
<https://doi.org/10.1007/s10086-006-0835-y>.
- (110) Scheirs, J.; Camino, G.; Tumiatti, W. Overview of Water Evolution during the Thermal Degradation of Cellulose. *Eur. Polym. J.* **2001**, *37* (5), 933–942.
[https://doi.org/10.1016/S0014-3057\(00\)00211-1](https://doi.org/10.1016/S0014-3057(00)00211-1).
- (111) Tang, M. M.; Bacon, R. Carbonization of Cellulose Fibers-I. Low Temperature Pyrolysis. *Carbon N. Y.* **1964**, *2* (3), 211–220. [https://doi.org/10.1016/0008-6223\(64\)90035-1](https://doi.org/10.1016/0008-6223(64)90035-1).
- (112) Degroot, W. F.; Pan, W. P.; Rahman, M. D.; Richards, G. N. First Chemical Events in Pyrolysis of Wood. *J. Anal. Appl. Pyrolysis* **1988**, *13* (3), 221–231.
[https://doi.org/10.1016/0165-2370\(88\)80024-X](https://doi.org/10.1016/0165-2370(88)80024-X).
- (113) Kashiwagi, T.; Nambu, H. Global Kinetic Constants for Thermal Oxidative Degradation of a Cellulosic Paper. *Combust. Flame* **1992**, *88* (3–4), 345–368.
[https://doi.org/10.1016/0010-2180\(92\)90039-R](https://doi.org/10.1016/0010-2180(92)90039-R).
- (114) Easton, M. W.; Nash, J. J.; Kenttämaa, H. I. Dehydration Pathways for Glucose and Cellobiose during Fast Pyrolysis. *J. Phys. Chem. A* **2018**, *122* (41), 8071–8085.
<https://doi.org/10.1021/acs.jpca.8b02312>.
- (115) Nimlos, M. R.; Blanksby, S. J.; Qian, X.; Himmel, M. E.; Johnson, D. K. Mechanisms of Glycerol Dehydration. *J. Phys. Chem. A* **2006**, *110* (18), 6145–6156.
<https://doi.org/10.1021/jp060597q>.

- (116) Zhang, M.; Geng, Z.; Yu, Y. Density Functional Theory (DFT) Study on the Dehydration of Cellulose. *Energy and Fuels* **2011**, *25* (6), 2664–2670.
<https://doi.org/10.1021/ef101619e>.
- (117) Pecha, M. B.; Montoya, J. I.; Chejne, F.; Garcia-Perez, M. Effect of a Vacuum on the Fast Pyrolysis of Cellulose: Nature of Secondary Reactions in a Liquid Intermediate. *Ind. Eng. Chem. Res.* **2017**, *56* (15), 4288–4301. <https://doi.org/10.1021/acs.iecr.7b00476>.
- (118) Denson, M. D.; Terrell, E.; Kostetsky, P.; Olarte, M.; Broadbelt, L.; Garcia-perez, M. Elucidation of Structure and Physical Properties of Pyrolytic Sugar Oligomers Derived from Cellulose Depolymerization / Dehydration Reactions : A Density Functional Theory Study. **2023**. <https://doi.org/10.1021/acs.energyfuels.3c00641>.
- (119) Nimlos, M. R.; Blanksby, S. J.; Barney Ellison, G.; Evans, R. J. Enhancement of 1,2-Dehydration of Alcohols by Alkali Cations and Protons: A Model for Dehydration of Carbohydrates. *J. Anal. Appl. Pyrolysis* **2003**, *66* (1), 3–27. [https://doi.org/10.1016/S0165-2370\(02\)00103-1](https://doi.org/10.1016/S0165-2370(02)00103-1).
- (120) Zhang, X.; Yang, W.; Dong, C. Levoglucosan Formation Mechanisms during Cellulose Pyrolysis. *J. Anal. Appl. Pyrolysis* **2013**, *104*, 19–27.
<https://doi.org/10.1016/J.JAAP.2013.09.015>.
- (121) Zhang, X.; Yang, W.; Blasiak, W. Thermal Decomposition Mechanism of Levoglucosan during Cellulose Pyrolysis. *J. Anal. Appl. Pyrolysis* **2012**, *96*, 110–119.
<https://doi.org/10.1016/j.jaap.2012.03.012>.
- (122) Richards, A. P.; Haycock, D.; Frandsen, J.; Fletcher, T. H. A Review of Coal Heating Value Correlations with Application to Coal Char, Tar, and Other Fuels. *Fuel* **2021**, *283* (June 2020), 118942. <https://doi.org/10.1016/j.fuel.2020.118942>.

- (123) Di Blasi, C.; Branca, C.; Galgano, A. Products and Global Weight Loss Rates of Wood Decomposition Catalyzed by Zinc Chloride. *Energy and Fuels* **2008**, *22* (1), 663–670. <https://doi.org/10.1021/ef700464s>.
- (124) Patwardhan, P. R.; Satrio, J. A.; Brown, R. C.; Shanks, B. H. Influence of Inorganic Salts on the Primary Pyrolysis Products of Cellulose. *Bioresour. Technol.* **2010**, *101* (12), 4646–4655. <https://doi.org/10.1016/j.biortech.2010.01.112>.
- (125) Kostetskyy, P.; Coile, M. W.; Terrian, J. M.; Collins, J. W.; Martin, K. J.; Brazdil, J. F.; Broadbelt, L. J. Selective Production of Glycolaldehyde via Hydrothermal Pyrolysis of Glucose: Experiments and Microkinetic Modeling. *J. Anal. Appl. Pyrolysis* **2020**, *149*, 104846. <https://doi.org/10.1016/J.JAAP.2020.104846>.
- (126) Assary, R. S.; Curtiss, L. A. Comparison of Sugar Molecule Decomposition through Glucose and Fructose: A High-Level Quantum Chemical Study. *Energy and Fuels* **2012**, *26* (2), 1344–1352. <https://doi.org/10.1021/ef201654s>.
- (127) Denson, M. D.; Terrell, E.; Kostetskyy, P.; Broadbelt, L.; Ollarte, M.; Garcia-Perez, M. Theoretical Insights on the Fragmentation of Cellulosic Oligomers to Form Hydroxyacetone and Hydroxyacetaldehyde. *Energy and Fuels* **2023**. <https://doi.org/10.1021/acs.energyfuels.3c01924>.
- (128) Mortensen, P. M.; Grunwaldt, J. D.; Jensen, P. A.; Knudsen, K. G.; Jensen, A. D. A Review of Catalytic Upgrading of Bio-Oil to Engine Fuels. *Appl. Catal. A Gen.* **2011**, *407* (1–2), 1–19. <https://doi.org/10.1016/j.apcata.2011.08.046>.
- (129) Yang, Y.; Xu, X.; He, H.; Huo, D.; Li, X.; Dai, L.; Si, C. The Catalytic Hydrodeoxygenation of Bio-Oil for Upgradation from Lignocellulosic Biomass. *Int. J. Biol. Macromol.* **2023**, *242* (May). <https://doi.org/10.1016/j.ijbiomac.2023.124773>.

- (130) Cordero-Lanzac, T.; Rodríguez-Mirasol, J.; Cordero, T.; Bilbao, J. Advances and Challenges in the Valorization of Bio-Oil: Hydrodeoxygenation Using Carbon-Supported Catalysts. *Energy and Fuels* **2021**, *35* (21), 17008–17031. <https://doi.org/10.1021/acs.energyfuels.1c01700>.
- (131) Zhang, M.; Hu, Y.; Wang, H.; Li, H.; Han, X.; Zeng, Y.; Xu, C. C. A Review of Bio-Oil Upgrading by Catalytic Hydrotreatment: Advances, Challenges, and Prospects. *Mol. Catal.* **2021**, *504* (September 2020), 111438. <https://doi.org/10.1016/j.mcat.2021.111438>.
- (132) Furimsky, E. Selection of Catalysts and Reactors for Hydroprocessing. *Appl. Catal. A Gen.* **1998**, *171* (2), 177–206. [https://doi.org/10.1016/S0926-860X\(98\)00086-6](https://doi.org/10.1016/S0926-860X(98)00086-6).
- (133) Choudhary, T. V.; Phillips, C. B. Renewable Fuels via Catalytic Hydrodeoxygenation. *Appl. Catal. A Gen.* **2011**, *397* (1–2), 1–12. <https://doi.org/10.1016/j.apcata.2011.02.025>.
- (134) Lin, F.; Xu, M.; Ramasamy, K. K.; Li, Z.; Klinger, J. L.; Schaidle, J. A.; Wang, H. Catalyst Deactivation and Its Mitigation during Catalytic Conversions of Biomass. *ACS Catal.* **2022**, *12* (21), 13555–13599. <https://doi.org/10.1021/acscatal.2c02074>.
- (135) Kerr, J. A. Bond Dissociation Energies by Kinetic Methods. **1970**, *227* (5256), 419–419. <https://doi.org/10.1038/227419a0>.
- (136) Han, Y.; Pires, A. P. P.; Garcia-Perez, M. Co-Hydrotreatment of the Bio-Oil Lignin-Rich Fraction and Vegetable Oil. *Energy and Fuels* **2020**, *34* (1), 516–529. <https://doi.org/10.1021/acs.energyfuels.9b03344>.
- (137) Furimsky, E. Catalytic Hydrodeoxygenation. *Appl. Catal. A Gen.* **2000**, *199* (2), 147–190. [https://doi.org/10.1016/S0926-860X\(99\)00555-4](https://doi.org/10.1016/S0926-860X(99)00555-4).
- (138) Wang, Y.; Wu, J.; Wang, S. Hydrodeoxygenation of Bio-Oil over Pt-Based Supported Catalysts: Importance of Mesopores and Acidity of the Support to Compounds with

- Different Oxygen Contents. *RSC Adv.* **2013**, 3 (31), 12635–12640.
<https://doi.org/10.1039/c3ra41405a>.
- (139) Qu, L.; Jiang, X.; Zhang, Z.; Zhang, X. G.; Song, G. Y.; Wang, H. L.; Yuan, Y. P.; Chang, Y. L. A Review of Hydrodeoxygenation of Bio-Oil: Model Compounds, Catalysts, and Equipment. *Green Chem.* **2021**, 23 (23), 9348–9376. <https://doi.org/10.1039/d1gc03183j>.
- (140) Lee, C. R.; Yoon, J. S.; Suh, Y. W.; Choi, J. W.; Ha, J. M.; Suh, D. J.; Park, Y. K. Catalytic Roles of Metals and Supports on Hydrodeoxygenation of Lignin Monomer Guaiacol. *Catal. Commun.* **2012**, 17, 54–58. <https://doi.org/10.1016/j.catcom.2011.10.011>.
- (141) Wan, H.; Chaudhari, R. V.; Subramaniam, B. Aqueous Phase Hydrogenation of Acetic Acid and Its Promotional Effect on P-Cresol Hydrodeoxygenation. *Energy and Fuels* **2013**, 27 (1), 487–493. <https://doi.org/10.1021/ef301400c>.
- (142) Cheah, Y. W.; Salam, M. A.; Arora, P.; Öhrman, O.; Creaser, D.; Olsson, L. Role of Transition Metals on MoS₂-Based Supported Catalysts for Hydrodeoxygenation (HDO) of Propylguaiacol. *Sustain. Energy Fuels* **2021**, 5 (7), 2097–2113.
<https://doi.org/10.1039/d1se00184a>.
- (143) Olivas, A.; Zepeda, T. A.; Villalpando, I.; Fuentes, S. Performance of Unsupported Ni(Co,Fe)/MoS₂ Catalysts in Hydrotreating Reactions. *Catal. Commun.* **2008**, 9 (6), 1317–1328. <https://doi.org/10.1016/j.catcom.2007.11.025>.
- (144) Yin, W.; Venderbosch, R. H.; Alekseeva, M. V.; Figueirêdo, M. B.; Heeres, H.; Khromova, S. A.; Yakovlev, V. A.; Cannilla, C.; Bonura, G.; Frusteri, F.; Heeres, H. J. Hydrotreatment of the Carbohydrate-Rich Fraction of Pyrolysis Liquids Using Bimetallic Ni Based Catalyst: Catalyst Activity and Product Property Relations. *Fuel Process. Technol.* **2018**, 169 (October 2017), 258–268.

- <https://doi.org/10.1016/j.fuproc.2017.10.006>.
- (145) Ruddy, D. A.; Schaidle, J. A.; Ferrell, J. R.; Wang, J.; Moens, L.; Hensley, J. E. *Recent Advances in Heterogeneous Catalysts for Bio-Oil Upgrading via “Ex Situ Catalytic Fast Pyrolysis”*: Catalyst Development through the Study of Model Compounds; 2014; Vol. 16. <https://doi.org/10.1039/c3gc41354c>.
- (146) Sitthisa, S.; Resasco, D. E. Hydrodeoxygenation of Furfural over Supported Metal Catalysts: A Comparative Study of Cu, Pd and Ni. *Catal. Letters* **2011**, *141* (6), 784–791. <https://doi.org/10.1007/s10562-011-0581-7>.
- (147) Elliott, D. C.; Hart, T. R.; Neuenschwander, G. G.; Rotness, L. J.; Olarte, M. V.; Zacher, A. H.; Solantausta, Y. Catalytic Hydroprocessing of Fast Pyrolysis Bio-Oil from Pine Sawdust. *Energy and Fuels* **2012**, *26* (6), 3891–3896. <https://doi.org/10.1021/ef3004587>.
- (148) Elliott, D. C. Historical Developments in Hydroprocessing Bio-Oils. *Energy and Fuels* **2007**, *21* (3), 1792–1815. <https://doi.org/10.1021/ef070044u>.
- (149) Han, Y.; Gholizadeh, M.; Tran, C. C.; Kaliaguine, S.; Li, C. Z.; Olarte, M.; Garcia-Perez, M. Hydrotreatment of Pyrolysis Bio-Oil: A Review. *Fuel Process. Technol.* **2019**, *195* (May). <https://doi.org/10.1016/j.fuproc.2019.106140>.
- (150) Hansen, S.; Mirkouei, A.; Diaz, L. A. A Comprehensive State-of-Technology Review for Upgrading Bio-Oil to Renewable or Blended Hydrocarbon Fuels. *Renew. Sustain. Energy Rev.* **2020**, *118* (October 2019), 109548. <https://doi.org/10.1016/j.rser.2019.109548>.
- (151) Zhang, M.; Hu, Y.; Wang, H.; Li, H.; Han, X.; Zeng, Y.; Xu, C. C. A Review of Bio-Oil Upgrading by Catalytic Hydrotreatment: Advances, Challenges, and Prospects. *Mol. Catal.* **2021**, *504* (September 2020). <https://doi.org/10.1016/j.mcat.2021.111438>.
- (152) Pujro, R.; García, J. R.; Bertero, M.; Falco, M.; Sedran, U. Review on Reaction Pathways

- in the Catalytic Upgrading of Biomass Pyrolysis Liquids. *Energy and Fuels* **2021**, *35* (21), 16943–16964. <https://doi.org/10.1021/acs.energyfuels.1c01931>.
- (153) Gea, S.; Hutapea, Y. A.; Piliang, A. F. R.; Pulungan, A. N.; Rahayu, R.; Layla, J.; Tikoalu, A. D.; Wijaya, K.; Saputri, W. D. A Comprehensive Review of Experimental Parameters in Bio-Oil Upgrading from Pyrolysis of Biomass to Biofuel Through Catalytic Hydrodeoxygenation. *Bioenergy Res.* **2023**, *16* (1), 325–347. <https://doi.org/10.1007/s12155-022-10438-w>.
- (154) Gholizadeh, M.; Zhang, S.; Hu, X.; Wang, Y. Advances and Perspectives of Bio-Oil Hydrotreatment for Biofuel Production. *Energy and Fuels* **2023**, *37* (14), 10134–10154. <https://doi.org/10.1021/acs.energyfuels.3c01647>.
- (155) Nolte, M. W.; Saraeian, A.; Shanks, B. H. Hydrodeoxygenation of Cellulose Pyrolysis Model Compounds Using Molybdenum Oxide and Low Pressure Hydrogen. *Green Chem.* **2017**, *19* (15), 3654–3664. <https://doi.org/10.1039/c7gc01477e>.
- (156) Hočevar, B.; Grilc, M.; Huš, M.; Likozar, B. Mechanism, Ab Initio Calculations and Microkinetics of Hydrogenation, Hydrodeoxygenation, Double Bond Migration and Cis–Trans Isomerisation during Hydrotreatment of C6 Secondary Alcohol Species and Ketones. *Appl. Catal. B Environ.* **2017**, *218*, 147–162. <https://doi.org/10.1016/j.apcatb.2017.06.046>.
- (157) Ruinart De Brimont, M.; Dupont, C.; Daudin, A.; Geantet, C.; Raybaud, P. Deoxygenation Mechanisms on Ni-Promoted MoS₂ Bulk Catalysts: A Combined Experimental and Theoretical Study. *J. Catal.* **2012**, *286*, 153–164. <https://doi.org/10.1016/j.jcat.2011.10.022>.
- (158) Dupont, C.; Lemeur, R.; Daudin, A.; Raybaud, P. Hydrodeoxygenation Pathways

- Catalyzed by MoS₂ and NiMoS Active Phases: A DFT Study. *J. Catal.* **2011**, 279 (2), 276–286. <https://doi.org/10.1016/j.jcat.2011.01.025>.
- (159) Vispute, T. P.; Huber, G. W. Production of Hydrogen, Alkanes and Polyols by Aqueous Phase Processing of Wood-Derived Pyrolysis Oils. *Green Chem.* **2009**, 11 (9), 1433–1445. <https://doi.org/10.1039/b912522c>.
- (160) Sanna, A.; Vispute, T. P.; Huber, G. W. Hydrodeoxygenation of the Aqueous Fraction of Bio-Oil with Ru/C and Pt/C Catalysts. *Appl. Catal. B Environ.* **2015**, 165, 446–456. <https://doi.org/10.1016/j.apcatb.2014.10.013>.
- (161) Adams, P.; Bridgwater, T.; Lea-Langton, A.; Ross, A.; Watson, I. *Biomass Conversion Technologies*; Elsevier Inc., 2017. <https://doi.org/10.1016/B978-0-08-101036-5.00008-2>.
- (162) Elliott, D. C.; Neuenschwander, G. G.; Hart, T. R. Hydroprocessing Bio-Oil and Products Separation for Coke Production. *ACS Sustain. Chem. Eng.* **2013**, 1 (4), 389–392. <https://doi.org/10.1021/sc300103y>.
- (163) Adkins, H.; Connor, R. Hydrogenolysis of Oxygenated Organic Compounds. **1932**, 54 (1931).
- (164) Sinfelt, J. H. Catalytic Hydrogenolysis over Supported Metals. *Catal. Rev.* **1970**, 3 (1), 175–205. <https://doi.org/10.1080/01614947008076859>.
- (165) Wang, Y.; Zhou, J.; Guo, X. Catalytic Hydrogenolysis of Glycerol to Propanediols: A Review. *RSC Adv.* **2015**, 5 (91), 74611–74628. <https://doi.org/10.1039/c5ra11957j>.
- (166) Dasari, M. A.; Kiatsimkul, P. P.; Sutterlin, W. R.; Suppes, G. J. Low-Pressure Hydrogenolysis of Glycerol to Propylene Glycol. *Appl. Catal. A Gen.* **2005**, 281 (1–2), 225–231. <https://doi.org/10.1016/j.apcata.2004.11.033>.
- (167) Oasmaa, A.; Kuoppala, E.; Ardiyanti, A.; Venderbosch, R. H.; Heeres, H. J.

- Characterization of Hydrotreated Fast Pyrolysis Liquids. *Energy and Fuels* **2010**, *24* (9), 5264–5272. <https://doi.org/10.1021/ef100573q>.
- (168) Elliott, D. C.; Baker, E. G. Method for Upgrading Biomass Pyrolyzates. **1989**, No. 19.
- (169) Elliott, D. C.; Beckman, D.; Bridgewater, A. V.; Diebold, J. P.; Gevert, S. B.; Solantausta, Y. Developments in Direct Thermochemical Liquefaction of Biomass:1983-1990. *Energy & Fuels* **1991**, *5*, 399–410.
- (170) Gagnon, J.; Kaliaguine, S. Catalytic Hydrotreatment of Vacuum Pyrolysis Oils from Wood. *Ind. Eng. Chem. Res.* **1988**, *27* (10), 1783–1788.
<https://doi.org/10.1021/ie00082a008>.
- (171) Şenol, O. I.; Ryymin, E. M.; Viljava, T. R.; Krause, A. O. I. Reactions of Methyl Heptanoate Hydrodeoxygenation on Sulphided Catalysts. *J. Mol. Catal. A Chem.* **2007**, *268* (1–2), 1–8. <https://doi.org/10.1016/j.molcata.2006.12.006>.
- (172) Wildschut, J.; Arentz, J.; Rasrendra, C. B.; Venderbosch, R. H.; Heeres, H. J. Catalytic Hydrotreatment of Fast Pyrolysis Oil: Model Studies on Reaction Pathways for the Carbohydrate Fraction. *Environ. Prog. Sustain. Energy* **2009**, *28* (3), 450–460.
<https://doi.org/10.1002/EP.10390>.
- (173) Garcia-Perez, M.; Wang, X. S.; Shen, J.; Rhodes, M. J.; Tian, F.; Lee, W. J.; Wu, H.; Li, C. Z. Fast Pyrolysis of Oil Mallee Woody Biomass: Effect of Temperature on the Yield and Quality of Pyrolysis Products. *Ind. Eng. Chem. Res.* **2008**, *47* (6), 1846–1854.
<https://doi.org/10.1021/ie071497p>.
- (174) Hu, X.; Zhang, Z.; Gholizadeh, M.; Zhang, S.; Lam, C. H.; Xiong, Z.; Wang, Y. Coke Formation during Thermal Treatment of Bio-Oil. *Energy and Fuels* **2020**, *34* (7), 7863–7914. <https://doi.org/10.1021/acs.energyfuels.0c01323>.

- (175) Gholizadeh, M.; Gunawan, R.; Hu, X.; De Miguel Mercader, F.; Westerhof, R.; Chaitwat, W.; Hasan, M. M.; Mourant, D.; Li, C. Z. Effects of Temperature on the Hydrotreatment Behaviour of Pyrolysis Bio-Oil and Coke Formation in a Continuous Hydrotreatment Reactor. *Fuel Process. Technol.* **2016**, *148*, 175–183.
<https://doi.org/10.1016/j.fuproc.2016.03.002>.
- (176) Li, Y.; Zhang, C.; Liu, Y.; Hou, X.; Zhang, R.; Tang, X. Coke Deposition on Ni/HZSM-5 in Bio-Oil Hydrodeoxygenation Processing. *Energy and Fuels* **2015**, *29* (3), 1722–1728.
<https://doi.org/10.1021/ef5024669>.
- (177) Qiao, Z.; Wang, Z.; Zhang, C.; Yuan, S.; Zhu, Y.; Wang, J. PVAm–PIP/PS Composite Membrane with High Performance for CO₂/N₂ Separation. *AIChE J.* **2012**, *59* (4), 215–228. <https://doi.org/10.1002/aic>.
- (178) Venderbosch, R. H.; Ardiyanti, A. R.; Wildschut, J.; Oasmaa, A.; Heeres, H. J. Stabilization of Biomass-Derived Pyrolysis Oils. *J. Chem. Technol. Biotechnol.* **2010**, *85* (5), 674–686. <https://doi.org/10.1002/jctb.2354>.
- (179) Xu, X.; Zhang, C.; Liu, Y.; Zhai, Y.; Zhang, R. Two-Step Catalytic Hydrodeoxygenation of Fast Pyrolysis Oil to Hydrocarbon Liquid Fuels. *Chemosphere* **2013**, *93* (4), 652–660.
<https://doi.org/10.1016/j.chemosphere.2013.06.060>.
- (180) Czernik, S.; Johnson, D. K.; Black, S. Stability of Wood Fast Pyrolysis Oil. *Biomass and Bioenergy* **1994**, *7* (1–6), 187–192. [https://doi.org/10.1016/0961-9534\(94\)00058-2](https://doi.org/10.1016/0961-9534(94)00058-2).
- (181) Fratini, E.; Bonini, M.; Oasmaa, A.; Solantausta, Y.; Teixeira, J.; Baglioni, P. SANS Analysis of the Microstructural Evolution during the Aging of Pyrolysis Oils from Biomass. *Langmuir* **2006**, *22* (1), 306–312. <https://doi.org/10.1021/la051990a>.
- (182) Lu, Q.; Yang, X. L.; Zhu, X. F. Analysis on Chemical and Physical Properties of Bio-Oil

- Pyrolyzed from Rice Husk. *J. Anal. Appl. Pyrolysis* **2008**, 82 (2), 191–198.
<https://doi.org/10.1016/j.jaap.2008.03.003>.
- (183) Diebold, J. P. A Review of the Chemical and Physical Mechanisms of the Storage Stability of Fast Pyrolysis Bio-Oils. *Nrel/Sr-570-27613* **2000**, No. January, 59.
- (184) Kadarwati, S.; Oudenhoven, S.; Schagen, M.; Hu, X.; Garcia-Perez, M.; Kersten, S.; Li, C. Z.; Westerhof, R. Polymerization and Cracking during the Hydrotreatment of Bio-Oil and Heavy Fractions Obtained by Fractional Condensation Using Ru/C and NiMo/Al₂O₃ Catalyst. *J. Anal. Appl. Pyrolysis* **2016**, 118, 136–143.
<https://doi.org/10.1016/j.jaap.2016.01.011>.
- (185) Gao, X.; Xu, Q.; Hu, X.; Shao, Y.; Gao, G.; Zhang, S.; Wang, Z.; Zhang, L. Hydrothermal Treatment of Furfural and Sugar Monomers and Oligomers: A Model-Compound Approach to Probe the Cross-Polymerization Reactions in Heating Bio-Oil. *Biomass Convers. Biorefinery* **2022**, No. 0123456789. <https://doi.org/10.1007/s13399-022-02503-3>.
- (186) Zhang, L.; Hu, X.; Li, C.; Zhang, S.; Wang, Y.; Esmaili, V.; Gholizadeh, M. Fates of Heavy Organics of Bio-Oil in Hydrotreatment: The Key Challenge in the Way from Biomass to Biofuel. *Sci. Total Environ.* **2021**, 778, 146321.
<https://doi.org/10.1016/j.scitotenv.2021.146321>.
- (187) Pollard, A. S.; Rover, M. R.; Brown, R. C. Characterization of Bio-Oil Recovered as Stage Fractions with Unique Chemical and Physical Properties. *J. Anal. Appl. Pyrolysis* **2012**, 93, 129–138. <https://doi.org/10.1016/j.jaap.2011.10.007>.
- (188) Furimsky, E. Catalytic Hydrodeoxygenation. *Appl. Catal. A Gen.* **2000**, 199 (2), 147–190.
[https://doi.org/10.1016/S0926-860X\(99\)00555-4](https://doi.org/10.1016/S0926-860X(99)00555-4).

- (189) Cai, Q.; Xu, J.; Zhang, S. Upgrading of Bio-Oil Aqueous Fraction by Dual-Stage Hydrotreating-Cocracking with Methanol. *ACS Sustain. Chem. Eng.* **2017**, *5* (7), 6329–6342. <https://doi.org/10.1021/acssuschemeng.7b01505>.
- (190) Kadarwati, S. Coke Formation during the Hydrotreatment of Bio-Oil. **2016**, No. September, 60.
- (191) Furimsky, E. Chemistry of Catalytic Hydrodeoxygenation. *Catal. Rev.* **1983**, *25* (3), 421–458. <https://doi.org/10.1080/01614948308078052>.
- (192) Cordero-Lanzac, T.; Palos, R.; Hita, I.; Arandes, J. M.; Rodríguez-Mirasol, J.; Cordero, T.; Bilbao, J.; Castaño, P. Revealing the Pathways of Catalyst Deactivation by Coke during the Hydrodeoxygenation of Raw Bio-Oil. *Appl. Catal. B Environ.* **2018**, *239* (July), 513–524. <https://doi.org/10.1016/j.apcatb.2018.07.073>.
- (193) Tang, Z.; Lu, Q.; Zhang, Y.; Zhu, X.; Guo, Q. One Step Bio-Oil Upgrading through Hydrotreatment, Esterification, and Cracking. *Ind. Eng. Chem. Res.* **2009**, *48* (15), 6923–6929. <https://doi.org/10.1021/ie900108d>.
- (194) Wang, H.; Wang, Y. Characterization of Deactivated Bio-Oil Hydrotreating Catalysts. *Top. Catal.* **2016**, *59* (1), 65–72. <https://doi.org/10.1007/s11244-015-0506-6>.

CHAPTER THREE: ELUCIDATION OF STRUCTURE AND PHYSICAL PROPERTIES OF
PYROLYTIC SUGAR OLIGOMERS DERIVED FROM CELLULOSE
DEPOLYMERIZATION/DEHYDRATION REACTIONS: A
DENSITY FUNCTIONAL THEORY STUDY

Denson, M. D., Terrell, E., Kostetskyy, P., Olarte, M., Broadbelt, L., & Garcia-Perez, M. (2023). Elucidation of Structure and Physical Properties of Pyrolytic Sugar Oligomers Derived from Cellulose Depolymerization/Dehydration Reactions: A Density Functional Theory Study. *Energy & Fuels*, 37(11), 7834-7847. <https://doi.org/10.1021/acs.energyfuels.3c00641>

Originally published in the *Energy & Fuels* and reproduced here.

Attributions:

- ✓ M. Denson – concept, computations/investigation, analysis of data, writing of first draft
- ✓ E. Terrell – concept, computational help/investigation and review and editing of drafts
- ✓ P. Kostetskyy – concept, computational help/investigation, review and editing of drafts
- ✓ M. Olarte – concept, review and editing of drafts, supervision
- ✓ L. Broadbelt – computational help, supervision
- ✓ M. Garcia-Perez – concept, review and editing of drafts, supervision

Abstract

Fast pyrolysis of lignocellulosic materials is a promising research area to produce renewable fuels and chemicals. Dehydration is known to be among the most important reaction families during cellulose pyrolysis; water is the most important product. Together with water, dehydration reactions also form a range of poorly known oligomer species of varying molecular sizes, often collected as part of the bio-oil water-soluble (WS) fraction. In this work, we used electronic structure calculations to evaluate the relative thermodynamic stabilities of several oligomer species from cellulose depolymerization intermediates undergoing three consecutive dehydration events. A library of the thermodynamically favored candidate molecular structures was compiled. Results revealed that most of the water molecules are eliminated from the non-reducing end, forming thermodynamically more stable conjugated compounds. This is consistent with results reported in literature where dehydration reactions occur preferably at the non-reducing ends of oligomers. The theoretical FTIR and NMR spectra of these proposed sugar oligomers conform qualitatively to the experimental result of pyrolytic sugars. Understanding their chemical structure could help to develop rational strategies to mitigate coke formation as sugars are often blamed to cause coke formation during bio-oil refining. The estimated physical-chemical properties (boiling point, melting point, Gibbs free energy of formation, enthalpy of formation, and solubility parameters among others) are also fundamental to conducting first principle engineering calculations to design and analyze new pyrolysis reactors and bio-oil upgrading units.

3.1 Introduction

Continued global population growth, industrialization, environmental concerns, and depletion of fossil fuel reserves demand the diversification of our energy portfolio.^{1,2,3} Lignocellulosic biomass, abundant, inexpensive, and non-competing for food resources, is a renewable source of C to produce fuels and chemicals. Cellulose is the most abundant biomolecule synthesized by photosynthesis.^{4,5,6} It is composed of repeating D-glucose units connected by β -1-4 glycosidic bonds.^{7,8} Cellulose can be decomposed into various chemical species through different methods including thermal decomposition (for example, fast pyrolysis).³

Fast pyrolysis is a promising conversion method where biomass is subjected to moderately high temperatures (673 to 873 K) without oxygen.^{9,10} Several chemical transformations occur in a complex network of chemical reactions as the cellulose polymer chain breaks apart. During fast pyrolysis, dehydration reactions result in water formation and poorly known anhydrous-sugars.^{11,12,13} This is coherent with the experimental results from Stankovikj et al.¹⁴ Terrell and Garcia-Perez¹⁵ compared experimental results with hypothetical pathways and assigned tentative chemical structures to the dehydrated oligomers observed by Fourier transform ion cyclotron resonance mass spectrometry (FT-ICR MS).

While experimental results give significant insights regarding molecular mass and elemental composition of anhydrosugars, complementing these results with first principle calculations could generate new information on the reaction mechanisms and molecular structure of pyrolysis products. Hu et al.¹⁶ and Kostetsky and Broadbelt¹⁷ discussed the recent developments in using electronic structure calculations to assess the mechanisms of biomass pyrolysis via quantum chemistry (QC). They concluded that the use of QC modeling provides

deep insights to obtain a whole image of the complex biomass pyrolysis chemistry (for both reaction mechanisms and product structures) which are experimentally difficult to grasp. Nimlos et al.^{18,19} used electronic structure calculations to study the dehydration mechanism of alcohols and glycerol and concluded that their work could be extended for carbohydrates. Hosoya and Sakaki²⁰ investigated the formation of levoglucosan using dimer and hexamer oligomeric carbohydrate models to represent the native cellulose. Results of their study showed that dimer degradation occurs by means of a concerted mechanism. The one-chain hexamer model showed no formation of levoglucosan instead depolymerization occurred; two-chain models with interchain H bonds clearly showed the formation of levoglucosan; and three-chain models indicated selective degradation on the crystalline surface. Easton et al.¹³ studied four water loss mechanisms of glucose and cellobiose during cellulose-fast pyrolysis. Their results showed that aldol condensation has the lowest free energy barrier which is consistent with cellobiose, and therefore could be applicable to glucooligosaccharides with a higher degree of polymerization. Zhang et al.²¹ modeled the mechanism of levoglucosan thermal decomposition during pyrolysis employing direct C-C bond breaking, C-O bond breaking, and 1,2-dehydration and found that the latter is the most favorable pathway, removing the hydroxyl group from C2 and a hydrogen atom from C3. These computational works contribute toward a comprehensive understanding of the elementary reaction mechanisms of cellulose and could pave ways to further study the heavy unknown oligomeric fractions of the bio-oil.

The presence of anhydrosugar oligomers in bio-oil formed during cellulose pyrolysis was discussed by Mamleev et al.²² The study of Pecha et al.²³ on the fast pyrolysis of hybrid poplar between 0.4 and 100 kPa revealed the effect of pressure on the formation of bio-oil anhydrosugars. Stankovikj et al.¹⁴ also confirmed the presence of highly dehydrated oligomeric

sugars in fast pyrolysis from cellulose using FT-ICR/MS. The mechanistic modeling of fast pyrolysis of neat glucose-based carbohydrates by Zhou et al.²⁴ predicted the formation of anhydrosugar products. These pyrolytic sugars are becoming an important field of research because they can be converted easily to platform chemicals such as furanics.^{25,26}

The thermodynamic and physical properties of these compounds, such as boiling point, critical temperature, and pressure, enthalpy of formation and vaporization, enthalpy of fusion, standard Gibbs free energy of formation, solubility parameters, etc. are fundamental to understanding their behavior in the mixtures and needed for the design of extraction/conversion, separation, and upgrading processes.²⁷ In the absence of experimental data due to cost or time constraint, methods for estimation of thermophysical properties of compounds must rely on theoretical tools, such as quantum mechanics, empirical correlations, and group additivity-based methods. Estimation methods usually apply the concepts of quantitative structure-property relationships (QSPRs) and quantitative property-property relationships (QPPRs), varying by the type of input data. QSPR methods require only knowledge of the molecular structures of the compound to estimate their physical properties while QPPR uses thermodynamic data.²⁸ The group contribution method (GCM), a special case of QSPR approach, is a simple, quick and extensively used technique that relies on the additivity principle of individual group contributions.²⁹ The best known GCM include the first-order approximations by Joback,³⁰ Joback & Reid et al.⁶⁰, Lydersen et al.⁵⁵, and Stein and Brown.³¹ These authors developed mathematical models employing multiple linear regression techniques to determine the group contributions from each fragment.

In this work, we aim to elucidate and propose potential structures of the oligomeric sugar compounds found in bio-oil through electronic structure calculations and then estimate their

physical and thermodynamic properties. Dehydrated sugars, particularly levoglucosan, being the main product of fast cellulose pyrolysis,^{32,33} and its oligomeric units (up to tetra-state), linked by 1,4- β -glycosidic bonds, were used as the starting model compounds. An in-depth understanding of these compounds' structure will contribute to developing and advancing biomass pyrolysis techniques and product upgrading strategies, especially hydrotreatment where coke formation is believed to be caused by the presence of sugar oligomers.

3.2 Methodology

3.2.1 Computational Details

The model compounds, shown in Figure 3.1, were subjected to dehydration reaction by means of the Maccoll elimination mechanism (otherwise known as 1-2 dehydration), where a C-O bond is broken with a concerted proton loss from a beta position, moving to the oxygen atom to form a C=C (double bond) and eliminate water.¹³ Sequential dehydrations (up to 3x) of these model compounds were completed in the gas phase with and typical fast pyrolysis temperature of 773.15 K and pressure of 1 atm. All possible pathway permutations eliminating water around the model molecules were investigated. For example, the double dehydration of the cellobiosan water molecule is eliminated from the levoglucosan-end (LG-end) and the second, from the nonreducing-end (NR-end). Another possible route is eliminating both water molecules from the same ring structure. It should be noted that the kinetics of these dehydration events was not considered, only the relative thermodynamics stabilities of the different isomers were studied as the study focused more on the structure of the final product and not the rate of reaction. The most thermodynamically stable structure has the minimum Gibbs free energy, and these calculated stabilities also provide information on whether the reaction is endothermic or exothermic. Though, kinetics is also a good parameter to consider for future studies.

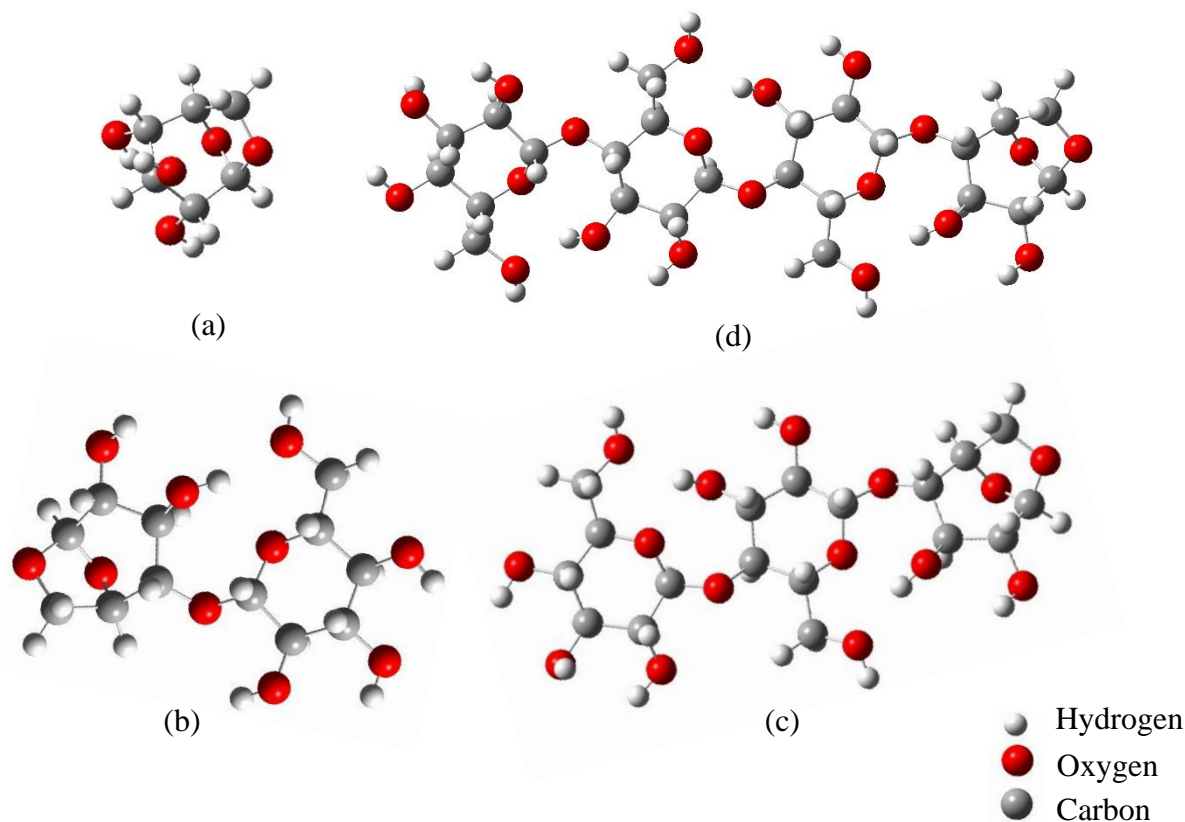


Figure 3.1: Optimized structures of the model compounds: (a) levoglucosan, (b) cellobiosan, (c) cellotriosan, and (d) celloquatrostan.

A systematic naming convention was assigned to identify the reactants, intermediates, and products. LG was used for levoglucosan, CBN for cellobiosan, CTN for cellotriosan, and CQN for celloquatrostan. Citing CBN34A as an example, CBN stands for cellobiosan as the name of the molecule under study; A refers to ring 1 being the LG-end, the first number “3” specifies the carbon position where the hydroxyl group is removed, and the second number “4” identifies the hydrogen atom being eliminated. This numbering convention is illustrated in Figure 3.2.

Geometry optimization and frequency calculations of all reactants, intermediates, and products were performed using the Gaussian 16 (Revision C.01) electronic structure code.⁶¹ Errors associated with the calculations of structure and electronic properties include the inaccurate description of electron correlation, anharmonicity, and the solvation of the Schrodinger equation³⁴ but can be corrected by using scaling factors to obtain a more accurate result. The choice of correct functionals and basis set are then important to consider. M05-2X hybrid functional³⁵ is recommended for carbohydrates but we employed the newer version, M06-2X³⁶ and 6-311++G(d,p) basis set for the O, C, and H atoms. Each converged geometry was verified with vibrational frequency calculations for all structures. A scaling factor of 0.9567 was used for the calculated vibrational frequencies, based on the work of Unal et al.³⁴ The change in free energy for subsequent dehydration events of the model compounds was calculated according to Equation 1 where $E_{\text{deh, H}_2\text{O}}$ corresponds to the

$$E_{\text{deh, H}_2\text{O}} - E_{\text{carb}} \quad (1)$$

energy of the dehydrated carbohydrate-H₂O complex and E_{carb} is the energy of the reacting carbohydrate. The structure of the reactant carbohydrate used for each subsequent dehydration event was then that of a carbohydrate-only, assuming desorption of water.

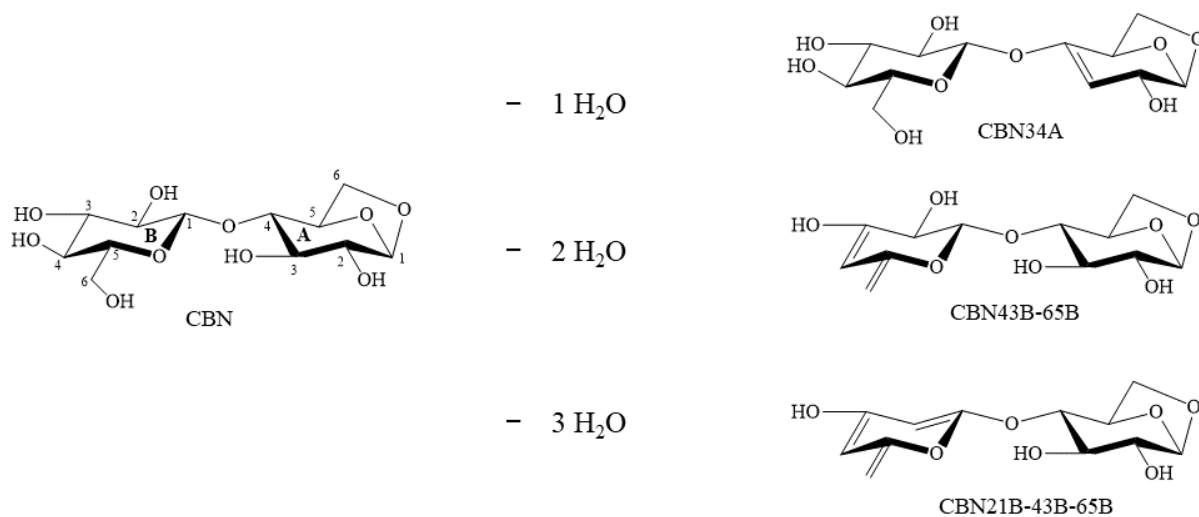


Figure 3.2: Sequential dehydration and numbering scheme for CBN. CBN stands for cellobiosan, A is for the LG-end, and B for the NR-end (in the case of cellotriosan, B is for the internal unit and C for the NR-end, the same pattern was followed for celloquatrosan).

With the optimized and most stable product structures being identified, the theoretical Nuclear Magnetic Resonance (both $^1\text{H-NMR}$ and $^{13}\text{C-NMR}$) spectra was calculated using the M06-2X hybrid functional, 6-311+G(d,p) basis set, and the Gauge-Independent Atomic Orbital (GIAO) method. It is necessary to understand that nuclear magnetic resonance (NMR) spectra strongly depend on the molecular structure since they are constantly in motion. Thus, we make sure to use the lowest energy structure of the molecule of interest to generate the NMR spectra of the stable products. Also, NMR spectra of the typically used reference molecule, deuterated dimethyl sulfoxide (DMSO), was calculated and the shielding value was subtracted from the spectrum of the stable products to obtain the relative shifts. Theoretical results may slightly vary for different functionals and basis sets and the type of reference molecule employed for NMR calculations.

3.2.2 Validation of Simulations

Selected model compounds, namely D-glucose (Dextrose) anhydrous ($\geq 99\%$, Thermo Scientific Chemicals), D(+)-mannose ($\geq 99\%$, Sigma Aldrich), and levoglucosan (99.3%, AK Scientific, Inc.) were subjected to both experimental and theoretical Fourier-Transform Infrared Spectroscopy (FTIR) and NMR analyses to assess the validity of the modeling results.

Experimental FTIR results were recorded in the solid phase using a Shimadzu IRPrestige 21 spectrometer equipped with a MIRacle single reflection ATR Ge probe. Enough samples were applied to cover the crystal window for measurement. Spectra were acquired at 600-4000 cm^{-1} and a resolution of 4 cm^{-1} but only the fingerprint region is shown in Figure 3.3. Modeling results were calculated in the gas phase employing the same method described earlier.

Comparable results were observed between the experimental and modeling for the model compounds, as shown in Figure 3.3. The sum of areas under the bands from 950 to 1200 cm^{-1} wavenumbers are assigned to C-O stretch vibrations of alcohols.^{37,38} The calculated spectra are harmonic frequencies and thus shifted to a higher energy than the experimental spectra.³⁹

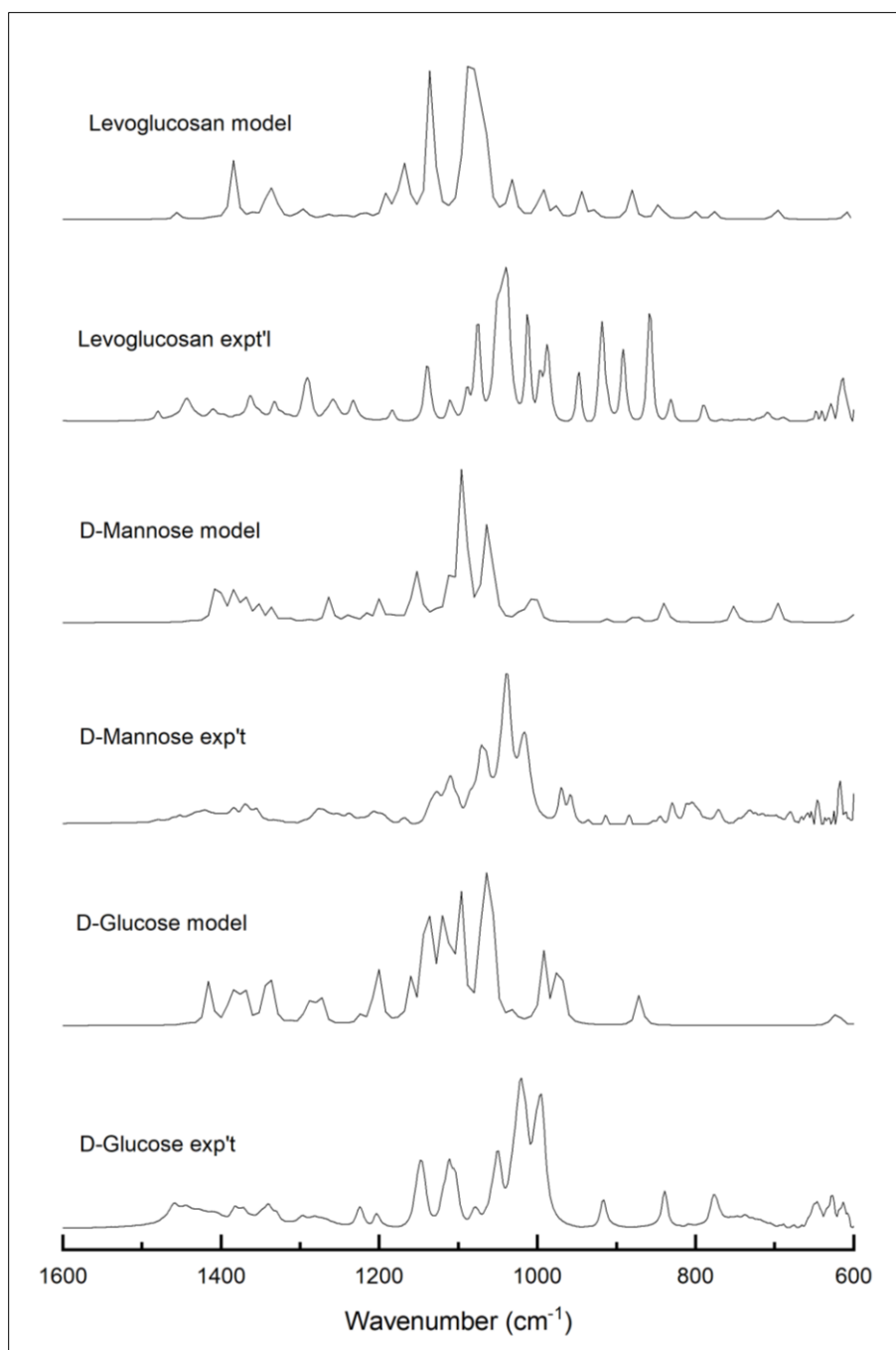


Figure 3.3: Comparison between experimental and modeled FTIR spectra of selected sugars.

Experimental ^{13}C -NMR and ^1H -NMR of the whole sugar were also obtained and compared with modeling yields. Pyrolytic sugars were separated from the whole bio-oil (BTG, The Netherlands) by means of cold-water precipitation⁴⁰ followed by column chromatography (Sepabeads SP207)⁴¹ to separate the sugars from phenols and finally rotary evaporation to concentrate the sugars. The ^{13}C -NMR spectra were acquired on a Bruker 500 Neo spectrometer equipped with a 5 mm Prodigy broadband cryoprobe with Z-axis gradients. An amount of 30 mg each of the selected model compounds was dissolved in 0.7 ml of DMSO- d_6 (99.9%, Cambridge Isotope Laboratories, Inc.). The ^{13}C -NMR spectra were acquired at 125.77 MHz with 90° pulse angle (10.0 ms), 1.08 s acquisition time, relaxation delay d_1 of 2 s, and inverse-gated ^1H composite pulse decoupling using 4000 scans, a spectral width of 30120.5 Hz and 32768 points. The FID was apodized with 8 Hz exponential line broadening for the model compounds. MestreNova 14.3.0 software was used for post processing spectra. Results (Figure 3.4) showed a good agreement between the experimental and modeling yield except for the shifting at 39.7 ppm in experimental results that is attributed to the solvent used (DMSO- d_6). The integration region between 60 to 80 ppm belongs to the aliphatic C-O associated with hydroxyl groups of the sugar compounds.¹²

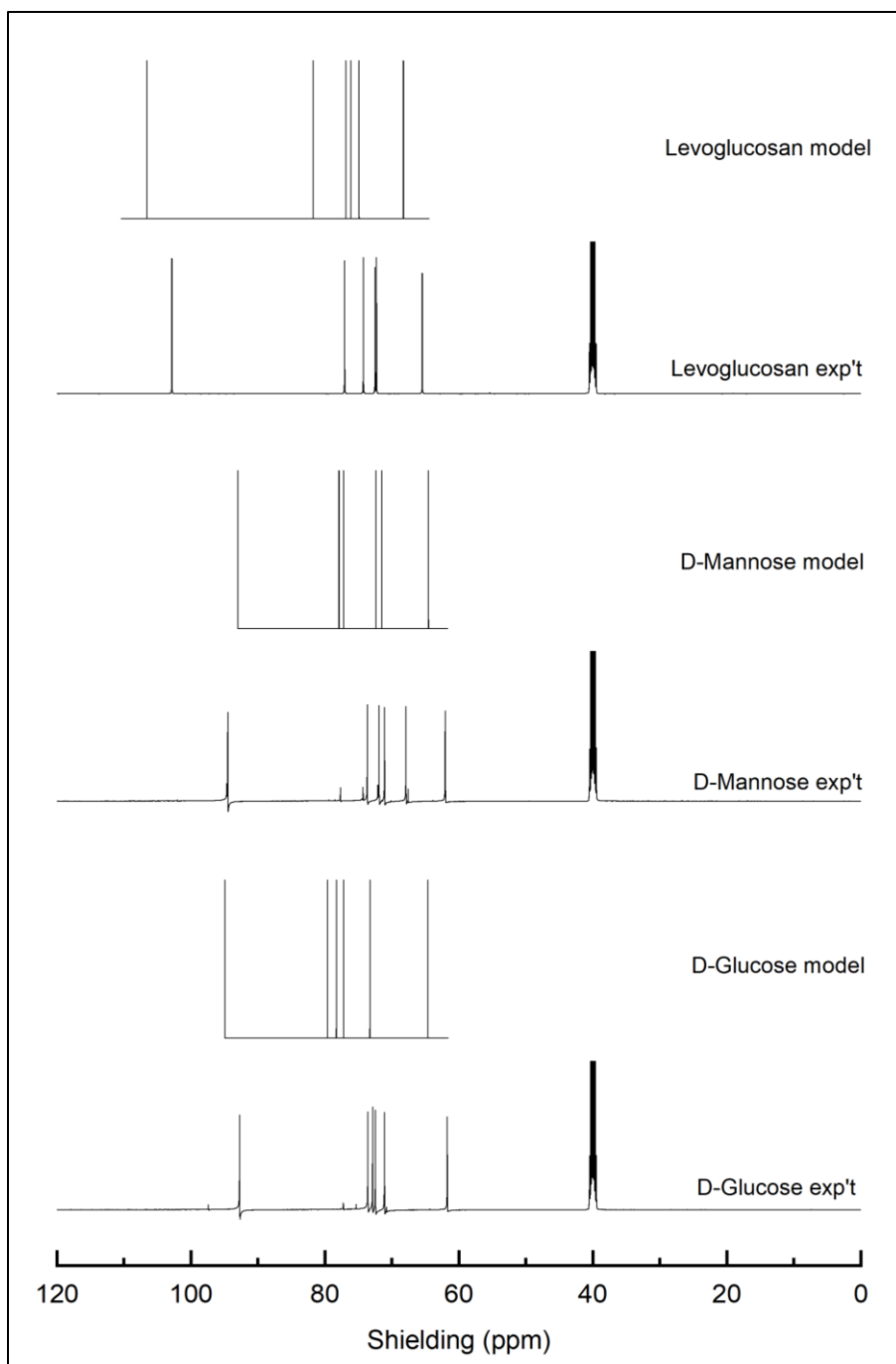


Figure 3.4: Comparison between experimental and modeled ^{13}C -NMR spectra of selected sugars (solvent peak: DMSO = 39.7 ppm).

3.2.3 Estimation of Properties of the Proposed Structures

QPPRs and GCM methods were applied to estimate the important physical and thermodynamic properties of the proposed oligomeric sugar structures. The complete equations and procedures are found elsewhere.⁴² Briefly, the number frequency of each group that constitute the pure compound or mixture was summed up and then multiplied by their corresponding group contribution terms. Among the discrepancies associated with these methods include reliability due to over simplicity of the molecular structures which makes isomers indistinguishable, size of model compounds, and the need of experimental data which may not be always available.²⁷ Therefore, the second-order group contributions was built on the first-order groups to atleast capture more information on the molecular structure of compounds like the fine differences among isomers and conjugate forms.^{27,43} In this work, the first-group contributions was employed for reasons of model simplification and user friendliness. Fonts et al.⁴² and Manrique et al.⁴⁴ used these same methods to estimate the physical and thermodynamic properties of bio-oil compounds derived from the fast pyrolysis of lignocellulosic compounds.

The parameters evaluated in this study are the critical properties, ideal gas properties, and condensed gas properties. The critical properties such as critical temperature (T_c), critical volume (V_c), and critical pressure (P_c) were estimated employing the methods of Joback³⁰ and Lydersen et al.⁵⁵; the enthalpy of vaporization via the methods of Joback³⁰, Riedel⁵⁷, and QPPR methods; the enthalpy of fusion by Joback³⁰ method; the normal boiling point by Joback³⁰, and Stein and Brown³¹ methods; and the normal melting point by Joback & Reid⁶⁰, and Perez-Ponce et al.⁵⁸ methods. The thermodynamic properties estimated using DFT were heat capacity, standard Gibbs free energy, change in enthalpy, and change in entropy. The methods of Joback, and Harrison & Seaton⁴⁵ were also employed for gas heat capacity estimation. Lastly, the condensed

phase properties considered were liquid heat capacity by Chueh & Swanson⁵⁹ method; the solid heat capacity by Hurst & Harrison⁴⁶ method; the liquid enthalpy of formation of individual compounds via QPPR approach; and the Hansen solubility parameters by Stefanis & Panayiotou⁴⁷ method.

3.3 Results and Discussion

3.3.1 Stable Structures of the Anhydrosugars

Table 3.1 shows the most thermodynamically stable molecular structures identified as the likely constituents of the dehydrated anhydro-oligo-sugars. The selection of the most stable structure was based on the conformer that gives the minimum Gibbs free energy. Note that although water is a product, it was not shown in the table. Dehydration of depolymerized cellulose oligomers is one of the main pyrolytic chemical transformations. A library of product structures, assessing all possible permutations of three dehydration events, and their corresponding stability is shown in Appendix A, Tables S1 through S11.

Monomer


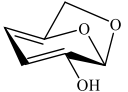
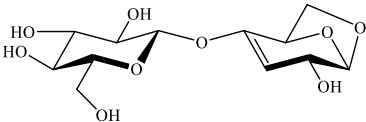
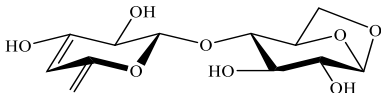
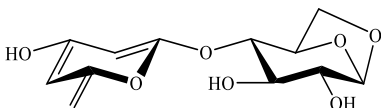
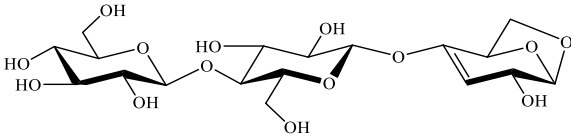
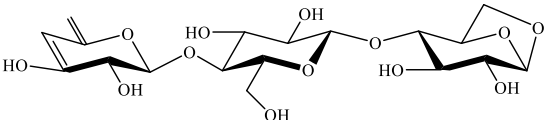
There are six (6) possible routes by which water can be removed from a levoglucosan molecule (Appendix A, Table S1). The result shows that pathway LG23 gave the most thermodynamically stable dehydration route with the lowest Gibbs free energy (ΔG) change of -88.6 kJ/mol. This means that the loss of a hydroxyl group from carbon 2 and hydrogen from carbon 3 is the most thermodynamically stable product. This finding is consistent with the result of Zhang et al.²¹ where they reported that the dehydration reaction is most favorable when H is removed from carbon 3 and the hydroxyl group is removed from carbon 2. On the one hand, LG21 and LG45 are less stable due to the presence of the bridged ring. Further, the change in

enthalpy (ΔH) and entropy (ΔS) of the most thermodynamically favored structure accounts for 38.4 kJ/mol and 164 J/mol K, respectively.

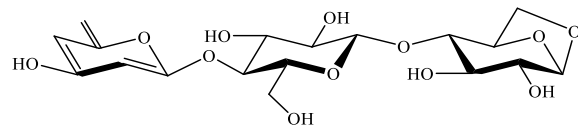
For the double dehydration of levoglucosan, a total of eleven (11) possible pathways were investigated (Appendix A, Table S2). Results show that the double dehydration of levoglucosan is a non-spontaneous reaction as depicted by the positive value of the ΔG_{rxn} . This result is coherent with experimental results, wherein we only observe levoglucosenone products, and no other dehydrated product of levoglucosenone. Also, since levoglucosan is very volatile, it significantly vaporizes upon formation,^{24,48} justifying the abundance of levoglucosan in experimental results.^{12,22}

It was observed that not only water and molecules with alkene moieties are formed as products but also some alkynes. Further, conjugated, isolated, and cumulated dienes are formed. However, results showed that conjugated alkenes are the most stable products. Reaction LG32A-45B, a conjugated diene, gives the most thermodynamically stable structure with Gibbs free energy change of 18.1 kJ/mol. The first water is eliminated from the LG-end at carbon 3 and carbon 2, while the second is removed at carbon 4 and 5. This result is supported by the basic knowledge on diene stability. Conjugated dienes are most stable compared to isolated and cumulated diene due to several factors like delocalization of charge through resonance and hybridization energy. Also, when comparing alkenes and alkynes, alkenes are more thermodynamically stable than alkynes. Moreover, this most stable reaction's enthalpy and entropy change accounts for 272.7 kJ/mol and 329 J/mol K, respectively. The same result was observed with the single dehydration reaction, where the dehydration routes near the bridge ring give the least favorable pathway.

Table 3.1. Most thermodynamically stable structures of the dehydrated sugars.

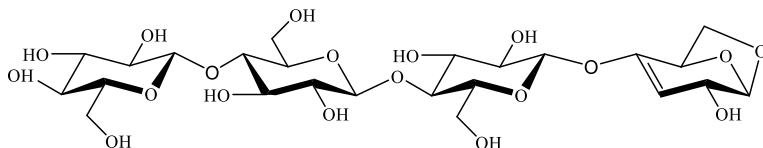
reaction label	product structure	molecular formula	molar mass (g/mol)	ΔG_{rxn} (kJ/mol)	ΔH_{rxn} (kJ/mol)	ΔS_{rxn} (J/mol K)
LG23		$C_6H_8O_4$	144.13	-88.63	38.43	164.0
LG32-45B		$C_6H_6O_3$	126.11	18.12	272.67	329.0
CBN34A		$C_{12}H_{18}O_9$	306.27	-76.85	59.27	175.0
CBN43B-65B		$C_{12}H_{16}O_8$	288.25	-171.67	88.63	337.0
CBN21B-43B-65B		$C_{12}H_{14}O_7$	270.07	-257.53	137.70	510.0
CTN34A		$C_{18}H_{28}O_{14}$	468.41	-82.95	53.25	180.0
CTN43C-65C		$C_{18}H_{26}O_{13}$	450.39	-177.84	79.97	333.0

CTN21C-
43C-65C



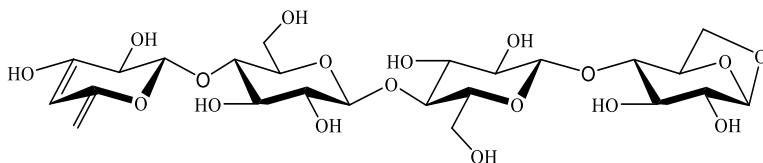
$C_{18}H_{24}O_{12}$ 432.13 -269.79 129.25 516.0

CQN34A



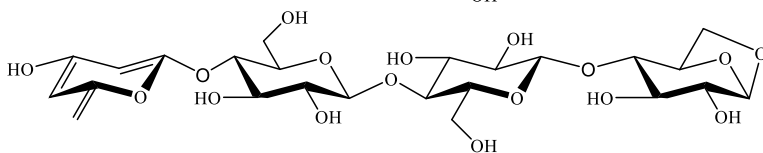
$C_{24}H_{38}O_{19}$ 630.20 -79.07 53.91 172.0

CQN43D-
65D



$C_{24}H_{36}O_{18}$ 612.19 -164.53 93.48 334.0

CQN21D-
43D-65D



$C_{24}H_{34}O_{17}$ 594.18 -255.00 131.13 499.0

**Note: Water is also a product but is not shown here.*

Dimer

A total of eleven (11) reaction pathways were examined for the single dehydration of cellobiosan (Appendix A, Table S3). The result shows that reaction CBN34A results in the most thermodynamically stable product with a ΔG_{rxn} of -76.9 kJ/mol. This pathway involves removing the hydroxyl group from carbon 3 and hydrogen from carbon 4. Enthalpy and entropy changes were calculated to be 59.7 kJ/mol and 175 J/mol K, respectively.

The double dehydration of cellobiosan can evolve through a total of forty-eight (48) reaction permutations (Appendix A, Table S4). Results show that CBN43B-65B with a ΔG_{rxn} of -171.7 kJ/mol resulted in the most thermodynamically stable product among all the reactions. This involves the removal of two water molecules from the NR-end. The first hydroxyl group of the first water is desorbed from carbon 4 and the hydrogen atom from carbon 3. In contrast, for the second dehydration event, the hydroxyl group is eliminated from carbon six and the hydrogen atom from carbon 5. Water elimination is more facile from the NR-end relative to the LG-end due to the stability of the levoglucosan end. The same observation as in the double dehydration of the monomer is seen here, where there are formations of alkenes and a few alkynes. The most thermodynamically favorable route, which is CBN43B-65B, is a conjugated alkene. Enthalpy and entropy changes are calculated to be 88.6 kJ/mol and 337 J/mol K, respectively.

For the triple dehydration of cellobiosan, a total of forty-four (44) dehydration reactions were investigated (Appendix A, Table S5). Pathway CBN21B-43B-65B resulted in the most thermodynamically stable product with Gibbs free energy change of -257.5 kJ/mol. All three water molecules were eliminated from the NR-end, that is, from 21B, 43B, and 65B positions.

The calculated enthalpy and entropy changes amounted to 137.7 kJ/mol and 510 J/mol K, respectively.

Trimer

A total of sixteen (16) reactions were investigated for the single dehydration of cellotriosan (Appendix A, Table S6). Results show that CTN34A gives the most thermodynamic product with Gibbs free energy change equal to -82.3 kJ/mol. This pathway entails the cleavage of the hydroxyl group from carbon 3 with a concerted proton loss from carbon 4 in the LG-end. Enthalpy and entropy changes of this route accounted for 53.3 kJ/mol and 184 J/mol K, respectively.

For the double dehydration of cellotriosan, a total of one hundred eleven (111) dehydration permutations were studied (Appendix A, Table S7). Results reveal that CTN43C-65C showed the most thermodynamically stable product, with Gibbs free reaction energy equal to -177.8 kJ/mol. That is, removing both water molecules from the NR-end. Specifically, the hydroxyl group is lost from carbon four and the hydrogen from carbon 3 for the first water molecule, while for the second water molecule, the hydroxyl group and hydrogen originate from carbon six and carbon 5, respectively. Additionally, the enthalpy and entropy changes of the second dehydration event were calculated to be 80.0 kJ/mol and 333 J/mol K, respectively.

Moreover, removing three water molecules from cellotriosan resulted in the investigation of one hundred seven (107) reaction pathways (Appendix A, Table S8). CTN21C-43C-65C was observed to be the most thermodynamically stable product with Gibbs free energy change of -269.8 kJ/mol. All three water molecules were lost from the NR-end, again indicating the ease of dehydration reactions at the NR-end. Enthalpy and entropy changes of this pathway correspond to 129.3 kJ/mol and 516 J/mol K, respectively.

Tetramer

Single dehydration of celloquatrosan resulted in a total of twenty-one (21) potential dehydration pathways (Appendix A, Table S9), revealing CQN34MacA as the most stable product with Gibbs free energy change equal to -79.1 kJ/mol. This pathway involves the removal of the hydroxyl group from carbon 3 and proton loss from carbon 4 in the LG-end. Enthalpy and entropy change of this route accounted for 53.9 kJ/mol and 172 J/mol K, respectively.

For the double dehydration of celloquatrosan, a total of sixty-six (66) reaction pathways (Appendix A, Table S10) were investigated. Reaction pathways which are expected to yield less stable products as evidenced in the dimers and trimers were not considered in this calculation. The CQN43D-65D pathway was found to be the most stable route with Gibbs free energy of -164.5 kJ/mol. Both water molecules were desorbed from the NR end. The enthalpy and entropy changes were correspondingly 93.5 kJ/mol and 334 J/mol K.

Finally, a total of sixty-nine (69) reaction pathways was studied for the triple dehydration of celloquatrosan (Appendix A, Table S11), resulting to CQN21D-43D-65D as the most thermodynamically stable product with Gibbs free energy change of -255.0 kJ/mol. All three water molecules were lost from the NR end. Enthalpy and entropy changes accounted for 131.13 kJ/mol and 500 J/mol K, respectively. Similarly, the reaction pathways expected to yield less stable products were not investigated.

In summary, results revealed that the LG-end is more stable than the NR-end. The thermodynamic stabilities of product molecules undergoing sequential dehydration events showed that most of the water molecules are eliminated from the NR-end, forming conjugated compounds. This result is consistent for the oligomeric units of the anhydrosugars (dimer, trimer, and tetramer) except for the single dehydration reactions exhibiting greater stability of products

when water is eliminated from carbons 3 and 4 of the LG-end. According to Mamleev et al.^{5,22}, dehydration reaction mostly happens at the NR-end and not from the LG-end because LG is a stable product.

3.3.2 Theoretical Spectra of the Dehydrated Anhydrosugars

FTIR

Figure 3.5 shows the theoretical FTIR spectra of the proposed structures of dehydrated anhydrosugars and the experimental result of the whole sugar. A scale factor of 0.9567 was applied to the calculated vibrational frequencies toward generating the theoretical IR spectra.³⁴ The theoretical peaks conform to experimental results reported in previous works.^{37,38} These include the hydroxyl functional group seen at 3500 to 3887 cm^{-1} , C-H vibrations from the alkane groups (2875 to 3000 cm^{-1}), alkenes and conjugated C=C bond (1605 to 1750 cm^{-1}), C-C stretch from alkanes (1500 to 1550 cm^{-1}), and the C-O stretch from alcohols (1047 to 1250 cm^{-1}). The region under 1605 to 1750 cm^{-1} was shown to be more intense when more water molecules are eliminated resulting in the formation of conjugated systems upon dehydration. The discrepancies on the OH stretches, which is observed to be broad in the experimental result could be attributed to residual water. Nonetheless, there is a strong qualitative agreement of the FTIR results of the model compounds and the experimental analysis of the whole sugar especially in the fingerprint region. The fingerprint regions of both experimental and modeling yields are within the absorbance range of the WS bio-oil fraction reported in the literature¹².

NMR

Figure 3.6 displays the theoretical ^1H -NMR spectra of the dehydrated anhydrosugar oligomers and the experimental result of the whole sugar. Results show that the most downfield/de-shielded regions at 4.5 to 6.1 ppm are the proton types originating from alkenes

and conjugated C=C systems, where the dehydration reaction occurred. The spectral areas at 3.0 to 4.5 ppm are the protons attached to carbon atoms associated with the alcohol groups. Lastly, regions at 0.2 to 2.2 ppm are attributed to the protons from alkanes. The peak observed at 2.5 ppm for the experimental sugar is traced back to the DMSO solvent. Compared to the experimental $^1\text{H-NMR}$ result of the whole sugar, the peaks of the proposed dehydrated sugar structures are within the range of chemical shifts. These modeling and experimental chemical shifts of the pyrolytic sugar also confirm qualitatively to the experimental results for pyrolysis bio-oils reported previously.¹⁴

Figure 3.7 shows the theoretical $^{13}\text{C-NMR}$ spectra of the proposed structures and the experimental spectra of the whole sugar. The C=C bond from 160.0 to 180.0 ppm and 100 to 120 ppm represented the alkenes and conjugated structure of the dehydrated sugars. Spectral regions between 60.0 to 100.0 ppm originated from the singly bonded carbon atoms attached to hydroxyl/alcohol groups (aliphatic C-O), with the non-ring carbon atom (carbon 6) being the most up-field. Most of the crowding is seen in this region due to the significant presence of alkane and aliphatic groups. These modeling yields are in good qualitative agreement with the experimental result of the whole sugar. A ^{13}C NMR analysis on the WS bio-oil fraction from which the whole sugar was extracted (Figure 8) also shows that our modeling results are within the expected chemical shift range.¹² Though there are more peaks in the WS fraction due to the presence of phenols and other aromatic compounds. The integration region under 60.8 to 95.8 ppm of the WS fraction was reported to represent the aliphatic C-O associated with hydroxyl groups, peaks at 95.8 to 125.0 ppm, 125.0-142.0 ppm and 142.0 to 166.5 ppm represented aromatic C-H, aromatic C-C and aromatic C-O, respectively.¹² The aliphatic C-O region is consistent with our modeling result. The aromatic regions in the WS fractions under 142.0 to

160.0 ppm and 170.0 to 180.0 ppm are shown to have very low intensity in our experimental ^{13}C NMR result because the phenols and aromatic compounds are no longer present in the pyrolytic sugar.

These theoretical 1-D ^1H and ^{13}C NMR of the sugar conforms to the experimental 2-D heteronuclear single quantum coherence spectroscopy (HSQC) NMR of bio-oil showing the presence of pyrolytic sugars as evidenced by the alcohol functional groups around 60 to 100 ppm chemical shifts for the ^{13}C NMR and 3 to 5 ppm for the ^1H NMR.⁴⁹ The functional groups found in the theoretical NMR results are consistent with the functional groups identified in the FTIR results.

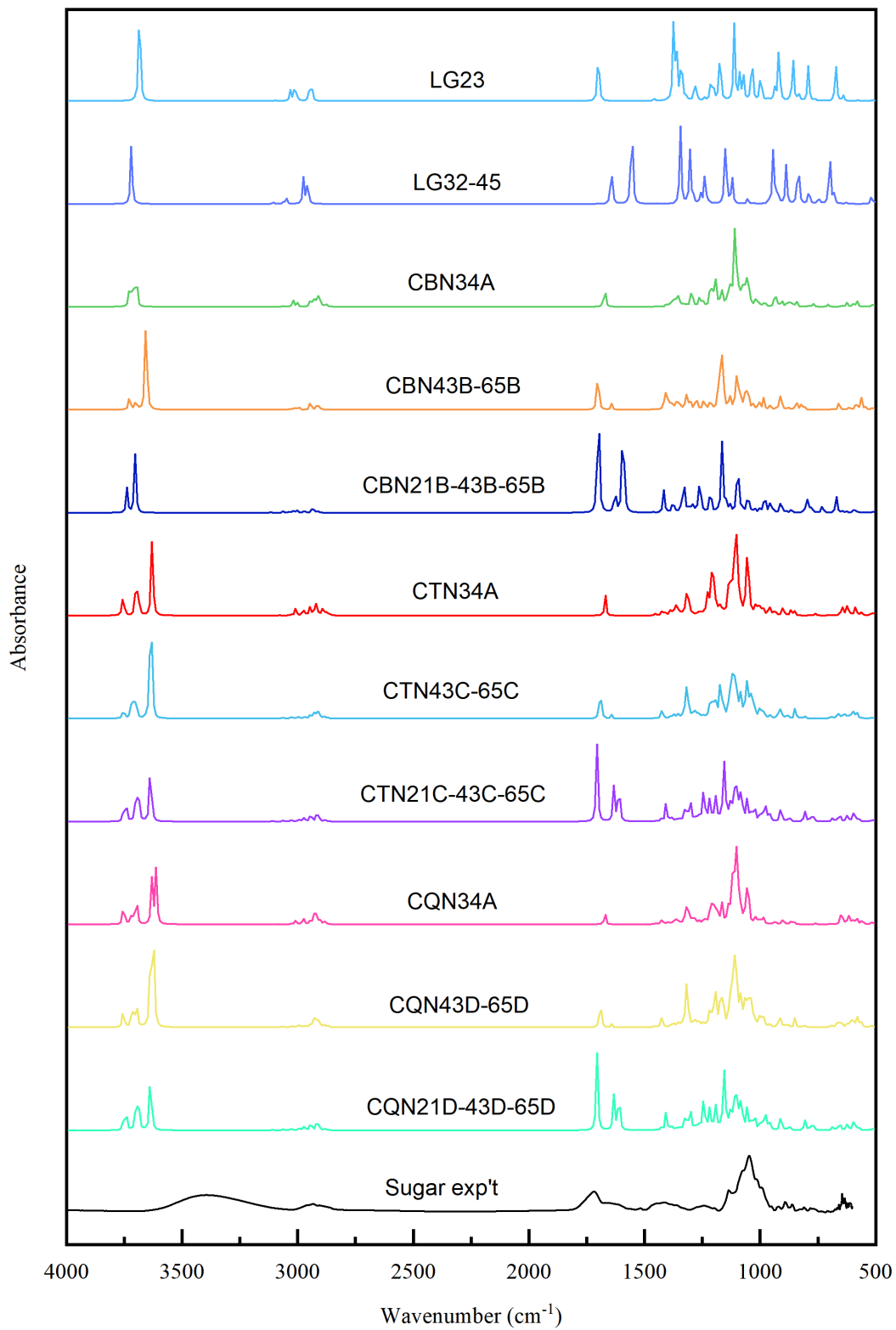


Figure 3.5: Theoretical FTIR spectra of the identified dehydrated anhydrosugars.

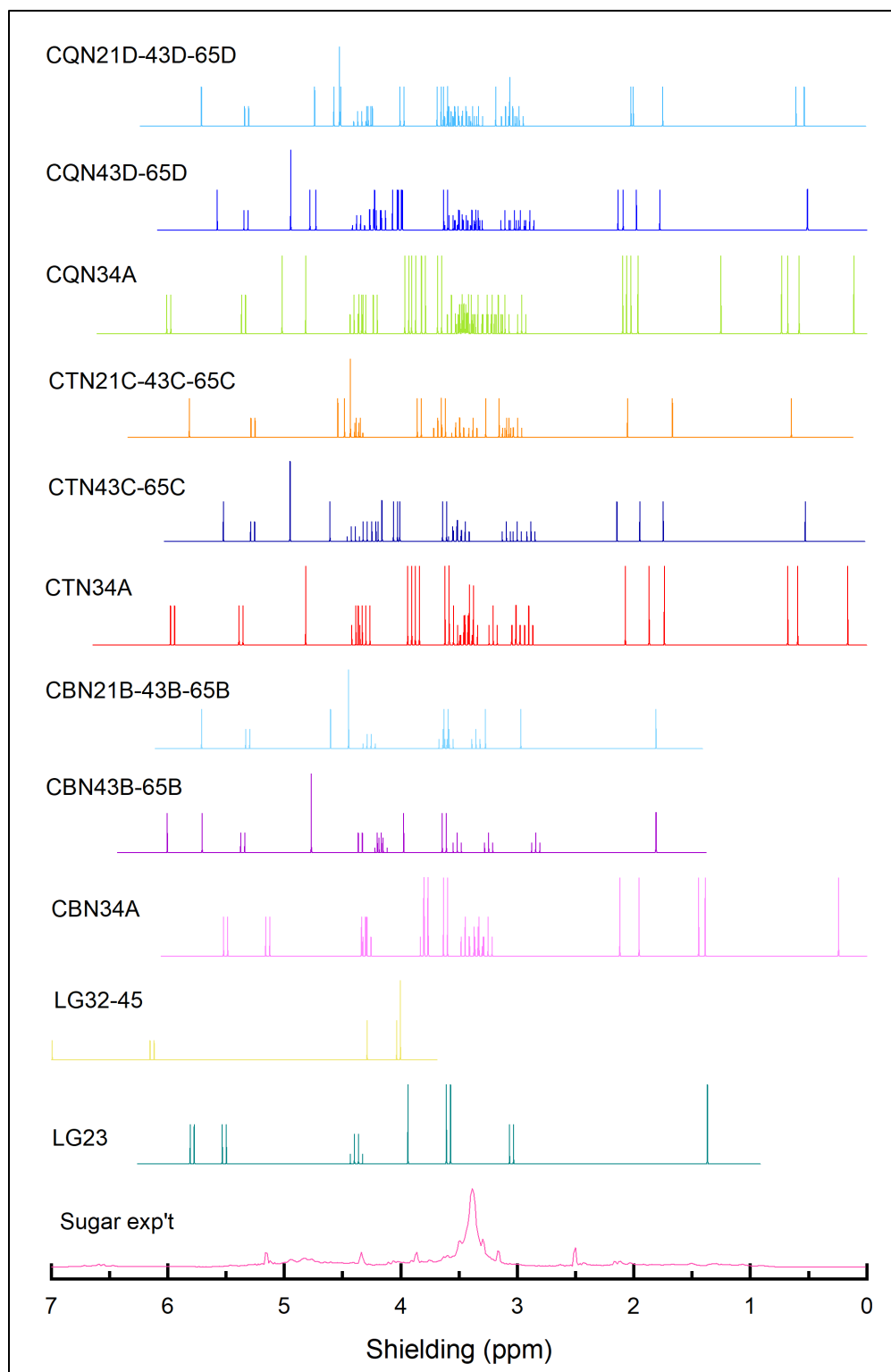


Figure 3.6: Theoretical ^1H -NMR spectra of the dehydrated anhydrosugars.

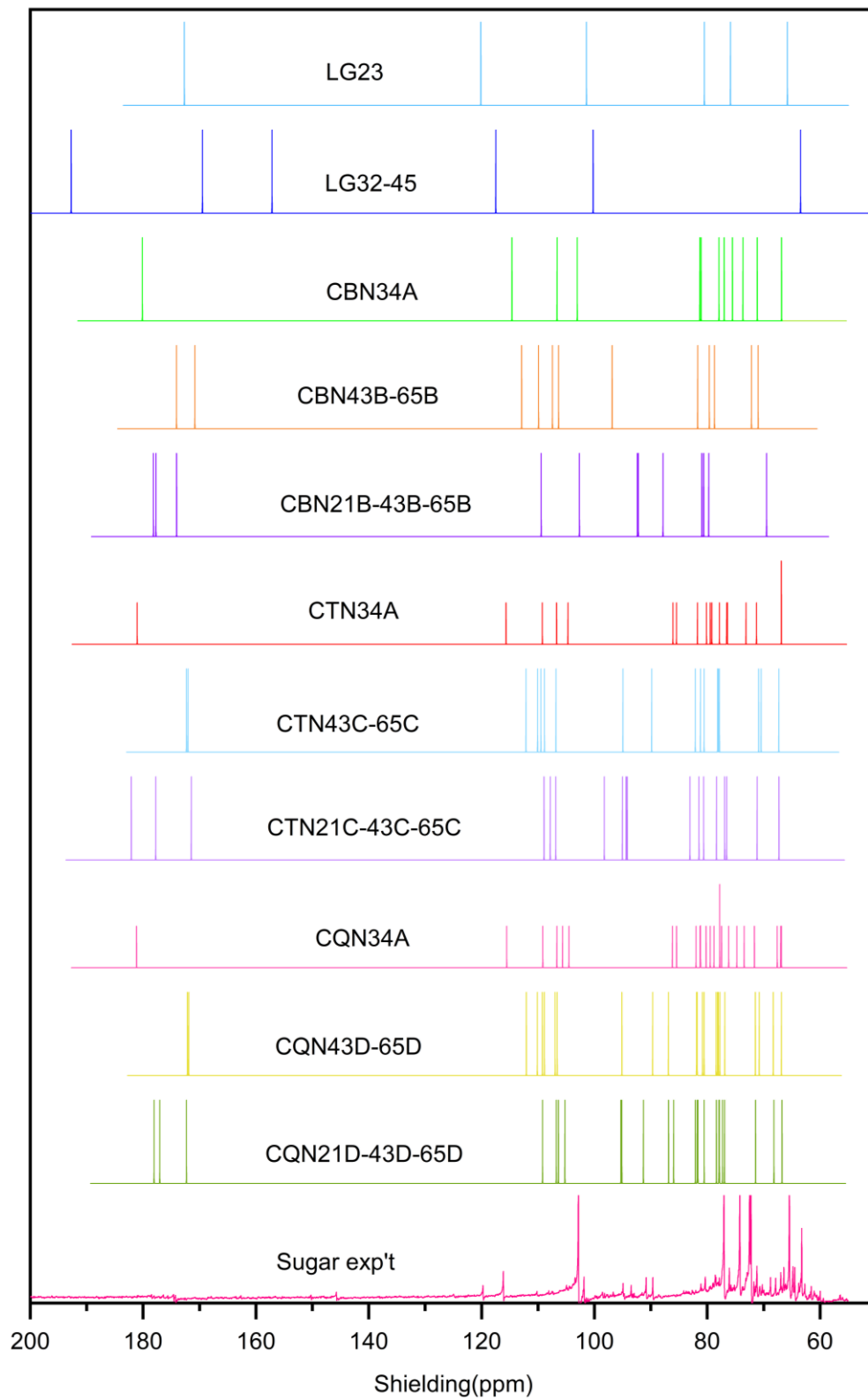


Figure 3.7: Theoretical ^{13}C -NMR spectra of the dehydrated anhydrosugars.

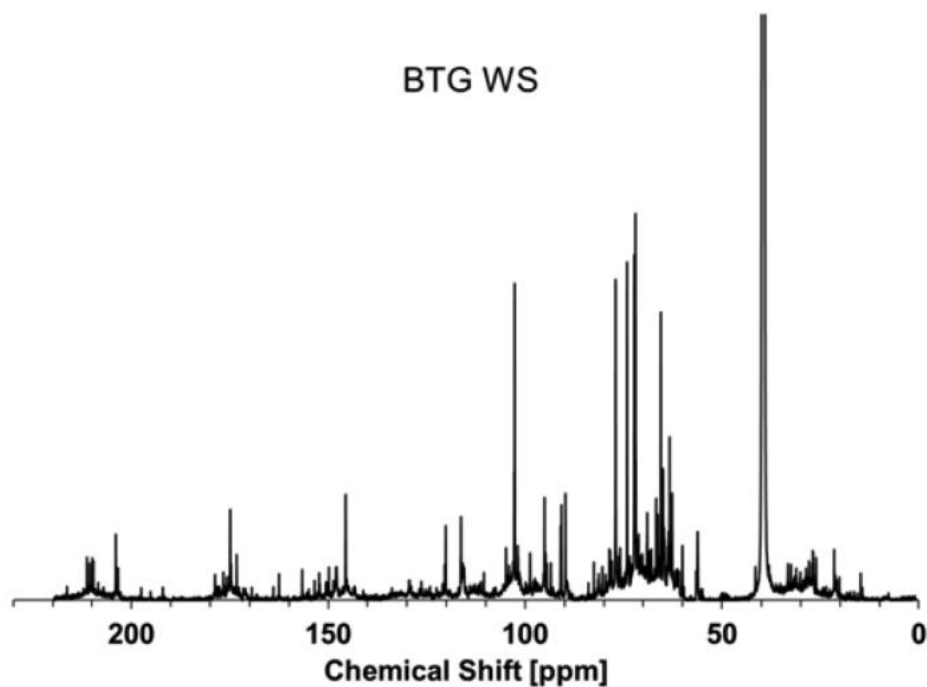


Figure 3.8: Experimental ^{13}C -NMR spectra of the WS BTG bio-oil fraction. Reproduced with permission from Ref.12. Copyright 2023. ACS Publications.

3.3.3 Thermodynamic and Physical Properties of the Proposed Oligomeric Structures

Physical Properties

Table 3.2 shows the results for the estimated physical properties of the proposed oligomeric sugar. The dehydrated oligomeric sugars were first broken down into sets of functional groupings as proposed in the literature.^{29,42,47} The physical properties investigated include critical properties like temperature, pressure, and volume, normal boiling point and melting point, and enthalpy of vaporization and fusion. These properties are fundamental parameters to predict thermodynamic behavior. The procedures used is described elsewhere.⁴² There are no literature data found for comparison for the thermodynamic and physical properties

of anhydrous-oligo-sugar molecules as they have not been studied in the past¹⁴. Thus, we've used experimental data for levoglucosan and cellobiosan as the point of reference, only if available. Otherwise, the estimation of Fonts et al.⁴² for levoglucosan and cellobiosan was used as point references.

For the critical temperature, the Joback³⁰ method gave a higher value than the Lydersen et al.⁵⁵ method except for the trimer which has a very high value and thus needs to be treated with caution, since these molecules are bigger than the molecules used for GCM models. Similarly, Fonts et al. estimated a high value averaging to 832.25 K and 1456.1 K for the levoglucosan and cellobiosan, respectively. The more dehydrated the compound, the lower is the critical temperature. That is, the twice dehydrated cellobiosan has the lowest critical temperature. Critical temperature is the maximum possible temperature at which the compound can exist as a liquid. Estimation of the critical pressure and critical volume resulted in quite closer values for both the Joback³⁰ and Lydersen et al.⁵⁵ methods. Also, these values are not too far from Fonts et al.⁴² estimated values for levoglucosan (5.12 MPa, 375 cm³/mol) and cellobiosan (3.32 MPa, 739 cm³/mol).

For the normal boiling point, using the Joback³⁰ method gave a closer value to experimental results for levoglucosan, cellobiosan, and cellotriosan accounting for 658 K⁵⁰, 853 K¹¹, and 1,063 K²², respectively. Similarly, Lede et. al.⁵⁶ obtained almost the same values of 612 K, 854 K, and 1065 K for the levoglucosan, cellobiosan, and cellotriosan, respectively. Mamleev et al.²² also reported a true boiling point of levoglucosan which is in the range of 563 to 573 K. The estimated T_b values for the cellobiosan and cellotriosan are higher than the typical fast pyrolysis temperature (773 K). This is consistent with the experimental results reported by Pecha et al.²³ where these molecules are driven by ejection mechanism instead of vaporizing during the

fast pyrolysis reaction. Similarly, Gong et al.⁵¹ reported that at 773 K, there are no sugars or anhydrosugars detected during the reaction, because almost all of the cellulose have already decomposed at such high temperature. For the normal melting point, estimation using both Joback and Perez-Ponce⁴⁸ methods gave quite closer value. Oja and Suuberg⁵² recorded a melting point of 453 K for levoglucosan and 513 K for cellobiose. The enthalpy of vaporization at boiling point and room temperature (298 K) resulted in a closer value for both the methods applied, except for the thrice dehydration of cellotriosan which has values quite far from each other.

Table 3.2. Estimated physical property values for each proposed structure of the anhydrosugars.

Physical property	Monomer		Dimer			Trimer			Tetramer			Ref
	LG 23	LG 32-45	CBN 34A	CBN 43B-65B	CBN 21B-43B-65B	CTN 34A	CTN 43C-65C	CTN 21C-43C-65C	CQN 34A	CQN 34D-65D	CQN 21D-43D-65D	
Critical temp. (T _c , K)	789	726	1310	1190	1101	2356	2034	1808	7420	5006	3840	30,60
	668	611	1072	1030	1127	2794	2827	5674	-4361 ^b	-3794 ^b	-2001 ^b	55
Critical pressure, (P _c , MPa)	5.6	5.6	4.0	3.8	3.8	3.0	2.8	2.8	2.3	2.2	2.2	30,60
	4.7	4.8	2.7	2.7	2.8	1.8	1.9	1.9	1.4	1.4	1.4	55
Critical volume, (V _c , cm ³ /mol)	334	304	696	662	630	1057	1022	992	1418	1384	1353	30,60
	348	312	716	678	642	1082	1046	1010	1450	1413	1373	55
Normal boiling point, (T _b , K)	597	518	1061	972	894	1525	1436	1358	1989	1900	1821	30,60
	545	496	764	725	693	979	936	904	1190	1147	1114	31
Enthalpy of vaporization @ T _b , (ΔH _{vap,Tb} , kJ/mol)	72	57	142	125	110	211	195	180	281	264	249	30,60
	71	47	174	167	139	75	96	115	22	34	47	57
Enthalpy of vaporization, (@298.15K) (ΔH _{vap,298.15K} , kJ/mol)	106	77	250	224	192	293	301	306	304	300	295	53
	106	73	252	262	206	706	591	506	1208	1054	928	*
Normal melting point (T _m , K)	370	331	659	616	577	949	906	867	1238	1195	1156	30,60
	392	370	618	564	541	844	789	767	1070	1015	993	58
Enthalpy of fusion, (ΔH _{fus,Tm} , kJ/mol)	29.4	24.0	62.0	56.2	50.8	96.6	89.3	84	129	122	117	30,60

* - thermodynamic equation; b - unreasonable

Table 3.3 shows estimated enthalpy of formation, standard Gibbs free energy of formation and the heat capacity estimated under ideal gas by Joback, Harrison & Seaton, and DFT methods. Standard Gibbs free energy is a useful parameter to determine the spontaneity of a reaction. The standard enthalpy of formation is widely used to conduct energy balances. It is the energy released or consumed during the formation of one mole of the substance at standard conditions. Entropy reflects the change in the degree of system disorder during the reaction. The values estimated in this work for the singly dehydrated levoglucosan and cellobiosan for both the gas standard enthalpy and Gibbs free energy of formations are reasonable compared to the values obtained by Fonts et al. for levoglucosan ($\Delta H^{\circ}_{f,G} = -815.1$ kJ/mol , $\Delta G^{\circ}_{f,G} = -508.6$ kJ/mol) and cellobiosan ($\Delta H^{\circ}_{f,G} = -1686.3$ kJ/mol , $\Delta G^{\circ}_{f,G} = -1065.7$ kJ/mol) using the Joback method. For the gas heat capacity, results obtained from Joback, Harrison & Seaton, and the DFT methods seem to agree with each other resulting in quite closer values. Fonts et al. reported a gas heat capacity at constant pressure equivalent to 187.2 J/mol.K for levoglucosan. This result is not too far from the estimated value for the single dehydration of levoglucosan reported in this work.

Table 3.3. Estimated ideal gas property values for each proposed structure of the anhydrosugars.

Ideal gas property	Monomer		Dimer			Trimer			Tetramer			Ref
	LG 23	LG 32-45	CBN 34A	CBN 43B-65B	CBN 21B-43B-65B	CTN 34A	CTN 43C-65C	CTN 21C-43C-65C	CQN 34A	CQN 43D-65D	CQN 21D-43D-65D	
Gas standard enthalpy of formation ($\Delta H^{\circ}_{f,G}$, kJ/mol)	-576	-337	-1448	-1191	-952	-2320	-2063	-1824	-3192	-2935	-2696	30, 60
Gas standard Gibbs free energy of formation ($\Delta G^{\circ}_{f,G}$, kJ/mol)	-336	-164	-894	-696	-524	-1451	-1254	-1081	-2009	-1811	-1638	30, 60
Gas heat capacity at	163	156	311	341	334	526	522	516	708	704	697	30, 60

constant pressure (@298K) (C_p , J/mol.K)	149	126	315	292	258	481	459	436	647	625	602	45
	132	112	315	289	272	495	470	451	674	651	631	61

Table 3.4 presents the estimated condensed gas properties of the proposed structures of anhydrosugars. These properties include the liquid heat capacity, solid heat capacity, liquid standard enthalpy of formation, and the Hansen solubility parameters. Again, no literature data were found for comparison of results obtained in this paper. Generally, estimated values for the monomers and dimers seem to agree with each other for the methods applied but are seemingly far for bigger compounds like the trimer and tetramers. This may be attributed to the reason that GCM was developed and patterned for small molecules and not for the bigger ones.

For the liquid heat capacity, solid heat capacity, and liquid standard enthalpy of formation properties, Fonts et al.⁴² estimated values that are close to experimental results. Hence, we can conclude that the estimated results in this work are within the range of validity of the method, considering we applied exactly the same method. Lastly, Hansen solubility parameters predict the ability of one substance to dissolve into another and thus an important factor to determine suitable solvents for extraction of bio-oil compounds. The estimated Hansen solubility parameters included dispersion forces (δ_d), dipole-dipole interactions (δ_p), and hydrogen bonding (δ_{hb}).

Table 3.4. Estimated condensed gas property values for each proposed structure of the anhydrosugars.

Condensed gas property	Monomer		Dimer			Trimer			Tetramer			Ref
	LG23	LG 32-45	CBN 34A	CBN 43B-65B	CBN 21B-43B-65B	CTN 34A	CTN 43C-65C	CTN 21C-43C-65C	CQN 34A	CQN 43D-65D	CQN 21D-43D-65D	
Liquid heat capacity at constant pressure, (C_p, L , J/mol-K)	275	228.03	590	543	495	929	870	822	1256	1197	1149	59

Solid heat capacity at constant pressure, ($C_{p,s}$, J/mol-K)	180	150.96	388	359	317	596	567	539	804	775	747	46
Liquid standard enthalpy of formation of individual compounds, ($\Delta H_{f,L}^\circ$, kJ/mol)	-682	-410	-1812	-1453	-1159	-3026	-2655	-2330	-4400	-3989	-3624	*
Hansen solubility parameter												54
δ_d	19.6	19.2	20.4	19.0	19.3	20.7	20.0	20.2	21.7	20.9	21.2	
δ_p	11.9	8.6	26.3	23.1	30.3	37.1	34.8	42.1	58.8	56.5	53.8	
δ_{hb}	20.4	11.7	40.8	33.1	33.6	61.2	53.7	54.2	91.1	83.7	74.8	
δ_T	30.7	24.0	52.6	44.6	49.2	74.5	67.1	71.5	110.6	103.1	94.6	

* - thermodynamic equation

3.4 Conclusion

In this work, we were able to identify and propose potential structures of the heavy oligomeric sugars obtained during cellulose pyrolysis using the DFT method and glucose-based carbohydrates as model compounds. Several potential products have been investigated as shown in the library compiled in Appendix A. It is concluded that water is typically removed from the non-reducing end. The theoretical FTIR and NMR spectra of the proposed structures of oligomeric sugars qualitatively conform to the experimental result of pyrolytic sugars. The use of QSPRs and QPPRs for the thermophysical characterization of resulting structures also shined some light on the oligomers found in bio-oil, which are fundamental for the efficient design of extraction, conversion, separation, and refining/upgrading technologies and processes. Results for the thermophysical properties cannot be compared with experimental data as they have not been studied in the past. Future efforts will explore extending this approach to the analysis of more heterogeneous feedstocks such as lignin or aggregate biomass.

3.5 REFERENCES

- (1) Asif, M.; Muneer, T. Energy Supply, Its Demand and Security Issues for Developed and Emerging Economies. *Renew. Sustain. Energy Rev.* **2007**, *11* (7), 1388–1413.
<https://doi.org/10.1016/j.rser.2005.12.004>.
- (2) Li, X. Diversification and Localization of Energy Systems for Sustainable Development and Energy Security. *Energy Policy* **2005**, *33* (17), 2237–2243.
<https://doi.org/10.1016/j.enpol.2004.05.002>.
- (3) Collard, F. X.; Blin, J. A Review on Pyrolysis of Biomass Constituents: Mechanisms and Composition of the Products Obtained from the Conversion of Cellulose, Hemicelluloses and Lignin. *Renew. Sustain. Energy Rev.* **2014**, *38*, 594–608.
<https://doi.org/10.1016/j.rser.2014.06.013>.
- (4) Krumm, C.; Pfaendtner, J.; Dauenhauer, P. J. Millisecond Pulsed Films Unify the Mechanisms of Cellulose Fragmentation. *Chem. Mater.* **2016**, *28* (9), 3108–3114.
<https://doi.org/10.1021/acs.chemmater.6b00580>.
- (5) Mamleev, V.; Bourbigot, S.; Yvon, J. Kinetic Analysis of the Thermal Decomposition of Cellulose: The Main Step of Mass Loss. *J. Anal. Appl. Pyrolysis* **2007**, *80* (1), 151–165.
<https://doi.org/10.1016/j.jaap.2007.01.013>.
- (6) Shen, D. K.; Gu, S. The Mechanism for Thermal Decomposition of Cellulose and Its Main Products. *Bioresour. Technol.* **2009**, *100* (24), 6496–6504.
<https://doi.org/10.1016/j.biortech.2009.06.095>.
- (7) Shen, D.; Jin, W.; Hu, J.; Xiao, R.; Luo, K. An Overview on Fast Pyrolysis of the Main Constituents in Lignocellulosic Biomass to Valued-Added Chemicals: Structures, Pathways and Interactions. *Renew. Sustain. Energy Rev.* **2015**, *51*, 761–774.

- <https://doi.org/10.1016/j.rser.2015.06.054>.
- (8) Shen, D.; Xiao, R.; Gu, S.; Luo, K. The Pyrolytic Behavior of Cellulose in Lignocellulosic Biomass: A Review. *RSC Adv.* **2011**, *1* (9), 1641–1660.
<https://doi.org/10.1039/c1ra00534k>.
- (9) Zhou, X.; Nolte, M. W.; Mayes, H. B.; Shanks, B. H.; Broadbelt, L. J. Experimental and Mechanistic Modeling of Fast Pyrolysis of Neat Glucose-Based Carbohydrates. 1. Experiments and Development of a Detailed Mechanistic Model. *Ind. Eng. Chem. Res.* **2014**, *53* (34), 13274–13289. <https://doi.org/10.1021/ie502259w>.
- (10) Abdilla-Santes, R. M.; Agarwal, S.; Xi, X.; Heeres, H.; Deuss, P. J.; Heeres, H. J. Valorization of Humin Type Byproducts from Pyrolytic Sugar Conversions to Biobased Chemicals. *J. Anal. Appl. Pyrolysis* **2020**, *152* (October).
<https://doi.org/10.1016/j.jaap.2020.104963>.
- (11) Pecha, M. B.; Montoya, J. I.; Chejne, F.; Garcia-Perez, M. Effect of a Vacuum on the Fast Pyrolysis of Cellulose: Nature of Secondary Reactions in a Liquid Intermediate. *Ind. Eng. Chem. Res.* **2017**, *56* (15), 4288–4301. <https://doi.org/10.1021/acs.iecr.7b00476>.
- (12) Stankovikj, F.; McDonald, A. G.; Helms, G. L.; Olarte, M. V.; Garcia-Perez, M. Characterization of the Water-Soluble Fraction of Woody Biomass Pyrolysis Oils. *Energy and Fuels* **2017**, *31* (2), 1650–1664. <https://doi.org/10.1021/acs.energyfuels.6b02950>.
- (13) Easton, M. W.; Nash, J. J.; Kenttämä, H. I. Dehydration Pathways for Glucose and Cellobiose during Fast Pyrolysis. *J. Phys. Chem. A* **2018**, *122* (41), 8071–8085.
<https://doi.org/10.1021/acs.jpca.8b02312>.
- (14) Stankovikj, F.; McDonald, A. G.; Helms, G. L.; Garcia-Perez, M. Quantification of Bio-Oil Functional Groups and Evidences of the Presence of Pyrolytic Humins. *Energy and*

- Fuels* **2016**, *30* (8), 6505–6524. <https://doi.org/10.1021/acs.energyfuels.6b01242>.
- (15) Terrell, E.; Garcia-Perez, M. Novel Strategy to Analyze Fourier Transform Ion Cyclotron Resonance Mass Spectrometry Data of Biomass Pyrolysis Oil for Oligomeric Structure Assignment. *Energy and Fuels* **2020**, *34* (7), 8466–8481. <https://doi.org/10.1021/acs.energyfuels.0c01687>.
- (16) Hu, B.; Zhang, B.; Xie, W. L.; Jiang, X. Y.; Liu, J.; Lu, Q. Recent Progress in Quantum Chemistry Modeling on the Pyrolysis Mechanisms of Lignocellulosic Biomass. *Energy and Fuels* **2020**, *34* (9), 10384–10440. <https://doi.org/10.1021/acs.energyfuels.0c01948>.
- (17) Kostetsky, P.; Broadbelt, L. J. Progress in Modeling of Biomass Fast Pyrolysis: A Review. *Energy and Fuels* **2020**, *34* (12), 15195–15216. <https://doi.org/10.1021/acs.energyfuels.0c02295>.
- (18) Nimlos, M. R.; Blanksby, S. J.; Barney Ellison, G.; Evans, R. J. Enhancement of 1,2-Dehydration of Alcohols by Alkali Cations and Protons: A Model for Dehydration of Carbohydrates. *J. Anal. Appl. Pyrolysis* **2003**, *66* (1), 3–27. [https://doi.org/10.1016/S0165-2370\(02\)00103-1](https://doi.org/10.1016/S0165-2370(02)00103-1).
- (19) Nimlos, M. R.; Blanksby, S. J.; Qian, X.; Himmel, M. E.; Johnson, D. K. Mechanisms of Glycerol Dehydration. *J. Phys. Chem. A* **2006**, *110* (18), 6145–6156. <https://doi.org/10.1021/jp060597q>.
- (20) Hosoya, T.; Sakaki, S. Levoglucosan Formation from Crystalline Cellulose: Importance of a Hydrogen Bonding Network in the Reaction. *ChemSusChem* **2013**, *6* (12), 2356–2368. <https://doi.org/10.1002/cssc.201300338>.
- (21) Zhang, X.; Yang, W.; Blasiak, W. Thermal Decomposition Mechanism of Levoglucosan during Cellulose Pyrolysis. *J. Anal. Appl. Pyrolysis* **2012**, *96*, 110–119.

- <https://doi.org/10.1016/j.jaap.2012.03.012>.
- (22) Mamleev, V.; Bourbigot, S.; Le Bras, M.; Yvon, J. The Facts and Hypotheses Relating to the Phenomenological Model of Cellulose Pyrolysis. Interdependence of the Steps. *J. Anal. Appl. Pyrolysis* **2009**, *84* (1), 1–17. <https://doi.org/10.1016/j.jaap.2008.10.014>.
- (23) Pecha, M. B.; Terrell, E.; Montoya, J. I.; Stankovikj, F.; Broadbelt, L. J.; Chejne, F.; Garcia-Perez, M. Effect of Pressure on Pyrolysis of Milled Wood Lignin and Acid-Washed Hybrid Poplar Wood. *Ind. Eng. Chem. Res.* **2017**, *56* (32), 9079–9089. <https://doi.org/10.1021/acs.iecr.7b02085>.
- (24) Zhou, X.; Nolte, M. W.; Shanks, B. H.; Broadbelt, L. J. Experimental and Mechanistic Modeling of Fast Pyrolysis of Neat Glucose-Based Carbohydrates. 2. Validation and Evaluation of the Mechanistic Model. **2014**. <https://doi.org/10.1021/ie502259w>.
- (25) Gallo, J. M. R.; Alonso, D. M.; Mellmer, M. A.; Dumesic, J. A. Production and Upgrading of 5-Hydroxymethylfurfural Using Heterogeneous Catalysts and Biomass-Derived Solvents. *Green Chem.* **2013**, *15* (1), 85–90. <https://doi.org/10.1039/c2gc36536g>.
- (26) Westerhof, R. J. M.; Oudenhoven, S. R. G.; Marathe, P. S.; Engelen, M.; Garcia-Perez, M.; Wang, Z.; Kersten, S. R. A. The Interplay between Chemistry and Heat/Mass Transfer during the Fast Pyrolysis of Cellulose. *React. Chem. Eng.* **2016**, *1* (5), 555–566. <https://doi.org/10.1039/c6re00100a>.
- (27) Constantinou, L.; Gani, R. New Group Contribution Method for Estimating Properties of Pure Compounds. *AIChE J.* **1994**, *40* (10), 1697–1710. <https://doi.org/10.1002/aic.690401011>.
- (28) Kolska, Z.; Zabransky, M.; Randov, A. Group Contribution Methods for Estimation of Selected Physico-Chemical Properties of Organic Compounds. *Thermodyn. - Fundam. Its*

- Appl. Sci.* **2012**. <https://doi.org/10.5772/49998>.
- (29) Gani, R. Group Contribution-Based Property Estimation Methods: Advances and Perspectives. *Curr. Opin. Chem. Eng.* **2019**, *23*, 184–196. <https://doi.org/10.1016/J.COCHE.2019.04.007>.
- (30) Joback, K. G. A Unified Approach to Physical Property Estimation Using Multivariate Statistical Techniques. 1984. <http://dspace.mit.edu/handle/1721.1/15374>.
- (31) Stein, S. E.; Brown, R. L. Estimation of Normal Boiling Points from Group Contributions. *J. Chem. Inf. Comput. Sci.* **2002**, *34* (3), 581–587. <https://doi.org/10.1021/CI00019A016>.
- (32) Mayes, H. B.; Broadbelt, L. J. Unraveling the Reactions That Unravel Cellulose. *J. Phys. Chem. A* **2012**, *116*. <https://doi.org/10.1021/jp300405x>.
- (33) Patwardhan, P. R.; Brown, R. C.; Shanks, B. H. Understanding the Fast Pyrolysis of Lignin. <https://doi.org/10.1002/cssc.201100133>.
- (34) Ünal, Y.; Nassif, W.; Özyaydin, B. C.; Sayin, K. Scale Factor Database for the Vibration Frequencies Calculated in M06-2X, One of the DFT Methods. *Vib. Spectrosc.* **2021**, *112* (November 2020), 1–6. <https://doi.org/10.1016/j.vibspec.2020.103189>.
- (35) Taylor, C. J.; Nix, M. G. D.; Dessent, C. E. H. Noncovalent Interactions in the Gas-Phase Conformers of Anionic Iduronate (Methyl 2-O-Sulfo- α -L-Iduronate): Variation of Subconformer versus Ring Conformer Energetics for a Prototypical Anionic Monosaccharide Studied Using Computational Methods. *J. Phys. Chem. A* **2010**, *114* (42), 11153–11160. <https://doi.org/10.1021/jp102657t>.
- (36) Zhao, Y.; Truhlar, D. G. The M06 Suite of Density Functionals for Main Group Thermochemistry, Thermochemical Kinetics, Noncovalent Interactions, Excited States, and Transition Elements: Two New Functionals and Systematic Testing of Four M06-

- Class Functionals and 12 Other Function. *Theor. Chem. Acc.* **2008**, *120* (1–3), 215–241.
<https://doi.org/10.1007/s00214-007-0310-x>.
- (37) Han, Y.; Pinheiro Pires, A. P.; Denson, M.; McDonald, A. G.; Garcia-Perez, M. Ternary Phase Diagram of Water/Bio-Oil/Organic Solvent for Bio-Oil Fractionation. *Energy and Fuels* **2020**, *34* (12), 16250–16264. <https://doi.org/10.1021/acs.energyfuels.0c03100>.
- (38) Stankovikj, F.; Garcia-Perez, M. TG-FTIR Method for the Characterization of Bio-Oils in Chemical Families. *Energy and Fuels* **2017**, *31* (2), 1689–1701.
<https://doi.org/10.1021/acs.energyfuels.6b03132>.
- (39) Nimlos, M. R.; Evans, R. J. Levoglucosan Pyrolysis. *Fuel Chem. Div. Prepr.* **2002**, *47* (1), 393.
- (40) Zhou, S.; Garcia-Perez, M.; Pecha, B.; Kersten, S. R. A.; McDonald, A. G.; Westerhof, R. J. M. Effect of the Fast Pyrolysis Temperature on the Primary and Secondary Products of Lignin. *Energy and Fuels* **2013**, *27* (10), 5867–5877. <https://doi.org/10.1021/ef4001677>.
- (41) Stanford, J. P.; Hall, P. H.; Rover, M. R.; Smith, R. G.; Brown, R. C. Separation of Sugars and Phenolics from the Heavy Fraction of Bio-Oil Using Polymeric Resin Adsorbents. *Sep. Purif. Technol.* **2018**, *194* (July 2017), 170–180.
<https://doi.org/10.1016/j.seppur.2017.11.040>.
- (42) Fonts, I.; Atienza-Martínez, M.; Carstensen, H. H.; Benés, M.; Pinheiro Pires, A. P.; Garcia-Perez, M.; Bilbao, R. Thermodynamic and Physical Property Estimation of Compounds Derived from the Fast Pyrolysis of Lignocellulosic Materials. *Energy and Fuels* **2021**. <https://doi.org/10.1021/acs.energyfuels.1c01709>.
- (43) Marrero, J.; Gani, R. Group-Contribution Based Estimation of Pure Component Properties. *Fluid Phase Equilib.* **2001**, *183–184*, 183–208. <https://doi.org/10.1016/S0378->

3812(01)00431-9.

- (44) Terrell, E. Estimation of Hansen Solubility Parameters with Regularized Regression for Biomass Conversion Products: An Application of Adaptable Group Contribution. *Chem. Eng. Sci.* **2022**, *248*. <https://doi.org/10.1016/J.CES.2021.117184>.
- (45) Keith Harrison, B.; Seaton, W. H. Solution to Missing Group Problem for Estimation of Ideal Gas Heat Capacities. *Ind. Eng. Chem. Res.* **1988**, *27* (8), 1536–1540. <https://doi.org/10.1021/ie00080a031>.
- (46) Hurst, J. E.; Harrison, B. K. Estimation of Liquid and Solid Heat Capacities Using a Modified Kopp's Rule. *Chem. Eng. Commun.* **1992**, *112* (1), 21–30. <https://doi.org/10.1080/00986449208935989>.
- (47) Stefanis, E.; Panayiotou, C. Prediction of Hansen Solubility Parameters with a New Group-Contribution Method. *Int J Thermophys* **2008**, *29*, 568–585. <https://doi.org/10.1007/s10765-008-0415-z>.
- (48) Teixeira, A. R.; Mooney, K. G.; Kruger, J. S.; Williams, C. L.; Suszynski, W. J.; Schmidt, L. D.; Schmidt, D. P.; Dauenhauer, P. J. Aerosol Generation by Reactive Boiling Ejection of Molten Cellulose. *Energy Environ. Sci.* **2011**, *4* (10), 4306–4321. <https://doi.org/10.1039/C1EE01876K>.
- (49) Yu, Y.; Chua, Y. W.; Wu, H. Characterization of Pyrolytic Sugars in Bio-Oil Produced from Biomass Fast Pyrolysis. *Energy and Fuels* **2016**, *30* (5), 4145–4149. <https://doi.org/10.1021/acs.energyfuels.6b00464>.
- (50) Shoji, T.; Kawamoto, H.; Saka, S. Boiling Point of Levoglucosan and Devolatilization Temperatures in Cellulose Pyrolysis Measured at Different Heating Area Temperatures. *J. Anal. Appl. Pyrolysis* **2014**, *109*, 185–195. <https://doi.org/10.1016/j.jaap.2014.06.014>.

- (51) Gong, X.; Yu, Y.; Gao, X.; Qiao, Y.; Xu, M.; Wu, H. Formation of AnhydroSugars in the Primary Volatiles and Solid Residues from Cellulose Fast Pyrolysis in a Wire-Mesh Reactor. **2014**. <https://doi.org/10.1021/ef501112q>.
- (52) Oja, V.; Suuberg, E. M. Vapor Pressures and Enthalpies of Sublimation of D-Glucose, D-Xylose, Cellobiose, and Levoglucosan. *J. Chem. Eng. Data* **1999**, *44* (1), 26–29. <https://doi.org/10.1021/je980119b>.
- (53) Watson, K. M. Thermodynamics of the Liquid State. *Ind. Eng. Chem.* **1943**, *35* (4), 398–406.
- (54) Hansen, C.M. *Hansen Solubility Parameters Second Edition: A User's Handbook*; 2007. A User's Handbook; CRC Press: Boca Raton, FL, 2007; pp 10–11, 347, 423.
- (55) Lydersen, A. L.; Greenkorn, R. A.; Hougen, O. A. Estimation of Critical Properties of Organic Compounds. Engineering Experiment Station Report 3; College of Engineering, University of Wisconsin: Madison, WI, 1955; pp 1–22
- (56) Le´ de´ , J. Diebold, J.P., Peacocke, G.V.C., Piskorz, J. in: A.V. Bridgwater (Ed.), *Fast Pyrolysis of Biomass: A Handbook*, *CPL Press*, Newbury, 1999, pp. 51–65
- (57) Riedel, L. Eine neue universelle Dampfdruckformel Untersuchungen über eine Erweiterung des Theorems der übereinstimmenden Zustände. Teil I. *Chem. Ing. Tech.* **1954**, *26* (2), 83–89.
- (58) Pérez Ponce, A. A.; Salfate, I.; Pulgar-Villaruel, G.; PalmaChilla, L.; Lazzus, J. A. New group contribution method for the prediction of normal melting points. *J. Eng. Thermophys.* **2013**, *22* (3), 226–235.
- (59) Chueh, C. F.; Swanson, A. C. Estimation of liquid heat capacity. *Can. J. Chem. Eng.* **1973**, *51* (5), 596–600.

- (60) Joback, K. G.; Reid, R. C. Estimation of pure-component properties from group-contributions. *Chem. Eng. Comm.* **1987**, *57*, 233-243.
- (61) M. J. Frisch, G. W. Trucks, H. B. Schlegel, G. E. Scuseria, M. A. Robb, J. R. Cheeseman, G. Scalmani, V. Barone, G. A. Petersson, H. Nakatsuji, X. Li, M. Caricato, A. V. Marenich, J. Bloino, B. G. Janesko, R. Gomperts, B. Mennucci, H. P. Hratchian, J. V. Ortiz, A. F. Izmaylov, J. L. Sonnenberg, D. Williams-Young, F. Ding, F. Lipparini, F. Egidi, J. Goings, B. Peng, A. Petrone, T. Henderson, D. Ranasinghe, V. G. Zakrzewski, J. Gao, N. Rega, G. Zheng, W. Liang, M. Hada, M. Ehara, K. Toyota, R. Fukuda, J. Hasegawa, M. Ishida, T. Nakajima, Y. Honda, O. Kitao, H. Nakai, T. Vreven, K. Throssell, J. A. Montgomery, Jr., J. E. Peralta, F. Ogliaro, M. J. Bearpark, J. J. Heyd, E. N. Brothers, K. N. Kudin, V. N. Staroverov, T. A. Keith, R. Kobayashi, J. Normand, K. Raghavachari, A. P. Rendell, J. C. Burant, S. S. Iyengar, J. Tomasi, M. Cossi, J. M. Millam, M. Klene, C. Adamo, R. Cammi, J. W. Ochterski, R. L. Martin, K. Morokuma, O. Farkas, J. B. Foresman, and D. J. Fox, Gaussian 16, Revision C.01, Gaussian, Inc., Wallingford CT, 2019.

CHAPTER FOUR: THEORETICAL INSIGHTS ON THE FRAGMENTATION OF
CELLULOSIC OLIGOMERS TO FORM HYDROXYACETONE
AND HYDROXYACETALDEHYDE

Denson, M. D., Terrell, E., Kostetskyy, P., Broadbelt, L., Olarte, M., & Garcia-Perez, M. (2023). Theoretical Insights on the Fragmentation of Cellulosic Oligomers to Form Hydroxyacetone and Hydroxyacetaldehyde. *Energy & Fuels*, 37(18), 13997-14005.
<https://doi.org/10.1021/acs.energyfuels.3c01924>

Originally published in the *Energy & Fuels* and reproduced here.

Attributions:

- ✓ M. Denson – concept, computations/investigation, analysis of data, writing of first draft
- ✓ E. Terrell – concept, computational help/investigation and review and editing of drafts
- ✓ P. Kostetskyy – concept, computational help/investigation, review and editing of drafts
- ✓ M. Olarte – concept, review and editing of drafts, supervision
- ✓ L. Broadbelt – computational help, supervision
- ✓ M. Garcia-Perez – concept, review and editing of drafts, supervision

Abstract

The presence of heavy unknown oligomeric sugar products in bio-oil is evidenced in experimental results reported in the literature. In this paper, we studied the fragmentation reactions yielding hydroxyacetone and hydroxyacetaldehyde from oligomeric sugars following previous work on dehydration reactions to propose structures of these oligomers. Hydroxyacetone and hydroxyacetaldehyde are primary products of cellulose fast pyrolysis but the fragmentation reaction mechanism of these compounds from oligomers merits further study. The density functional theory (DFT) approach was employed to study this reaction. Results revealed that hydroxyacetone and hydroxyacetaldehyde fragments are more favorably removed from the non-reducing end based on their thermodynamic stabilities. As a result of this study, we proposed new potential structures of the unknown oligomeric sugars. Theoretical FTIR and NMR spectra were calculated so that in the future when these molecules are separated, their experimental spectra and the theoretical ones herein reported can be used to confirm the structures of these oligomeric sugars. Also, the thermodynamics and physical properties of these compounds were estimated using the Group Contribution Method (GCM). These properties are essential in the design of technologies for bio-oil refining.

4.1 Introduction

Pyrolysis oil, often called bio-oil, is a complex, dark liquid product of fast pyrolysis. It is formed by more than 50 wt.% high molecular mass compounds ($> 500 \text{ g mol}^{-1}$), which cannot be analyzed by GC/MS but can be experimentally studied by Fourier-transform ion cyclotron resonance mass spectrometry (FT-ICR MS).^{1,2,3} These oligomeric compounds are derived from cellulose, hemicellulose, and lignin and whose structures are poorly understood.^{2,4} Cellulose decomposition is initiated by depolymerization to yield 'active cellulose' which further undergoes competitive reactions of fragmentation and dehydration to form anhydrosugars and low molecular mass compounds. The presence of sugars in pyrolysis oils is believed to be the culprit of coke formation during upgrading and therefore the need to study these sugar oligomers. Stankovikj et al.⁴ studied the water-soluble fraction of the bio-oil and results showed the presence of unknown high molecular mass fractions accounting for 30-55 wt % which are believed to be products of highly dehydrated sugars.

Patwardhan et al.⁵ reported that the formation of levoglucosan and other low molecular mass compounds are formed via competitive reactions and not sequential reactions. The light products of fragmentation reactions such as hydroxyacetone and hydroxyacetaldehyde are well-known and among the most abundant single compounds found in pyrolysis oils.² Several works have been done to investigate the formation of these products during the biomass pyrolysis in the presence of alkaline compounds and mineral salts. While hydroxyacetaldehyde yield decreases dramatically in the presence of KOH even in small amounts, the yield of hydroxyacetone was not affected.⁶ The authors concluded that the action of KOH changes even with compounds of the same class. When using a Lewis acid such as ZnCl_2 , the yields of both hydroxyacetone and hydroxyacetaldehyde decrease very fast because Lewis acids acted as a dehydrating and cross-

linking agent promoting char and water formation.⁸ In the presence of $\text{Ca}(\text{OH})_2$, however, the yield of hydroxyacetone and hydroxyacetaldehyde increased very fast because mineral salts and higher temperature accelerated the formation of low molecular mass compounds compared to anhydrosugars.⁷ The yields of hydroxyacetaldehyde and hydroxyacetone reach maximum yields in the presence of NaCl and KCl. Much lower impact was observed when MgCl_2 and CaCl_2 were used.⁷ Further, Radelin et al.³⁰ studied the effect of temperature on the yield of hydroxyacetaldehyde and found that the maximum yield is achieved at 873 K. Higher temperatures resulted in a dramatic reduction in yield. In the literature, it has been reported that hydroxyacetone concentration in pyrolysis oils is between 2.6 to 8.6 wt.% while hydroxyacetaldehyde is found to be between 1.0 to 13.7 wt.%.^{2,9,10} These high contents could eventually justify their separation and commercialization as chemicals. Hydroxyacetone and hydroxyacetaldehyde are known for their use in medical applications, the food industry, and as precursors of other chemical products.^{11,12}

With reference to the work of Stankovikj et al.⁴, Terrell and Garcia-Perez³ coupled FT-ICR MS experimental results with combinatoric dehydration and fragmentation modeling to further propose structures of the unknown oligomers. Molecular formulas of the unknown oligomers were proposed. With the use of Density Functional Theory (DFT), this work aimed to propose structures of the unknown oligomers. Some modeling studies^{13,14} also investigated the formation of these compounds but only from the monomers. It was shown that these products are mostly generated from the $\text{C}_1\text{-C}_2\text{-C}_3$ and $\text{C}_4\text{-C}_5\text{-C}_6$ segments of monomers. Richards⁹ proposed a very preliminary mechanism to explain cellulose fragmentation. To the best of our knowledge, there is very limited available literature related to studying the reaction mechanisms producing hydroxyacetone and hydroxyacetaldehyde from oligomers.

The main goal of this work is to investigate the mechanism of hydroxyacetone and hydroxyacetaldehyde fragmentation from oligomeric sugars to propose potential structures of the heavy unknown oligomeric sugars in bio-oil. It is the first time in literature in the last 70 years to report the fragmentation mechanism of these compounds from cellulosic oligomers. This work will contribute towards understanding the composition and structural motifs of the unknown oligomers which are essential to design reactors and catalysts for downstream processing.

4.2 Methodology

4.2.1 Computational Details

The fragmentation reaction mechanism of hydroxyacetone and hydroxyacetaldehyde from oligomeric sugars was studied using the DFT specifically the Gaussian 16 software package³⁹ to perform geometry optimization and frequency calculations of all reactants, intermediates, and products at MO6-2X functional¹⁵ and 6-311++G(d,p) level of theory. A correction factor of 0.9567 developed by Unal et al.¹⁶ was applied to account for errors associated with the description of the electron correlation, anharmonicity and solvation of the Schrodinger equation to obtain a more accurate result. The dimer up to tetramer state of the carbohydrates were used as model compounds of the oligomeric sugars. Each equilibrium geometry for all calculations was verified to have no imaginary frequency. All possible positions from where the hydroxyacetaldehyde could be fragmented from the oligomer structures was assessed and the reaction that gives the lowest Gibbs free energy change is identified as the most thermodynamically stable product. It should be noted that only the thermodynamic stabilities of the isomeric compounds was considered in this paper.

Theoretical Nuclear Magnetic Resonance (NMR) was also calculated using the Gauge-Independent Atomic Orbital (GIAO) method to aid in elucidating the structures of the oligomeric

sugars. MO6-2X functional and 6-311+G(d,p) level of theory was used to generate the NMR spectra of the stable products. The NMR magnetic shielding tensor of the reference molecule, deuterated dimethyl sulfoxide (DMSO-d₆, 99.9%, Cambridge Isotope Laboratories, Inc.), was calculated and the shielding value was subtracted from the spectrum of the stable products to create the chemical shift values for the candidate structure under study. Theoretical results may slightly vary among types of functionals and basis sets applied and also the type of reference molecule employed for NMR calculations.

Validation of the simulations was performed by comparing simulation results of selected model compounds with experimental outputs, which were reported in our previous paper.¹⁷ Briefly, standard pure compounds such as D-glucose (Dextrose) anhydrous, ($\geq 99\%$, Thermo Scientific Chemicals), D(+)-mannose ($\geq 99\%$, Sigma Aldrich), and levoglucosan (99.3%, AK Scientific, Inc.) were subjected to Fourier-Transform Infrared Spectroscopy (FTIR) and NMR analyses for both experimental and modeling. The procedure for FTIR and NMR experimental analyses are described elsewhere.¹⁷ Results showed that the simulation yields are qualitatively comparable with the experimental results. Moreover, pyrolytic sugar was extracted from BTG bio-oil by means of cold-water precipitation, followed by column chromatography using Sepabeads resin to adsorb phenols from the water-soluble fraction. Subsequently, the sugar was concentrated via rotary evaporation. This sugar was then subjected to FTIR and NMR analyses.

4.2.2 Fragmentation Reaction Mechanisms of Hydroxyacetaldehyde and Hydroxyacetone

Removal from Oligomeric Sugars

Figures 4.1 and 4.2 show the fragmentation mechanisms of hydroxyacetone and hydroxyacetaldehyde from oligomeric sugars, portraying cellobiosan as an example. For the removal of hydroxyacetaldehyde, 1,2-dehydration happens first at C₃-C₂ of the non-reducing

end, followed by ring opening at C₁-O₁ and retro-Diels-Alder reaction at C₄-C₅.⁹ Finally, tautomerization reaction happens at C₄-C₃ to obtain a more stable sugar fragment. All possible pathways including the internal units where hydroxyacetaldehyde could be removed were investigated. For the naming convention of the final product, say CBN-HAAb, this means the hydroxyacetaldehyde (HAA) was fragmented from cellobiosan (CBN) at ring *b* (nonreducing end). The same pattern for the naming convention was used for all the compounds studied.

The proposed reaction mechanism of hydroxyacetone fragmentation from oligomeric sugars is initiated by 1,2-dehydration at C₅-C₆ of the non-reducing end, followed by ring opening at C₁-O₁ and proton transfer from C₂-C₁, tautomerization reaction at C₆-C₅, and then retro-aldol reaction at C₃-C₄. This proposed mechanism is only possible for the non-reducing end and does not work with the internal units of the trimer and tetramer structures.

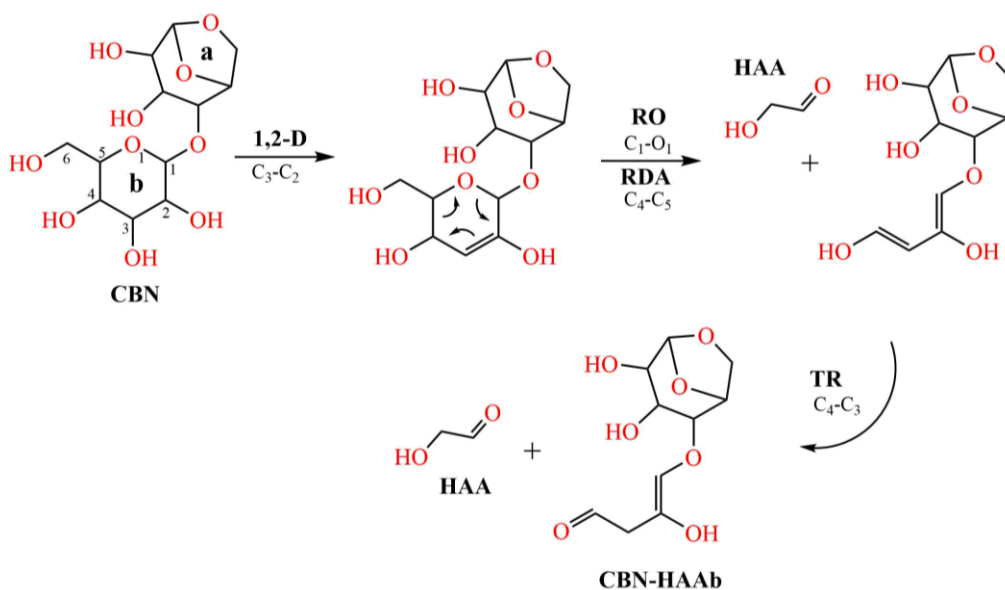


Figure 4.1: Proposed mechanism of hydroxyacetaldehyde fragmentation from oligomeric sugars. CBN: cellobiosan; a: ring *a* of the model compound; b: ring *b* of the model compound; 1,2-D: 1,2 dehydration reaction; RO: ring opening reaction; RDA: retro-Diels-Alder reaction; TR: tautomerization; HAA: hydroxyacetaldehyde; CBN-HAAb: final product.

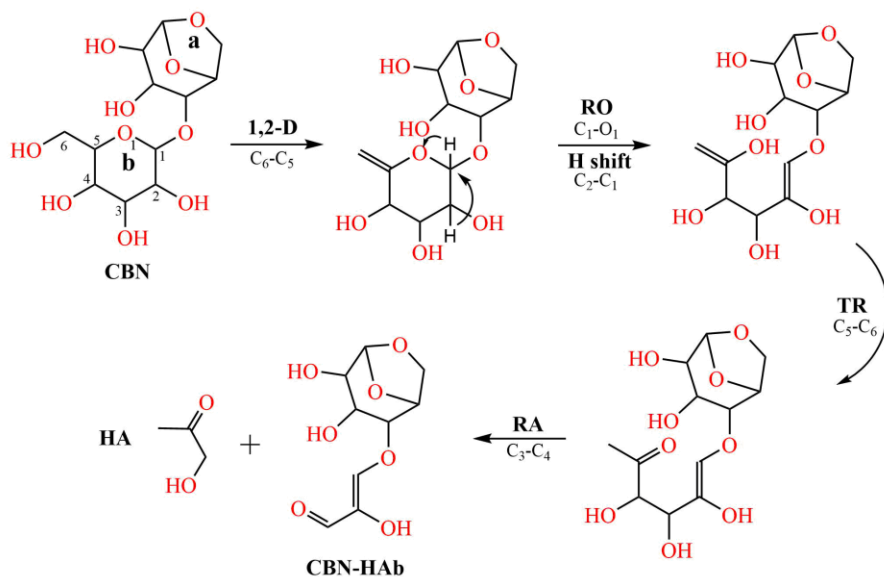


Figure 4.2: Proposed mechanism of hydroxyacetone fragmentation from oligomeric sugars. CBN stands for cellobiosan; a: ring *a* of the model compound; b: ring *b* of the model compound; 1,2-D: 1,2 dehydration reaction; RO: ring opening reaction; H shift: proton transfer; TR: tautomerization reaction; RA: retro-aldol reaction; HA: hydroxyacetone; CBN-HAb: final product.

4.2.3 Estimation of Thermophysical Properties of the Proposed Structures

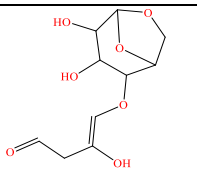
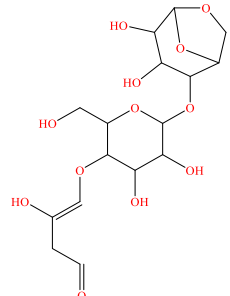
Group contribution method (GCM) using the approach described by Joback et al.^{18,31} and Lydersen et al.³² and other several authors was used to estimate the thermodynamics and physical properties of the proposed products. The detailed approach was described somewhere where Fonts et al.¹⁹ applied this method to estimate thermodynamic and physical properties of selected bio-oil compounds. Briefly, it works by summing up the number of similar fragments forming the structure of a compound then multiplied by their corresponding group contributions. The properties estimated in this paper include boiling point, melting point, Gibbs free energy and enthalpy of formation, enthalpy of vaporization, and solubility parameters, among others. These properties are essential for the design of processing/upgrading technologies and the selectivity of products.

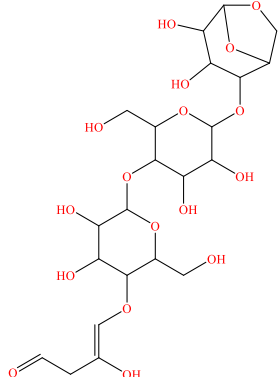
4.3 Results and Discussion

4.3.1 Proposed Structures of the Oligomeric Sugar Fragments

Tables 4.1 and 4.2 show the potential fragment structures of oligomeric sugars with their corresponding changes in Gibbs free energy, enthalpy, and entropy of reaction. Results showed that hydroxyacetaldehyde and hydroxyacetone compounds are most likely to be fragmented from the non-reducing end. These structures were proposed based on their thermodynamic stabilities. The reaction that gives the lowest Gibbs free energy change is identified as the most thermodynamically stable product. The proposed structures show the formation of aldehyde functional group where the hydroxyacetone and hydroxyacetaldehyde compounds were eliminated. Experimentally, bio-oil is reported to contain aldehyde compounds among its hundred individual components.^{2,20}

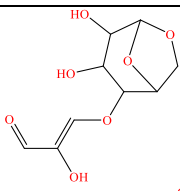
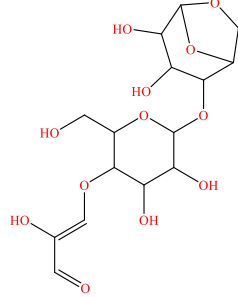
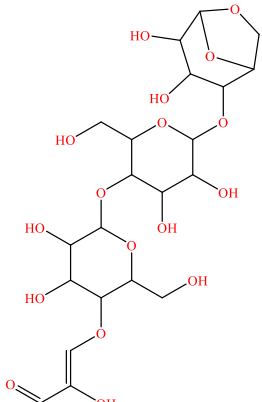
Table 4.1. Proposed structures of the oligomeric sugar fragments where hydroxyacetaldehyde is removed.^a

reaction label	product structure	molecular formula	molar mass (g mol ⁻¹)	ΔG_{rxn} (kJ mol ⁻¹)	ΔH_{rxn} (kJ mol ⁻¹)	ΔS_{rxn} (J mol ⁻¹ K ⁻¹)
CBN-HAAb		C ₁₀ H ₁₄ O ₇	246.07	-108.60	40.91	415
CTN-HAAc		C ₁₆ H ₂₄ O ₁₂	408.13	-103.37	42.75	411

CQN-HAAd		$C_{22}H_{34}O_{17}$	570.18	-84.00	51.94	398
----------	---	----------------------	--------	--------	-------	-----

^aNote: Hydroxyacetaldehyde is also a product but is not shown here.

Table 4.2. Proposed structures of the oligomeric sugar fragments where hydroxyacetone is removed.^b

reaction label	product structure	molecular formula	molar mass (g mol ⁻¹)	ΔG_{rxn} (kJ mol ⁻¹)	ΔH_{rxn} (kJ mol ⁻¹)	ΔS_{rxn} (J mol ⁻¹ K ⁻¹)
CBN-HAb		$C_9H_{12}O_7$	232.06	-170.9	147.22	411
CTN-HAc		$C_{15}H_{22}O_{12}$	394.11	-202.9	107.44	401
CQN-HAd		$C_{21}H_{32}O_{17}$	556.16	-162.5	152.11	407

^bNote: Hydroxyacetone is also a product but is not shown here.

4.3.2 Theoretical Spectra of the Oligomeric Sugar Fragments

NMR

Figure 4.3 presents the theoretical ^{13}C -NMR (a) and ^1H -NMR (b) spectra of the proposed oligomeric sugar fragments where hydroxyacetaldehyde was removed. The ^{13}C -NMR results showed that the most downfield (past 200 ppm) are the aldehyde group ($\text{C}=\text{O}$). Spectral regions between 137-157 ppm are the double bond carbon ($\text{C}=\text{C}$) atoms of the non-ring end associated with the alkene groups where hydroxyacetone and hydroxyacetaldehyde were fragmented. Regions at 65-100 ppm are the single bond carbons attached to the hydroxyl/alcohol groups ($\text{C}-\text{OH}$) and finally, regions at 48-52 ppm are the aliphatic $\text{C}-\text{C}$ atoms from the non-ring end. A good qualitative agreement was seen between the modeling and experimental results, especially at 50 to 100 ppm regions. Peaks seen at regions past 150 ppm were observed to have very weak intensity in the experimental result. The modeling result of the oligomeric sugar fragments are within the range of the experimental values obtained from the BTG water-soluble (WS) fraction of bio-oil⁴ where the oligomeric sugars were experimentally extracted.

^1H -NMR results show that the most downfield regions at 10.0 to 11.0 ppm originated from the protons of the aldehyde group ($\text{C}=\text{O}$). The spectral regions at 4.5 to 6.5 ppm are associated with alkenes and conjugated carbon ($\text{C}=\text{C}$) atoms. The dominant group seen at regions between 3 to 4.5 ppm corresponds to hydrogen atoms associated with the alcohol group. Lastly, regions at 0.5 to 3 ppm consisted of the protons from alkanes with the non-ring being the most upfield. The same functional groups identified from the ^{13}C -NMR, ^1H -NMR (Figure 4) and FTIR analyses (Figure 5b) of the sugar fragments where glycolaldehyde was removed were seen in the theoretical spectra of sugar fragments where hydroxyacetone was removed.

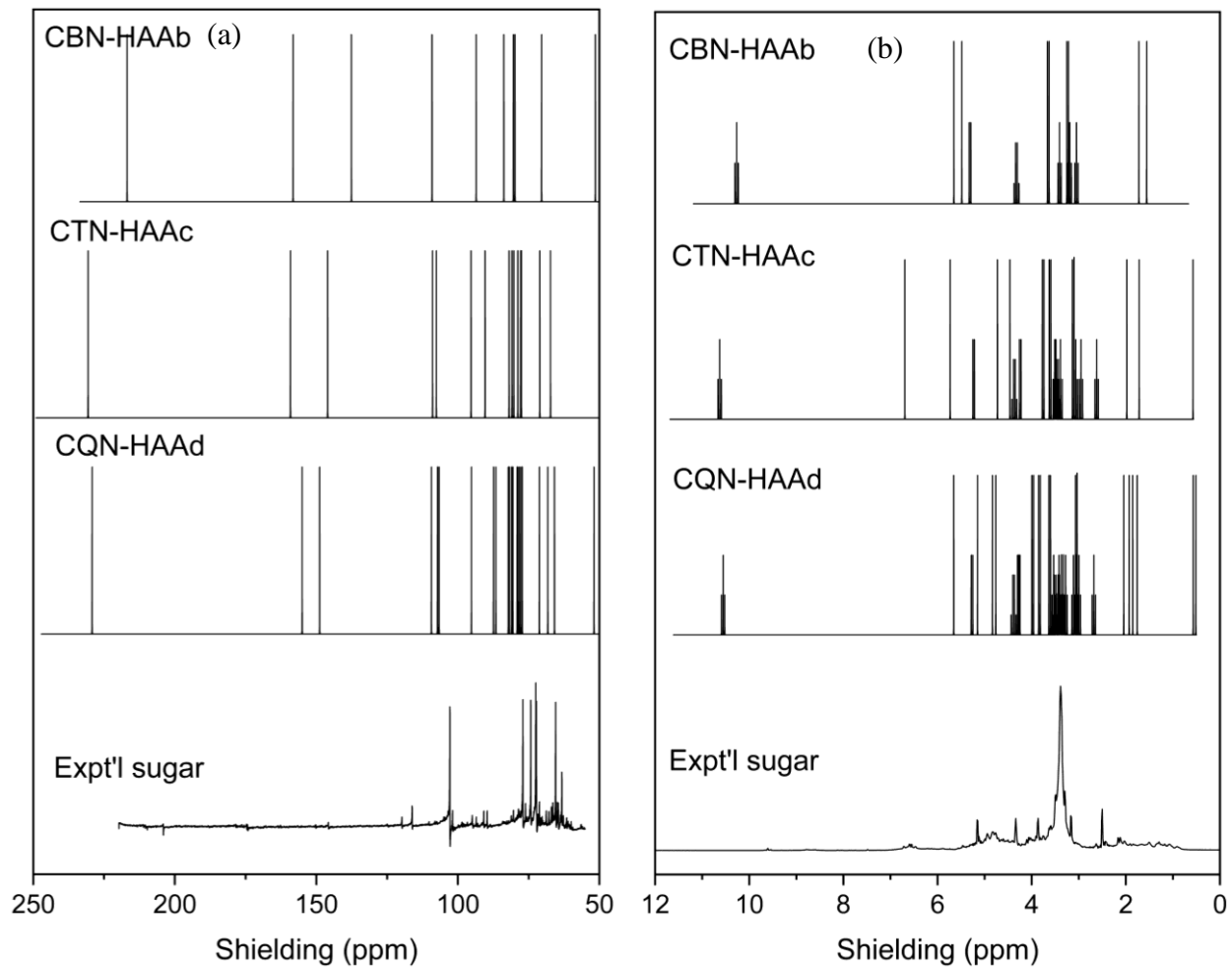


Figure 4.3: Theoretical ^{13}C -NMR (a) and ^1H -NMR (b) of the proposed oligomeric sugar fragments where hydroxyacetaldehyde was removed (experimental sugar solvent peak: DMSO- d_6 = 39.7 for ^{13}C -NMR and 2.5 ppm for ^1H -NMR).

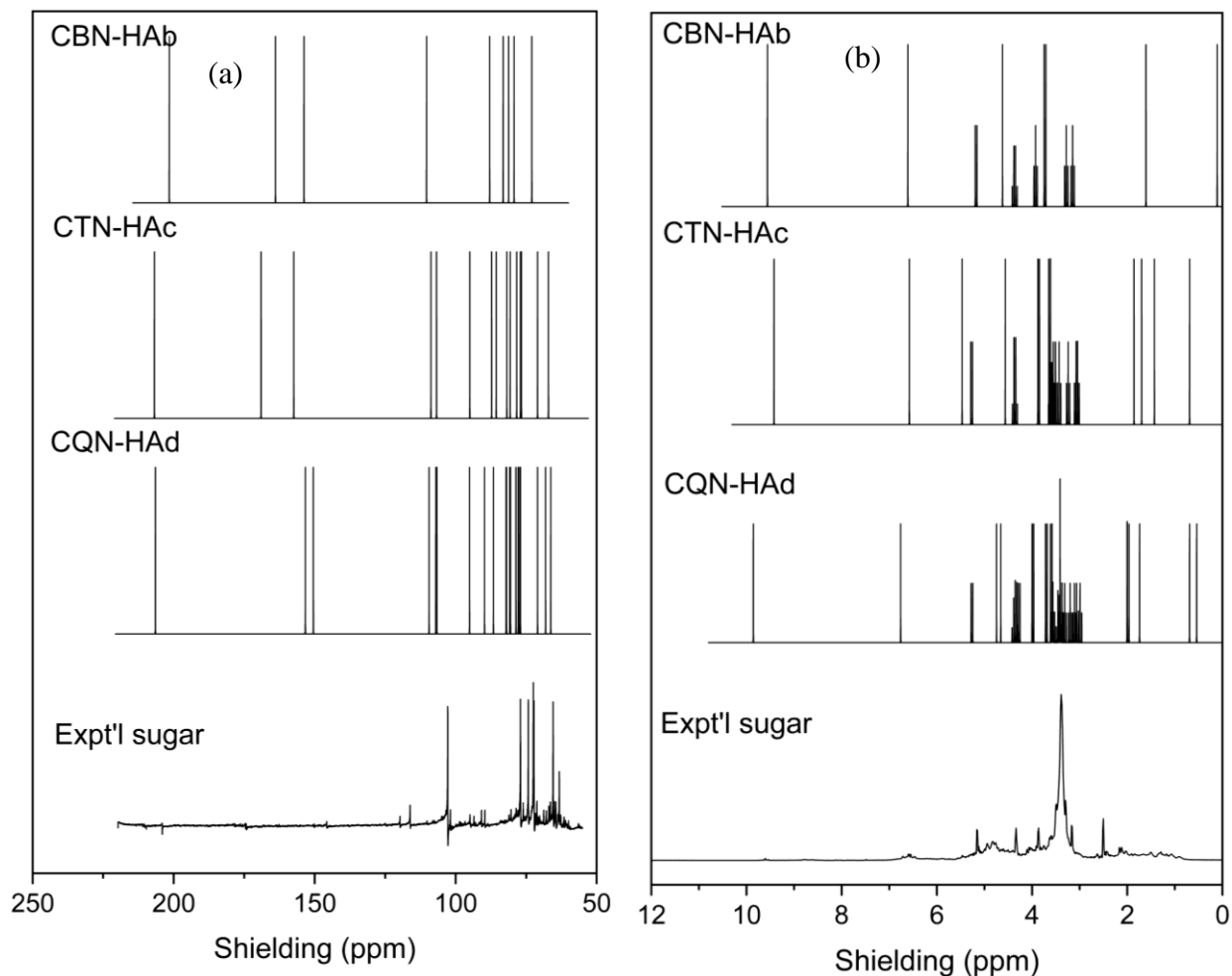


Figure 4.4: Theoretical ^{13}C -NMR (a) and ^1H -NMR (b) of the proposed oligomeric sugar fragments where hydroxyacetone was removed (DMSO peak at 39.7 ppm for ^{13}C -NMR and 2.5 ppm for the ^1H -NMR).

FTIR

Figure 4.5 shows the theoretical FTIR spectra of the oligomeric sugar fragments where hydroxyacetone and hydroxyacetaldehyde were removed. Result revealed a good qualitative agreement with the experimental values obtained from the whole sugar extracted from BTG bio-oil. The theoretical spectra was adjusted using a scale factor of 0.9567 to obtain a good agreement with the experimental vibrational frequencies.²¹ Peaks observed at 3500-3885 cm^{-1} are

assigned to the O-H stretches originating from the alcohol groups. The O-H stretches of the experimental resulted in a very broad peak which is attributed to moisture. Bands observed at 2800-3050 cm^{-1} wavenumbers correspond to C-H stretches from the alkane groups while regions at 1500-1700 cm^{-1} are drawn from the alkenes and conjugated C=C stretching. Lastly, C-O stretching were seen at 1000-1320 cm^{-1} wavenumbers from the alcohol groups. These FTIR modeling results of the model compounds correspond qualitatively well with the experimental analysis of the whole sugar. Further, these modeling yields conform to experimental results reported in the literature.^{22,23}

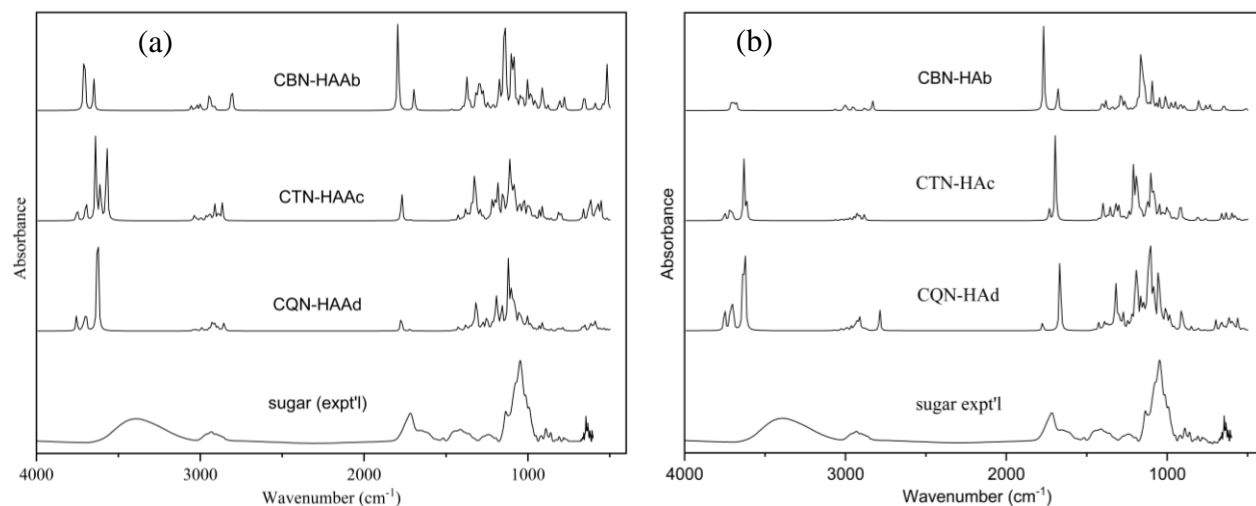


Figure 4.5: Theoretical FTIR spectra of the oligomeric sugar fragments where the hydroxyacetaldehyde (a) and hydroxyacetone (b) were removed.

4.3.3 Thermodynamic and Physical Properties of the Oligomeric Sugar Fragments

Tables 4.3 and 3.4 show the estimated thermodynamic and physical properties of the proposed structures of oligomeric sugar fragments with hydroxyacetone and hydroxyacetaldehyde removal, respectively. The structure of oligomeric sugars has not been

studied before and therefore there is no reference for comparison of the estimated thermodynamic and physical properties. The critical properties (temperature, pressure and volume) of the dimer are not too far from the estimated properties of cellobiosan by Fonts et al.¹⁹ The estimated values for the trimer and tetramer sugar fragments are high and should be treated with caution because these compounds are bigger than the compounds used for GCM development. Both methods, Joback^{18,31} and Lydersen et al.³², seem to agree with each other giving quite closer values.

Table 4.3. Estimated property values for each proposed structure of the oligomeric sugar fragments where hydroxyacetone is removed.

property	dimer	trimer	tetramer	refs
	CBN-HAAb	CTN-HAAc	CQN-HAAc	
Critical temp. (T_c , K)	1013	1689	3530	18, 31
	829	1370	3228	32
Critical pressure, (P_c , MPa)	4.5	3.3	2.5	18, 31
	5.5	2.5	1.7	32
Critical volume, (V_c , cm ³ mol ⁻¹)	550	911	1272	18, 31
	479	844	1284	32
Normal boiling point, (T_b , K)	819	1283	1747	18, 31
	666	837	1300	24
Enthalpy of vaporization @ T_b , ($\Delta H_{vap, T_b}$ kJ mol ⁻¹)	103	173	242	18, 31
	138	129	40	35
Enthalpy of vaporization, (@298.15K,) ($\Delta H_{vap, 298.15K}$, kJ mol ⁻¹)	176	286	289	25
	242	537	960	*
	488	784	1073	18, 31

Normal melting point (T_m , K)	557	783	1009	36
Enthalpy of fusion, ($\Delta H_{fus, T_m}$, kJ mol ⁻¹)	45	78	111	18, 31
Gas standard enthalpy of formation ($\Delta H_{f, G}^\circ$, kJ mol ⁻¹)	-988	-1964	-2709	18, 31
Gas standard Gibbs free energy of formation ($\Delta G_{f, G}^\circ$, kJ mol ⁻¹)	-616	-1258	-1741	18, 29
Gas heat capacity at constant pressure (@298 K) ($C_{p, G}$, J mol ⁻¹ K ⁻¹)	201	424	621	18, 31
	252	418	584	38
Liquid heat capacity at constant pressure ($C_{p, L}$, J mol ⁻¹ K ⁻¹)	466	794	1117	37
Solid heat capacity at constant pressure, ($C_{p, s}$, J mol ⁻¹ K ⁻¹)	309	517	725	26
Liquid standard enthalpy of formation of individual compounds, ($\Delta H_{f, L}^\circ$, kJ mol ⁻¹)	-1248	-2439	-2637	*
Hansen solubility parameter				33
dispersion, δ_d	18.7	19.7	20.7	
polar, δ_p	22.2	33.9	55.6	
hydrogen bonding, δ_{hb}	27.1	47.7	77.7	
total, δ_T	39.7	61.8	97.8	

* - thermodynamic equation

Table 4.4. Estimated physical change property values for each proposed structure of the oligomeric sugar fragments where hydroxyacetaldehyde is removed.

property	Dimer	trimer	tetramer	refs
	CBN-HAAb	CTN-HAAc	CQN-HAAd	
Critical temp. (T_c , K)	1037	1740	3741	18, 31
	833	1209	3476	32
Critical pressure, (P_c , MPa)	3.9	2.9	2.3	18, 31
	3.5	2.2	1.5	32
Critical volume, (V_c , cm ³ mol ⁻¹)	606	967	1326	18, 31
	605	972	1339	32
Normal boiling point, (T_b , K)	842	1306	1770	18, 31
	678	877	1312	24
Enthalpy of vaporization @ T_b , ($\Delta H_{vap, T_b}$ kJ mol ⁻¹)	105	175	244	18, 31
	140	117	35	35
Enthalpy of vaporization, (@298.15K,) ($\Delta H_{vap, 298.15K}$, kJ mol ⁻¹)	182	286	289	25
	221	524	886	*
Normal melting point (T_m , K)	499	789	1078	18, 31
	546	790	1016	36
Enthalpy of fusion, ($\Delta H_{fus, T_m}$, kJ mol ⁻¹)	48	81	114	18, 31
Gas standard enthalpy of formation ($\Delta H_{f, G}^\circ$, kJ mol ⁻¹)	-1009	-1880	-2752	18, 31
Gas standard Gibbs free energy of formation ($\Delta G_{f, G}^\circ$, kJ mol ⁻¹)	-608	-1166	-1723	18, 31
Gas heat capacity at constant pressure (@298K) ($C_{p, G}$, J mol ⁻¹ K ⁻¹)	284	468	715	18, 31
	252	418	584	38

Liquid heat capacity at constant pressure, ($\Delta H_{f,G}^{\circ}$, J mol ⁻¹ K ⁻¹)	497	815	1151	37
Solid heat capacity at constant pressure, ($\Delta G_{f,G}^{\circ}$, J mol ⁻¹ K ⁻¹)	309	517	725	26
Liquid standard enthalpy of formation of individual compounds, ($\Delta H_{f,L}^{\circ}$, kJ mol ⁻¹)	497	815	1151	*
Hansen solubility parameter				33
dispersion, δ_d	18.7	19.7	20.6	
polar, δ_p	21.9	33.6	55.3	
hydrogen bonding, δ_{hb}	26.7	47.3	77.3	
total, δ_T	39.2	61.2	97.3	

* - *thermodynamic equation*

For the normal boiling point, cellobiosan and cellotriosan were reported to have experimental results accounting for 853 K¹, and 1,063 K²⁷, respectively. Le´de´ et al.³⁴ reported almost the same values for cellobiosan (854 K) and cellotriosan (1065 K). In this work, the estimated boiling point of the dimer (819 K) and trimer (1283 K) sugar fragments are closer to the values obtained when using the Joback method. These values are higher than the typical temperature (773 K) of fast pyrolysis which further supports the proposed mechanism that these anhydrosugar oligomers are ejected during the pyrolysis process rather than vaporized.^{1,28}

The estimated enthalpies of vaporization are quite close for the dimeric sugar fragments for both the methods applied. However, estimated results for the trimer and tetramer fragments are significantly higher when using the TMD_VAP_ENTH compared to the Watson²⁵ method and therefore needs to be treated with caution. This result is similar to what Fonts et al.¹⁹

obtained for larger compounds. For normal melting point, both methods (Joback³¹ and Pérez-Ponce³⁶) applied seem to agree with each other giving quite closer values. The estimated values for the dimer fragments in this work are close to the melting point of cellobiose (513 K) reported in the literature.²⁹ The enthalpy of fusion was estimated using Joback method which is reported to give accurate results. An estimated value of 45 kJ/mol for the dimeric fragment would be reasonable compared to the result (67.9 kJ/mol) reported by Fonts et al.¹⁹ for cellobiosan.

The ideal gas properties such as standard Gibbs free energy and enthalpy of formation were estimated using Joback method, which is reported to have yield reasonable estimates for these properties¹⁹. In comparison to the estimated values of cellobiosan by Fonts et al.¹⁹, the results obtained in this work for the dimeric fragments are reasonable. Similarly, the values obtained in this work for the heat capacities (gas, solid, liquid) at constant pressure and the liquid standard enthalpy of formation are reasonable when compared with the results obtained by Fonts et al. for cellobiosan. Finally, the estimated values for the solubility parameters of the dimeric fragments using the Hansen method are reasonable compared to the values reported for cellobiosan¹⁹.

4.4 Conclusion

The goal of this work is to unravel the structure of the heavy unknown oligomeric sugars obtained by fast pyrolysis of cellulose. It specifically aimed to study the mechanism of fragmentation reaction to form hydroxyacetone and hydroxyacetaldehyde from the oligomeric sugars. Glucose-based oligomers (dimer to tetramer) were used as model compounds. The Gaussian software package was employed to obtain and propose potential structures of the oligomers. Results showed that both hydroxyacetone and hydroxyacetaldehyde could be directly fragmented from the sugar oligomers and are most favorably removed from the non-reducing

end of the oligomers. Theoretical FTIR and NMR were also calculated to reveal functional groups of the proposed products which are essential to build and understand their structures. The thermodynamic and physical properties of these proposed products were estimated employing the GCM. These properties are deemed necessary for the design of processing and upgrading technologies.

4.5 REFERENCES

- (1) Pecha, M. B.; Terrell, E.; Montoya, J. I.; Stankovikj, F.; Broadbelt, L. J.; Chejne, F.; Garcia-Perez, M. Effect of Pressure on Pyrolysis of Milled Wood Lignin and Acid-Washed Hybrid Poplar Wood. *Ind. Eng. Chem. Res.* **2017**, *56* (32), 9079–9089. <https://doi.org/10.1021/acs.iecr.7b02085>.
- (2) Stankovikj, F.; McDonald, A. G.; Helms, G. L.; Garcia-Perez, M. Quantification of Bio-Oil Functional Groups and Evidences of the Presence of Pyrolytic Humins. *Energy and Fuels* **2016**, *30* (8), 6505–6524. <https://doi.org/10.1021/acs.energyfuels.6b01242>.
- (3) Terrell, E.; Garcia-Perez, M. Novel Strategy to Analyze Fourier Transform Ion Cyclotron Resonance Mass Spectrometry Data of Biomass Pyrolysis Oil for Oligomeric Structure Assignment. *Energy and Fuels* **2020**, *34* (7), 8466–8481. <https://doi.org/10.1021/acs.energyfuels.0c01687>.
- (4) Stankovikj, F.; McDonald, A. G.; Helms, G. L.; Olarte, M. V.; Garcia-Perez, M. Characterization of the Water-Soluble Fraction of Woody Biomass Pyrolysis Oils. *Energy and Fuels* **2017**, *31* (2), 1650–1664. <https://doi.org/10.1021/acs.energyfuels.6b02950>.
- (5) Patwardhan, P. R.; Satrio, J. A.; Brown, R. C.; Shanks, B. H. Product Distribution from Fast Pyrolysis of Glucose-Based Carbohydrates. *J. Anal. Appl. Pyrolysis* **2009**, *86* (2), 323–330. <https://doi.org/10.1016/j.jaap.2009.08.007>.
- (6) Blasi, C. Di; Galgano, A.; Branca, C. Effects of Potassium Hydroxide Impregnation on Wood Pyrolysis. *Energy and Fuels* **2009**, *23* (2), 1045–1054. <https://doi.org/10.1021/ef800827q>.
- (7) Patwardhan, P. R.; Satrio, J. A.; Brown, R. C.; Shanks, B. H. Influence of Inorganic Salts on the Primary Pyrolysis Products of Cellulose. *Bioresour. Technol.* **2010**, *101* (12),

- 4646–4655. <https://doi.org/10.1016/j.biortech.2010.01.112>.
- (8) Di Blasi, C.; Branca, C.; Galgano, A. Products and Global Weight Loss Rates of Wood Decomposition Catalyzed by Zinc Chloride. *Energy and Fuels* **2008**, *22* (1), 663–670. <https://doi.org/10.1021/ef700464s>.
- (9) Richards, G. N. Glycolaldehyde from Pyrolysis of Cellulose. *J. Anal. Appl. Pyrolysis* **1987**, *10* (3), 251–255. [https://doi.org/10.1016/0165-2370\(87\)80006-2](https://doi.org/10.1016/0165-2370(87)80006-2).
- (10) Pinheiro Pires, A. P.; Arauzo, J.; Fonts, I.; Domine, M. E.; Fernández Arroyo, A.; Garcia-Perez, M. E.; Montoya, J.; Chejne, F.; Pfromm, P.; Garcia-Perez, M. Challenges and Opportunities for Bio-Oil Refining: A Review. *Energy and Fuels* **2019**, *33* (6), 4683–4720. <https://doi.org/10.1021/acs.energyfuels.9b00039>.
- (11) Mohamad, M. H.; Awang, R.; Yunus, W. M. Z. W. A Review of Acetol: Application and Production. *Am. J. Appl. Sci.* **2011**, *8* (11), 1135–1139. <https://doi.org/10.3844/ajassp.2011.1135.1139>.
- (12) Vitasari, C. R.; Meindersma, G. W.; de Haan, A. B. Laboratory Scale Conceptual Process Development for the Isolation of Renewable Glycolaldehyde from Pyrolysis Oil to Produce Fermentation Feedstock. *Green Chem.* **2012**, *14* (2), 321–325. <https://doi.org/10.1039/c1gc16200d>.
- (13) Lu, Q.; Hu, B.; Zhang, Z. xi; Wu, Y. ting; Cui, M. shu; Liu, D. jia; Dong, C. qing; Yang, Y. ping. Mechanism of Cellulose Fast Pyrolysis: The Role of Characteristic Chain Ends and Dehydrated Units. *Combust. Flame* **2018**, *198*, 267–277. <https://doi.org/10.1016/j.combustflame.2018.09.025>.
- (14) Kostetsky, P.; Coile, M. W.; Terrian, J. M.; Collins, J. W.; Martin, K. J.; Brazdil, J. F.; Broadbelt, L. J. Selective Production of Glycolaldehyde via Hydrothermal Pyrolysis of

- Glucose: Experiments and Microkinetic Modeling. *J. Anal. Appl. Pyrolysis* **2020**, *149*, 104846. <https://doi.org/10.1016/J.JAAP.2020.104846>.
- (15) Zhao, Y.; Truhlar, D. G.; Zhao, Y.; Truhlar, · D G. The M06 Suite of Density Functionals for Main Group Thermochemistry, Thermochemical Kinetics, Noncovalent Interactions, Excited States, and Transition Elements: Two New Functionals and Systematic Testing of Four M06-Class Functionals and 12 Other Functionals and Inorganometallic Chemistry and for Noncovalent Interactions. *Theor Chem Acc.* **2008**, *120*, 215–241. <https://doi.org/10.1007/s00214-007-0310-x>.
- (16) Ünal, Y.; Nassif, W.; Özyaydin, B. C.; Sayin, K. Scale Factor Database for the Vibration Frequencies Calculated in M06-2X, One of the DFT Methods. *Vib. Spectrosc.* **2021**, *112*. <https://doi.org/10.1016/J.VIBSPEC.2020.103189>.
- (17) Denson, M. D.; Terrell, E.; Kostetsky, P.; Olarte, M.; Broadbelt, L.; Garcia-perez, M. Elucidation of Structure and Physical Properties of Pyrolytic Sugar Oligomers Derived from Cellulose Depolymerization / Dehydration Reactions : A Density Functional Theory Study. **2023**. <https://doi.org/10.1021/acs.energyfuels.3c00641>.
- (18) Joback, K. G. A Unified Approach to Physical Property Estimation Using Multivariate Statistical Techniques. 1984. <http://dspace.mit.edu/handle/1721.1/15374>.
- (19) Fonts, I.; Atienza-Martínez, M.; Carstensen, H. H.; Benés, M.; Pinheiro Pires, A. P.; Garcia-Perez, M.; Bilbao, R. Thermodynamic and Physical Property Estimation of Compounds Derived from the Fast Pyrolysis of Lignocellulosic Materials. *Energy and Fuels* **2021**. <https://doi.org/10.1021/acs.energyfuels.1c01709>.
- (20) Diebold, J. P. A Review of the Chemical and Physical Mechanisms of the Storage Stability of Fast Pyrolysis Bio-Oils. *Nrel/Sr-570-27613* **2000**, No. January, 59.

- (21) Ünal, Y.; Nassif, W.; Özyaydin, B. C.; Sayin, K. Scale Factor Database for the Vibration Frequencies Calculated in M06-2X, One of the DFT Methods. *Vib. Spectrosc.* **2021**, *112* (November 2020), 1–6. <https://doi.org/10.1016/j.vibspec.2020.103189>.
- (22) Han, Y.; Pinheiro Pires, A. P.; Denson, M.; McDonald, A. G.; Garcia-Perez, M. Ternary Phase Diagram of Water/Bio-Oil/Organic Solvent for Bio-Oil Fractionation. *Energy and Fuels* **2020**, *34* (12), 16250–16264. <https://doi.org/10.1021/acs.energyfuels.0c03100>.
- (23) Stankovikj, F.; Garcia-Perez, M. TG-FTIR Method for the Characterization of Bio-Oils in Chemical Families. *Energy and Fuels* **2017**, *31* (2), 1689–1701. <https://doi.org/10.1021/acs.energyfuels.6b03132>.
- (24) Stein, S. E.; Brown, R. L. Estimation of Normal Boiling Points from Group Contributions. *J. Chem. Inf. Comput. Sci.* **2002**, *34* (3), 581–587. <https://doi.org/10.1021/CI00019A016>.
- (25) Watson, K. M. Liquid State GENERALIZED PREDICTION OF PROPERTIES. **2021**.
- (26) Hurst, J. E.; Harrison, B. K. Estimation of Liquid and Solid Heat Capacities Using a Modified Kopp's Rule. *Chem. Eng. Commun.* **1992**, *112* (1), 21–30. <https://doi.org/10.1080/00986449208935989>.
- (27) Mamleev, V.; Bourbigot, S.; Le Bras, M.; Yvon, J. The Facts and Hypotheses Relating to the Phenomenological Model of Cellulose Pyrolysis. Interdependence of the Steps. *J. Anal. Appl. Pyrolysis* **2009**, *84* (1), 1–17. <https://doi.org/10.1016/j.jaap.2008.10.014>.
- (28) Teixeira, A. R.; Mooney, K. G.; Kruger, J. S.; Williams, C. L.; Suszynski, W. J.; Schmidt, L. D.; Schmidt, D. P.; Dauenhauer, P. J. Aerosol Generation by Reactive Boiling Ejection of Molten Cellulose. *Energy Environ. Sci.* **2011**, *4* (10), 4306–4321. <https://doi.org/10.1039/c1ee01876k>.
- (29) Oja, V.; Suuberg, E. M. Vapor Pressures and Enthalpies of Sublimation of D-Glucose, D-

- Xylose, Cellobiose, and Levoglucosan. *J. Chem. Eng. Data* **1999**, *44* (1), 26–29.
<https://doi.org/10.1021/je980119b>.
- (30) Radlein D, Piskorz J, Scott DS: Fast Pyrolysis of natural polysaccharides as a potential industrial process. *Journal of Analytical and Applied Pyrolysis*, **1991**, *19*, 41-63)
- (31) Joback, K. G.; Reid, R. C. Estimation of pure-component properties from group-contributions. *Chem. Eng. Comm.* **1987**, *57*, 233-243.
- (32) Lydersen, A. L.; Greenkorn, R. A.; Hougen, O. A. Estimation of Critical Properties of Organic Compounds. Engineering Experiment Station Report 3; College of Engineering, University of Wisconsin: Madison, WI, **1955**; pp 1–22
- (33) Hansen, C. M. Hansen Solubility Parameters: A User's Handbook; CRC Press: Boca Raton, FL, **2007**; pp 10–11, 347, 423.
- (34) Le´de´, J. Diebold, J.P., Peacocke, G.V.C., Piskorz, J. in: A.V. Bridgwater (Ed.), Fast Pyrolysis of Biomass: A Handbook, *CPL Press*, Newbury, **1999**, pp. 51–65
- (35) Riedel, L. Kritischer Koeffizient, Dichte des gesättigten Dampfes und Verdampfungswärme. Untersuchungen über eine Erweiterung des Theorems der übereinstimmenden Zustände. Teil III. *Chem. Ing. Tech.* **1954**, *26* (12), 679–683.
- (36) Pérez Ponce, A. A.; Salfate, I.; Pulgar-Villaruel, G.; PalmaChilla, L.; Lazzus, J. A. New group contribution method for the prediction of normal melting points. *J. Eng. Thermophys.* **2013**, *22* (3), 226–235.
- (37) Chueh, C. F.; Swanson, A. C. Estimation of liquid heat capacity. *Can. J. Chem. Eng.* **1973**, *51* (5), 596–600.
- (38) Harrison, B. K.; Seaton, W. H. Solution to missing group problem for estimation of ideal gas heat capacities. *Ind. Eng. Chem. Res.* **1988**, *27* (8), 1536–1540.

(39) M. J. Frisch, G. W. Trucks, H. B. Schlegel, G. E. Scuseria, M. A. Robb, J. R. Cheeseman, G. Scalmani, V. Barone, G. A. Petersson, H. Nakatsuji, X. Li, M. Caricato, A. V. Marenich, J. Bloino, B. G. Janesko, R. Gomperts, B. Mennucci, H. P. Hratchian, J. V. Ortiz, A. F. Izmaylov, J. L. Sonnenberg, D. Williams-Young, F. Ding, F. Lipparini, F. Egidi, J. Goings, B. Peng, A. Petrone, T. Henderson, D. Ranasinghe, V. G. Zakrzewski, J. Gao, N. Rega, G. Zheng, W. Liang, M. Hada, M. Ehara, K. Toyota, R. Fukuda, J. Hasegawa, M. Ishida, T. Nakajima, Y. Honda, O. Kitao, H. Nakai, T. Vreven, K. Throssell, J. A. Montgomery, Jr., J. E. Peralta, F. Ogliaro, M. J. Bearpark, J. J. Heyd, E. N. Brothers, K. N. Kudin, V. N. Staroverov, T. A. Keith, R. Kobayashi, J. Normand, K. Raghavachari, A. P. Rendell, J. C. Burant, S. S. Iyengar, J. Tomasi, M. Cossi, J. M. Millam, M. Klene, C. Adamo, R. Cammi, J. W. Ochterski, R. L. Martin, K. Morokuma, O. Farkas, J. B. Foresman, and D. J. Fox, Gaussian 16, Revision C.01, Gaussian, Inc., Wallingford CT, **2019**.

CHAPTER FIVE: TOWARDS A RATIONAL DESCRIPTION OF THE CHEMICAL COMPOSITION OF BIO-OIL WATER SOLUBLE FRACTIONS

Abstract

The primary objective of this study is to separate and characterize pyrolytic sugars present in the whole bio-oil. The heavy, unidentified compounds found in bio-oil consist of oligomeric sugars and are known for their significant role in coke formation during bio-oil upgrading. Consequently, it is of paramount importance to characterize these compounds.

To achieve this, BTG bio-oil was subjected to cold water precipitation to separate the water-soluble fraction of the bio-oil. Subsequent steps involved column chromatography using Sepabeads resin to effectively partition sugars from phenols. The extracted sugars were then concentrated through rotary evaporation. Further fractionation was carried out using silica gel column chromatography. To refine the separation process, semi-preparative HPLC was utilized, resulting in a chromatogram exhibiting several peaks that necessitate additional techniques to characterize the sugar compounds. The outcomes of this empirical research were synthesized with our previous modeling work to shed light into the potential structures of these oligomeric sugars. Results showed that bio-oil is a very complex mixture. Hundreds to thousands of compounds were found in the sugar sub-fraction samples obtained from the HPLC. Interestingly, the proposed molecular structures/formulas of sugar oligomers from Chapters 3 and 4 were detected experimentally.

5.1 Introduction

Pyrolysis oil or bio-oil, obtained through the pyrolysis of lignocellulosic biomass, has attracted significant attention among researchers due to its potential applications in the production of biofuels and chemicals. Biofuels play a critical role as an alternative to traditional fossil fuels, reducing global greenhouse gas emissions. However, bio-oil conversion into biofuels poses a significant challenge due to coke formation during the upgrading process, which is recognized to originate from heavy non-volatile compounds (i.e., sugar and lignin oligomers)^{1,2,3,4,5} Bio-oil is a complex mixture comprising hundreds to thousands of compounds with diverse molecular masses, functional groups, and polarities.^{6,7} Although, a fraction of the bio-oil still remains poorly understood at the moment.

The py-GC-MS analysis of Lin et al.⁸ on cellulose pyrolysis revealed an unidentified compound constituting 9.8 % of the composition. Further HPLC-MS analysis of these compounds revealed higher molar masses, specifically 347, 509, 671, 833, 922, 995, and 1157. Lédé et al.⁹ reported that these compounds are ionized anhydro-oligomers, corresponding to levoglucosan, cellobiosan (DP2), cellotriosan (DP3) and up to septaosan (DP7), respectively. More experimental studies^{1,10} further confirmed the existence of heavy unknown compounds, which were subsequently identified as oligomers from sugars. The characterization of the water-soluble fraction of bio-oil revealed the presence of unknown compounds, accounting for 30 to 55 wt. %.¹ It is speculated that these compounds originated from the highly dehydrated sugars containing abundant carbonyl groups, along with water-soluble phenols. These compounds are currently poorly understood and thus underscore further investigation to advance the understanding of bio-oil composition and their properties.

To elucidate bio-oil compositions, researchers employ separation techniques to isolate and analyze its constituent compounds. The most familiar method of separating bio-oil compounds is by liquid-liquid extraction.^{11,12,13,14} Cold-water precipitation is commonly used to extract the water-soluble bio-oil fraction containing highly polar sugar-rich compounds.^{4,10,13,15,16,17} Several solvents, such as n-hexane, toluene, dichloromethane, chloroform, ethyl acetate, ethanol, butanol, acetonitrile, and methanol are used to fractionate bio-oils, depending on the specific compound of interest.^{13,14,18,19,20,21,22,23} The mechanism of separation relies on the differences in solubility or affinity between the stationary and mobile phases. Compounds with stronger affinity interact with the stationary phase therefore they elute later than the compounds with weak affinity.

Pyrolytic sugars account for 15-30 wt.% in typical bio-oils.²⁴ When using a pure cellulose, levoglucosan yield can be as high as 59%.²⁵ Because the unknown bio-oil compounds are reported to be highly dehydrated sugars and among the compounds responsible to cause coke formation, it is necessary to isolate and analyze them. Results are important towards an in-depth understanding of their properties leading to efficient designs of valorization techniques. On the one hand, sugar fractions are attractive sources of bioethanol via hydrolysis of levoglucosan to glucose then subsequently undergo fermentation.²⁶ Other notable sugar-derived platform chemicals include levulinic acid, polyols and other platform chemicals.²⁷

Few modeling works have attempted to unveil potential structures of these sugar oligomeric compounds. Terrell and Garcia-Perez²⁸ proposed hypothetical structures of these compounds based on experimental FT-ICR MS analyses. Our previous modeling works on the dehydration²⁹ and fragmentation³⁰ mechanism of oligomeric sugars proposed several potential

structures of these compounds and showed that water, and hydroxyacetaldehyde, hydroxyacetone are most favorably formed from the nonreducing end of the sugar oligomers.

To our knowledge, no prior experimental efforts have been dedicated to the extraction and characterization of the heavy unknown bio-oil fractions which are associated to highly dehydrated sugars. Therefore, the primary objective of this study is to isolate and characterize the sugar fractions to shed light on their chemical constituents because they affect bio-oil quality. The isolation of the oligomers from the bio-oil was accomplished through a combination of cold-water precipitation and several column chromatography techniques. The findings from this experimental work were then integrated with the results obtained from our previous modeling endeavors to determine identity and propose potential structure of the unknown sugar fractions. This knowledge is of utmost importance for the design and development of upstream and/or downstream processing and technologies, especially to mitigate coke formation during bio-oil upgrading.

5.2 Methodology

5.2.1 Materials

BTG bio-oil (pyrolysis oil) was procured from The Netherlands and stored in the refrigerator at 5 °C prior to experiments. This oil is produced from sized pine woods (average of 3 mm particle size, < 5% MC) using a rotating cone reactor (<http://www.btg-btl.com/>) under the following conditions: ambient pressure, an average of 510 °C reactor temperature, < 2 s gas residence time and 40 °C condensation temperature (one step). The bio-oil container was vigorously hand-shaken to achieve homogeneity before taking out samples. HPLC-grade organic solvents such as dichloromethane (DCM, $\geq 99.8\%$, J.T. Baker), tetrahydrofuran (THF, $\geq 99.9\%$,

OmniSolv), ethyl acetate (EA, $\geq 99.5\%$, Macron Fine Chemicals), methanol (MeOH, $\geq 99.9\%$, J.T. Baker) were used in the fractionation step. These chemicals were used as received. Ultrapure water ($>18.18\text{ M}\Omega\cdot\text{cm}$) was produced in the laboratory. Silica gel (SiO_2 , ultrapure 40-60 μm , 60 \AA) was procured from Acros Organics. Sepabeads SP207 adsorption resin (250 μm , 110 \AA , Alfa Aesar) was purchased from Sigma Aldrich. Sand (J.T. Baker) was procured from Sigma Aldrich, while the cotton wool was bought from a local store.

5.2.2 Experimental Set-up

Figure 5.1 shows the experimental scheme of separating pyrolytic sugars from the whole BTG bio-oil.

Separation of Oligomeric Sugars

BTG bio-oil was rotary evaporated (Büchi Rotavapor R-3000, Thermo Scientific, Hanover Park, IL) to evaporate the light oxygenates (water, acetic acid, hydroxyacetone, hydroxyacetaldehyde) at 55 °C bath temperature and 28 inHg. Light oxygenates have a yield of 26%. The resulting bio-oil was mixed with methanol (1:0.25 wt.%) prior to cold precipitation. Cold water precipitation was employed to fractionate bio-oil and the complete procedure is described somewhere^{14,15, 31, 32,33} Briefly, a bucket of ice-cooled water was prepared where another vessel filled with DI water was inserted. The water in the beaker was allowed to chill down before use. An amount of 10 g of the bio-oil and MeOH mixture was slowly introduced into the cold DI water while simultaneously doing magnetic stirring at a rate of 600 rpm (VWR stirrer). After adding all the mixture, vortex stirring (Daigger Vortex Genie 2) was done to enhance separation. Vacuum filtration (Whatman No. 42 filter paper) was done to separate the water-soluble (WS) from the water-insoluble (WIS, also called pyrolytic lignin) fractions of bio-

oil. Re-filtration of the WS fraction was done to remove impurities while the WIS fraction was thoroughly washed with ultrapure water.

The WS fraction contains majority of the pyrolytic sugars and some phenols.^{1,16} Therefore, column chromatography using Sepabeads SP207 resin was used to separate these compounds.²⁰ Sepabeads resin is reported as a good adsorbent of phenols from the aqueous phase. Prior to use, the resin was extensively washed in running water (ultrapure) for 1 hour and methanol for another 2 hours then dried in the oven set at 80 °C for 2 hours. The WS and sepabeads resin were combined at 1:5 wt. % and shaken (VWR DS-500E orbital shaker) at 200 rpm for 2 hours to allow for phenol adsorption. The mixture was then poured into a column (2.8 mm outside diameter, 9.5 in high) with a base filter to hold the beads while sugars are being separated. Ultrapure water was used to wash the beads to remove all the sugars. The aqueous sugar-rich phase was then concentrated using a rotary evaporator at 80 °C and 28 inHg to eliminate the water. The thick, concentrated pyrolytic sugar (syrup) was collected, and the yield was reported.

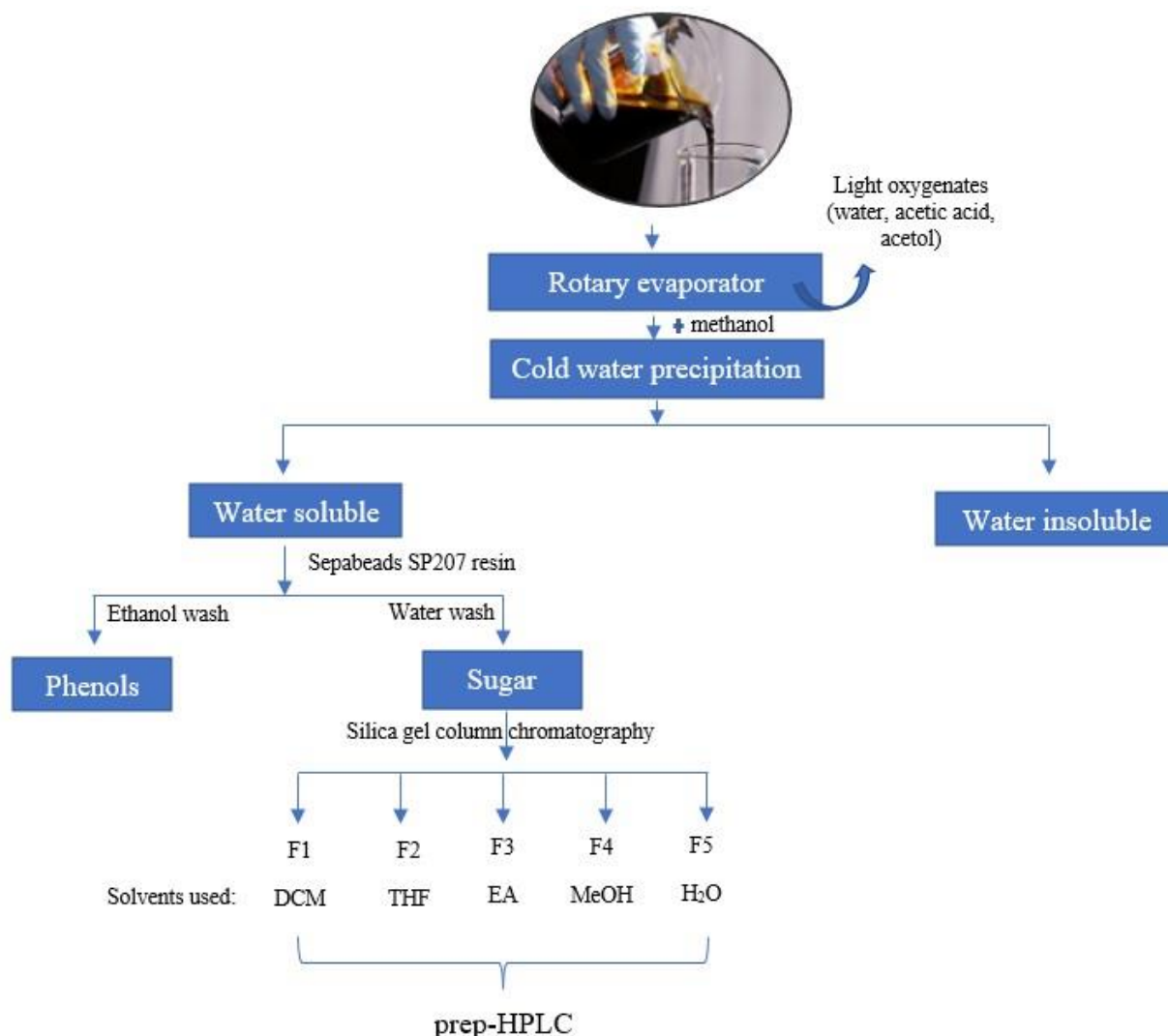


Figure 5.1: Separation scheme of sugars from the bio-oil.

Silica gel column chromatography was employed to sub-fractionate the sugars.^{19,22} The compounds were separated through the varying interaction between the stationary and mobile phases. Silica gel has the property of having a lot of oxygen atoms with high electronegativity around the silicon. The use of mobile phase with increasing polarity will allow the analytes to pass through the stationary phase at different speeds of movement. Because silica gel is extremely polar, compounds of least polarity are eluted first as they

have least affinity with the silica gel. Similarly, the highly polar compounds are adsorbed by the highly polar silica gel, thus elutes later.

For the fractionation process, a burette glass tube (17 mm outside diameter and 100 ml volume) served as the column. It was plugged securely with cotton wool ball at the base followed by sand (2.7 g) to hold the stationary phase (silica gel) in place and at the same time serve as a filter. The wet method of column preparation was employed where a slurry of 36 g silica gel and the first eluent (DCM) was prepared and poured into the column. The column was saturated with the first eluent (DCM) and allowed to stabilize for at least 3 hours before fractionation. A layer of sand (2.7 g) was introduced at the top of the column to serve as protection of the silica column when adding solvents. The retention volume of the column is 30 ml. HPLC-grade solvents of increasing polarity (DCM–3.1, THF–4.0, EA–4.4, MeOH–5.1, and H₂O–10.2)³⁴ were used as the mobile phase. These sub-fractions were labeled as F1, F2, F3, F4, and F5, respectively.

About 523 mg of pyrolytic sugar was dissolved in 1 mL of methanol. The sample was loaded to the top of the column. Right after it was absorbed in the sand layer, the first 30 ml of the DCM solvent was added, and the collection process started. A total of 90 ml of each solvent was used to extract the sub-fractions (60 mL to extract the sub-fraction and 30 mL to clean the column to avoid contamination). The elution time was recorded. The same procedure was employed until 5 sub-fractions were obtained. It is important to keep the top solvent level above the top of the silica to prevent drying out of the column.

The sub-fractions were filtered (Syringe filter nylon 0.22 µm) to eliminate impurities prior to rotary evaporation at specific conditions. The parameters used to concentrate the sub-fractions are as follows: DCM–eluted fraction (F1) = 50 °C bath temperature and vacuum

pressure of 14 inHg; THF-eluted (F2) = 35 °C and 22 inHg; EA-eluted (F3) = 60 °C and 21 inHg; MeOH-eluted (F4) = 30 °C and 26 inHg; and H₂O-eluted (F5) = 50 °C and 28 inHg.

These sub-fractions were gathered in a glass vial and extra solvents were evaporated. The yield of the sub-fractions was calculated using the equation below.

$$\text{Yield} = \frac{\text{Wt. of sugar subfraction}}{\text{Total feed intake}} * 100\%$$

Semi-Preparative High Performance Liquid Chromatography

Initially, samples were dissolved in 5 mL of Mili-Q water and filtered through a 0.45 µm disk filter. These samples underwent analysis and fractionation using the 1260 Infinity II system from Agilent (Germany), composed of a quarterly pump (G7111B), a thermostated autoinjector (G7129A), a refractive index detector (G1362A), and a thermostated fraction collector unit (G1364F). The separation was done through a Bio-Rad Aminex HPX-87C column (300 mm x 7.9 mm x 9 µm, CA, USA) (Part Number: 125-0095) with Guard Column Carbo-C (Part Number: 125-0128) at 85 °C. Mili-Q water was used as a mobile phase at a 0.6 mL/min flow rate. An amount of 10 µL of sample is injected per run. The autoinjector and fraction collector compartment temperatures are maintained at 10 °C. More information about the Aminex column is found elsewhere.³⁵ Data acquisition and treatment are performed using an Agilent OpenLab CDS ChemStation software.

5.2.3 Analytical Methods

The following characterization techniques were done to aid in building the structures of the oligomeric sugars.

Fourier-Transform Infrared Spectroscopy (FTIR)

A Shimadzu IRPrestige 21 spectrometer equipped with a MIRacle single reflection ATR Ge probe was used to obtain the infrared spectra of absorption of the samples. The samples were spread into the crystal window in a thin layer and spectra were acquired at a wavenumber range of 600-4000 cm^{-1} , 64 scans, 4 cm^{-1} resolution, and Harp-Genzel for the apodization. A background scan was always run before each sample measurement.

Ultraviolet (UV)-Fluorescence

Samples were dissolved in HPLC-grade DCM at 500 ppm. The synchronous fluorescence spectra were recorded with a Shimadzu RF 5301 pc spectrometer at a constant wavelength difference. The excitation wavelengths were scanned from 250 to 700 nm while the emission wavelengths were registered from 265 to 715 nm. Both the excitation and emission slit widths were set at 3 nm, and data were recorded every 1 nm. Post-processing of spectra was performed using Panorama Fluorescence 2.1 software.

Heated Electrospray Ionization–Fourier Transform–Orbitrap Mass Spectroscopy (H–ESI–FT–Orbitrap MS)

A comprehensive chemical speciation of the sugar samples was performed on the Orbitrap Exactive Plus (Thermo-Fisher Scientific) coupled with a heated electrospray ionization source. Solutions of pyrolytic sugar samples and their subfractions were prepared with a concentration of 300 $\mu\text{g mL}^{-1}$ in methanol and were directly infused into the ionization source at a flow rate of 30 $\mu\text{L min}^{-1}$. The mass spectra were acquired at a mass resolution (FWHM) of 140,000 (m/z 200). Both negative and positive ion ESI-MS scans in the range m/z 100–2000 were performed for the samples. For negative ion mode, the conditions were as follows: sheath gas flow, 10 arbitrary units (AU); ion source temperature, 100 °C; capillary temperature, 300 °C;

and spray voltage, -3.5 kV and $+3.5$ kV; the scanning range from 100 to 1000 Da. For the elemental compositions that were observed concurrently within the sample and blank spectra, final intensities were determined as the difference between sample and blank spectra intensities. Molecular formulas were assigned using XCalibur v. 3.1 software (Thermo Scientific, Bremen, Germany) and confirmed using a processing algorithm, which was implemented in Microsoft Excel, and developed by the Petroleum and Energy from Biomass Research Group (PEB) research group in Brazil. Mass peaks relevant to isotopic distributions were identified and deleted. Criteria for the assignments of elemental compositions were: tolerance error of ± 3 ppm, charge equals to -1 , and DBE less than 30. Regarding the elements, normal conditions for bio-oil data ($CcHhNnOoSs$, $3 \leq c \leq 200$, $3 \leq h \leq 1000$, $n = 0$, $s = 0$, and $1 \leq o \leq 45$) were used for these calculations.³⁶ Only ions with signal/noise ratio greater or equal to 3 were analyzed.

The determination of statistical values such as the number-average molecular weight (M_n) and the weight-average molecular weight (M_w) were calculated from the following equations:

$$M_n = \frac{\sum_i M_i I_i}{\sum_i I_i}; M_w = \frac{\sum_i M_i^2 I_i}{\sum_i M_i I_i}$$

where M_i is the m/z value of peak i and I_i is the peak intensity.³⁷ Both parameters represent a weighted average of the molecular mass of the components, with M_w slightly overestimating the heavier ones.

Nuclear Magnetic Resonance (NMR)

The ^{13}C -NMR, ^1H -NMR, and the Heteronuclear Single Quantum Coherence (HSQC) spectra were acquired on a Bruker 500 Neo spectrometer, equipped with a 5 mm Prodigy broadband cryoprobe with Z-axis gradients. An amount of 30 mg of each sugar sub-fraction was diluted in 0.7 mL of deuterated dimethyl sulfoxide (DMSO- d_6). The ^{13}C -NMR spectra were

acquired at 125.77 MHz at 303 K with 90° pulse angle (10.0 ms), 1.08 s acquisition time, relaxation delay d1 of 2 s, and inverse-gated ¹H composite pulse decoupling using 4000 scans, a spectral width of 30120.5 Hz and 32768 points. The FID was apodized with 8 Hz exponential line broadening for the model compounds. MestreNova 14.3.0 software was used for post-processing the spectra.

¹H-NMR spectra were acquired under the following conditions: 16 scans, 90° pulse (12.00 ms), 3 s relaxation delay, 4.4 s acquisition time, 32768 points, and 7463 Hz spectral width. Proton data were apodized with 1.3 Hz of line broadening.

5.3 Results and Discussion

5.3.1 Yield of the Sugars

Figure 5.2 shows the sugar sub-fractions (dissolved in MeOH). The resulting yield showed that the first fraction (DCM-eluted) has the highest yield accounting to 62%, followed by sub-fraction 2 (THF-eluted) yielding 17%, then sub-fraction 3 (EA-eluted) accounting for 15%, sub-fraction 4 (MeOH-eluted) giving 4% and the last sub-fraction (H₂O-eluted) with 2% yield. When the solvent is evaporated from these sugar sub-fractions, a syrup-like substance is formed. Meanwhile, F5 gives both syrup-like and powder-like substances.



Figure 5.2: Yield of the sugar sub-fractions obtained from silica gel chromatography (left figure is the sugar sub-fractions dissolved in MeOH).

5.3.2 Characteristics of the Sugar Sub-fractions from Silica Gel Chromatography

FTIR

Figure 5.3 shows the FTIR of the sugars obtained after silica gel chromatography. The broad peaks observed within the range of $3340\text{--}3380\text{ cm}^{-1}$ are attributed to the O-H groups, indicating the presence of hydroxyl groups and some residual water. The C-H stretch vibrations between $2800\text{ to }3000\text{ cm}^{-1}$ and C-H bends at 1442 cm^{-1} corresponds to saturated compounds. The broad band present at 1605 cm^{-1} is indicative of C=C bonds (alkenes) while the strong peak at 1714 cm^{-1} in the whole sugar (pyrolytic sugar) is assigned to C=O stretches. This peak could be attributed to carboxyl, carbonyl and aldehyde groups likely associated to acetic acid, hydroxyacetaldehyde, hydroxyacetone and acetic acid. However, its disappearance in the subfractions suggests a potential retention of these functional groups on the silica gel (stationary phase) during the separation process. C=O groups can form hydrogen bonds with the silanol groups of the silica gel. This interaction leads to stronger retention of polar compounds on the silica gel column. On one hand, these compounds could have also been removed from the

subfractions during rotary evaporation. Lastly, the sharp peak between 1000 to 1200 cm^{-1} corresponds to C-O stretches, possibly attributed to glycosidic or ether bonds connecting sugar structures. This peak appears significantly sharper in the sugar subfractions compared to the whole sugar, indicating strong absorbance of the well-defined and specific ether bond functional group. This implies that the subfractions mainly composed of sugars with glycosidic bonds. The expected broadness of the whole sugar spectrum implies a greater complexity of compounds compared to the more specific compounds present in the already fractionated samples. The presence of C-O deformation in alcohols is noted at 1047 cm^{-1} .

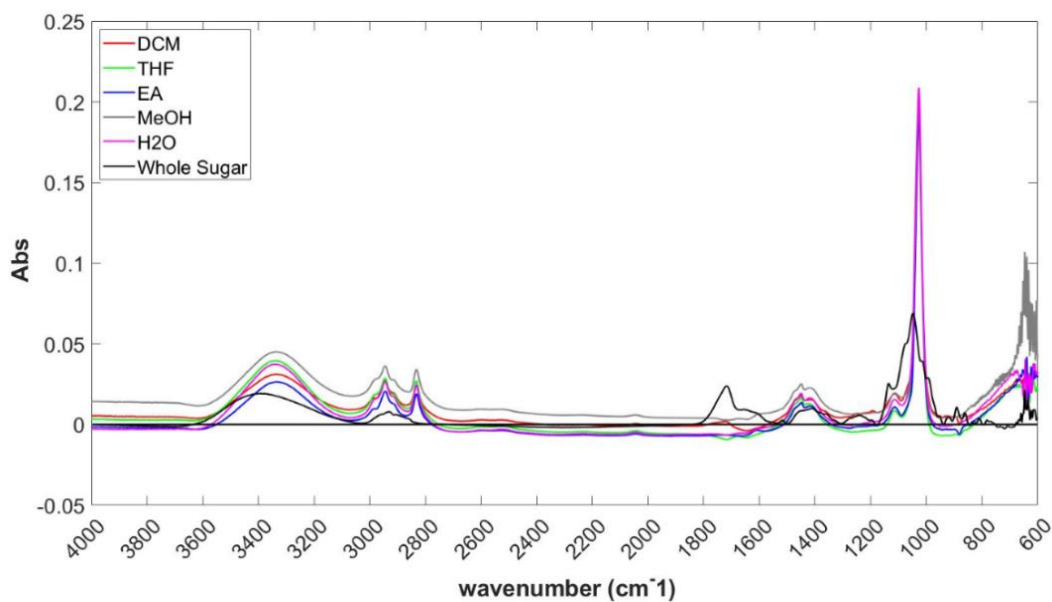


Figure 5.3: FTIR spectra of the sugar and its sub-fractions.

UV Fluorescence

Figure 5.4 shows the UV Fluorescence spectra of the sugar sub-fractions after silica gel chromatography. The results reveal that subfractions eluted with THF and H₂O composed of small, conjugated ring systems, as evidenced by the peaks at 275 nm wavelength. Notably, the THF-eluted subfraction exhibits a high peak, likely attributed to the elution of monophenols in addition to the small, conjugated sugar compounds. This observation aligns with the findings from ¹³C and ¹H-NMR analyses, indicating aromatic regions at 125 to 150 nm and 6.5 to 6.8 nm, respectively. In contrast, the whole sugar and DCM-eluted fractions show small conjugated systems which correspond mostly to dimers that have lost few H₂O molecules, evident from peaks in the 289 to 307 nm range. Interestingly, the subfractions eluted with EA and the MeOH indicate the presence of larger conjugated ring systems (350 to 500 nm), suggesting molecules that have lost more water molecules. This confirms the existence of oligomeric sugars in bio-oil. This finding is important as the two subfractions may represent fractions prone to coke formation. The presence of highly dehydrated fractions indicates a trajectory toward coke formation, emphasizing the importance of understanding these bio-oil compounds.

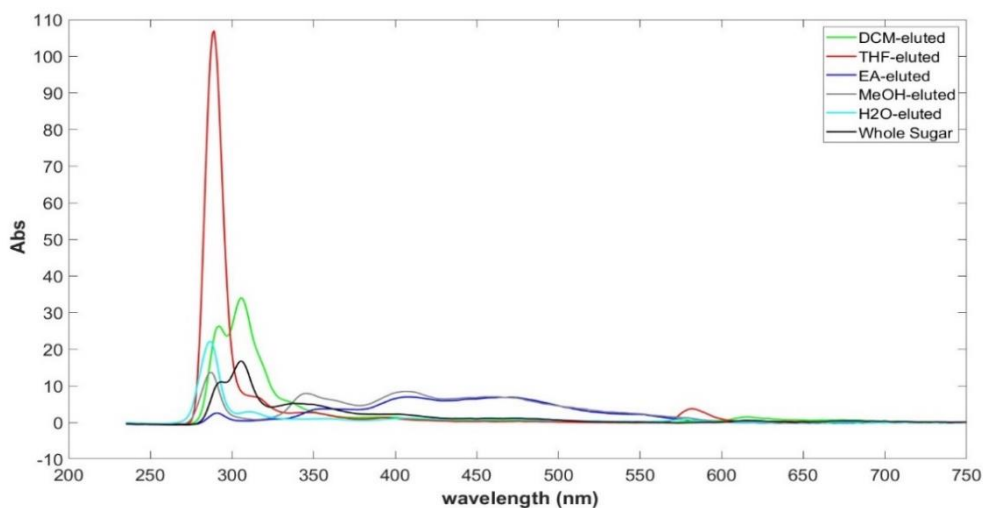


Figure 5.4: UV-Fluorescence analysis of the sugar and its sub-fractions.

NMR

Figure 5 shows the ^{13}C -NMR (left) and ^1H -NMR (right) spectra of the sugar sub-fractions obtained after silica gel chromatography. Results of the ^{13}C -NMR analysis showed peak at 39.75 ppm which is attributed to the DMSO solvent. Long and branched aliphatics, mostly from secondary and tertiary carbons, (C-H) contribute to peaks observed in the 20 to 50 ppm range, while carbons directly attached to alcohols/hydroxyl (C-OH) are represented by peaks in the 60 to 80 ppm range. Interestingly, a notable trend reveals a decreasing peak intensity in the hydroxyl group from the DCM to MeOH soluble fractions. This trend is likely a result of higher dehydration reactions indicating that the use of solvents of increasing polarity is directly proportional to extracting more dehydrated sugars. This is supported by the UV-fluorescence analysis wherein the EA and MeOH soluble fractions mostly contain polycondensed/conjugated ring systems. Alkenes/conjugated ring systems (C=C) as a product of dehydration are reflected in signals at 90 to 105 ppm, and aromatics from phenols are identified in the 115 to 150 ppm range. It's noteworthy that phenols persist in the sugar fractions even after employing several separation techniques, a finding supported by their presence in the 2D HSQC (Figure 6) and in the phenolic region ($\text{H/C} = 1.2\text{-}0.8$; $\text{O/C} = 0.1\text{-}0.4$) of the van Krevelen plot especially for DCM and THF soluble fractions (Figure 7). These phenolic compounds may be involved in the formation of hybrid oligomers (lignin-carbohydrate structures) or humins as described in other references.¹ Additionally, peaks observed at 180 ppm in the EA-eluted subfraction are assigned to aldehydes (C=O).

The DCM- and THF-eluted subfractions qualitatively share similar compound groups, portraying defined peaks in the alkyl and aromatic regions of the subfractions due to higher concentration post-separation. Aromatic region peaks in the DCM and THF fractions are likely

attributed to phenols. The less polar nature of DCM and THF solvents allows for the elution of phenols during separation.

Conversely, the EA- and MeOH-eluted subfractions qualitatively display similar compound groups, with a subtle, low-intensity peak in the aromatic region for the EA fraction. The subdued peaks in the alkyl region are attributed to the predominance of polycondensed/conjugated ring systems in these compounds, as depicted in the UV-fluorescence analysis (Figure 4). The presence of a peak around 88 to 95 ppm in both the whole sugar and methanol fractions is linked to hemiacetals in sugars. The H₂O-eluted fraction exhibits qualitatively identical peaks to those observed in the whole sugar spectrum.

In the ¹H-NMR spectra, the peak signal at 2.52 ppm is indicative of the DMSO solvent. The most upfield signals within the range of 0.5 to 1.5 ppm are ascribed to aliphatic protons connected to carbon atoms. Protons on aliphatic carbons α -to heteroatom or unsaturation (C=O or C=C moieties) contribute to signals falling between 1.5 to 3.0 ppm. The region spanning 3.5 to 4.2 ppm corresponds to protons situated on carbon atoms adjacent to OH functional groups. Peaks within the 4.2 to 6 ppm range are attributed to aromatic ether protons (methoxy) and hydrogen atoms derived from carbohydrate-like molecules. Signals ranging from 6.0 to 9.2 ppm emanate from alkenes/conjugated rings and aromatics found in phenols. Lastly, the most deshielded spectral region between 9.2 to 10 is likely associated with aldehydes.¹

The whole sugar and DCM, THF and EA, as well as the MeOH and H₂O soluble subfractions, display qualitatively similar groups of compounds. The whole sugar and DCM soluble fraction show mostly alcohol groups from sugars. Interestingly, both THF and EA soluble fractions do not reveal protons originating from the alcohol region; instead, they exhibit protons originating from methoxy/carbohydrate-like molecules in the spectrum regions of 4.5 to

5.5 ppm. These molecules might be associated to sugars containing minimal OH groups, such as conjugated ring systems resulting from dehydration reactions or hybrid oligomers (lignin-carbohydrate structure). The presence of these conjugated structures is further substantiated by the UV-fluorescence analysis, which indicates that the EA fraction is primarily characterized by polycondensed/conjugated structures. The hybrid oligomers could also be linked to the FT-Orbitrap MS results, suggesting the existence of structures that resemble hybrids.

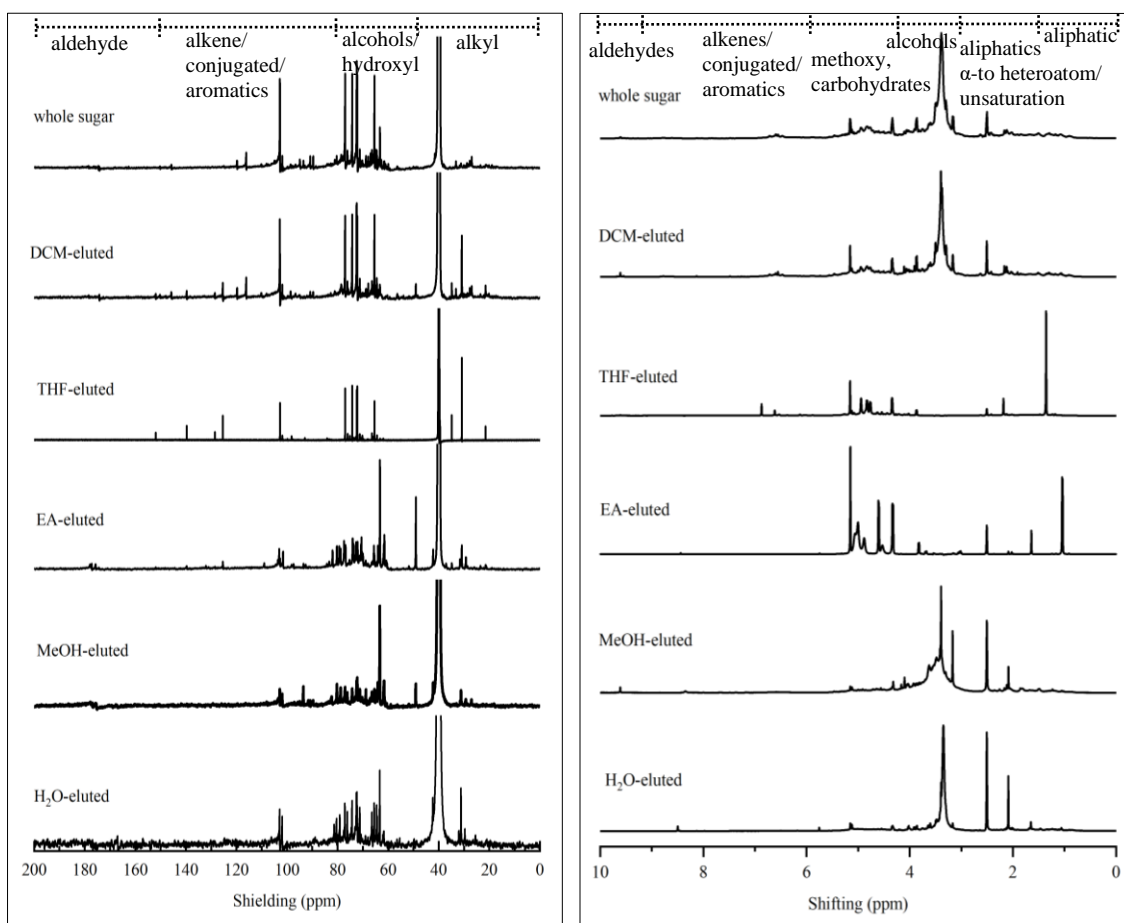


Figure 5.5: ^{13}C -NMR (left) and ^1H -NMR (right) of the sugar and its sub-fractions (solvent and impurity peaks: DMSO = 2.52 ppm for ^1H , 39.75 ppm for ^{13}C ; and H_2O = 3.29 ppm for ^1H).

Lastly, the relatively intense peak observed between 2.0 to 2.5 ppm in the MeOH and H₂O soluble fractions correspond to hydrogen atoms α -to heteroatom or unsaturation. The predominance of protons originating from alcohols is also evident. This result strongly suggests the presence of conjugated molecules in the MeOH and H₂O soluble fractions.

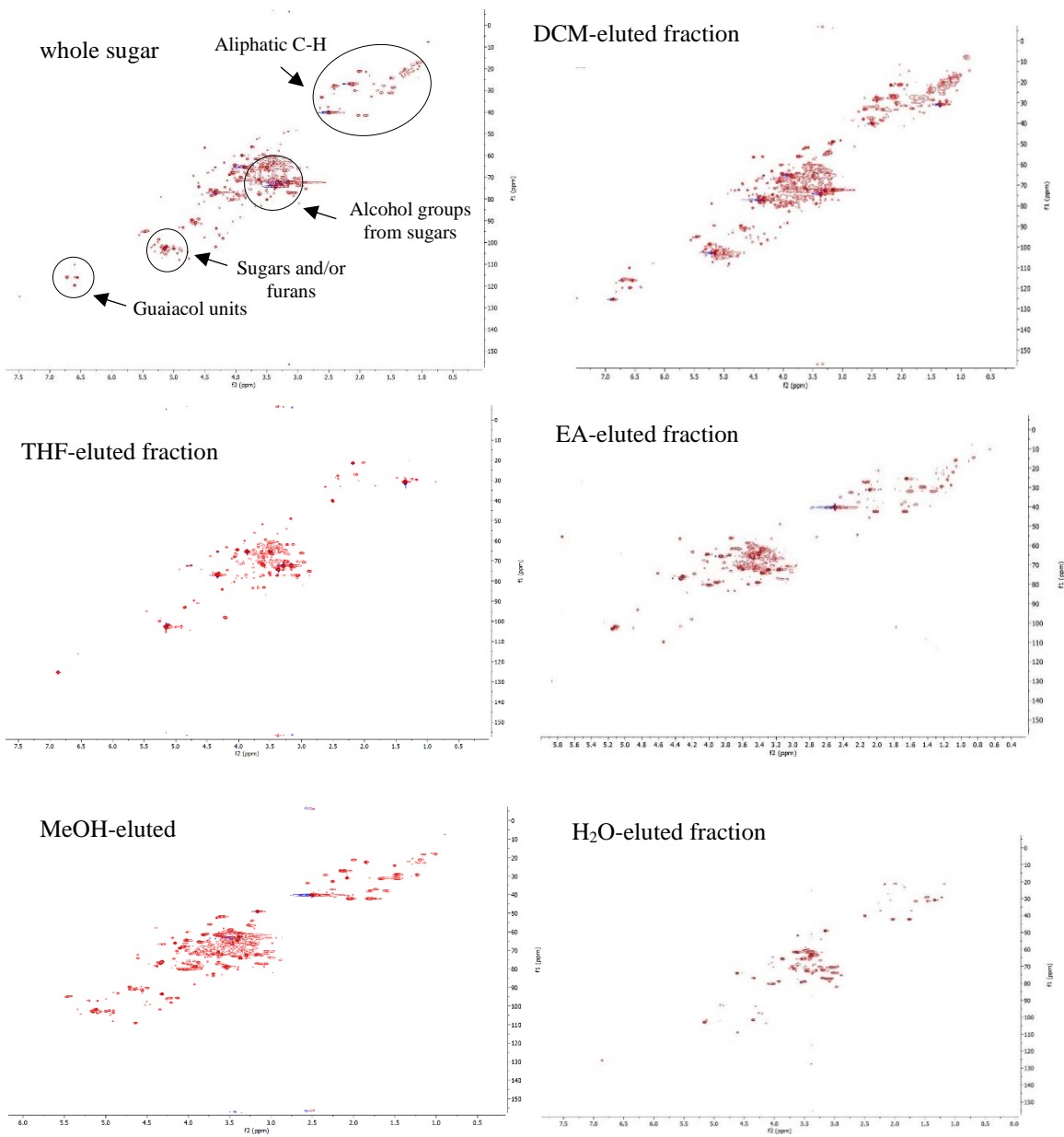


Figure 5.6: 2D HSQC NMR of the whole sugar and its sub-fractions.

Figure 5.6 shows a 2D ^1H - ^{13}C HSQC NMR of the sugar sub-fractions obtained after silica gel chromatography. The whole sugar and DCM qualitatively show similar functional groups such as the aliphatic groups in the 15.0-45.0 ppm and 1.0-2.8 ppm integration region, alcohol groups in the 60.0-80.0 ppm and 3.0-4.0 ppm region, sugars or furans in the 100.0-110.0 ppm and 4.6-5.5 ppm region, and guaiacol units in the 115.0-120.0 and 6.5-7.0 region. DCM, being the least polar solvent, eluted mostly the guaiacol units. THF and EA soluble fractions show similar group of compounds predominantly alcohol groups. The aliphatic C-H and guaiacol units could also be seen but at a very low intensity. The MeOH soluble fraction is dominantly composed of alcohols and some aliphatic C-H but no lignin units. Finally, the water-soluble fraction is composed of alcohol groups with few aliphatic groups.

H-ESI-FT-Orbitrap MS

The complexity of pyrolytic sugars primarily stems from the vast diversity of representative compounds across different chemical classes, resulting in an intricate mixture. Given that pyrolytic sugars are predominantly composed by anhydrosugars, dimers, and oligomers of sugar units, the direct infusion of the sample into (\pm)H-ESI-FT-Orbitrap MS analysis without prior pre-treatment can significantly facilitate the identification of these organic compounds. Tables 5.1 and 5.2 summarize the general information about the sugar sub-fractions spectra.

The FT-Orbitrap MS spectra of the pyrolytic sugars ranged from 8,000 to 14,000 detected ions in the negative mode H-ESI (Table 1). Among these detected ions, ~15% had their chemical formulas assigned with an error below ± 3 ppm. Despite an increase in the total number of detected peaks for each fraction during fractionation with DCM, THF, EA, MeOH, and H_2O , no significant variation was observed in the number of assigned ions. Furthermore, based on the

statistical values of the number-average molecular weight (M_n) and weight-average molecular weight (M_w), when comparing the fractions, a trend of decreasing M_n and M_w values with increasing solvent polarity was observed.

For the positive mode of H-ESI, the spectra of pyrolytic sugars fractions ranged from 2,000 to 12,000 detected ions (Table 5.2). Among these detected ions, ~20 to ~30% had their chemical formulas assigned with an error below ± 3 ppm. No significant variations or specific trends were observed for the detected peaks and assigned peaks of sugars fractions eluted with DCM, THF, EA, and H₂O solvents. Based on the statistical values of number-average molecular weight (M_n) and weight-average molecular weight (M_w), when comparing

Table 5.1. Number of ions and mass distribution of pyrolytic sugar sub-fractions based on the (-)H-ESI-FT-Orbitrap MS spectra.

Parameter	DCM	THF	EA	MeOH	H ₂ O syrup	H ₂ O powder
Detected ions	8809	9146	11245	11381	10629	13866
Assigned ions	1827	1748	1684	1525	1517	1693
Signal-to-noise > 3	1158	1174	855	699	626	600
M_n	238	266	234	213	211	207
M_w	309	320	289	250	243	236
PDI	1.30	1.20	1.23	1.17	1.15	1.14

Table 5.2. Number of ions and mass distribution of pyrolytic sugar sub-fractions based on the (+)H-ESI-FT-Orbitrap MS spectra.

Parameter	DCM	THF	EA	MeOH	H ₂ O syrup	H ₂ O powder
Detected ions	9660	8882	10503	1953	7993	11783
Assigned ions	2359	1816	2043	620	1597	2029
Signal-to-noise > 3	1396	884	947	390	531	715

M _n	322	358	271	227	348	223
M _w	368	395	310	252	428	246
PDI	1.14	1.10	1.14	1.11	1.23	1.10

the fractions, the H₂O powder showed the lowest values of Mn and Mw, and H₂O syrup showed the highest values of Mw and Polydispersity index (PDI).

Based on the values of Mn, Mw, and PDI determined by the negative mode H-ESI, it was observed that all sub-fractions are primarily composed of sugars and anhydrosugars dimer units. In contrast, the structure of pyrolytic sugars varied among the sub-fractions based on the values of Mn, Mw, and PDI determined by the positive mode H-ESI. Aligned with the negative mode, the EA, MeOH, and H₂O powder sub-fractions are also primarily composed of dehydrated dimer units. Conversely, the DCM, THF, and H₂O syrup sub-fractions are primarily composed of sugars and anhydrosugars dimers units, as the values found fall within the range of dimer units. Although ESI is among the softest ionization methods, the negative mode could lead to higher levels of fragmentation than the positive mode when analyzing sugars and anhydrosugars.³⁹ In this way, the low values of Mn observed for DCM, THF and H₂O syrup might be associated with this mechanism. To evaluate the chemical speciation that could be varying among these samples, an approach based on petroleomics was applied.

For molecular characterization, only ions with a signal-to-noise ratio ≥ 3 were considered for data analysis, which accounted for more than 50% of the total assigned ions. Given that molecules with acidic characteristics are preferentially ionized in the negative mode of analysis, the processing conditions were tailored to focus on compounds falling within the O_x class (where *x* ranges from 1 to 20). The characterized ions were sorted into different chemical classes

according to the number of heteroatoms present in their molecular formulas. The molecular distribution plots are shown in Figures 1 and 2.

The chemical analysis of the pyrolytic sugar subfractions, as determined by (-)HESI-FT-Orbitrap MS (Figure 5.7), exhibited a notable intensity compound within the mass range of monomers to dimers (100 to 300 Da). Among these, the most intense compounds demonstrated a high O/C ratio ($O/C > 0.4$) as shown in Figure 5.7 topmost row diagrams. Less intense ions extend up to 700 Da. The subfractions showed different molecular distributions when comparing the diagrams of number of carbons versus values of Double-Bond-Equivalents (DBE), shown in Figure 5.7 middle row diagrams. They can be sorted into three different groups. The first group, DCM and THF showed a similar molecular distribution, the compounds encompassed a range from C_4 to C_{30} with DBE values spanning from 0 to 11. The second group, composed of EA and MeOH sub-fractions, showed molecular distributions from C_4 to C_{28} with DBE values spanning from 0 to 10. The third group, composed of H_2O syrup and H_2O powder sub-fractions, the molecular distribution falls within a range of C_4 to C_{25} and DBE values spanning from 0 to 10.

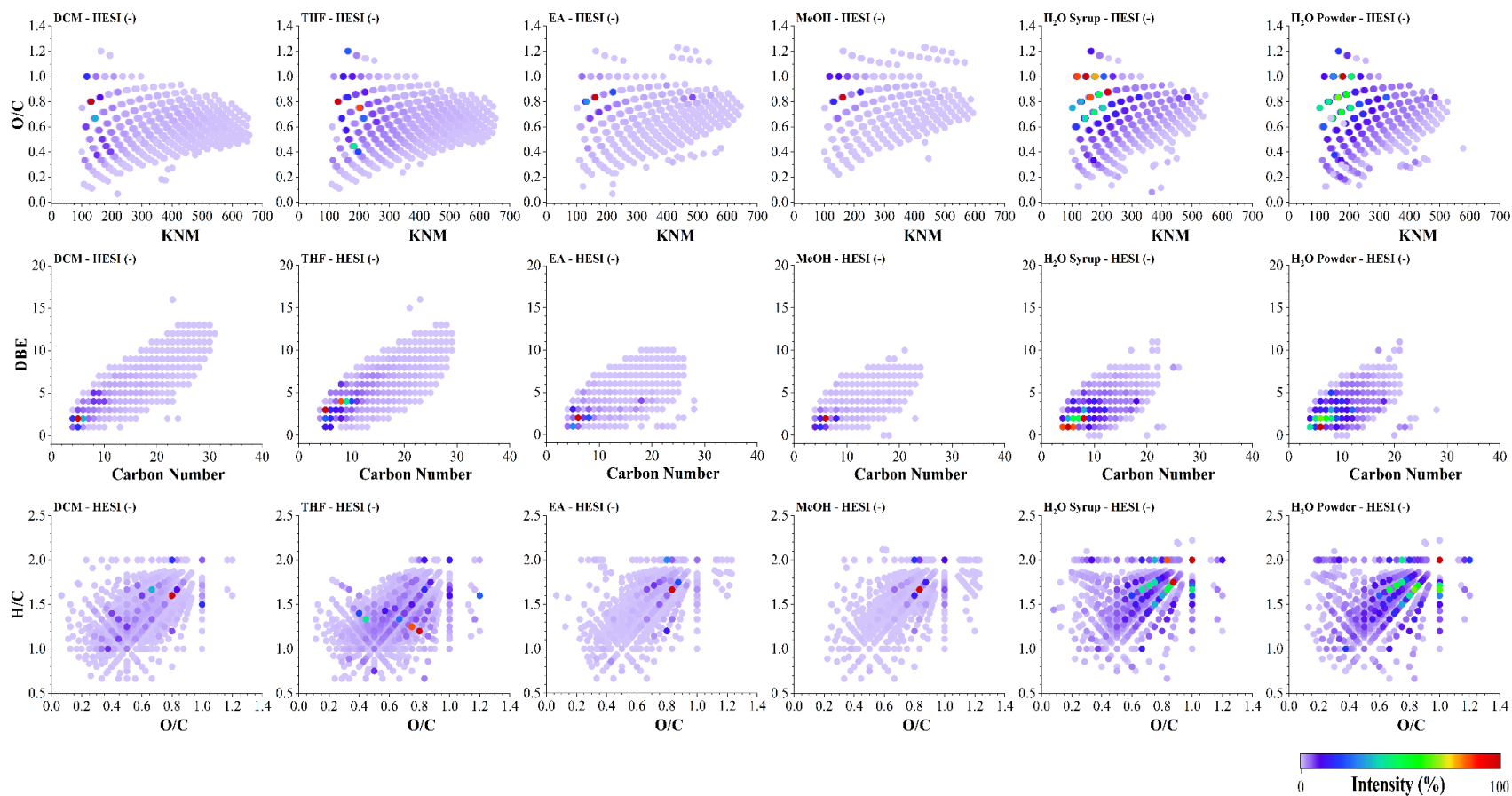


Figure 5.7: Compositional characterization of pyrolytic sugar from BTG bio-oil and their subfractions by (-)H-ESI-FT Orbitrap MS. (Top) Diagrams of O/C ratio vs. Kendrick mass; (Middle) Diagrams of DBE vs. Carbon Number; and (Bottom) Diagrams of van Krevelen for H/C ratio vs. O/C ratio.

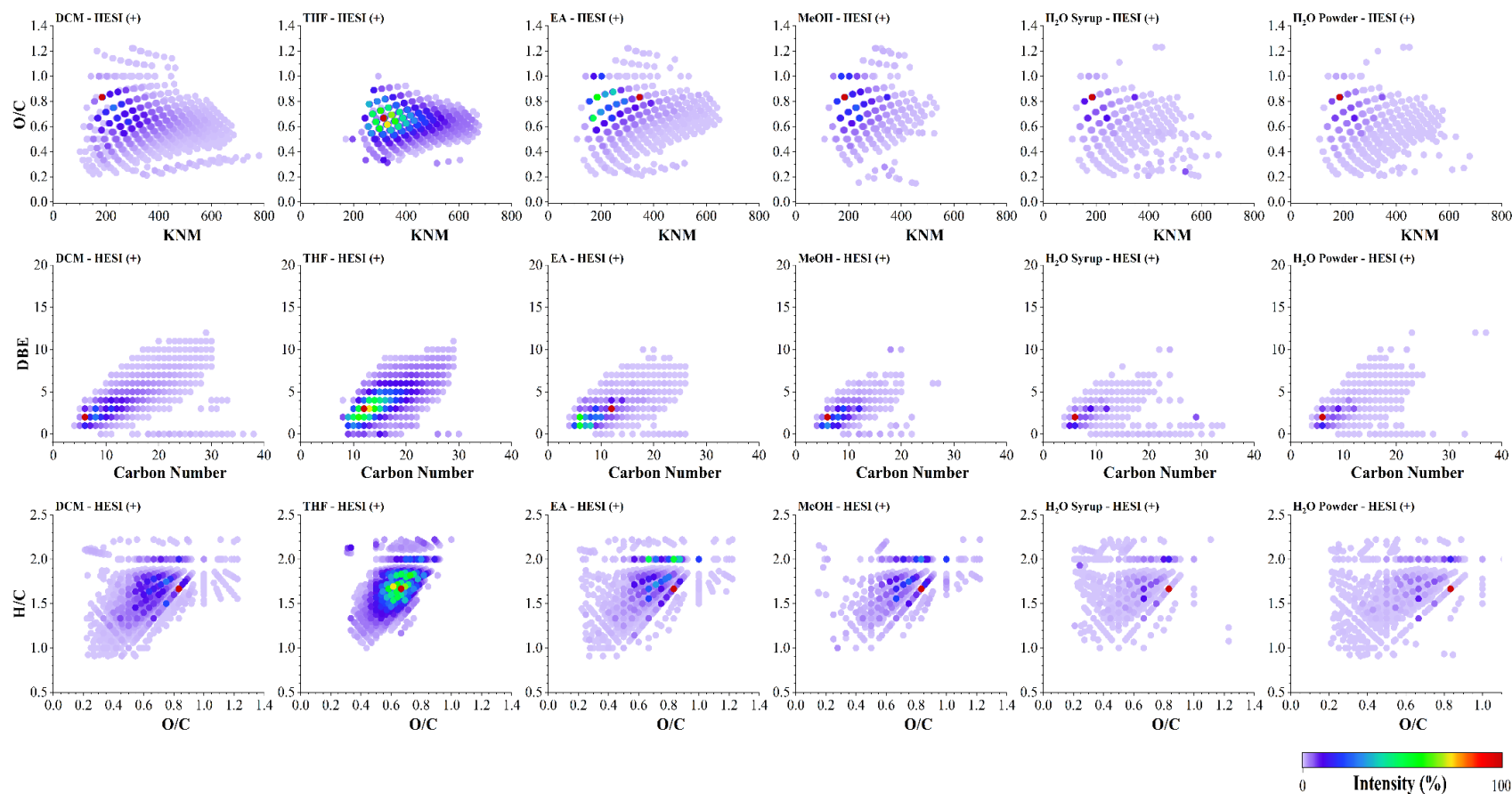


Figure 5.8: Compositional characterization of pyrolytic sugars from BTG bio-oil and their subfractions (+)H-ESI-FT Orbitrap MS. (Top) Diagrams of O/C ratio vs. Kendrick mass; (Middle) Diagrams of DBE vs. Carbon Number; and (Bottom) Diagrams of van Krevelen for H/C ratio vs. O/C ratio.

Although the molecular distribution is similar to the second group, the third group showed a broader range of intense compounds. The most intense compounds in the H₂O sub-fractions (syrup and powder) have carbon number values from 1 to 5, and DBE values from 4 to 11. Considering the chemical classes, the van Krevelen diagram (Figure 5.7, bottom row) for each pyrolytic sugar sub-fraction demonstrated that these samples are predominantly composed of sugar-like and anhydrosugar-like compounds (H/C= 1.4-2.0; O/C= 0.6-1.0), with a minimal presence of lipid-like compounds (H/C= 1.4-2.0; O/C= 0.0-0.3) and phenolic compounds (H/C= 1.2-0.8; O/C= 0.1-0.4).

Analyzing the molecular distribution determined by (+)HESI-FT-Orbitrap MS (Figure 5.8), the general molecular distribution was similar to the observed negative mode of H-ESI. Despite the similarities, a notable intensity of anhydrosugars compounds in DCM, EA, and THF subfractions was observed. They were found primarily within the mass range of dimers and trimers (200 to 400 Da) in the EA-eluted and DCM-eluted subfractions, and dimers to tetramers (200 to 550 Da) in the THF-eluted subfraction. The presence of pyrolytic lignin in the pyrolytic sugar fractions of bio-oil might raise questions about the efficiency of the separation process. However, it's crucial to consider that the ionization in H-ESI positive mode has a preferential tendency to ionize sugar-like compounds over phenolic derivatives. Based on the diagrams of the BTG bio-oil and the analysis of its behavior during separation using the described solvents in this study, it is concluded that the pyrolytic lignin is in low intensity. They only become noticeable in the DCM-eluted and THF-eluted fractions, as the other solvents do not exhibit sufficient elution strength to remove residual pyrolytic lignin.

5.3.3 Integrating Experimental and Modeling Yields for Sugar Oligomer Insights

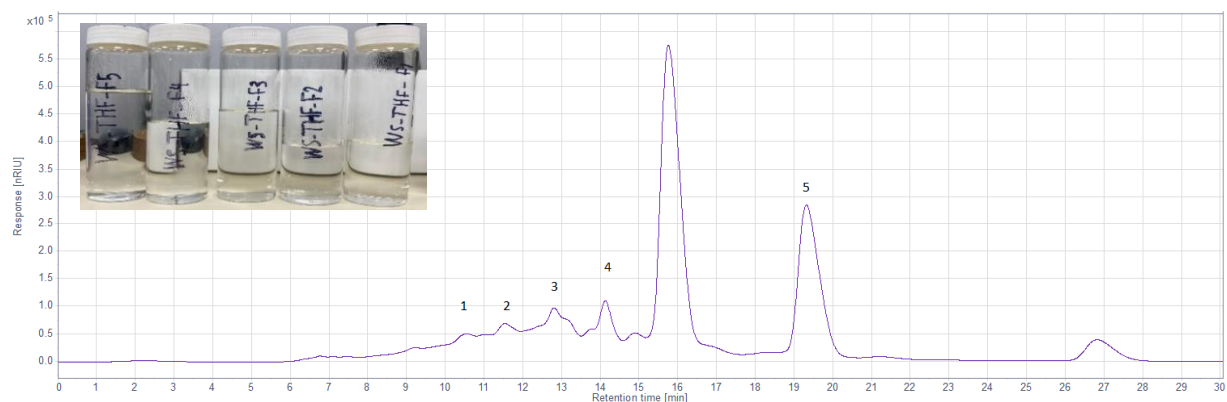
Figure 5.9 illustrates the chromatograms obtained through semi-preparative HPLC, where each of the numbered peaks corresponds to the collected samples from THF (a), MeOH (b), and H₂O (c) sub-fractions. THF and MeOH fractions yielded five sub-fractions each, whereas the H₂O fraction produced ten. No peaks were detected in DCM and EA sub-fractions.

Subsequently, the collected samples from the THF, MeOH, and H₂O are subjected to the H-ESI-FT Orbitrap MS technique to determine the compounds present within each sample. However, despite employing several separation techniques, the results revealed the presence of hundreds to thousands of compounds in each of the sugar sub-fractions collected from the semi-preparative HPLC. Table 5.3 details the compounds with the highest relative intensity identified in the sugar sub-fractions acquired through semi-preparative HPLC in positive and negative ion modes. THF-1 corresponds to peak 1 and sample bottle 1 from the THF sub-fraction in Figure 5.9, and so on.

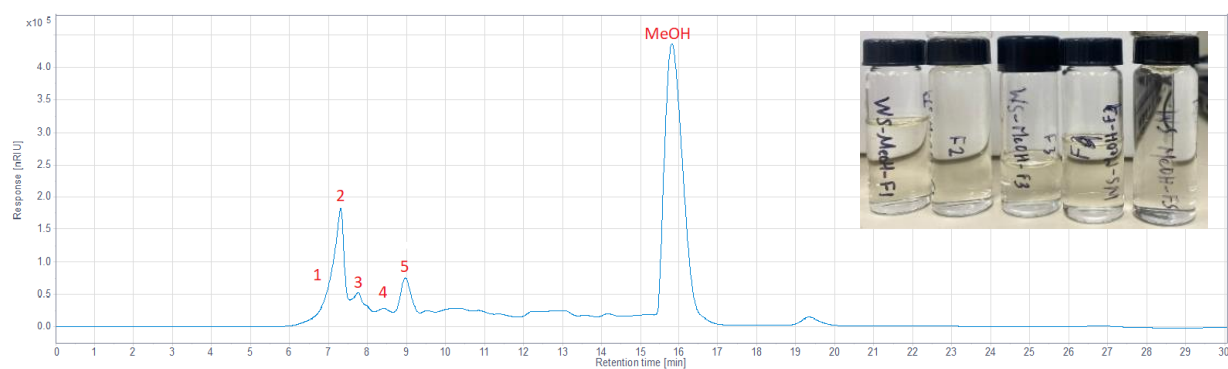
In the ESI-FT Orbitrap MS, the positive ion mode detects analyte compounds that are easily protonated, while the negative ion mode targets those readily deprotonated, such as acidic compounds. Some compounds may appear in both positive and negative ion modes due to the vast functional groups comprising a bio-oil compound.

Interestingly, Table 5.4 shows that the proposed molecular structures/formulas through dehydration²⁹ and fragmentation³⁰ modeling in Chapters 3 and 4, respectively, were detected experimentally in the bio-oil sub-fractions obtained through semi-preparative HPLC. The table also indicates in which sample these proposed structures/formulas were detected and the ionization mode responsible for their identification. However, their presence is noted at a low relative intensity, except for the C₆H₆O₃, C₁₂H₁₈O₉, and C₁₀H₁₄O₇, which exhibited a relative intensity exceeding 10%.

(a) Chromatogram from THF sub-fraction



(b) Chromatogram from MeOH sub-fraction



(c) Chromatogram form H₂O sub-fraction

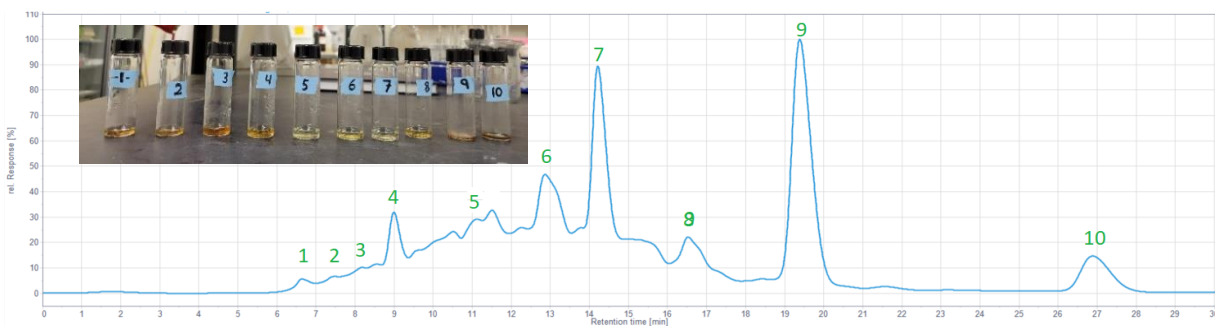


Figure 5.9: Semi-preparative HPLC chromatograms of the sugar sub-fractions obtained from: (a) THF-eluted sub-fractions, (b) MeOH-eluted sub-fractions, and (c) water-eluted sub-fractions.

Table 5.3. Highest relative intensity compounds identified in the sugar sub-fractions by (\pm)H-ESI-FT Orbitrap MS.

	Detected compound of highest intensity	
	Negative mode	Positive mode
THF-1	C ₆ H ₆ O ₄	C ₆ H ₁₀ O ₅
THF-2	C ₆ H ₁₀ O ₅	C ₉ H ₁₄ O ₆
THF-3	C ₅ H ₁₀ O ₅	C ₆ H ₁₂ O ₅
THF-4	C ₅ H ₁₀ O ₅	C ₈ H ₁₂ O ₆
THF-5	C ₁₂ H ₆ O ₃	C ₉ H ₁₄ O ₆
MeOH-1	C ₃₂ H ₆₄ O ₄	C ₆ H ₁₀ O ₅
MeOH-2	C ₈ H ₈ O ₂	C ₅ H ₈ O ₄
MeOH-3	C ₇ H ₆ O ₂	C ₁₂ H ₁₄ O ₄
MeOH-4	C ₅ H ₆ O ₄	C ₆ H ₁₂ O ₆
MeOH-5	C ₈ H ₁₄ O ₇	C ₁₂ H ₂₀ O ₁₀
H ₂ O-1	C ₈ H ₁₄ O ₇	C ₈ H ₁₄ O ₇
H ₂ O-2	C ₁₂ H ₁₆ O ₈	C ₆ H ₁₀ O ₅
H ₂ O-3	C ₈ H ₁₄ O ₇	C ₈ H ₁₄ O ₇
H ₂ O-4	C ₆ H ₁₀ O ₅	C ₆ H ₁₀ O ₅
H ₂ O-5	C ₆ H ₁₀ O ₅	C ₉ H ₁₆ O ₇
H ₂ O-6	C ₅ H ₁₀ O ₄	C ₉ H ₁₆ O ₇
H ₂ O-7	C ₅ H ₁₀ O ₄	C ₈ H ₁₄ O ₆
H ₂ O-8	C ₄ H ₈ O ₄	C ₇ H ₁₂ O ₅
H ₂ O-9	C ₂₂ H ₄₂ O ₇	C ₆ H ₁₀ O ₅
H ₂ O-10	C ₂₂ H ₄₂ O ₇	C ₆ H ₁₀ O ₅

Table 5.4. Proposed structures/formulas of the sugar oligomers that are experimentally detected.

Reaction	Molecule tag	Molecular Wt. (g/mol)	Molecular Formula	Detected (Exp't)	Sample #	Ion. Mode
Fragmentation ³⁰	CBN-HAAb	246.07	C ₁₀ H ₁₄ O ₇	Yes	H ₂ O-3	-
	CTN-HAAc	408.13	C ₁₆ H ₂₄ O ₁₂	No		
	CQN-HAAd	570.18	C ₂₂ H ₃₄ O ₁₇	Yes	H ₂ O-10	+
	CBN-HAb	232.06	C ₉ H ₁₂ O ₇	Yes	THF-3	-
	CTN-HAc	394.11	C ₁₅ H ₂₂ O ₁₂	Yes	H ₂ O-3	-
	CQN-HAd	556.16	C ₂₁ H ₃₂ O ₁₇	Yes	H ₂ O-10	+
Dehydration ²⁹	LG23	144.13	C ₆ H ₈ O ₄	Yes	H ₂ O-9	-
	LG32-45B	126.11	C ₆ H ₆ O ₃	Yes	H ₂ O-3	-
	CBN34A	306.27	C ₁₂ H ₁₈ O ₉	Yes	H ₂ O-4	-
	CBN43B-65B	288.25	C ₁₂ H ₁₆ O ₈	Yes	H ₂ O-3	-
	CBN21B-43B-65B	270.07	C ₁₂ H ₁₄ O ₇	Yes	H ₂ O-3	-
	CTN34A	468.41	C ₁₈ H ₂₈ O ₁₄	Yes	H ₂ O-5	-
	CTN43C-65C	450.39	C ₁₈ H ₂₆ O ₁₃	Yes	H ₂ O-5	-
	CTN21C-43C-65C	432.13	C ₁₈ H ₂₄ O ₁₂	Yes	H ₂ O-3	-
	CQN34A	630.2	C ₂₄ H ₃₈ O ₁₉	Yes	THF-3	+
	CQN43D-65D	612.19	C ₂₄ H ₃₆ O ₁₈	Yes	THF-3	-
	CQN21D-43D-65D	594.18	C ₂₄ H ₃₄ O ₁₇	Yes	THF-3	-

5.4 Conclusion

In this work, pyrolytic sugar was separated from the whole bio-oil (BTG) and characterized using several techniques to identify the heavy unknown sugar oligomers. Initially, cold-water precipitation was done to separate water-soluble from the water-insoluble bio-oil compounds, followed by column chromatography using Sepabeads resin to separate sugars from phenols and then concentrated by means of rotary evaporation. The sugar was further fractionated employing silica gel column chromatography and solvents of increasing polarity.

These sub-fractions were concentrated and subjected to semi-preparative HPLC to further purify the compounds. The samples collected are characterized to identify sugar oligomers present in the sub-fractions. The results revealed that bio-oil is an exceptionally intricate mixture, comprising hundreds to thousands of compounds, even after separation by semi-preparative HPLC. The pyrolytic sugars are predominantly composed of sugar and anhydrosugar dimer units, with the extension to tetramers observed at lower intensities. Notably, the proposed molecular structures/ formulas from the modeling works discussed in Chapters 3 and 4 were detected experimentally using (\pm)H-ESI-FT-Orbitrap MS.

5.5 REFERENCES

- (1) Stankovikj, F.; McDonald, A. G.; Helms, G. L.; Olarte, M. V.; Garcia-Perez, M. Characterization of the Water-Soluble Fraction of Woody Biomass Pyrolysis Oils. *Energy and Fuels* **2017**, *31* (2), 1650–1664. <https://doi.org/10.1021/acs.energyfuels.6b02950>.
- (2) Gagnon, J.; Kaliaguine, S. Catalytic Hydrotreatment of Vacuum Pyrolysis Oils from Wood. *Ind. Eng. Chem. Res.* **1988**, *27* (10), 1783–1788. <https://doi.org/10.1021/ie00082a008>.
- (3) Zhang, L.; Hu, X.; Li, C.; Zhang, S.; Wang, Y.; Esmaeili, V.; Gholizadeh, M. Fates of Heavy Organics of Bio-Oil in Hydrotreatment: The Key Challenge in the Way from Biomass to Biofuel. *Sci. Total Environ.* **2021**, *778*, 146321. <https://doi.org/10.1016/j.scitotenv.2021.146321>.
- (4) Pollard, A. S.; Rover, M. R.; Brown, R. C. Characterization of Bio-Oil Recovered as Stage Fractions with Unique Chemical and Physical Properties. *J. Anal. Appl. Pyrolysis* **2012**, *93*, 129–138. <https://doi.org/10.1016/j.jaap.2011.10.007>.
- (5) Bu, Q.; Lei, H.; Zacher, A. H.; Wang, L.; Ren, S.; Liang, J.; Wei, Y.; Liu, Y.; Tang, J.; Zhang, Q.; Ruan, R. A Review of Catalytic Hydrodeoxygenation of Lignin-Derived Phenols from Biomass Pyrolysis. *Bioresour. Technol.* **2012**, *124*, 470–477. <https://doi.org/10.1016/j.biortech.2012.08.089>.
- (6) Han, Y.; Gholizadeh, M.; Tran, C. C.; Kaliaguine, S.; Li, C. Z.; Olarte, M.; Garcia-Perez, M. Hydrotreatment of Pyrolysis Bio-Oil: A Review. *Fuel Process. Technol.* **2019**, *195* (May). <https://doi.org/10.1016/j.fuproc.2019.106140>.
- (7) Hertzog, J.; Garnier, C.; Mase, C.; Mariette, S.; Serve, O.; Hubert-Roux, M.; Afonso, C.; Giusti, P.; Barrère-Mangote, C. Fractionation by Flash Chromatography and Molecular Characterization of Bio-Oil by Ultra-High-Resolution Mass Spectrometry and NMR Spectroscopy. *J. Anal. Appl. Pyrolysis* **2022**, *166* (April), 1–8. <https://doi.org/10.1016/j.jaap.2022.105611>.
- (8) Lin, Y. C.; Cho, J.; Tompsett, G. A.; Westmoreland, P. R.; Huber, G. W. Kinetics and Mechanism of Cellulose Pyrolysis. *J. Phys. Chem. C* **2009**, *113* (46), 20097–20107. <https://doi.org/10.1021/jp906702p>.
- (9) Lédé, J.; Blanchard, F.; Boutin, O. Radiant Flash Pyrolysis of Cellulose Pellets: Products and Mechanisms Involved in Transient and Steady State Conditions. *Fuel* **2002**, *81* (10), 1269–1279. [https://doi.org/10.1016/S0016-2361\(02\)00039-X](https://doi.org/10.1016/S0016-2361(02)00039-X).
- (10) Stankovikj, F.; McDonald, A. G.; Helms, G. L.; Garcia-Perez, M. Quantification of Bio-Oil Functional Groups and Evidences of the Presence of Pyrolytic Humins. *Energy and Fuels* **2016**, *30* (8), 6505–6524. <https://doi.org/10.1021/acs.energyfuels.6b01242>.
- (11) Li, X.; Kersten, S. R. A.; Schuur, B. Extraction of Acetic Acid, Glycolaldehyde and Acetol from Aqueous Solutions Mimicking Pyrolysis Oil Cuts Using Ionic Liquids. *Sep. Purif. Technol.* **2017**, *175*, 498–505. <https://doi.org/10.1016/j.seppur.2016.10.023>.

- (12) Westerhof, R. J. M.; Brillman, D. W. F.; Garcia-Perez, M.; Wang, Z.; Oudenhoven, S. R. G.; Van Swaaij, W. P. M.; Kersten, S. R. A. Fractional Condensation of Biomass Pyrolysis Vapors. *Energy and Fuels* **2011**, *25* (4), 1817–1829. <https://doi.org/10.1021/ef2000322>.
- (13) Han, Y.; Pinheiro Pires, A. P.; Denson, M.; McDonald, A. G.; Garcia-Perez, M. Ternary Phase Diagram of Water/Bio-Oil/Organic Solvent for Bio-Oil Fractionation. *Energy and Fuels* **2020**, *34* (12), 16250–16264. <https://doi.org/10.1021/acs.energyfuels.0c03100>.
- (14) Garcia-Perez, M.; Chaala, A.; Pakdel, H.; Kretschmer, D.; Roy, C. Characterization of Bio-Oils in Chemical Families. *Biomass and Bioenergy* **2007**, *31* (4), 222–242. <https://doi.org/10.1016/j.biombioe.2006.02.006>.
- (15) Vitasari, C. R.; Meindersma, G. W.; de Haan, A. B. Water Extraction of Pyrolysis Oil: The First Step for the Recovery of Renewable Chemicals. *Bioresour. Technol.* **2011**, *102* (14), 7204–7210. <https://doi.org/10.1016/j.biortech.2011.04.079>.
- (16) Yu, Y.; Chua, Y. W.; Wu, H. Characterization of Pyrolytic Sugars in Bio-Oil Produced from Biomass Fast Pyrolysis. *Energy and Fuels* **2016**, *30* (5), 4145–4149. <https://doi.org/10.1021/acs.energyfuels.6b00464>.
- (17) Oasmaa, A.; Kuoppala, E. Fast Pyrolysis of Forestry Residue. 3. Storage Stability of Liquid Fuel. *Energy and Fuels* **2003**, *17* (4), 1075–1084. <https://doi.org/10.1021/ef030011o>.
- (18) Lu, Y.; Wei, X. Y.; Cao, J. P.; Li, P.; Liu, F. J.; Zhao, Y. P.; Fan, X.; Zhao, W.; Rong, L. C.; Wei, Y. Bin; Wang, S. Z.; Zhou, J.; Zong, Z. M. Characterization of a Bio-Oil from Pyrolysis of Rice Husk by Detailed Compositional Analysis and Structural Investigation of Lignin. *Bioresour. Technol.* **2012**, *116*, 114–119. <https://doi.org/10.1016/j.biortech.2012.04.006>.
- (19) García-Pérez, M. E.; Royer, M.; Herbette, G.; Desjardins, Y.; Pouliot, R.; Stevanovic, T. Picea Mariana Bark: A New Source of Trans-Resveratrol and Other Bioactive Polyphenols. *Food Chem.* **2012**, *135* (3), 1173–1182. <https://doi.org/10.1016/j.foodchem.2012.05.050>.
- (20) Rover, M. R.; Aui, A.; Wright, M. M.; Smith, R. G.; Brown, R. C. Production and Purification of Crystallized Levoglucosan from Pyrolysis of Lignocellulosic Biomass. *Green Chem.* **2019**, *21* (21), 5980–5989. <https://doi.org/10.1039/c9gc02461a>.
- (21) Wei, Y.; Lei, H.; Wang, L.; Zhu, L.; Zhang, X.; Liu, Y.; Chen, S.; Ahring, B. Liquid-Liquid Extraction of Biomass Pyrolysis Bio-Oil. *Energy and Fuels* **2014**, *28* (2), 1207–1212. <https://doi.org/10.1021/ef402490s>.
- (22) Wang, S.; Wang, Y.; Leng, F.; Chen, J.; Qiu, K.; Zhou, J. Separation and Enrichment of Catechol and Sugars from Bio-Oil Aqueous Phase. *BioResources* *11* (1), 1707–1720.
- (23) Oasmaa, A.; Kuoppala, E.; Elliott, D. C. Development of the Basis for an Analytical Protocol for Feeds and Products of Bio-Oil Hydrotreatment. *Energy and Fuels* **2012**, *26*

- (4), 2454–2460. <https://doi.org/10.1021/ef300252y>.
- (24) Lu, Y.; Li, G. S.; Lu, Y. C.; Fan, X.; Wei, X. Y. Analytical Strategies Involved in the Detailed Componential Characterization of Biooil Produced from Lignocellulosic Biomass. *Int. J. Anal. Chem.* **2017**, *2017*. <https://doi.org/10.1155/2017/9298523>.
- (25) Kuzhiyil, N.; Dalluge, D.; Bai, X.; Kim, K. H.; Brown, R. C. Pyrolytic Sugars from Cellulosic Biomass. *ChemSusChem* **2012**, *5* (11), 2228–2236. <https://doi.org/10.1002/cssc.201200341>.
- (26) Yu, Z.; Zhang, H. Erratum to Ethanol Fermentation of Acid-Hydrolyzed Cellulosic Pyrolysate with *Saccharomyces Cerevisiae* (DOI:10.1016/S0960-8524(03)00093-2). *Bioresour. Technol.* **2009**, *100* (19), 4539. <https://doi.org/10.1016/j.biortech.2009.04.006>.
- (27) Hu, X.; Li, C. Z. Levulinic Esters from the Acid-Catalysed Reactions of Sugars and Alcohols as Part of a Bio-Refinery. *Green Chem.* **2011**, *13* (7), 1676–1679. <https://doi.org/10.1039/c1gc15272f>.
- (28) Terrell, E.; Garcia-Perez, M. Novel Strategy to Analyze Fourier Transform Ion Cyclotron Resonance Mass Spectrometry Data of Biomass Pyrolysis Oil for Oligomeric Structure Assignment. *Energy and Fuels* **2020**, *34* (7), 8466–8481. <https://doi.org/10.1021/acs.energyfuels.0c01687>.
- (29) Denson, M. D.; Terrell, E.; Kostetskyy, P.; Olarte, M.; Broadbelt, L.; Garcia-perez, M. Elucidation of Structure and Physical Properties of Pyrolytic Sugar Oligomers Derived from Cellulose Depolymerization / Dehydration Reactions : A Density Functional Theory Study. **2023**. <https://doi.org/10.1021/acs.energyfuels.3c00641>.
- (30) Denson, M. D.; Terrell, E.; Kostetskyy, P.; Broadbelt, L.; Olarte, M.; Garcia-Perez, M. Theoretical Insights on the Fragmentation of Cellulosic Oligomers to Form Hydroxyacetone and Hydroxyacetaldehyde. *Energy and Fuels* **2023**. <https://doi.org/10.1021/acs.energyfuels.3c01924>.
- (31) Zhou, S.; Garcia-Perez, M.; Pecha, B.; Kersten, S. R. A.; McDonald, A. G.; Westerhof, R. J. M. Effect of the Fast Pyrolysis Temperature on the Primary and Secondary Products of Lignin. *Energy and Fuels* **2013**, *27* (10), 5867–5877. <https://doi.org/10.1021/ef4001677>.
- (32) Oasmaa, A.; Sundqvist, T.; Kuoppala, E.; Garcia-Perez, M.; Solantausta, Y.; Lindfors, C.; Paasikallio, V. Controlling the Phase Stability of Biomass Fast Pyrolysis Bio-Oils. *Energy and Fuels* **2015**, *29* (7), 4373–4381. <https://doi.org/10.1021/acs.energyfuels.5b00607>.
- (33) Sukhbaatar, B.; Li, Q.; Wan, C.; Yu, F.; Hassan, E. B.; Steele, P. Inhibitors Removal from Bio-Oil Aqueous Fraction for Increased Ethanol Production. *Bioresour. Technol.* **2014**, *161*, 379–384. <https://doi.org/10.1016/j.biortech.2014.03.051>.
- (34) Oasmaa, A.; Fonts, I.; Pelaez-Samaniego, M. R.; Garcia-Perez, M. E.; Garcia-Perez, M. Pyrolysis Oil Multiphase Behavior and Phase Stability: A Review. *Energy and Fuels* **2016**, *30* (8), 6179–6200. <https://doi.org/10.1021/acs.energyfuels.6b01287>.
- (35) Huck CW, Huber CG, Bonn GK. Chapter 5 HPLC of carbohydrates with cation- and

- anion-exchange silica and resin-based stationary phases. *J Chromatogr Libr.* **2002**;66(C):165-205. doi:10.1016/S0301-4770(02)80030-6.
- (36) Staš M, Chudoba J, Kubička D, Blažek J, Pospíšil M. Petroleomic Characterization of Pyrolysis Bio-oils: A Review. *Energy and Fuels.* **2017**;31(10):10283-10299. doi:10.1021/acs.energyfuels.7b00826.
- (37) Santos JM, Vetere A, Wisniewski A, Eberlin MN, Schrader W. Modified SARA method to unravel the complexity of resin fraction(s) in crude oil. *Energy and Fuels.* **2020**;34(12):16006-16013. doi:10.1021/acs.energyfuels.0c02833.
- (38) Qu W, Xue Y, Gao Y, Rover M, Bai X. Repolymerization of pyrolytic lignin for producing carbon fiber with improved properties. *Biomass and Bioenergy.* **2016**;95:19-26. doi:10.1016/j.biombioe.2016.09.013.
- (39) Chen Z, Jin X, Wang Q, Lin Y, Gan L. Confirmation and determination of sugars in soft drink products by IEC with ESI-MS. *Chromatographia.* **2009**;69(7-8):761-764. doi:10.1365/s10337-009-0969-3.

CHAPTER SIX: CO-HYDROTREATMENT OF BIO-OIL AND WASTE COOKING OIL TO PRODUCE BIOFUEL

Abstract

This study practically aimed to upgrade the heavy bio-oil fraction, containing both pyrolytic sugars and lignin, by co-hydrotreating it with waste cooking oil (WCO) using a NiMo/ γ -Al₂O₃ catalyst. BTG bio-oil was rotary evaporated to remove the light-oxygenated compounds, mixed with 1-butanol to mitigate coke formation, and then blended with WCO. The co-hydrotreatment was done in two phases: stabilization to saturate the highly reactive hydrogen-deficient compounds and deoxygenation to expel oxygen, mostly in the form of H₂O. The yield, composition, and properties of the upgraded oil as affected by different bio-oil concentrations (0, 10, 20, 30, 40 wt.% of WCO) were reported. The resulting hydrotreated oil was distilled at <150°C, 150-250°C, and 250-350°C to obtain gasoline, kerosene, and diesel, respectively.

The yield of the hydrotreated oil shows that as the bio-oil concentration increases, the amounts of coke (0.7-2.4 %) and water (2-10 %) increase, and the amount of organic layer decreases (80-63 %). The coke yield was relatively low and is comparable to coke yield obtained when utilizing solely the pyrolytic lignin fraction. This implies that coke formation is not solely attributed to sugar oligomers; rather, both sugars and lignin contribute to this process. Based on the coke formation, the recommended bio-oil blend in WCO is 20 wt.% accounting for 0.8 % coke.

The yield of distillation cuts shows that an increase in bio-oil concentration leads to a slight increase in gasoline yield and a decrease in kerosene and diesel yields. The UV-fluorescence analysis on the hydrotreated oil shows that more polycondensed and conjugated ring system compounds form as the bio-oil concentration increases. These compounds are

precursors to coke formation but are mitigated by the addition of 1-butanol. FTIR results showed that most of the raw materials were converted to biofuels after the hydrotreatment. The identified carbon species found in the fuel cuts include n-paraffin, iso-paraffin, cycloparaffin, and aromatics. Further, the characteristics of the jet fuel cut (kerosene) in terms of density, surface tension, and viscosity conform to the standard specifications for sustainable aviation fuels (Jet A-1). Further research is suggested to fine-tune the operating parameters for achieving reduced coke yield and enhanced kerosene yield.

6.1 Introduction

Faced with energy shortfalls, higher prices, and the issues associated with environmental concerns, researchers around the world are motivated to explore the potential of bio-oil from biomass.¹ Biomass is abundant and a direct carbon source, therefore making it an interesting candidate to fulfill the world's search for a renewable and sustainable fuel source. The conversion of lignocellulosic biomass to bio-oil is achieved through hydrothermal liquefaction (HTL) and fast pyrolysis. Fast pyrolysis is a mature technology that converts lignocellulosic biomass into bio-oil up to 75 wt. % yield^{2,3} under a temperature range of 450 to 600 °C in the absence of oxygen.^{4,5,6}

Bio-oil consists of hundreds of compounds, including water (15 to 30 wt. %), light oxygenates (8 to 26 wt. %), monophenols (2 to 7 wt. %), water-insoluble oligomers derived from lignin 15 to 25 (wt. %), and water-soluble (WS) molecules (10 to 30 wt. %).^{7,8,9,10,11,12} The high amounts of water and oxygen in a variety of chemical functionalities result in poor bio-oil properties such as corrosiveness, high viscosity, low energy density, and thermal instability thereby limiting the use of bio-oil as 'drop-in' transportation fuel.^{13,14,15,16,17} This means that bio-oil must be upgraded with additional physical and chemical processes to produce a hydrocarbon stream similar to the properties of existing liquid transportation fuels. Various techniques such as catalytic hydrotreating, zeolite upgrading, fractionation, and emulsification have been employed to get rid of these unwanted properties and improve the quality of bio-oil.^{16,18} Catalytic hydrotreatment, a promising route of bio-oil upgrading, involves the treatment of bio-oil with H₂ under high pressure and temperature conditions. The Battelle, Pacific Northwest Laboratory has developed and patented a two-stage process steps of hydrodeoxygenation (HDO): stabilization and deoxygenation to reduce coke formation.^{19,20,21} Stabilization involves the pretreatment of the

hydrogen-deficient compounds, specifically the carboxyl and carbonyl functional groups, at a lower temperature (below 280 °C) to form a more stable oil intermediate that can be hydrotreated at a higher temperature, typically 350 °C. The second stage involves cracking and oxygen removal (deoxygenation), usually in the form of H₂O. The most extensively used HDO catalysts in petroleum refineries are NiMo/ γ -Al₂O₃ and CoMo/ γ -Al₂O₃.^{22,23} These catalysts are widely available and cheaper.

Bio-oil upgrading has been studied for many years. However, coke formation remains the top concern and is believed to be caused by the heavy unknown oligomeric compounds, especially those from the sugars.^{10,24,25,26} Therefore, researchers have explored various routes to mitigate coke formation, including fractionation^{17,27} to get rid of the sugar-rich fraction, addition of organic solvents like methanol and butanol to stabilize the bio-oil, and co-hydrotreatment with hydrogen-rich chemicals like vegetable oils and/or waste cooking oils prior to upgrading. For example, Kloekhorst et al.²⁸ and Figueiredo et al.²⁹ hydrotreated pyrolytic lignin fraction over Ru/C and Pd/C catalysts, respectively, and their result indicated the potential use of lignin to produce phenols and aromatics. Another study³⁰ reported that lignin feed has shown a significant impact on the oil quality compared to using the whole bio-oil. A few works have also investigated the upgrading of the aqueous (water-soluble, sugar-rich) fraction. Sanna et al.³¹ employed the two-step hydrogenation of WS bio-oil fraction over Ru/C and Pt/C catalysts and successfully produced up for 45 % carbon in the WS to useful products such as gasoline cuts and diols. Similarly, Li et al.³² employed the two-stage process to upgrade the aqueous fraction produced by hydrolysis and obtained gasoline range products with a carbon yield of up to 57 %. Yin et al.³³ studied both the sugar and lignin fractions and reported that coke formation from the sugars is higher. On the one hand, Kadarwati et al.³⁴ showed that the addition of levoglucosan

into bio-oil prior to hydrotreatment did not yield more coke compared to pure bio-oil under identical conditions; coke yield was increased in the absence of catalyst instead.

Further efforts on the blending of bio-oil with organic solvents and co-hydrotreating with hydrogen-rich oils have been made. The work of Han et al.³⁵ on the co-hydrotreatment of bio-oil lignin-rich oil (LRO) fraction and vegetable oil showed that coke yield without the addition of butanol was very high, accounting for 25-50 wt. % in all cases depending on the amount of added LRO. However, the blending of 1-butanol into the mixture mitigated coke formation, which decreased from 34.73 wt. % to 6.65 wt. %. Another study³⁶ explored the addition of butanol to the water-insoluble fraction and co-hydrotreated it with waste cooking oil over a sulfided NiMo/ γ -Al₂O₃ catalyst and reported a coke yield close to 2 wt. %. The study of Cai et al.³⁷ on the influence of bio-oil aqueous fraction (BAF) and methanol mixing ratio confirmed the role and importance of methanol blending in the feed before hydrotreatment. Methanol acted as a hydrogen donor to the bio-oil components and mitigated coke formation. This is evident when the BAF to methanol ratio is high (2:1) because the insufficient supply of hydrogen leads to accelerated deactivation of the catalyst. These various techniques have demonstrated a compelling route for converting biomass pyrolysis oil into liquid transportation fuels and chemicals.

Despite these studies, further research is still needed to upgrade the whole bio-oil while minimizing coke formation. In this work, the bio-oil (light oxygenates were removed by rotary evaporation) was blended with 1-butanol and co-hydrotreated with waste cooking oil over a pre-sulfided NiMo/ γ -Al₂O₃ to produce bio-jet fuels. The practical aim of this work was to upgrade the bio-oil containing the heavy fractions from both sugar and lignin oligomers. It also aimed to

assess whether the bio-oil containing the sugars would result in a higher coke yield. This will give an idea of whether it is worth fractionating bio-oils before hydrotreatment.

6.2 Methodology

6.2.1 Chemicals

Bio-oil (pyrolysis oil) was sourced from the Biomass Technology Group (BTG) company in Enschede, The Netherlands, and stored in the refrigerator at -5 °C. The BTG bio-oil was produced from pine wood using a rotating cone reactor (<http://www.btg-btl.com/>) at the following conditions: ambient pressure, reactor temperature of approximately 500 °C, and short gas residence time (<2 s). The pre-filtered waste cooking oil (yellow grease) was procured from Baker Commodities Inc. and stored at room temperature. The bio-oil and WCO were characterized in terms of elemental and proximate analyses prior to utilization. The waste cooking oil characterization is found somewhere.³⁶ The NiMo/ γ -Al₂O₃ catalyst (granular) commercially procured by PNNL was used. Dimethyl disulfide (DMDS) ($\geq 99.0\%$) was purchased from Sigma-Aldrich, while analytical grade hydrogen and nitrogen (> 99.99%) were from Linde.

6.2.2 Preparation of Samples

BTG bio-oil was subjected to rotary evaporation (Büchi Rotavapor R-3000, Thermo Scientific, Hanover Park, IL) at 55 °C and 29 in. of mercury³⁸ to remove the light oxygenates (LO) which contain mostly water, acetol, acetic acid, and glycolaldehyde. Bio-oil without the light oxygenates was used for the hydrotreatment study. This bio-oil was thoroughly pre-mixed with 1-butanol (99 %, Alfa Aesar) (1 g bio-oil: 0.5 g 1-butanol) to mitigate coke formation.³⁵ The resulting mixture was subsequently blended with WCO at different concentrations (0, 10,

20, 30, 40 wt. % WCO). The final feedstock blends were thoroughly mixed by hand shaking until homogeneity was achieved.

The batch-type Parr reactor consists of a 250 mL vessel and can operate at maximum conditions of 500 °C and 5000 psi. The system was equipped with a gas injection stirrer to promote the mixing of the feedstocks and, therefore, better hydrogen transfer into the bio-oil. Initially, the reactor vessel was weighed with the catalyst inside ready for drying. The reactor was closed and subsequently purged with N₂ gas at 150 psi and at room temperature to remove air. A leak test was performed several times by introducing pressurized H₂ gas at 150 psi and at room temperature into the autoclave reactor using a leak detector (catalog number 22655, Restek). Analysis of the light-oxygenated compounds that were removed from the bio-oil is shown in the Appendix C, Figures S1 through S3.

6.2.3 Co-hydrotreatment Experiment

The hydrotreatment procedure is described elsewhere.^{15,35} Initially, the reactor was loaded with the NiMo/ γ -Al₂O₃ catalyst and subsequently subjected to drying. The reactor was then cooled down using an air blower and depressurized to safely introduce the DMDS. DMDS was introduced into the system to activate the catalyst then flushed with N₂ gas to remove air from the autoclave reactor. The reactor was pressurized with H₂ gas to perform a leak test. Upon successfully completing the leak test, the reactor was pressurized with H₂ gas, subsequently heated to desired temperature. The reactor was then allowed to cool down to safely introduce the feedstock. This completes the sulfidation process. The feedstock (50 g) was injected into the system through the input valve using a 500 mL syringe. The system was again flushed with N₂ gas to remove air, then pressurized with H₂ gas to check possible leaks. The system was then pressurized with H₂ at the desired operating condition and stirred at 500 rpm. This process is

called stabilization where hydrogen-deficient compounds react with hydrogen atoms and are converted to alcohols. Finally, the temperature was elevated to a higher operating temperature to reject the oxygen in the form of water. This is the deoxygenation process. Before opening, the reactor was cooled down to room temperature and depressurized.

6.2.4 Collection of Products

The reactor was opened to collect solid (coke) and liquid products. The vessel with the hydrotreated oil and catalyst inside was weighed for proper mass balance calculations. The few amounts of liquid formed in the ceiling of the reactor were also collected using a syringe. The liquid was separated from the solid products and transferred to a coned centrifuge tube. The liquid, containing both water and the hydrotreated oil, was centrifuged (Centaur 2 benchtop centrifuge) in a set at 3000 rpm for 30 minutes to separate the water. The organic layer was then separated from the water products. The spent catalyst and coke were vacuum filtered (Whatman No. 42 filter paper) and thoroughly rinsed with acetone multiple times to eliminate any residue from the hydrotreated oil. The catalyst and coke were then dried in the hood overnight before recording the weight. The coke accumulated on the stirrer and ceiling of the reactor was also collected. The total amount of coke was determined. The yields were reported and the hydrotreated oil was analyzed using UV-fluorescence and FTIR.

6.2.5 Distillation of Hydrotreated Oils

The hydrotreated oil was distilled using a simple distillation setup (ASTM D86-12) described elsewhere.^{39,36} Briefly, an amount of 20 g of the hydrotreated oil was distilled at <150 °C, 150 to 250 °C, and 250 to 350 °C to obtain gasoline, kerosene, and diesel, respectively. At > 350 °C, some residuals formed. The yields were reported, and the distillation cuts (fuel cuts)

were characterized in terms of elemental composition, carbon distribution analysis, density, surface tension, and viscosity.

6.2.6 Characterization of Feed and Upgraded Product

The following characterization techniques were performed to analyze the feedstock and product samples:

Proximate Analysis

A thermogravimetric analyzer, SDTA 851e (Mettler Toledo, U.S.) was used in accordance with a previously documented procedure⁴⁰ to ascertain the fixed carbon, volatile matter, and ash content of the feedstocks.

Fourier Transform Infrared (FTIR) Spectroscopy

FTIR spectra were acquired using a Shimadzu IRPrestige 21 spectrometer equipped with a MIRacle single reflection ATR Ge probe. Enough samples were introduced into the crystal window and spectra were recorded at a range of 600-4000 cm^{-1} , 64 scans, 4 cm^{-1} resolution, and Harp-Genzel for the apodization. Background correction was done before each sample measurement.

Ultraviolet (UV)-Fluorescence

Samples were dissolved in HPLC-grade dichloromethane (DCM) at 500 ppm. Analysis was done using a Shimadzu RF 5301 pc (software: Panorama Fluorescence 2.1) spectrometer. The synchronous fluorescence spectra at a constant wavelength difference were set. The excitation and emission wavelengths were scanned from 250 to 700 nm and 265 to 715 nm, respectively. The excitation and emission slit widths were configured to 3 nm, and data were recorded at 1 nm intervals.

Elemental Analysis (CHNO-S)

The elemental composition (C, H, N, O, and S content) of the distillation cuts were analyzed at PNNL using an automated Euro Vector EA3000 CHNS analyzer with acetanilide as the calibration reference. Every sample was subjected to duplicate analysis, and the reported value represents the average. The combustion and reduction tubes were appropriately filled to facilitate the analysis of carbon, nitrogen, sulfur, and hydrogen. The combustion tube was subjected to a temperature of 1150 °C, while the reduction tube reached 850 °C. Helium served as the carrier gas. Sample sizes typically fell within the range of 10 to 30 uL.

Density

The Gay-Lussac's pycnometer (2 mL) was used to determine the density of the distillation cuts. The complete procedure is described somewhere.⁴¹ Briefly, the pycnometer was completely filled with samples and weighed. Density was calculated by multiplying the mass of the samples with their corresponding volumes. The test was done in triplicates.

Surface Tension

The surface tension measurement was done employing the same method described elsewhere.⁴¹ Briefly, the Du Noüy Ring (R=9.55 mm, r=0.2 mm) method with a LAUDA TD 2 tensiometer. Before each measurement, the Du Noüy ring is washed with acetone and flamed using a mini torch to avoid any contamination. Calibration was done using a calibration weight of 500.00 mg (standard deviation = 0.1 mg). Enough samples were loaded into the sample vessel. During measurement, the ring should be at least 2 to 3 mm below the surface of the sample. The measuring parameters were configured as follows: movement speed = 5; movement optimization = 20 %; pause = 1 min; maximum time = 15 min; standard points = 5; standard deviation = 0.01 mN/m. Analysis was done in triplicates and the average was reported with standard deviations.

Kinematic Viscosity

The viscosity was determined using a KV1000 digital constant temperature kinematic viscosity bath. The procedure is described elsewhere.⁴¹ Each sample was subjected to viscosity measurement at four different temperatures (15, 25, 35, and 45 °C). The viscosity bath (Borosilicate glass jar) was filled with distilled water that serves as the heat transfer fluid up to 5 cm from the rim of the bath to allow for fluid expansion. The glass viscometer was submerged in the bath and samples were loaded into it. An air supply was used to apply pressure into the sample to push it up at 7 mm above the first timing mark of the viscometer arm. The sample was allowed to flow naturally under the influence of gravity until it reached the second timing mark, all while recording the time. The viscosity was calculated by multiplying the recorded time (s) by the viscometer calibration constant (mm^2/s^2). The measurements were carried out in triplicate, and average values were reported. The density at -20 °C was extrapolated.

Gas Chromatography - Flame Ionization Detector

The two-dimensional gas chromatography with flame ionization detector (GCxGC-FID) analysis was employed to identify the carbon species found in the fuel cuts. An Agilent 8890 with a SepSolve flow modulator was used. The first-dimension column is a Restek Rxi-17Sil (60m x 0.32mm x 0.50um), and the second-dimension column is a Restek Rxi-1ms (15m x 0.32mm x 0.50um). The carrier gas is grade 5.0 helium with flows of 1.2 mL/min and 48mL/min through the first- and second-dimension columns, respectively. The GC oven starts at 40 °C for 30 seconds and then increases at 1°C/min until 280 °C. The modulation time is 10 seconds. The injection volume is 1 uL. The hydrocarbon group type analysis was performed with the method described by Vozka et al.⁴²

Samples for the oxygen content analysis were analyzed using an Elementar Rapid Oxy-Cube. The combustion tube was packed according to manufacturer specifications and heated to 1450 °C. Helium was used as the carrier gas. Sample size should not exceed 20uL.

6.3 Results and Discussion

6.3.1 Characteristics of the Feedstocks

The characteristics of the oil feedstocks are presented in Table 6.1. Results showed a higher value for the initial oxygen content.

Table 6.1. Composition of the BTG bio-oil and WCO.

	BTG bio-oil (without light oxygenates)	WCO (Pires et al., 2023) ³⁶
	Elemental Analysis:	
C (wt.%)	55.25	78.0±0.3
H (wt.%)	6.75	9.3±0.0
N (wt.%)	0.19	0.2±0.0
O (wt.%)	37.81	12.5±0.3
	Proximate analysis:	
Volatiles	82.4	61.7
Ash	0.0	0.0
Fixed Carbon	17.6	38.3

6.3.2 Yields of the Hydrotreated Oil and Distillation Cuts

Figure 6.1 shows the hydrotreated oil at different bio-oil concentrations (left) and a representative of the distillation cuts (gasoline, kerosene, and diesel) (right). Figure 6.2 shows the yield of the hydrotreated oil on a feedstock basis. As the bio-oil concentration is increased, the amount of organic layers decreases (80.3 to 62.9 wt.%) and the amounts of coke (0.7 to 2.4 wt.%), gas (17.2 to 24.4 wt.%) and water (1.8 to 10.3wt.%) increase. The amount of coke was comparable to a previous study utilizing the pyrolytic lignin fraction under similar conditions yielding a value close to 2%.³⁶ This may suggest that light oxygenates also play a big role

towards coke formation. The result also shows the possibility of hydrotreating the bio-oil (only the light oxygenates are removed by rotary evaporation) and that extensive chemical fractionation prior to upgrading is unnecessary. Therefore, saving time and resources.

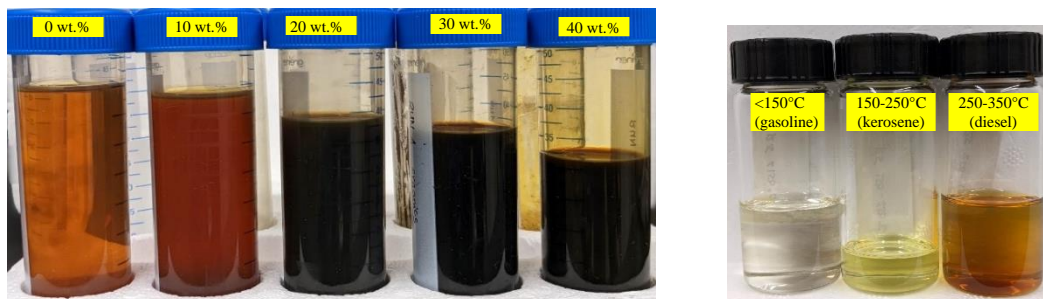


Figure 6.1: Hydrotreated oil at different bio-oil concentrations (left) and representative distillation cuts (right).

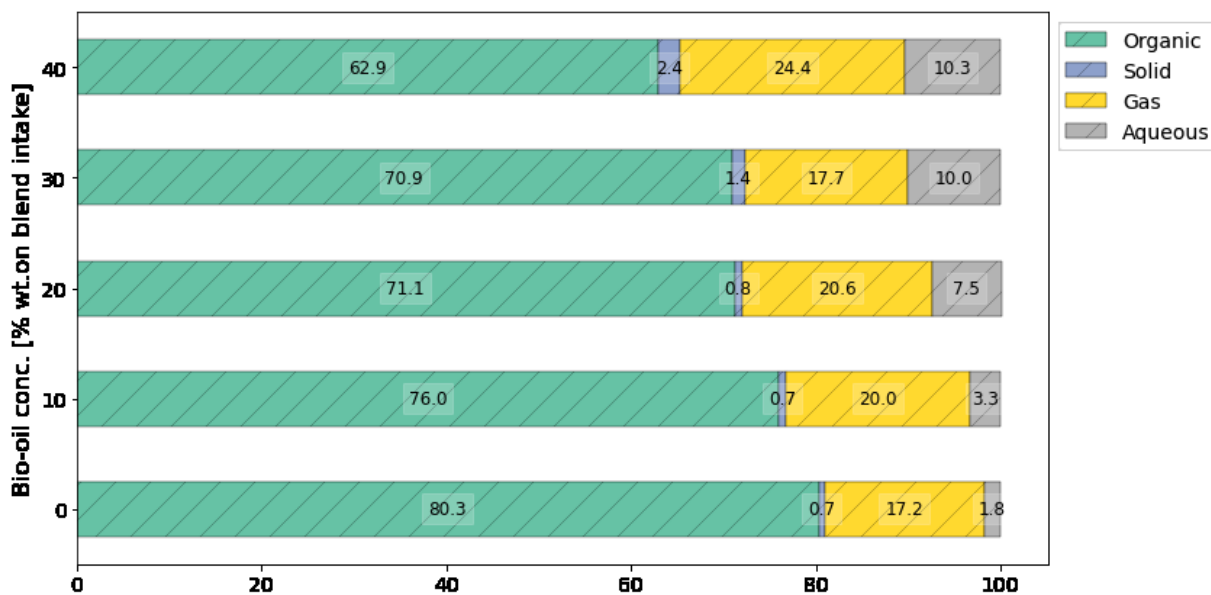


Figure 6.2: Product yields of the co-hydrotreated bio-oil and WCO.

Figure 6.3 shows the yield of the distillation cuts on a feedstock basis (mass of bio-oil + waste cooking oil + 1-butanol). It is observed that the yield is not much affected by the increase

in bio-oil concentration. Diesel cut has the highest yield regardless of the bio-oil concentration but decreases 10 to 40 wt. % of bio-oil concentration. The yield of both gasoline and kerosene cuts decreased slightly with an increase in bio-oil concentration, especially evident at 20 to 40 wt. % bio-oil concentration. The yield of residuals is directly related to the increase of bio-oil concentration. However, it is important to note that these products are not strictly gasoline, kerosene, and diesel cuts for the reason of the difference in distillation set up employed in this work compared to the commercially used method to obtain these cuts.

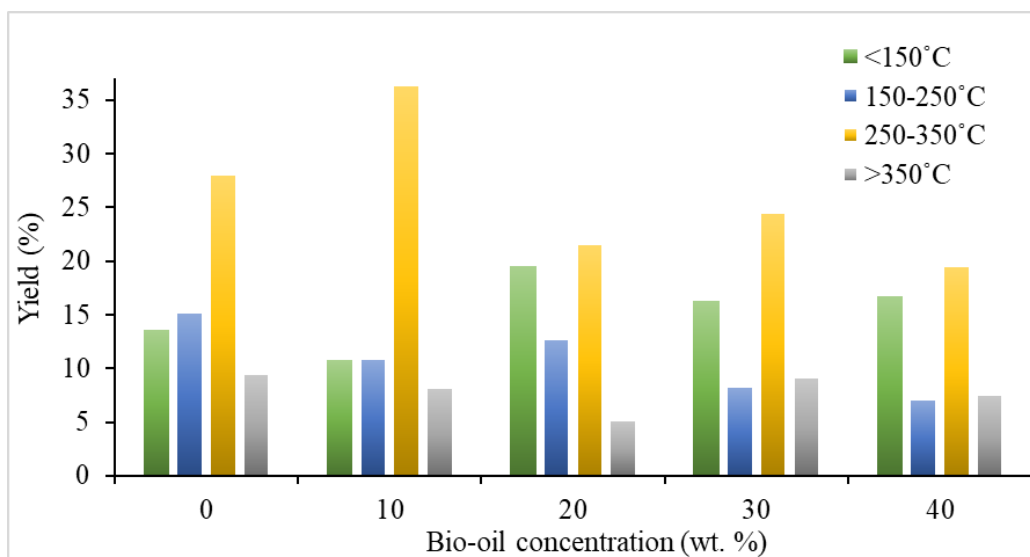


Figure 6.3: Product yield (%) of the distillation cuts.

6.3.3 Characteristics of the Hydrotreated Oils and Distillation Cuts

FTIR

The FTIR spectra of the feedstocks and hydrotreated oils is shown in Figure 6.4. The results indicated that most of the raw materials underwent conversion into biofuels following the hydrotreatment process. The broad, high peaks observed between 1700 to 1800 cm^{-1} and 1000 to

1300 cm^{-1} associated to C=O stretches (carboxylic acids, carbonyls) and C-O stretches (alcohols and carboxylic acids from the bio-oil and ester groups from the WCO), respectively, were eliminated after the hydrotreatment. However, a small peak can still be seen at 30 and 40 wt.% bio-oil concentration. The peaks observed at 1600 cm^{-1} are associated with aromatic C=C stretching. Small peaks can still be seen at 20, 30 and 40 wt.% bio-oil concentration which means that the C=C are not fully converted to alkanes during the hydrotreatment. Sharp peaks are observed between 1380 and 1470 cm^{-1} associated to -CH₃ and -CH₂, respectively. These peaks correspond to the alkanes formed during the hydrotreatment.

UV-Fluorescence

Figure 6.5 shows the UV-fluorescence spectra of the feedstocks and hydrotreated oil. Monomers are observed at 283 nm. Conjugated ring systems are evidenced in the 300 to 450 nm wavelengths. More polycondensed and conjugated ring system compounds are formed at higher bio-oil concentrations. These compounds are precursors to coke formation but are mitigated by the addition of 1-butanol.³⁵

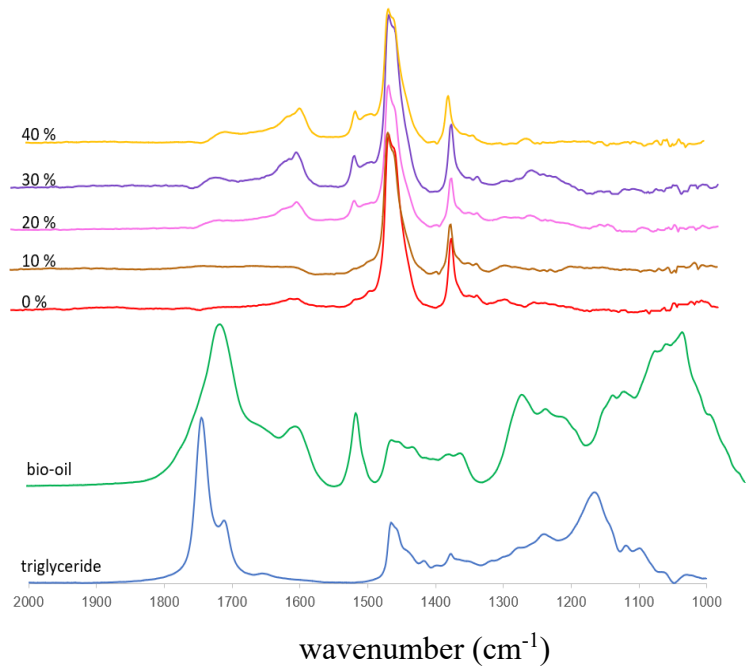


Figure 6.4: FTIR spectra of the feedstocks and hydrotreated oils.

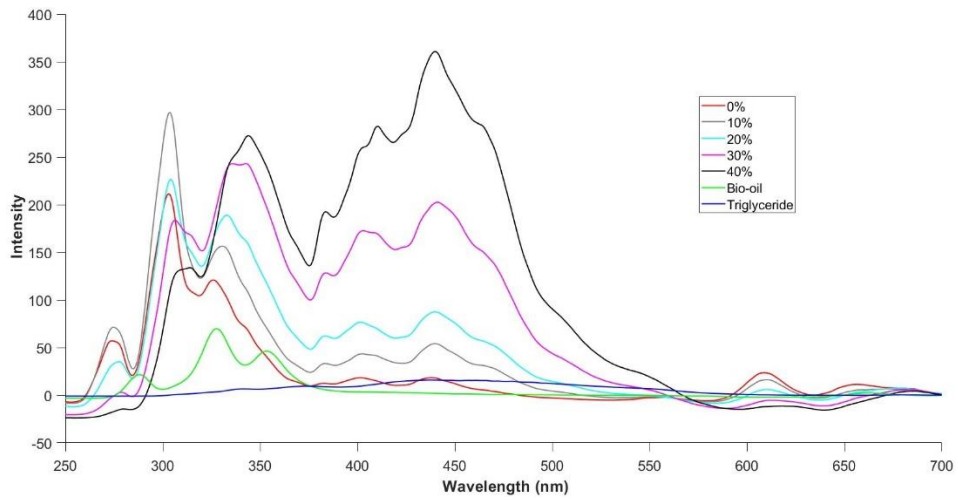


Figure 6.5: UV-Fluorescence spectra of the feedstocks and hydrotreated oils.

Elemental Analysis (CHNO-S)

Table 6.2 displays the elemental composition of the distillation cuts. It is shown that both C and H content of the cuts were increased compared to the initial content of raw feedstock. The O content was also significantly lowered from 38% from the bio-oil and 12.5% from the waste cooking oil to <1.0 wt.%. These results prove the successful hydrodeoxygenation of the bio-oil.

Table 6.2. Elemental composition of the distillation cuts (wt.%).

bio-oil concentration (wt.% of WCO)	distilling temp. (°C)	C	H	N	O	S
0	<150	80.86	14.67	0.67	0.02	0.24
	150 - 250	85.9	15.39	0.15	0.05	0.08
	250 - 350	86.41	15.19	0.42	0.07	0.05
10	<150	78.08	14.99	0.69	0.03	0.24
	150 - 250	85.52	15.75	0.14	0.05	0.08
	250 - 350	86.57	15.61	0.44	0.06	0.03
20	<150	84.37	15.74	0.43	0.51	0.03
	150 - 250	86.16	15.54	0.70	0.45	0.02
	250 - 350	86.35	15.7	0.65	0.26	0.03
30	<150	83.90	15.37	0.51	0.87	0.04
	150 - 250	85.44	14.94	0.52	1.25	0.03
	250 - 350	86.82	15.20	0.52	0.69	0.02
40	150 - 250	86.00	14.59	0.67	2.01	0.04
	250 - 350 °C	86.07	14.71	0.66	1.24	0.03

Density

Table 6.3 shows the density of the distillation cuts. Gasoline cut ranges from 0.71 to 0.74 g/mL, kerosene cut varies from 0.75 to 0.80 g/mL, and the diesel cut accounts for 0.81 g/mL. As the bio-oil concentration is increased, the density of the distillation cuts increased. The results obtained for the kerosene cut conform to the Jet A-1 standards, which stipulate a range of 0.775 g/mL to 0.840 g/mL at 15 °C.⁴¹

Table 6.3. Density (g/mL) of the distillation cuts.

Bio-oil concentration (wt.% WCO)	<150 °C (gasoline)	150 to 250 °C (kerosene)	250 to 350 °C (diesel)
0	0.7114	0.7537	0.8066
10	0.7129	0.7402	0.7931
20	0.7282	0.7898	0.8148
30	0.7312	0.7831	0.8081
40	0.7408	0.8027	0.8122

Surface Tension

Table 6.4 shows the surface tension of the distillation cuts. The gasoline cut has the highest surface tension, followed by the diesel cut, then kerosene cut. As the bio-oil concentration is increased, the surface tension of the distillation cuts increased. Although no specific standards has been specified, it's worth noting that the Handbook of Aviation Fuel Properties (Coordinating Research Council Incorporated 1983) did provide an average value of 23.5 mN/m.⁴¹

Table 6.4. Surface tension (mN/m) of the distillation cuts.

Bio-oil concentration (wt.% of WCO)	<150 °C (gasoline)	150 to 250 °C (kerosene)	250 to 350 °C (diesel)
0	20.94±0.0	23.10±0.0	21.30±0.01
10	20.76±0.0	23.09±0.0	23.65±0.02
20	21.68±0.01	23.75±0.01	23.50±0.01
30	21.53±0.01	24.06±0.01	24.03±0.01
40	21.69±0.01	24.15±0.01	24.65±0.01

Viscosity

The viscosity of the distillation cuts is shown in Table 6.5. Results showed that the kerosene cut is within the recommended density for aviation fuels which is < 8 mm²/s at -20 °C.⁴¹ The diesel cut has the highest viscosity (5.6 to 7.34 mm²/s), followed by kerosene (1.89 to

5.60 mm²/s) and gasoline cut (0.86 to 1.17 mm²/s). This is because diesel cut contains more products with a high number of carbon atoms, followed by kerosene then gasoline. This is evident in the GC results. In the literature, it is reported that viscosity is directly related to the number of carbon atoms⁴³ or molecular weight.⁴⁵ It was also observed that viscosity decreased with an increase in temperature and is consistent with the literature.^{41,44,46}

Table 6.5. Viscosity (mm²/s) of the distillation cuts.

Bio-oil concentration (wt.% of WCO)	Distilling temp. (°C)	-20 °C	15 °C	25 °C	35 °C	45 °C
0	<150	1.02	0.72	0.65	0.62	0.54
	150 - 250	1.89	1.52	1.31	1.14	1.00
	250 - 350	6.17	4.88	3.84	3.10	2.54
10	<150	0.86	0.69	0.63	0.58	0.53
	150 - 250	1.96	1.48	1.27	1.14	0.99
	250 - 350	5.60	4.50	3.50	2.90	2.41
20	<150	1.17	0.85	0.78	0.73	0.69
	150 - 250	4.45	3.54	2.86	2.36	1.98
	250 - 350	7.34	5.93	4.57	3.63	2.96
30	<150	0.99	0.82	0.73	0.66	0.60
	150 - 250	3.51	2.48	2.02	1.72	1.39
	250 - 350	6.54	5.28	4.09	3.26	2.66
40	≤ 150	1.32	0.88	0.67	0.57	0.51
	150 - 250	4.48	3.38	2.71	2.22	1.81
	250 - 350	7.51	6.11	4.64	3.63	2.93

GC x GC-FID

Figure 6.6 shows the carbon species found in the fuel cuts. These include n-paraffins as the main product, followed by cycloparaffins, aromatics, and iso-paraffins regardless of bio-oil concentration. The aromatics is dominantly composed of alkylbenzene followed by cycloaromatic, toluene, naphthalene, benzene, and heavy aromatics (C18+). The cycloparaffins included both mono- and polycycloparaffins. Results show that as the bio-oil concentration is

increased, the yield of n-paraffin and iso-paraffin products decreased while cycloparaffin and aromatic yields are increased, especially evident in the 20 to 40 wt. % bio-oil concentration. This is consistent among the three fuel cuts except for the cycloparaffin yield in the gasoline cut which was directly related to the increase in bio-oil concentration. The percent yield (distillation cut yield basis) of n-paraffin in the kerosene cut ranges from 3.9 to 9.5 %, cycloparaffin yield ranges from 1.4 to 3.9 %, aromatic yield is from 0.95 to 1.8 % and iso-paraffin yield ranges from 0.2 to 0.7 %, depending on the bio-oil concentration.

Figure 6.7 shows the percent distribution of the number of carbon atoms found in the fuel cuts. The gasoline cut ranged from 7 to 12 carbon atoms, kerosene cut ranged from 14 to 20 carbon atoms and the diesel cut has 15 to 20 carbon atoms.

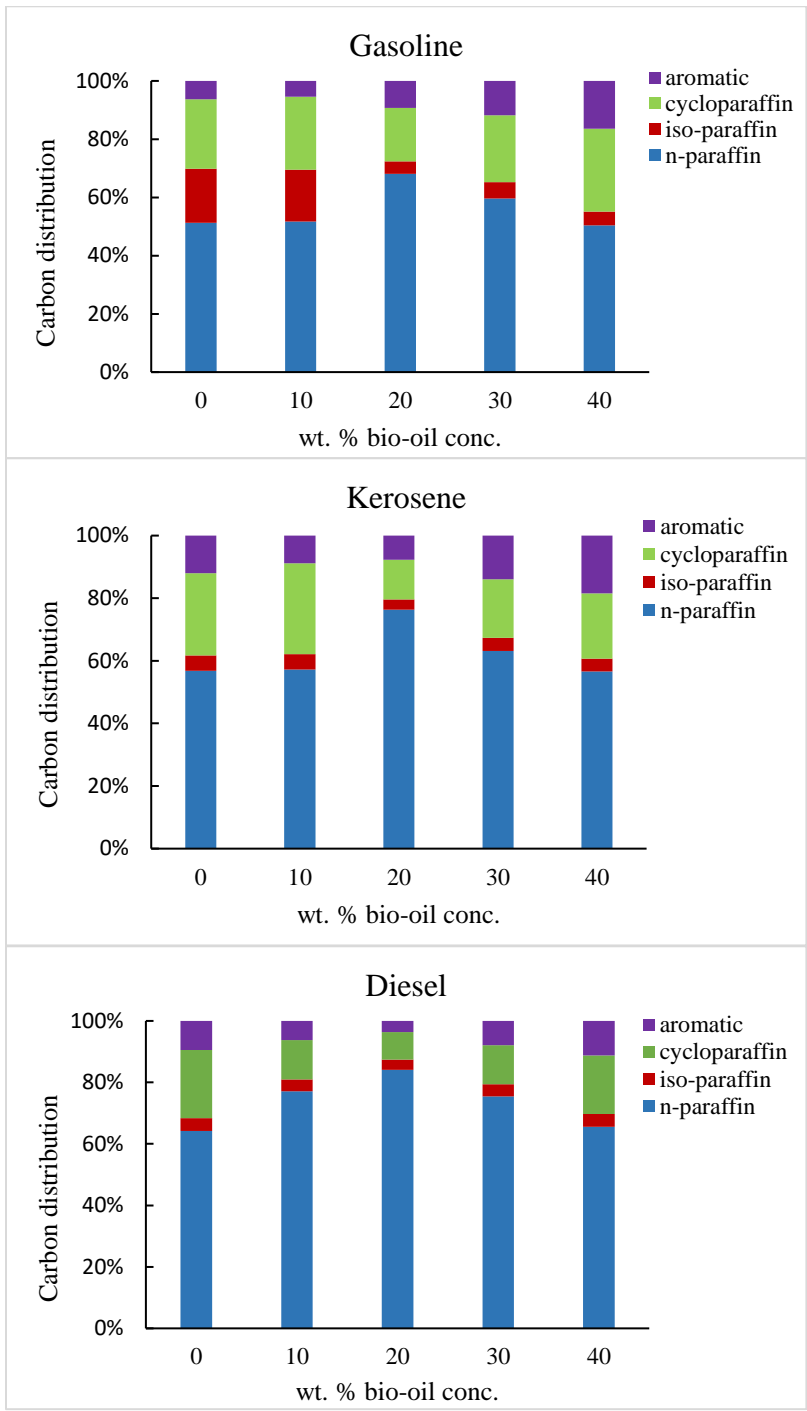


Figure 6.6: Percentage distribution of carbon species identified in the fuel cuts.

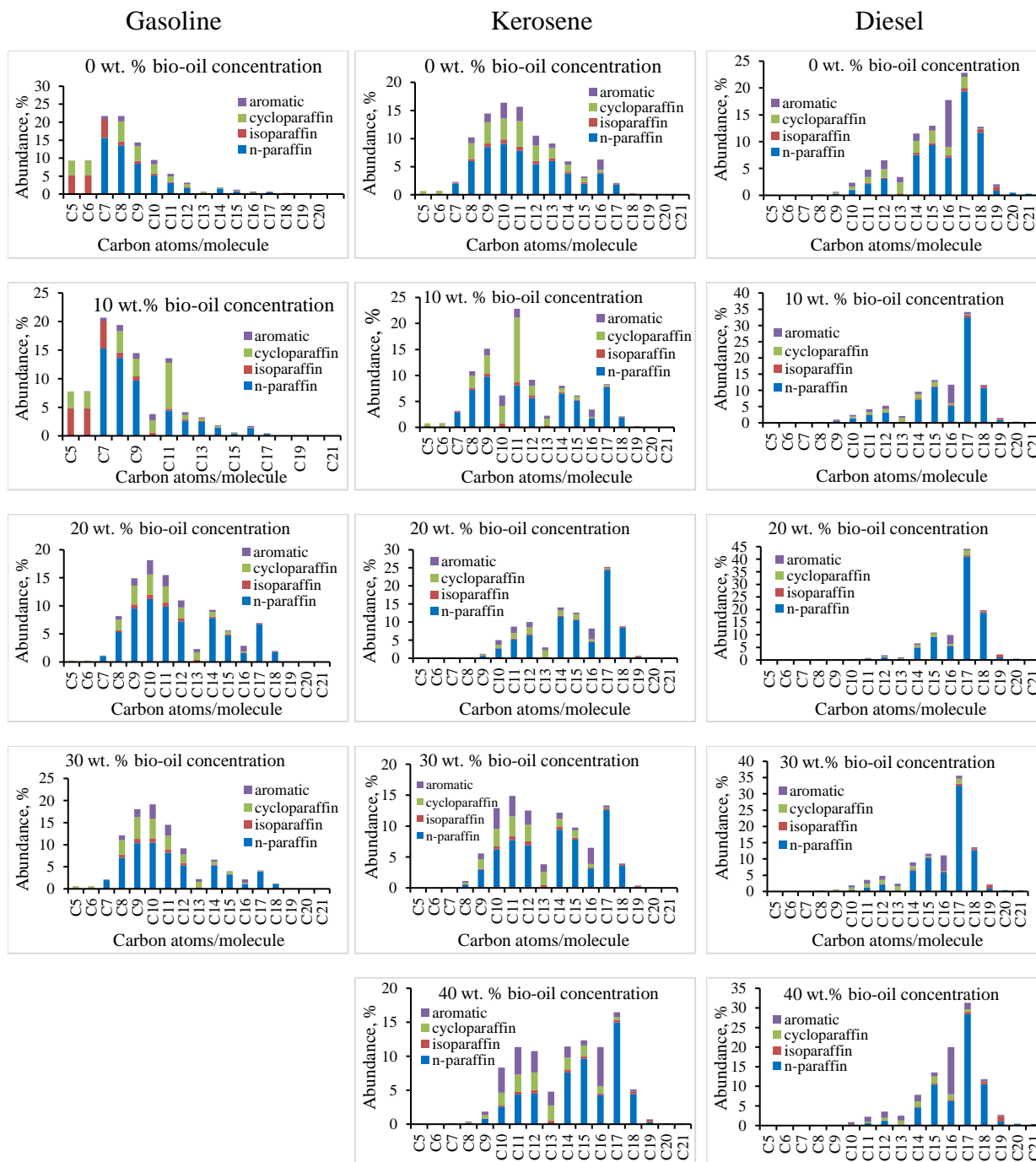


Figure 6.7: Percentage distribution of each class of hydrocarbons identified in the fuel cuts (Note: Samples were insufficient for the analysis of gasoline cut with 40 wt.% bio-oil concentration).

6.4 Conclusion

In this work, heavy bio-oil fraction was co-hydrotreated with WCO using NiMo catalyst supported on alumina to produce biofuels. The bio-oil was pre-mixed with 1-butanol (2:1) to mitigate coke formation and subsequently blended with WCO. Results demonstrated that co-hydrotreating the heavy bio-oil fraction with waste cooking oil led to coke formation results comparable to those achieved when using solely the lignin fraction of the bio-oil. This implies that coke formation is not mainly attributed to sugars; lignin fractions also play a significant role. Additionally, pre-fractionation to eliminate the sugar-rich fraction is unnecessary, maximizing bio-oil utilization while saving time and resources.

The characteristics of the fuel cuts, including density, viscosity, and surface tension, conform to the standards for jet fuels (Jet A-1). The predominant carbon species in the fuel cuts are primarily n-paraffins, cycloparaffins, aromatics, and iso-paraffins. The yield of n-paraffinic hydrocarbons decreased with an increase in bio-oil concentration, while the yields of cycloparaffin and aromatic were directly related to the bio-oil concentration. Moreover, it is recommended to use a 20 wt.% bio-oil mixture with the WCO to achieve a minimal coke yield (0.8%). Future research should consider fine-tuning the operating parameters to reduce coke formation further and enhance kerosene yield.

6.5 REFERENCES

- (1) International Energy Agency. International Energy Agency (IEA) World Energy Outlook 2022. [https://www.Iea.Org/Reports/World-Energy-Outlook-2022/Executive-Summary](https://www.iea.org/reports/world-energy-outlook-2022/executive-summary) **2022**, 524.
- (2) Mohan, D.; Pittman, C. U.; Steele, P. H. Pyrolysis of Wood /Biomass for Bio-Oil. *Prog. Energy Combust. Sci.* **2017**, 62 (4), 848–889.
- (3) Bridgwater, A. V. Review of Fast Pyrolysis of Biomass and Product Upgrading. *Biomass and Bioenergy* **2012**, 38, 68–94. <https://doi.org/10.1016/j.biombioe.2011.01.048>.
- (4) Abdilla-Santes, R. M.; Agarwal, S.; Xi, X.; Heeres, H.; Deuss, P. J.; Heeres, H. J. Valorization of Humin Type Byproducts from Pyrolytic Sugar Conversions to Biobased Chemicals. *J. Anal. Appl. Pyrolysis* **2020**, 152 (October). <https://doi.org/10.1016/j.jaap.2020.104963>.
- (5) Garcia-Perez, M.; Wang, S.; Shen, J.; Rhodes, M.; Lee, W. J.; Li, C. Z. Effects of Temperature on the Formation of Lignin-Derived Oligomers during the Fast Pyrolysis of Mallee Woody Biomass. *Energy and Fuels* **2008**, 22 (3), 2022–2032. <https://doi.org/10.1021/ef7007634>.
- (6) Wang, X.; Kersten, S. R. A.; Prins, W.; Van Swaaij, W. P. M. Biomass Pyrolysis in a Fluidized Bed Reactor. Part 2: Experimental Validation of Model Results. *Ind. Eng. Chem. Res.* **2005**, 44 (23), 8786–8795. <https://doi.org/10.1021/ie050486y>.
- (7) Garcia-Perez, M.; Chaala, A.; Pakdel, H.; Kretschmer, D.; Roy, C. Characterization of Bio-Oils in Chemical Families. *Biomass and Bioenergy* **2007**, 31 (4), 222–242. <https://doi.org/10.1016/j.biombioe.2006.02.006>.
- (8) Stankovikj, F.; McDonald, A. G.; Helms, G. L.; Garcia-Perez, M. Quantification of Bio-Oil Functional Groups and Evidences of the Presence of Pyrolytic Humins. *Energy and Fuels* **2016**, 30 (8), 6505–6524. <https://doi.org/10.1021/acs.energyfuels.6b01242>.
- (9) Lu, Y.; Li, G. S.; Lu, Y. C.; Fan, X.; Wei, X. Y. Analytical Strategies Involved in the Detailed Componential Characterization of Biooil Produced from Lignocellulosic

- Biomass. *Int. J. Anal. Chem.* **2017**, 2017. <https://doi.org/10.1155/2017/9298523>.
- (10) Stankovikj, F.; McDonald, A. G.; Helms, G. L.; Olarte, M. V.; Garcia-Perez, M. Characterization of the Water-Soluble Fraction of Woody Biomass Pyrolysis Oils. *Energy and Fuels* **2017**, 31 (2), 1650–1664. <https://doi.org/10.1021/acs.energyfuels.6b02950>.
- (11) Bayerbach, R.; Meier, D. Characterization of the Water-Insoluble Fraction from Fast Pyrolysis Liquids (Pyrolytic Lignin). Part IV: Structure Elucidation of Oligomeric Molecules. *J. Anal. Appl. Pyrolysis* **2009**, 85 (1–2), 98–107. <https://doi.org/10.1016/j.jaap.2008.10.021>.
- (12) Pinheiro Pires, A. P.; Arauzo, J.; Fonts, I.; Domine, M. E.; Fernández Arroyo, A.; Garcia-Perez, M. E.; Montoya, J.; Chejne, F.; Pfromm, P.; Garcia-Perez, M. Challenges and Opportunities for Bio-Oil Refining: A Review. *Energy and Fuels* **2019**, 33 (6), 4683–4720. <https://doi.org/10.1021/acs.energyfuels.9b00039>.
- (13) Oasmaa, A.; Czernik, S. Fuel Oil Quality of Biomass Pyrolysis Oils - State of the Art for the End Users. *Energy and Fuels* **1999**, 13 (4), 914–921. <https://doi.org/10.1021/ef980272b>.
- (14) Czernik, S.; Bridgwater, A. V. Overview of Applications of Biomass Fast Pyrolysis Oil. *Energy and Fuels* **2004**, 18 (2), 590–598. <https://doi.org/10.1021/ef034067u>.
- (15) Elliott, D. C.; Hart, T. R.; Neuenschwander, G. G.; Rotness, L. J.; Olarte, M. V.; Zacher, A. H.; Solantausta, Y. Catalytic Hydroprocessing of Fast Pyrolysis Bio-Oil from Pine Sawdust. *Energy and Fuels* **2012**, 26 (6), 3891–3896. <https://doi.org/10.1021/ef3004587>.
- (16) Xiu, S.; Shahbazi, A. Bio-Oil Production and Upgrading Research: A Review. *Renew. Sustain. Energy Rev.* **2012**, 16 (7), 4406–4414. <https://doi.org/10.1016/j.rser.2012.04.028>.
- (17) Lindfors, C.; Kuoppala, E.; Oasmaa, A.; Arpiainen, V. Fractionation of Bio-Oil. **2014**.
- (18) Huber, G. W.; Iborra, S.; Corma, A. Synthesis of Transportation Fuels from Biomass: Chemistry, Catalysts, and Engineering. *Chem. Rev.* **2006**, 106 (9), 4044–4098. <https://doi.org/10.1021/cr068360d>.

- (19) Elliott, D. C.; Baker, E. G. Method for Upgrading Biomass Pyrolyzates. **1989**, No. 19.
- (20) Laboratories, P. N.; Beckman, D. Reviews Developments in Direct Thermochemical Liquefaction Of. *Energy & Fuels* **1991**, *5*, 399–410.
- (21) Elliott, D. C. Historical Developments in Hydroprocessing Bio-Oils. *Energy and Fuels* **2007**, *21* (3), 1792–1815. <https://doi.org/10.1021/ef070044u>.
- (22) Furimsky, E. Catalytic Hydrodeoxygenation. *Appl. Catal. A Gen.* **2000**, *199* (2), 147–190. [https://doi.org/10.1016/S0926-860X\(99\)00555-4](https://doi.org/10.1016/S0926-860X(99)00555-4).
- (23) He, Z.; Wang, X. Hydrodeoxygenation of Model Compounds and Catalytic Systems for Pyrolysis Bio-Oils Upgrading. *Catal. Sustain. Energy* **2013**, *1*, 28–52. <https://doi.org/10.2478/cse-2012-0004>.
- (24) Pollard, A. S.; Rover, M. R.; Brown, R. C. Characterization of Bio-Oil Recovered as Stage Fractions with Unique Chemical and Physical Properties. *J. Anal. Appl. Pyrolysis* **2012**, *93*, 129–138. <https://doi.org/10.1016/j.jaap.2011.10.007>.
- (25) Zhang, L.; Hu, X.; Li, C.; Zhang, S.; Wang, Y.; Esmaeili, V.; Gholizadeh, M. Fates of Heavy Organics of Bio-Oil in Hydrotreatment: The Key Challenge in the Way from Biomass to Biofuel. *Sci. Total Environ.* **2021**, *778*, 146321. <https://doi.org/10.1016/j.scitotenv.2021.146321>.
- (26) Bu, Q.; Lei, H.; Zacher, A. H.; Wang, L.; Ren, S.; Liang, J.; Wei, Y.; Liu, Y.; Tang, J.; Zhang, Q.; Ruan, R. A Review of Catalytic Hydrodeoxygenation of Lignin-Derived Phenols from Biomass Pyrolysis. *Bioresour. Technol.* **2012**, *124*, 470–477. <https://doi.org/10.1016/j.biortech.2012.08.089>.
- (27) De Miguel Mercader, F.; Groeneveld, M. J.; Kersten, S. R. A.; Geantet, C.; Toussaint, G.; Way, N. W. J.; Schaverien, C. J.; Hogendoorn, K. J. A. Hydrodeoxygenation of Pyrolysis Oil Fractions: Process Understanding and Quality Assessment through Co-Processing in Refinery Units. *Energy Environ. Sci.* **2011**, *4* (3), 985–997. <https://doi.org/10.1039/c0ee00523a>.
- (28) Kloekhorst, A.; Wildschut, J.; Heeres, H. J. Catalytic Hydrotreatment of Pyrolytic Lignins

- to Give Alkylphenolics and Aromatics Using a Supported Ru Catalyst. *Catal. Sci. Technol.* **2014**, *4* (8), 2367–2377. <https://doi.org/10.1039/c4cy00242c>.
- (29) Figueirêdo, M. B.; Deuss, P. J.; Venderbosch, R. H.; Heeres, H. J. Catalytic Hydrotreatment of Pyrolytic Lignins from Different Sources to Biobased Chemicals: Identification of Feed-Product Relations. *Biomass and Bioenergy* **2020**, *134* (June 2019). <https://doi.org/10.1016/j.biombioe.2020.105484>.
- (30) French, R. J.; Black, S. K.; Myers, M.; Stunkel, J.; Gjersing, E.; Iisa, K. Hydrotreating the Organic Fraction of Biomass Pyrolysis Oil to a Refinery Intermediate. *Energy and Fuels* **2015**, *29* (12), 7985–7992. <https://doi.org/10.1021/acs.energyfuels.5b01440>.
- (31) Sanna, A.; Vispute, T. P.; Huber, G. W. Hydrodeoxygenation of the Aqueous Fraction of Bio-Oil with Ru/C and Pt/C Catalysts. *Appl. Catal. B Environ.* **2015**, *165*, 446–456. <https://doi.org/10.1016/j.apcatb.2014.10.013>.
- (32) Li, N.; Tompsett, G. A.; Zhang, T.; Shi, J.; Wyman, C. E.; Huber, G. W. Renewable Gasoline from Aqueous Phase Hydrodeoxygenation of Aqueous Sugar Solutions Prepared by Hydrolysis of Maple Wood. *Green Chem.* **2011**, *13* (1), 91–101. <https://doi.org/10.1039/c0gc00501k>.
- (33) Yin, W.; Alekseeva, M. V.; Venderbosch, R. H.; Yakovlev, V. A.; Heeres, H. J. Catalytic Hydrotreatment of the Pyrolytic Sugar and Pyrolytic Lignin Fractions of Fast Pyrolysis Liquids Using Nickel Based Catalysts. *Energies* **2020**, *13* (1). <https://doi.org/10.3390/en13010285>.
- (34) Kadarwati, S.; Hu, X.; Gunawan, R.; Westerhof, R.; Gholizadeh, M.; Hasan, M. D. M.; Li, C. Coke Formation during the Hydrotreatment of Bio-Oil Using NiMo and CoMo Catalysts. *Fuel Process. Technol.* **2017**, *155*, 261–268. <https://doi.org/10.1016/j.fuproc.2016.08.021>.
- (35) Han, Y.; Pires, A. P. P.; Garcia-Perez, M. Co-Hydrotreatment of the Bio-Oil Lignin-Rich Fraction and Vegetable Oil. *Energy and Fuels* **2020**, *34* (1), 516–529. <https://doi.org/10.1021/acs.energyfuels.9b03344>.

- (36) Paiva Pinheiro Pires, A.; Olarte, M.; Terrell, E.; Garcia-Perez, M.; Han, Y. Co-Hydrotreatment of Yellow Greases and the Water-Insoluble Fraction of Pyrolysis Oil. Part I: Experimental Design to Increase Kerosene Yield and Reduce Coke Formation. *Energy and Fuels* **2023**, *37* (3), 2100–2114. <https://doi.org/10.1021/acs.energyfuels.2c03250>.
- (37) Cai, Q.; Xu, J.; Zhang, S. Upgrading of Bio-Oil Aqueous Fraction by Dual-Stage Hydrotreating-Cocracking with Methanol. *ACS Sustain. Chem. Eng.* **2017**, *5* (7), 6329–6342. <https://doi.org/10.1021/acssuschemeng.7b01505>.
- (38) Han, Y.; Pinheiro Pires, A. P.; Denson, M.; McDonald, A. G.; Garcia-Perez, M. Ternary Phase Diagram of Water/Bio-Oil/Organic Solvent for Bio-Oil Fractionation. *Energy and Fuels* **2020**, *34* (12), 16250–16264. <https://doi.org/10.1021/acs.energyfuels.0c03100>.
- (39) Han, Y.; Stankovikj, F.; Garcia-Perez, M. Co-Hydrotreatment of Tire Pyrolysis Oil and Vegetable Oil for the Production of Transportation Fuels. *Fuel Process. Technol.* **2017**, *159*, 328–339. <https://doi.org/10.1016/j.fuproc.2017.01.048>.
- (40) Pecha, M. B.; Terrell, E.; Montoya, J. I.; Stankovikj, F.; Broadbelt, L. J.; Chejne, F.; Garcia-Perez, M. Effect of Pressure on Pyrolysis of Milled Wood Lignin and Acid-Washed Hybrid Poplar Wood. *Ind. Eng. Chem. Res.* **2017**, *56* (32), 9079–9089. <https://doi.org/10.1021/acs.iecr.7b02085>.
- (41) Pires, A. P. P.; Han, Y.; Kramlich, J.; Garcia-Perez, M. Alternative Jet Fuel Properties. *BioResources* **2018**, *13* (2), 2632–2657.
- (42) Vozka, P.; Kilaz, G. How to Obtain a Detailed Chemical Composition for Middle Distillates via GC × GC-FID without the Need of GC × GC-TOF/MS. *Fuel* **2019**, *247* (March), 368–377. <https://doi.org/10.1016/j.fuel.2019.03.009>.
- (43) Knothe, G.; Steidley, K. R. Kinematic Viscosity of Biodiesel Fuel Components and Related Compounds. Influence of Compound Structure and Comparison to Petrodiesel Fuel Components. *Fuel* **2005**, *84* (9), 1059–1065. <https://doi.org/10.1016/j.fuel.2005.01.016>.
- (44) Berkhou, S. K. Thermal Oxidative Stability of Coal-Based Jp-900 Jet Fuel: Impact on

Selected Physical Properties. *Dep. Energy GeoEnvironmental Eng.* **2007**.

- (45) Detusheva, É. P., Klimova, A. P., Khramtsova, L. P., Zhalnin, A. M., and Muchinskii, Y. D. (1986). "Characteristics of narrow residual fractions of naphthenic-paraffinic hydrocarbons," *Chemistry and Technology of Fuels and Oils* 21(6), 310-312.
- (46) Hemighaus, G., Boval, T., Bacha, J., Barnes, F., Franklin, M., Gibbs, L., Hogue, N., Jones, J., Lesnini, D., Lind, J., and Morris, J. (2006). "Aviation fuels technical review (FTR-3)," Chevron Corporation.

CHAPTER SEVEN: HYDRODEOXYGENATION OF HYDROXYACETONE OVER NiMo CATALYST FROM FIRST PRINCIPLES

7.1 Introduction

Global concerns over dwindling fossil fuels, escalating fuel prices, and environmental issues have ignited the quest for alternative fuel sources. Bio-oil, derived from lignocellulosic biomass, has emerged as a viable candidate. However, it cannot readily serve as a direct substitute for transportation fuel due to its unfavorable properties such as low energy content and corrosiveness, associated with high oxygen (35 to 40 wt. %) ^{1,2} and water (19 to 30 wt. %) ^{2,3,4,5} contents, as well as chemical complexity. In particular, the highly oxygenated compounds in bio-oil, including sugars, guaiacols, phenol, carboxylic acids, and furanic rings, pose a significant challenge related to coke formation due to their inherent instability and reactivity. ^{6,7} Consequently, bio-oil upgrading becomes a necessity. Catalytic hydrotreatment, specifically hydrodeoxygenation (HDO), has shown significant promise for improving bio-oil quality. ⁸ Hydrotreatment, a well-established process in the petroleum industry for upgrading crude oils, is being adapted to refine bio-oil through HDO.

The chemistry of hydrodeoxygenation involves the elimination of oxygen from bio-oil compounds in the action of hydrogen atoms under high pressure and elevated temperature conditions and in the presence of active catalysts. ⁹ Initially, the bio-oil compounds and hydrogen atoms undergo chemisorption onto the catalyst surface. Following this initial adsorption, hydrogen dissociates onto the metal surface and then migrates towards the unsaturated bio-oil compounds, facilitating the hydrogenation process. As the bio-oil compounds become saturated and transformed into hydrocarbons, they desorb from the surface, releasing water as a byproduct, ultimately yielding hydrotreated oil.

Significant efforts have been committed to enhance the quality of biofuels from bio-oil, encompassing investigations that employed real bio-oils, model compounds, and calculations from the first principles. These efforts are directed towards mitigating coke formation, which remains the foremost concern in upgrading bio-oils.¹⁰ Coke formation arises from polymerization and polycondensation reactions involving the strong adsorption of alkenes, aromatics, heterocyclic, and highly oxygenated compounds onto the catalyst surface.⁶ Research studies have tackled this challenge by exploring approaches such as catalyst innovation, co-feeding with hydrogen-rich chemicals, and optimizing process conditions. Catalyst selection has spanned a range of metals, including noble metals (Pt, Pd, Ru, and Rh), transition metals (Ni, Mo, Fe, and Co), and bifunctional metals (mostly NiMo and CoMo).^{11,12,13} While noble metals exhibit high HDO activity, their practical use can be economically prohibitive. As a result, standard hydroprocessing catalysts like NiMo and CoMo supported on alumina, being well-established and inexpensive, remain prevalent in the industry.^{60,61,62,63}

Elliot et al.¹⁴ conducted a comprehensive review, highlighting the historical evolution of bio-oil hydroprocessing up to 2007, with the significant role played by PNNL in the development of a two-stage hydrotreatment process aimed at mitigating coke formation. To this day, this method remains extensively utilized. Because of the complex chemical makeup of bio-oil, only a few studies have utilized real bio-oil for hydrotreatment. In some cases, researchers have opted to fractionate bio-oil to remove the highly oxygenated sugar fraction, which is believed to cause coke formation, concentrating instead on the hydrotreatment of the lignin-rich fraction.^{15,16,17,18} Nevertheless, certain research efforts have endeavored to investigate the sugar-rich bio-oil fraction. Sanna et al.¹⁹ employed the two-stage process to hydrotreat aqueous phase fraction over Ru and Pt catalysts supported on carbon. The aqueous phase comprises diverse

light-oxygenated compounds, including aldehydes, ketones, acids, and carbohydrates. The study reported coke yields of approximately 19% and 22.5% of the starting carbon at 150 and 175 C, respectively. Kadarwati et al.²⁰ also used the two-stage to hydrotreat three distinct bio-oil fractions: the whole bio-oil, the heavy fraction (without light oxygenates), and the lignin fraction utilizing Ru/C and unsulfided NiMo/ γ -Al₂O₃ catalysts. Their results revealed the formation of heavy molecular weight compounds originating from the sugar-rich fraction, which proved challenging to crack. A follow-up study²¹ investigated the yield of coke formation by adding extra levoglucosan to the bio-oil. Their findings indicated that the additional levoglucosan did not increase coke formation. However, without a catalyst, the coke yield significantly escalated. Denson et al. (paper to be submitted) conducted co-hydrotreatment of the heavy bio-oil fraction (excluding light oxygenates but containing both lignin and sugar fractions) with waste cooking oil, reporting a coke yield ranging from 0.7 to 2.4 wt%, depending on bio-oil concentration. This coke yield closely resembled the coke formation observed when utilizing only the lignin fraction. Furthermore, additional studies^{15,22} have investigated the bio-oil's sugar-rich fraction using various catalysts. In addition to investigations using real bio-oil, most research has heavily focused on model compounds such as guaiacol, furfural, and acetic acid to represent the lignin, cellulosic, and hemicellulosic bio-oil components, respectively.²³

On one hand, simulation calculations based on first principles are immensely helpful to aid in a better understanding of the reaction mechanisms underlying HDO. Density functional theory (DFT) offers valuable insights regarding the energetics and thermodynamics of the system, catalyst surface reactivity, and reaction pathways, among others. These insights contribute significantly to the development of a more efficient and sustainable biofuel production process. However, due to the complex molecular structures of bio-oil compounds, most DFT

studies have focused on smaller compounds, typically containing one or two oxygen atoms. Specifically, DFT research has also focused on fundamental components like guaiacol^{24,25,26,27,28,29,30,31,32,33,34,35,36} and phenol^{37,38,39,40,41,42,43,44,45,46} from lignin, furans^{47,48} and furfurals^{49,50,51,52} from sugars, and linear low molecular weight compounds.^{53,54,55,56,57}

Despite numerous studies into the HDO of bio-oils, understanding the intricate reaction pathways remains a formidable challenge, particularly the highly oxygenated compounds, which are known contributors to catalyst deactivation due to coke formation. Compounds like carboxylic acids, ketones, hydroxy groups, and aldehydes are among the unfavorable constituents.^{4,58} Therefore, the primary objective of this study is to gain a more profound insight into the mechanism of hydrogenation and oxygen removal during the upgrading of hydroxyacetone (HA). HA comprises hydroxy and ketone functional groups, representing the highly reactive bio-oil compounds. It originates from the fragmentation of the carbohydrate fraction in bio-oil and constitutes approximately 2.6 to 8.6 wt.% of the bio-oil.^{4,59}

This work specifically aims to model the HDO mechanism of sugar fractions, drawing from our previous experimental HDO research on heavy bio-oil fractions.(paper to be submitted) However, to streamline the study, we employed hydroxyacetone, a sugar fragment, along with an unsupported Ni-promoted MoS₂ catalyst. It is important to emphasize that our previous experimental work did not involve characterizing the NiMoS catalyst, and as such, our NiMoS model is constructed based on existing literature.^{53,54,64,65,66}

A characterization technique based on transmission electron microscopy (TEM) revealed that the commercial MoS₂ possessed a stacking layer comprising over 12 slabs, with a length exceeding 120 nm and an interlayer distance of 0.62 nm. These findings aligned with results obtained through XRD.⁶⁷ Furthermore, it was observed in another study⁶⁸ that doping the MoS₂

with Ni led to a reduction in the slab length to a range of 4 to 6 nm. The stacks varied from 1 to 6, with one being the most prevalent, and the interlayer distance was measured at 0.64 nm. Similar investigations^{69,70} corroborated the structural attributes of the MoS₂ catalyst, characterized by parameters such as slab length and layer number. Notably, MoS₂ crystals possess two exposed surfaces: the 001 plane (basal plane) and the 100 plane, exposing the S-Mo edges (edge plane).⁷¹ It is important to mention that the edge plane is more active for catalytic activity than the basal plane, which is chemically inert.⁷² Hence, in this work, the 100 plane was the focus of our modeling efforts.

The findings from this study will offer a more extensive understanding of the reaction mechanisms involved in the HDO of the highly oxygenated compounds such as hydroxyacetone. This knowledge can be extended to investigate the HDO reaction of other bio-oil constituents, such as the oligomers.

7.2 Methodology

7.2.1 Computational Details

This study employed planewave periodic density functional density, specifically the Vienna ab-initio simulation package (VASP)^{73,74} to study the reaction mechanism of acetol hydrodeoxygenation. The generalized gradient approximation (GGA) functional, particularly Perdew-Burke-Ernzerhof (PBE)⁷⁵ and OptB86b-vdW⁷⁶ functionals, were utilized to better describe the exchange-correlation energy of the electrons being studied. The core electrons were treated with projector augmented waves (PAW)⁷⁷ to solve the Kohn-Sham equations with an energy cut-off of 400 eV. Energy and force tolerances were set at 1×10^{-4} eV and 0.05 eV/Å, respectively. Smearing and sigma values were set to 1 (relaxation in metals) and 0.1, respectively. The k-point mesh used was 20x20x20 for bulk structure calculations and 3x3x1 for

surface calculations. The optimized bulk structure, with the $P6_3/mmc$ space group, exhibited lattice constants of $a = b = 3.1687 \text{ \AA}$, and $c = 12.3920 \text{ \AA}$.

Initially, the structure of MoS_2 was obtained from the Materials Project,⁷⁸ and bulk volume optimization was performed. The optimized scale served as the foundation for constructing the catalyst slab (Appendix D, Figure S9). The final design of the catalyst periodic supercell was modeled based on previous studies,^{53,54,64,65,66} except that the new model contained both the Mo-edge and S-edge (Figure 7.1) to account for meaningful adsorption of the bio-oil model compound onto the slab surface. The supercell comprises 4 Mo units in the x-direction and 5 Mo units stacked in the z-direction. More precisely, the 5 Mo units in the z-direction are made up of 4 Mo sub-surface layers overlaid by a mixed Ni-Mo metallic row with a promotion rate of 50% and a sulfur coverage of 12.5%. The lower 2 Mo unit layers were fixed at their bulk positions, while the upper 3 Mo unit layers were allowed to relax. The slab length (number of Mo units in the z-direction) was determined by assessing the adsorption energy (eq'n 1), shown in Appendix D, Figure S10. Vacuum testing was also conducted to ensure sufficient room for free movement during simulation while preventing unwanted interactions with neighboring periodic images. This process resulted in the establishment of a 17 \AA -thick vacuum layer (shown in Appendix D, Figure S11). Moreover, the minimum energy pathways (MEPs) of the reactions will be evaluated using the nudged elastic band (NEB) method.

$$E_{\text{adsorption}} = E_{\text{total}} - E_{\text{clean}} - E_{\text{adsorbate}} \quad (\text{eq'n 1})$$

where: E_{total} – energy of slab + adsorbate, eV

E_{clean} – energy of slab, eV

$E_{\text{adsorbate}}$ – energy of adsorbate, eV

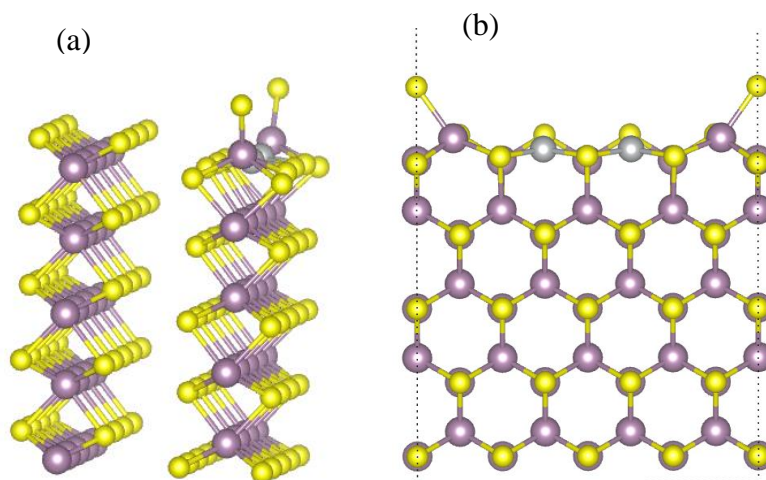


Figure 7.1: NiMoS model (100 surface) used in the study: (a) perspective view showing both Mo and S edges, and (b) front view showing the Ni-promoted Mo-edge. Color legend: Mo – magenta, Ni – gray, S – yellow.

7.3 Result and Discussion

7.3.1 Reaction Pathway of Hydroxyacetone HDO

Figure 7.2 shows the proposed HDO mechanisms of hydroxyacetone to propanediol. It is initiated by the hydrogenation of the ketone group to reduce it to alcohol. The hydrogenation of the alcohol leads to the cleavage of C-O bond, therefore desorbing the propanol from the catalyst surface and generating water as by-product. This mechanism assumes the abundant supply of molecular hydrogen into the system. In cases where hydrogen source is lacking, it is conceivable that hydrogen originates from the bio-oil compounds. Consequently, the formation of propenol is observed as intermediates in the HDO process of hydroxyacetone to propanediol. This pathway pertains to the concerted mechanism of alcohol dehydration leading to the formation of an olefin which are further hydrogenated to yield an alkane.⁵³ Another pathway called hydrogenolysis,

involves the direct cleavage of C-OH bond upon hydrogenation of the ketone group. This happens when the Mo-O dissociation bond energy is stronger than the C-O bond.

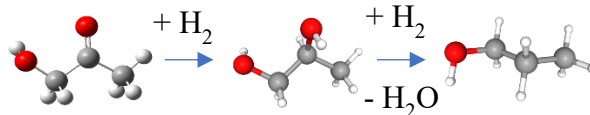


Figure 7.2: Hydrodeoxygenation pathway of hydroxyacetone to propanediol.

7.3.2 Adsorption of Hydroxyacetone

As reported in the literature,^{53,54,65,66} hydrogen atoms undergo dissociative binding, forming hydridic species with Ni and protonic species with S. In contrast, O and C atoms bind to the Mo atom. The adsorption of hydroxyacetone onto the catalyst is initiated by the ketone (C=O) group since it is more reactive than the alcohol group. Multiple adsorption sites (including Mo, Ni, and the bidentate state) and adsorption configurations were evaluated, as depicted in Figure 7.3. The assessment of the adsorption energy was performed using equation 1. The results indicated that the ketone group exhibited the most favorable adsorption energy when adsorbed on the Mo atom in an inclined configuration, with an energy of -1.57 eV. This preferred configuration was subsequently used for further calculations to evaluate the HDO mechanism.

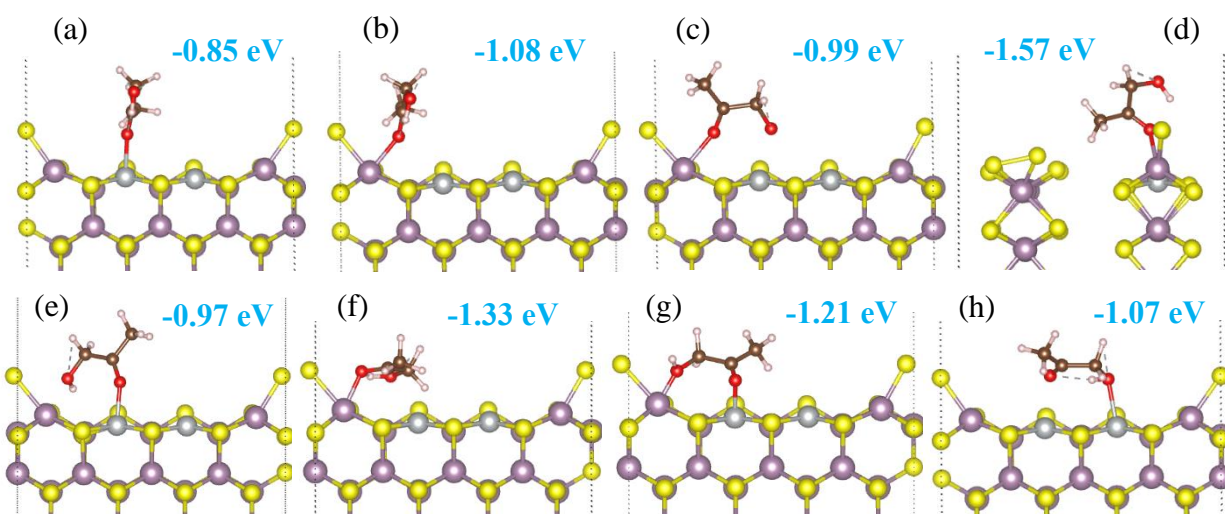


Figure 7.3: Adsorption sites and configurations of hydroxyacetone: (a) ketone on Ni-1 perpendicular, (b) ketone on Mo perpendicular, (c) ketone on Mo parallel, (d) ketone on Mo inclined, (e) ketone on Ni-1 parallel, (f) ketone on Mo perpendicular flat, (g) bidentate – ketone on Ni-1 and alcohol on Mo, and (h) ketone on Ni-2 parallel. Color legend: Mo magenta, Ni – gray, S – yellow, C – brown, O – red, and pinkish white – H.

7.3.3 HDO Mechanism

Two hydrogen atoms were dissociatively co-adsorbed onto the system. One H atom binds to the Ni site, while the other binds to the S-bridge. Subsequently, the H atom bound to the Ni site migrates to hydrogenate the C in the ketone group. This is followed by hydrogenation of the O atom in the ketone group, using the H atom from the S-bridge, thereby effectively converting the ketone group into an alcohol group, forming propanediol. A repetition of similar processes to hydrogenate the alcohol group (previously formed from the ketone group) leads to the breaking of the C-OH bond, resulting in the release of both water and propanol from the catalyst surface. These steps are illustrated in Figure 7.4.

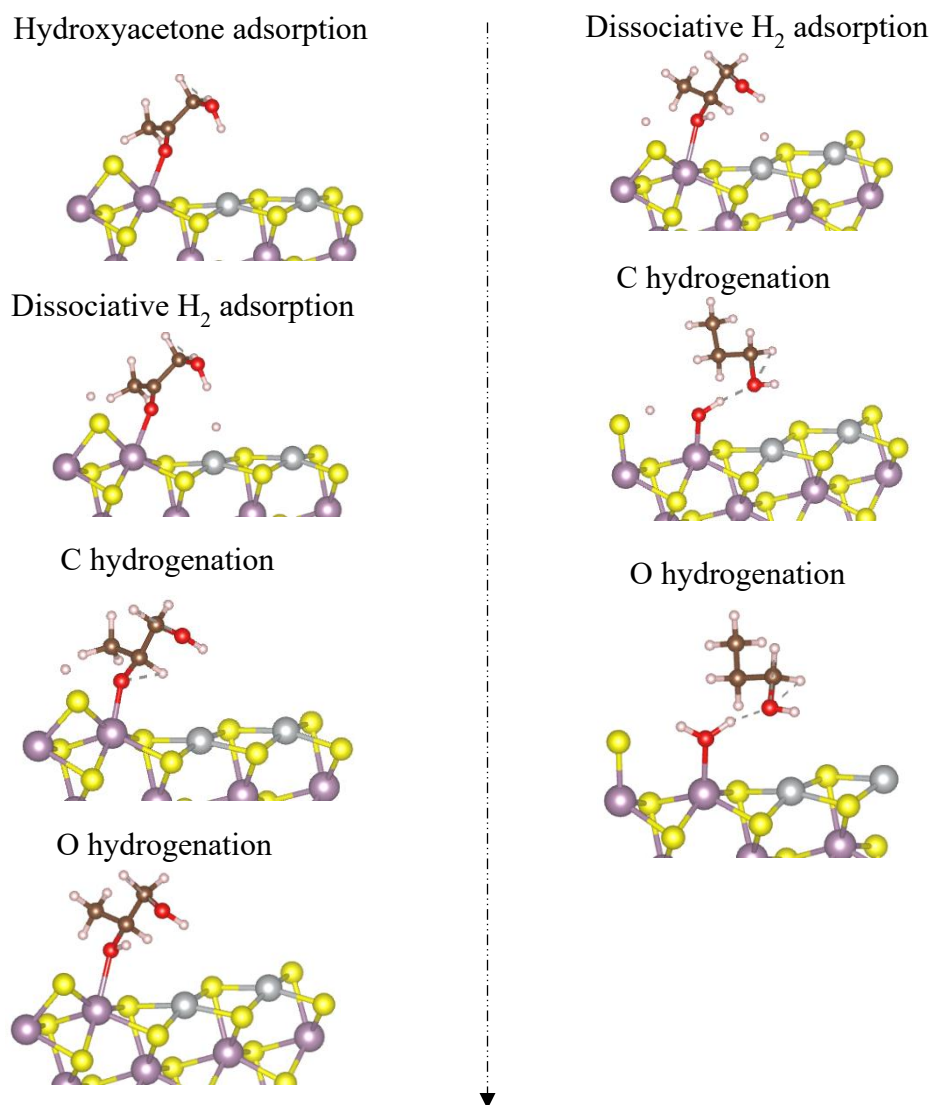


Figure 7.4: Hydrogenation steps of hydroxyacetone to propanediol.

7.4 Conclusion

The high oxygen and water content of bio-oil renders it unsuitable for use as a direct transportation fuel, thus mandating the need for an upgrading process. In this work, we investigated the reaction mechanism of hydroxyacetone hydrodeoxygenation over an unsupported NiMoS catalyst through the density functional theory (DFT). The

hydrodeoxygenation mechanism is initiated by the adsorption of the ketone group in an inclined configuration onto the active site of the catalyst surface, specifically, onto the Mo atom at the M-edge site. The dissociated hydrogen atoms onto the S-bridge and the Ni atom facilitate the hydrogenation of the ketone group, converting the hydroxyacetone to propanediol. Subsequently, the alcohol group formed from the ketone group undergoes further hydrogenation, resulting in the release of water and propanol as products. Further calculation is done to investigate the energy barriers required for the hydrodeoxygenation of hydroxyacetone. These research findings can be extended to study oligomers, offering a deeper understanding of how bio-oil interacts with catalysts to mitigate coke formation and innovate efficient HDO catalysts.

7.5 REFERENCES

- (1) Garcia-Perez, M.; Chaala, A.; Pakdel, H.; Kretschmer, D.; Roy, C. Characterization of Bio-Oils in Chemical Families. *Biomass and Bioenergy* **2007**, *31* (4), 222–242.
<https://doi.org/10.1016/j.biombioe.2006.02.006>.
- (2) Oasmaa, A.; Czernik, S. Fuel Oil Quality of Biomass Pyrolysis Oils - State of the Art for the End Users. *Energy and Fuels* **1999**, *13* (4), 914–921.
<https://doi.org/10.1021/ef980272b>.
- (3) Oasmaa, A.; Leppämäki, E.; Koponen, P.; Levander, J.; Tapola, E. Physical Characterisation of Biomass-Based Pyrolysis Liquids Application of Standard Fuel Oil Analyses. *VTT Publ.* **1997**, No. 306. [https://doi.org/10.1016/s0140-6701\(98\)97220-4](https://doi.org/10.1016/s0140-6701(98)97220-4).
- (4) Pinheiro Pires, A. P.; Arauzo, J.; Fonts, I.; Domine, M. E.; Fernández Arroyo, A.; Garcia-Perez, M. E.; Montoya, J.; Chejne, F.; Pfromm, P.; Garcia-Perez, M. Challenges and Opportunities for Bio-Oil Refining: A Review. *Energy and Fuels* **2019**, *33* (6), 4683–4720. <https://doi.org/10.1021/acs.energyfuels.9b00039>.
- (5) Terrell, E.; Garcia-Perez, M. Novel Strategy to Analyze Fourier Transform Ion Cyclotron Resonance Mass Spectrometry Data of Biomass Pyrolysis Oil for Oligomeric Structure Assignment. *Energy and Fuels* **2020**, *34* (7), 8466–8481.
<https://doi.org/10.1021/acs.energyfuels.0c01687>.
- (6) Furimsky, E.; Massoth, F. E. Deactivation of Hydroprocessing Catalysts. *Catal. Today* **1999**, *52* (4), 381–495. [https://doi.org/10.1016/S0920-5861\(99\)00096-6](https://doi.org/10.1016/S0920-5861(99)00096-6).
- (7) Wang, H.; Male, J.; Wang, Y. Recent Advances in Hydrotreating of Pyrolysis Bio-Oil and Its Oxygen-Containing Model Compounds. *ACS Catal.* **2013**, *3* (5), 1047–1070.
<https://doi.org/10.1021/cs400069z>.

- (8) Mortensen, P. M.; Grunwaldt, J. D.; Jensen, P. A.; Knudsen, K. G.; Jensen, A. D. A Review of Catalytic Upgrading of Bio-Oil to Engine Fuels. *Appl. Catal. A Gen.* **2011**, *407* (1–2), 1–19. <https://doi.org/10.1016/j.apcata.2011.08.046>.
- (9) Furimsky, E. Chemistry of Catalytic Hydrodeoxygenation. *Catal. Rev.* **1983**, *25* (3), 421–458. <https://doi.org/10.1080/01614948308078052>.
- (10) Pujro, R.; García, J. R.; Bertero, M.; Falco, M.; Sedran, U. Review on Reaction Pathways in the Catalytic Upgrading of Biomass Pyrolysis Liquids. *Energy and Fuels* **2021**, *35* (21), 16943–16964. <https://doi.org/10.1021/acs.energyfuels.1c01931>.
- (11) Ruddy, D. A.; Schaidle, J. A.; Ferrell, J. R.; Wang, J.; Moens, L.; Hensley, J. E. *Recent Advances in Heterogeneous Catalysts for Bio-Oil Upgrading via “Ex Situ Catalytic Fast Pyrolysis”*: Catalyst Development through the Study of Model Compounds; 2014; Vol. 16. <https://doi.org/10.1039/c3gc41354c>.
- (12) Lang, M.; Li, H. Heterogeneous Metal-Based Catalysts for Cyclohexane Synthesis from Hydrodeoxygenation of Lignin-Derived Phenolics. *Fuel* **2023**, *344* (March), 128084. <https://doi.org/10.1016/j.fuel.2023.128084>.
- (13) Kim, S.; Kwon, E. E.; Kim, Y. T.; Jung, S.; Kim, H. J.; Huber, G. W.; Lee, J. Recent Advances in Hydrodeoxygenation of Biomass-Derived Oxygenates over Heterogeneous Catalysts. *Green Chem.* **2019**, *21* (14), 3715–3743. <https://doi.org/10.1039/c9gc01210a>.
- (14) Elliott, D. C. Historical Developments in Hydroprocessing Bio-Oils. *Energy and Fuels* **2007**, *21* (3), 1792–1815. <https://doi.org/10.1021/ef070044u>.
- (15) Yin, W.; Venderbosch, R. H.; Alekseeva, M. V.; Figueirêdo, M. B.; Heeres, H.; Khromova, S. A.; Yakovlev, V. A.; Cannilla, C.; Bonura, G.; Frusteri, F.; Heeres, H. J. Hydrotreatment of the Carbohydrate-Rich Fraction of Pyrolysis Liquids Using Bimetallic

- Ni Based Catalyst: Catalyst Activity and Product Property Relations. *Fuel Process. Technol.* **2018**, *169* (October 2017), 258–268.
<https://doi.org/10.1016/j.fuproc.2017.10.006>.
- (16) Han, Y.; Pires, A. P. P.; Garcia-Perez, M. Co-Hydrotreatment of the Bio-Oil Lignin-Rich Fraction and Vegetable Oil. *Energy and Fuels* **2020**, *34* (1), 516–529.
<https://doi.org/10.1021/acs.energyfuels.9b03344>.
- (17) Paiva Pinheiro Pires, A.; Olarte, M.; Terrell, E.; Garcia-Perez, M.; Han, Y. Co-Hydrotreatment of Yellow Greases and the Water-Insoluble Fraction of Pyrolysis Oil. Part I: Experimental Design to Increase Kerosene Yield and Reduce Coke Formation. *Energy and Fuels* **2023**, *37* (3), 2100–2114. <https://doi.org/10.1021/acs.energyfuels.2c03250>.
- (18) Kloekhorst, A.; Wildschut, J.; Heeres, H. J. Catalytic Hydrotreatment of Pyrolytic Lignins to Give Alkylphenolics and Aromatics Using a Supported Ru Catalyst. *Catal. Sci. Technol.* **2014**, *4* (8), 2367–2377. <https://doi.org/10.1039/c4cy00242c>.
- (19) Sanna, A.; Vispute, T. P.; Huber, G. W. Hydrodeoxygenation of the Aqueous Fraction of Bio-Oil with Ru/C and Pt/C Catalysts. *Appl. Catal. B Environ.* **2015**, *165*, 446–456.
<https://doi.org/10.1016/j.apcatb.2014.10.013>.
- (20) Kadarwati, S.; Oudenhoven, S.; Schagen, M.; Hu, X.; Garcia-Perez, M.; Kersten, S.; Li, C. Z.; Westerhof, R. Polymerization and Cracking during the Hydrotreatment of Bio-Oil and Heavy Fractions Obtained by Fractional Condensation Using Ru/C and NiMo/Al₂O₃ Catalyst. *J. Anal. Appl. Pyrolysis* **2016**, *118*, 136–143.
<https://doi.org/10.1016/j.jaap.2016.01.011>.
- (21) Kadarwati, S.; Hu, X.; Gunawan, R.; Westerhof, R.; Gholizadeh, M.; Hasan, M. D. M.; Li, C. Coke Formation during the Hydrotreatment of Bio-Oil Using NiMo and CoMo

- Catalysts. *Fuel Process. Technol.* **2017**, *155*, 261–268.
<https://doi.org/10.1016/j.fuproc.2016.08.021>.
- (22) Yin, W.; Alekseeva, M. V.; Venderbosch, R. H.; Yakovlev, V. A.; Heeres, H. J. Catalytic Hydrotreatment of the Pyrolytic Sugar and Pyrolytic Lignin Fractions of Fast Pyrolysis Liquids Using Nickel Based Catalysts. *Energies* **2020**, *13* (1).
<https://doi.org/10.3390/en13010285>.
- (23) Elliott, D. C.; Hart, T. R. Catalytic Hydroprocessing of Chemical Models for Bio-Oil. *Energy and Fuels* **2009**, *23* (2), 631–637. <https://doi.org/10.1021/ef8007773>.
- (24) Hensley, A. J. R.; Wang, Y.; McEwen, J. S. Adsorption of Guaiacol on Fe (110) and Pd (111) from First Principles. *Surf. Sci.* **2016**, *648*, 227–235.
<https://doi.org/10.1016/j.susc.2015.10.030>.
- (25) Moon, J. S.; Kim, E. G.; Lee, Y. K. Active Sites of Ni₂P/SiO₂ Catalyst for Hydrodeoxygenation of Guaiacol: A Joint XAFS and DFT Study. *J. Catal.* **2014**, *311*, 144–152. <https://doi.org/10.1016/j.jcat.2013.11.023>.
- (26) Badawi, M.; Paul, J. F.; Cristol, S.; Payen, E. Guaiacol Derivatives and Inhibiting Species Adsorption over MoS₂ and CoMoS Catalysts under HDO Conditions: A DFT Study. *Catal. Commun.* **2011**, *12* (10), 901–905. <https://doi.org/10.1016/j.catcom.2011.02.010>.
- (27) Chiu, C. C.; Genest, A.; Borgna, A.; Rösch, N. Hydrodeoxygenation of Guaiacol over Ru(0001): A DFT Study. *ACS Catal.* **2014**, *4* (11), 4178–4188.
<https://doi.org/10.1021/cs500911j>.
- (28) Nania, C.; Bertini, M.; Gueci, L.; Ferrante, F.; Duca, D. DFT Insights into Competing Mechanisms of Guaiacol Hydrodeoxygenation on a Platinum Cluster. *Phys. Chem. Chem. Phys.* **2023**, *25* (15), 10460–10471. <https://doi.org/10.1039/d2cp06077a>.

- (29) Lee, K.; Gu, G. H.; Mullen, C. A.; Boateng, A. A.; Vlachos, D. G. Guaiacol Hydrodeoxygenation Mechanism on Pt(111): Insights from Density Functional Theory and Linear Free Energy Relations. *ChemSusChem* **2015**, *8* (2), 315–322.
<https://doi.org/10.1002/cssc.201402940>.
- (30) Tran, C. C.; Mohan, O.; Banerjee, A.; Mushrif, S. H.; Kaliaguine, S. A Combined Experimental and DFT Investigation of Selective Hydrodeoxygenation of Guaiacol over Bimetallic Carbides. *Energy and Fuels* **2020**, *34* (12), 16265–16273.
<https://doi.org/10.1021/acs.energyfuels.0c03102>.
- (31) Konadu, D.; Kwawu, C. R.; Tia, R.; Adei, E.; de Leeuw, N. H. Mechanism of Guaiacol Hydrodeoxygenation on Cu (111): Insights from Density Functional Theory Studies. *Catalysts* **2021**, *11* (4), 1–12. <https://doi.org/10.3390/catal11040523>.
- (32) Morteo-Flores, F.; Roldan, A. Mechanisms and Trends of Guaiacol Hydrodeoxygenation on Transition Metal Catalysts. *Front. Catal.* **2022**, *2* (May), 1–12.
<https://doi.org/10.3389/fctls.2022.861364>.
- (33) Zhang, H.; Yang, C.; Tao, Y.; Chen, M.; Xiao, R. Catalytic Cracking of Model Compounds of Bio-Oil: Characteristics and Mechanism Research on Guaiacol and Acetic Acid. *Fuel Process. Technol.* **2022**, *238* (September), 107512.
<https://doi.org/10.1016/j.fuproc.2022.107512>.
- (34) Gao, D.; Xiao, Y.; Varma, A. Guaiacol Hydrodeoxygenation over Platinum Catalyst: Reaction Pathways and Kinetics. *Ind. Eng. Chem. Res.* **2015**, *54* (43), 10638–10644.
<https://doi.org/10.1021/acs.iecr.5b02940>.
- (35) Liu, X.; An, W.; Wang, Y.; Turner, C. H.; Resasco, D. E. Hydrodeoxygenation of Guaiacol over Bimetallic Fe-Alloyed (Ni, Pt) Surfaces: Reaction Mechanism, Transition-

- State Scaling Relations and Descriptor for Predicting C-O Bond Scission Reactivity. *Catal. Sci. Technol.* **2018**, 8 (8), 2146–2158. <https://doi.org/10.1039/c8cy00282g>.
- (36) Lu, J.; Behtash, S.; Mamun, O.; Heyden, A. Theoretical Investigation of the Reaction Mechanism of the Guaiacol Hydrogenation over a Pt(111) Catalyst. *ACS Catal.* **2015**, 5 (4), 2423–2435. <https://doi.org/10.1021/cs5016244>.
- (37) Garcia-Pintos, D.; Voss, J.; Jensen, A. D.; Studt, F. Hydrodeoxygenation of Phenol to Benzene and Cyclohexane on Rh(111) and Rh(211) Surfaces: Insights from Density Functional Theory. *J. Phys. Chem. C* **2016**, 120 (33), 18529–18537. <https://doi.org/10.1021/acs.jpcc.6b02970>.
- (38) Zhang, J.; Fidalgo, B.; Shen, D.; Zhang, X.; Gu, S. Mechanism of Hydrodeoxygenation (HDO) in Anisole Decomposition over Metal Loaded Brønsted Acid Sites: Density Functional Theory (DFT) Study. *Mol. Catal.* **2018**, 454 (February), 30–37. <https://doi.org/10.1016/j.mcat.2018.05.015>.
- (39) Jain, V.; Bonita, Y.; Brown, A.; Taconi, A.; Hicks, J. C.; Rai, N. Mechanistic Insights into Hydrodeoxygenation of Phenol on Bimetallic Phosphide Catalysts. *Catal. Sci. Technol.* **2018**, 8 (16), 4083–4096. <https://doi.org/10.1039/c8cy00977e>.
- (40) Zhou, J.; An, W.; Wang, Z.; Jia, X. Hydrodeoxygenation of Phenol over Ni-Based Bimetallic Single-Atom Surface Alloys: Mechanism, Kinetics and Descriptor. *Catal. Sci. Technol.* **2019**, 9 (16), 4314–4326. <https://doi.org/10.1039/c9cy01082c>.
- (41) Nelson, R. C.; Baek, B.; Ruiz, P.; Goundie, B.; Brooks, A.; Wheeler, M. C.; Frederick, B. G.; Grabow, L. C.; Austin, R. N. Experimental and Theoretical Insights into the Hydrogen-Efficient Direct Hydrodeoxygenation Mechanism of Phenol over Ru/TiO₂. *ACS Catal.* **2015**, 5 (11), 6509–6523. <https://doi.org/10.1021/acscatal.5b01554>.

- (42) Jia, X.; An, W.; Wang, Z.; Zhou, J. Effect of Doped Metals on Hydrodeoxygenation of Phenol over Pt-Based Bimetallic Alloys: Caryl-OH Versus CaliphaticH-OH Bond Scission. *J. Phys. Chem. C* **2019**, *123* (27), 16873–16882.
<https://doi.org/10.1021/acs.jpcc.9b04457>.
- (43) Mäki-Arvela, P.; Murzin, D. Y. Hydrodeoxygenation of Lignin-Derived Phenols: From Fundamental Studies towards Industrial Applications. *Catalysts* **2017**, *7* (9).
<https://doi.org/10.3390/catal7090265>.
- (44) Gu, G. H.; Mullen, C. A.; Boateng, A. A.; Vlachos, D. G. Mechanism of Dehydration of Phenols on Noble Metals via First-Principles Microkinetic Modeling. *ACS Catal.* **2016**, *6* (5), 3047–3055. <https://doi.org/10.1021/acscatal.6b00776>.
- (45) Liu, D.; Li, G.; Yang, F.; Wang, H.; Han, J.; Zhu, X.; Ge, Q. Competition and Cooperation of Hydrogenation and Deoxygenation Reactions during Hydrodeoxygenation of Phenol on Pt(111). *J. Phys. Chem. C* **2017**, *121* (22), 12249–12260.
<https://doi.org/10.1021/acs.jpcc.7b03042>.
- (46) Nie, X.; Zhang, Z.; Wang, H.; Guo, X.; Song, C. Effect of Surface Structure and Pd Doping of Fe Catalysts on the Selective Hydrodeoxygenation of Phenol. *Catal. Today* **2021**, *371* (March 2020), 189–203. <https://doi.org/10.1016/j.cattod.2020.07.038>.
- (47) Wang, S.; Vorotnikov, V.; Vlachos, D. G. A DFT Study of Furan Hydrogenation and Ring Opening on Pd(111). *Green Chem.* **2014**, *16* (2), 736–747.
<https://doi.org/10.1039/c3gc41183d>.
- (48) Badawi, M.; Cristol, S.; Paul, J. F.; Payen, E. DFT Study of Furan Adsorption over Stable Molybdenum Sulfide Catalyst under HDO Conditions. *Comptes Rendus Chim.* **2009**, *12* (6–7), 754–761. <https://doi.org/10.1016/j.crci.2008.10.023>.

- (49) Banerjee, A.; Mushrif, S. H. Reaction Pathways for the Deoxygenation of Biomass-Pyrolysis-Derived Bio-Oil on Ru: A DFT Study Using Furfural as a Model Compound. *ChemCatChem* **2017**, *9* (14), 2828–2838. <https://doi.org/10.1002/cctc.201700036>.
- (50) Jiang, Z.; Wan, W.; Lin, Z.; Xie, J.; Chen, J. G. Understanding the Role of M/Pt(111) (M = Fe, Co, Ni, Cu) Bimetallic Surfaces for Selective Hydrodeoxygenation of Furfural. *ACS Catal.* **2017**, *7* (9), 5758–5765. <https://doi.org/10.1021/acscatal.7b01682>.
- (51) Banerjee, A.; Mushrif, S. H. Investigating Reaction Mechanisms for Furfural Hydrodeoxygenation on Ni and the Effect of Boron Doping on the Activity and Selectivity of the Catalyst. *J. Phys. Chem. C* **2018**, *122* (32), 18383–18394. <https://doi.org/10.1021/acs.jpcc.8b01301>.
- (52) Hsiao, Y. W.; Zong, X.; Zhou, J.; Zheng, W.; Vlachos, D. G. Selective Hydrodeoxygenation of 5-Hydroxymethylfurfural (HMF) to 2,5-Dimethylfuran (DMF) over Carbon Supported Copper Catalysts Using Isopropyl Alcohol as a Hydrogen Donor. *Appl. Catal. B Environ.* **2022**, *317* (July), 121790. <https://doi.org/10.1016/j.apcatb.2022.121790>.
- (53) Hočevar, B.; Grilc, M.; Huš, M.; Likozar, B. Mechanism, Ab Initio Calculations and Microkinetics of Hydrogenation, Hydrodeoxygenation, Double Bond Migration and Cis–Trans Isomerisation during Hydrotreatment of C6 Secondary Alcohol Species and Ketones. *Appl. Catal. B Environ.* **2017**, *218*, 147–162. <https://doi.org/10.1016/j.apcatb.2017.06.046>.
- (54) Hočevar, B.; Grilc, M.; Huš, M.; Likozar, B. Mechanism, Ab Initio Calculations and Microkinetics of Straight-Chain Alcohol, Ether, Ester, Aldehyde and Carboxylic Acid Hydrodeoxygenation over Ni-Mo Catalyst. *Chem. Eng. J.* **2019**, *359* (September 2018),

- 1339–1351. <https://doi.org/10.1016/j.cej.2018.11.045>.
- (55) Alcalá, R.; Greeley, J.; Mavrikakis, M.; Dumesic, J. A. Density-Functional Theory Studies of Acetone and Propanal Hydrogenation on Pt(111). *J. Chem. Phys.* **2002**, *116* (20), 8973–8980. <https://doi.org/10.1063/1.1471247>.
- (56) Jeffery, E. L.; Mann, R. K.; Hutchings, G. J.; Taylor, S. H.; Willock, D. J. A Density Functional Theory Study of the Adsorption of Acetone to the (1 1 1) Surface of Pt: Implications for Hydrogenation Catalysis. *Catal. Today* **2005**, *105* (1 SPEC. ISS.), 85–92. <https://doi.org/10.1016/j.cattod.2005.04.013>.
- (57) McManus, J. R.; Martono, E.; Vohs, J. M. Selective Deoxygenation of Aldehydes: The Reaction of Acetaldehyde and Glycolaldehyde on Zn/Pt(111) Bimetallic Surfaces. *ACS Catal.* **2013**, *3* (8), 1739–1750. <https://doi.org/10.1021/cs400355e>.
- (58) Furimsky, E. Catalytic Hydrodeoxygenation. *Appl. Catal. A Gen.* **2000**, *199* (2), 147–190. [https://doi.org/10.1016/S0926-860X\(99\)00555-4](https://doi.org/10.1016/S0926-860X(99)00555-4).
- (59) Stankovikj, F.; McDonald, A. G.; Helms, G. L.; Garcia-Perez, M. Quantification of Bio-Oil Functional Groups and Evidences of the Presence of Pyrolytic Humins. *Energy and Fuels* **2016**, *30* (8), 6505–6524. <https://doi.org/10.1021/acs.energyfuels.6b01242>.
- (60) Furimsky, E. Catalytic Hydrodeoxygenation. *Appl. Catal. A Gen.* **2000**, *199* (2), 147–190. [https://doi.org/10.1016/S0926-860X\(99\)00555-4](https://doi.org/10.1016/S0926-860X(99)00555-4).
- (61) He, Z.; Wang, X. Hydrodeoxygenation of Model Compounds and Catalytic Systems for Pyrolysis Bio-Oils Upgrading. *Catal. Sustain. Energy* **2013**, *1*, 28–52. <https://doi.org/10.2478/cse-2012-0004>.
- (62) Wang, Y.; Wu, J.; Wang, S. Hydrodeoxygenation of Bio-Oil over Pt-Based Supported Catalysts: Importance of Mesopores and Acidity of the Support to Compounds with

- Different Oxygen Contents. *RSC Adv.* **2013**, *3* (31), 12635–12640.
<https://doi.org/10.1039/c3ra41405a>.
- (63) Qu, L.; Jiang, X.; Zhang, Z.; Zhang, X. G.; Song, G. Y.; Wang, H. L.; Yuan, Y. P.; Chang, Y. L. A Review of Hydrodeoxygenation of Bio-Oil: Model Compounds, Catalysts, and Equipment. *Green Chem.* **2021**, *23* (23), 9348–9376. <https://doi.org/10.1039/d1gc03183j>.
- (64) Krebs, E.; Silvi, B.; Raybaud, P. Mixed Sites and Promoter Segregation: A DFT Study of the Manifestation of Le Chatelier's Principle for the Co(Ni)MoS Active Phase in Reaction Conditions. **2007**. <https://doi.org/10.1016/j.cattod.2007.06.081>.
- (65) Dupont, C.; Lemeur, R.; Daudin, A.; Raybaud, P. Hydrodeoxygenation Pathways Catalyzed by MoS₂ and NiMoS Active Phases: A DFT Study. *J. Catal.* **2011**, *279* (2), 276–286. <https://doi.org/10.1016/j.jcat.2011.01.025>.
- (66) Ruinat De Brimont, M.; Dupont, C.; Daudin, A.; Geantet, C.; Raybaud, P. Deoxygenation Mechanisms on Ni-Promoted MoS₂ Bulk Catalysts: A Combined Experimental and Theoretical Study. *J. Catal.* **2012**, *286*, 153–164.
<https://doi.org/10.1016/j.jcat.2011.10.022>.
- (67) Jiang, Y.; Wang, D.; Pan, Z.; Ma, H.; Li, M.; Li, J.; Zheng, A.; Lv, G.; Tian, Z. Microemulsion-Mediated Hydrothermal Synthesis of Flower-like MoS₂ Nanomaterials with Enhanced Catalytic Activities for Anthracene Hydrogenation. *Front. Chem. Sci. Eng.* **2018**, *12* (1), 32–42. <https://doi.org/10.1007/s11705-017-1677-4>.
- (68) Cheah, Y. W.; Salam, M. A.; Arora, P.; Öhrman, O.; Creaser, D.; Olsson, L. Role of Transition Metals on MoS₂-Based Supported Catalysts for Hydrodeoxygenation (HDO) of Propylguaiacol. *Sustain. Energy Fuels* **2021**, *5* (7), 2097–2113.
<https://doi.org/10.1039/d1se00184a>.

- (69) Lai, W.; Chen, Z.; Zhu, J.; Yang, L.; Zheng, J.; Yi, X.; Fang, W. A NiMoS Flower-like Structure with Self-Assembled Nanosheets as High-Performance Hydrodesulfurization Catalysts. *Nanoscale* **2016**, 8 (6), 3823–3833. <https://doi.org/10.1039/C5NR08841K>.
- (70) Cao, J.; Xia, J.; Zhang, Y.; Liu, X.; Bai, L.; Xu, J.; Yang, C.-A.; Zheng, S.; Yang, T.; Tang, K.; Zhang, C.; Zhou, C. Influence of the Alumina Crystal Phase on the Performance of CoMo/Al₂O₃ Catalysts for the Selective Hydrodesulfurization of Fluid Catalytic Cracking Naphtha. **2020**. <https://doi.org/10.1016/j.fuel.2020.119843>.
- (71) Sakashita, Y.; Yoneda, T. Orientation of MoS₂ Clusters Supported on Two Kinds of γ -Al₂O₃ Single Crystal Surfaces with Different Indices. *J. Catal.* **1999**, 185 (2), 487–495. <https://doi.org/10.1006/jcat.1999.2504>.
- (72) Lei, B.; Li, G. R.; Gao, X. P. Morphology Dependence of Molybdenum Disulfide Transparent Counter Electrode in Dye-Sensitized Solar Cells. *J. Mater. Chem. A* **2014**, 2 (11), 3919–3925. <https://doi.org/10.1039/c3ta14313a>.
- (73) Kresse, G.; Furthmüller, J. Efficient Iterative Schemes for Ab Initio Total-Energy Calculations Using a Plane-Wave Basis Set. *Phys. Rev. B. Condens. Matter* **1996**, 54 (16), 11169–11186. <https://doi.org/10.1103/PHYSREVB.54.11169>.
- (74) Kresse, G. Ab Initio Molecular Dynamics for Liquid Metals. *J. Non. Cryst. Solids* **1995**, 192–193, 222–229. [https://doi.org/10.1016/0022-3093\(95\)00355-X](https://doi.org/10.1016/0022-3093(95)00355-X).
- (75) Perdew, J. P.; Burke, K.; Ernzerhof, M. Generalized Gradient Approximation Made Simple. *Phys. Rev. Lett.* **1996**, 77 (18), 3865. <https://doi.org/10.1103/PhysRevLett.77.3865>.
- (76) Becke, A. D. Density Functional Calculations of Molecular Bond Energies. *J. Chem. Phys.* **1986**, 84 (8), 4524–4529. <https://doi.org/10.1063/1.450025>.

- (77) Lejaeghere, K.; Bihlmayer, G.; Björkman, T.; Blaha, P.; Blügel, S.; Blum, V.; Caliste, D.; Castelli, I. E.; Clark, S. J.; Dal Corso, A.; De Gironcoli, S.; Deutsch, T.; Dewhurst, J. K.; Di Marco, I.; Draxl, C.; Duřak, M.; Eriksson, O.; Flores-Livas, J. A.; Garrity, K. F.; Genovese, L.; Giannozzi, P.; Giantomassi, M.; Goedecker, S.; Gonze, X.; Grånäs, O.; Gross, E. K. U.; Gulans, A.; Gygi, F.; Hamann, D. R.; Hasnip, P. J.; Holzwarth, N. A. W.; Iuřan, D.; Jochym, D. B.; Jollet, F.; Jones, D.; Kresse, G.; Koepernik, K.; Küçükbenli, E.; Kvashnin, Y. O.; Locht, I. L. M.; Lubeck, S.; Marsman, M.; Marzari, N.; Nitzsche, U.; Nordström, L.; Ozaki, T.; Paulatto, L.; Pickard, C. J.; Poelmans, W.; Probert, M. I. J.; Refson, K.; Richter, M.; Rignanese, G. M.; Saha, S.; Scheffler, M.; Schlipf, M.; Schwarz, K.; Sharma, S.; Tavazza, F.; Thunström, P.; Tkatchenko, A.; Torrent, M.; Vanderbilt, D.; Van Setten, M. J.; Van Speybroeck, V.; Wills, J. M.; Yates, J. R.; Zhang, G. X.; Cottenier, S. Reproducibility in Density Functional Theory Calculations of Solids. *Science* (80-.). **2016**, *351* (6280). https://doi.org/10.1126/SCIENCE.AAD3000/SUPPL_FILE/AAD3000-LEJAEGERE-SM.PDF.
- (78) A. Jain*, S.P. Ong*, G. Hautier, W. Chen, W.D. Richards, S. Dacek, S. Cholia, D. Gunter, D. Skinner, G. Ceder, K.A. Persson (*=equal contributions) The Materials Project: A materials genome approach to accelerating materials innovation *APL Materials*, 2013, 1(1), 011002. doi:10.1063/1.4812323.

CHAPTER EIGHT: CONCLUSION AND RECOMMENDATION

8.1 Conclusions

The effectiveness of bio-oil processing and upgrading technologies is hinged on the fundamental understanding of bio-oil properties. This work aimed to elucidate the structure and properties of the unknown sugar oligomers derived from fast pyrolysis. In addition, the study investigated the behavior of pyrolytic sugars during bio-oil upgrading, integrating both experimental and computational modeling.

Based on the findings of this study, the following conclusions are drawn:

1. The study put forth several potential structures of the unidentified sugar oligomers. The study revealed that sequential dehydration predominantly removes water molecules from the non-reducing end of the sugar oligomers based on their thermodynamic stabilities. Additionally, the fragmentation reactions demonstrated that hydroxyacetone and hydroxyacetaldehyde can be directly generated from the sugar oligomers. These light-oxygenated fragments are most readily produced from the non-reducing end of sugar oligomers, per their thermodynamic stabilities.
2. The theoretical FTIR and NMR peaks of the proposed structures of sugar oligomers exhibited a strong qualitative agreement with the experimental results of the whole sugar.
3. The physical and thermochemical properties of the proposed sugar oligomers were estimated through the group contribution method. These properties are crucial for designing efficient upgrading reactors, fine-tuning process conditions, and improving product selectivity.
4. The isolation and characterization of the sugar oligomers confirms the high complexity of bio-oil composition. Despite employing several chromatographic techniques, the

chromatogram obtained from the preparative-HPLC shows clusters of peaks, underscoring the presence of myriad compounds in the sugar sub-fractions. The (\pm)H-ESI-FT Orbitrap MS analysis of the sugars showed that dimer units of sugars and anhydrosugars are predominantly found in the sugar sub-fractions. High molecular weight compounds up to 700 Da were also detected but at lower intensities. Interestingly, the proposed molecular structures/formulas from the modeling works in Chapters 3 and 4 were detected experimentally.

5. The co-hydrotreatment of the heavy bio-oil fraction (after removing only the light oxygenates) with waste cooking oil over NiMo/ γ -Al₂O₃ catalyst did not result in increased coke formation. The formed coke, ranging from 0.7 to 2.4 wt. %, is comparable to the coke yield achieved when using only the lignin fraction. This indicates that sugars are not the sole contributors to coke formation; instead, both pyrolytic sugars and lignin contribute to coke formation. Additionally, the utilization of the heavy bio-oil fraction suggests that pre-fractionation to remove the sugar-rich fraction before HDO is unnecessary, maximizing the utilization of bio-oil and conserving resources. The main carbon species identified in the biofuel include n-paraffins, iso-paraffins, cyclo-paraffins, and aromatics. The properties of the kerosene cut, such as density, viscosity, heating value, and surface tension, conform to the ASTM standards established for jet fuels. Moreover, the use of 1-butanol mitigated coke formation.
6. The density functional theory has provided insights into the reaction mechanism of hydrodeoxygenating hydroxyacetone, providing a foundational understanding of the chemistry underlying bio-oil upgrading. These findings have broader applications: (a) extending the examination of other bio-oil components, such as the heavy sugar and

lignin oligomers, known for their contribution to coke formation, (b) enabling the design of high-performance catalysts, (c) optimizing process parameters to maximize bio-fuel yield while simultaneously addressing cost and environmental concerns.

7. The application of cooperative research through integrating experimental and computational modeling is critical for a deeper understanding of the underlying mechanisms and product formation during the thermochemical conversion of biomass to hydrocarbons. DFT is a powerful tool to unravel the very complex reaction pathways, mechanisms and product structures of biomass pyrolysis and bio-oil upgrading. DFT can also provide thermodynamic data and estimate reaction rates and kinetics, among others. The accuracy of DFT entails a tradeoff between employing high-level functionals for better results and considering the computational cost.
8. In a broader context, the elucidation of the structure of sugar oligomers is a step forward toward bio-oil characterization. This contributes to efficient design of upstream and downstream processes. The conversion of biomass to biofuel offers a sustainable path to reduce fossil fuel dependence and address environmental issues.

8.2 Recommendations

Considering the study's findings, the following recommendations are proposed:





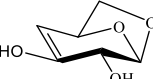

1. The prep-HPLC chromatogram, obtained during the isolation of sugar oligomers, showed bumps of peaks, vividly illustrating the complex nature of bio-oil. It is recommended to explore the selectivity of solvents in the silica column chromatography and consider using a new design of the HPLC column to enhance the separation process and obtain purer compounds.

2. The operating parameters for the co-hydrotreatment of the heavy bio-oil fraction with waste cooking oil could be optimized to improve the yield of kerosene cut (jet fuel cut) while minimizing coke yield and production cost.
3. The computational modeling of hydroxyacetone HDO could be extended to study sugar compounds (could be levoglucosan) to better understand the behavior of pyrolytic sugars during bio-oil upgrading.

APPENDICES

APPENDIX A: SUPPLEMENTAL INFORMATION FOR CHAPTER THREE

Table S1. Product structure and relative energetics of the singly dehydrated levoglucosan

Reaction label	Product structure	ΔG_{rxn} kJ/mol	ΔH_{rxn} kJ/mol	ΔS_{rxn} J/mol.K
LG21		78.27	208.14	168
LG23		-88.63	38.43	164
LG32		-84.20	48.45	172
LG34		-82.46	46.85	167
LG43		-86.38	42.62	167
LG45		55.95	185.49	168

*Water is also a product but is not shown here.

Table S2. Product structure and relative energetics of the doubly dehydrated levoglucosan








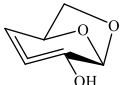
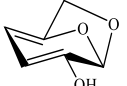
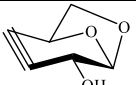
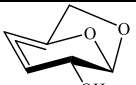
Reaction label	Product structure	ΔG_{rxn} kJ/mol	ΔH_{rxn} kJ/mol	ΔS_{rxn} J/mol.K
LG21-32		130.80	389.61	335
LG21-34		45.05	302.29	333
LG21-43		37.23	292.00	330
LG21-45		160.08	423.42	341
LG23-32		99.79	354.20	329
LG23-34		44.61	296.16	325
LG23-45		21.34	277.57	331
LG32-43		66.68	320.53	328
LG32-45		18.12	272.67	329
LG34-43		88.60	343.89	330
LG34-45		123.37	385.82	339

Table S3. Product structure and relative energetics of the singly dehydrated cellobiosan

Reaction label	Product structure	ΔG_{rxn} kJ/mol	ΔH_{rxn} kJ/mol	ΔS_{rxn} J/mol.K
CBN21A		81.80	202.93	157
CBN23A		-60.68	67.99	166
CBN32A		-65.04	56.09	157
CBN34A		-76.85	59.27	175
CBN21B		-63.96	74.55	179
CBN23B		-60.68	67.99	166
CBN32B		-59.15	73.08	171
CBN34B		-65.98	67.44	173
CBN43B		-69.38	58.29	165
CBN45B		-66.26	62.83	167
CBN65B		-74.53	60.91	175

Table S4. Product structure and relative energetics of the doubly dehydrated cellobiosan

Reaction label (48 reactions)	Product structure	ΔG_{rxn} kJ/mol	ΔH_{rxn} kJ/mol	ΔS_{rxn} J/mol.K
CBN21A-21B		24.19	275.19	325
CBN21A-23B		15.29	267.25	326
CBN21A-32B		19.15	272.24	327
CBN21A-34B		17.23	267.42	324
CBN21A-43B		9.65	259.55	323
CBN21A-45B		10.80	261.60	324
CBN21A-65B		4.49	261.57	333
CBN23A-21B		-126.46	115.54	313
CBN23A-23B		-121.13	118.43	310
CBN23A-32B		-116.46	123.40	310
CBN23A-34B		-128.99	111.24	311
CBN23A-43B		-134.39	103.79	308

CBN23A-45B		-129.36	110.96	311
CBN23A-65B		-148.84	101.77	324
CBN32A-21B		-127.26	121.80	322
CBN32A-23B		-128.14	128.39	332
CBN32A-32B		-126.04	133.48	336
CBN32A-34B		-139.50	120.51	336
CBN32A-43B		-143.76	112.73	332
CBN32A-45B		-132.79	121.12	328
CBN32A-65B		-143.54	105.11	322
CBN34A-21B		-128.27	115.66	315
CBN34A-23B		-152.36	124.57	358
CBN34A-32B		-129.55	135.48	343
CBN34A-34B		-149.97	109.33	335

CBN34A-43B		-157.08	102.13	335
CBN34A-45B		-141.95	124.10	344
CBN34A-65B		-150.70	105.31	331
CBN21A-32A		143.52	415.03	351
CBN21A-34A		49.13	305.03	331
CBN23A-32A		111.13	373.99	340
CBN23A-34A		48.91	307.71	335
CBN21B-32B		143.52	415.03	350
CBN21B-34B		-139.36	118.67	334
CBN21B-43B		-143.14	113.05	331
CBN21B-45B		-137.26	126.51	341
CBN21B-65B		-124.09	137.40	338
CBN23B-32B		118.24	380.94	340

CBN23B-34B		44.39	306.17	339
CBN23B-45B		-147.98	107.99	331
CBN23B-65B		-137.30	128.55	344
CBN32B-43B		65.84	326.39	337
CBN32B-45B		-146.13	104.41	324
CBN32B-65B		-128.91	137.33	344
CBN34B-43B		114.85	376.70	339
CBN34B-45B		61.97	323.73	339
CBN34B-65B		-159.50	107.27	345
CBN43B-65B		-171.67	88.63	337

Table S5. Product structure and relative energetics of the triply dehydrated cellobiosan

Reaction label (48 reactions)	Product structure	ΔG_{rxn} kJ/mol	ΔH_{rxn} kJ/mol	ΔS_{rxn} J/mol.K
CBN21A-21B-43B		-67.87	312.98	490
CBN21A-23B-45B		-70.19	306.78	490
CBN21A-34B-65B		-19.33	364.21	500

CBN21A-43B-65B		-93.33	288.98	490
CBN23A-21B-34B		-223.41	157.73	490
CBN23A-21B-43B		-232.53	151.08	502
CBN23A-21B-45B		-217.37	171.54	500
CBN23A-21B-65B		-213.83	171.43	500
CBN23A-23B-45B		-229.60	158.86	500
CBN23A-23B-65B		-214.14	167.86	490
CBN23A-32B-45B		-232.07	154.47	500
CBN23A-32B-65B		-208.40	175.35	500
CBN23A-34B-45B		-20.31	363.10	500
CBN23A-34B-65B		-234.08	144.318	500
CBN23A-43B-65B		-251.73	125.03	490
CBN32A-21B-34B		-219.01	174.24	510
CBN32A-21B-43B		-228.74	164.64	510
CBN32A-21B-45B		-218.72	185.28	520
CBN32A-21B-65B		-212.83	177.91	510

CBN32A-23B-34B		-28.39	364.78	510
CBN32A-23B-45B		-224.44	174.31	520
CBN32A-23B-65B		-206.01	182.43	500
CBN32A-43B-65B		-243.31	139.34	490
CBN32A-32B-45B		-223.26	169.37	510
CBN32A-32B-65B		-201.66	188.58	500
CBN32A-34B-45B		-14.03	384.11	510
CBN32A-34B-65B		-228.96	158.60	500
CBN34A-21B-34B		-211.21	172.72	500
CBN34A-21B-43B		-213.51	152.50	470
CBN34A-21B-45B		-210.80	181.39	510
CBN34A-21B-65B		-214.52	175.17	500
CBN34A-23B-45B		-240.20	150.91	510
CBN34A-23B-65B		-216.14	170.81	500
CBN34A-32B-45B		-226.59	160.33	500
CBN34A-32B-65B		-206.17	182.88	500

CBN34A-34B-45B		-22.01	377.72	520
CBN34A-34B-65B		-235.38	149.38	500
CBN34A-43B-65B		-249.99	132.24	490
CBN21B-34B-65B		-77.58	308.11	500
CBN21B-43B-65B		-257.53	137.70	510
CBN21A-34A-34B		-14.20	380.44	510
CBN21A-34A-43B		-24.57	359.50	500
CBN21A-34A-45B		-19.86	375.77	510
CBN21A-34A-65B		-19.33	364.21	500

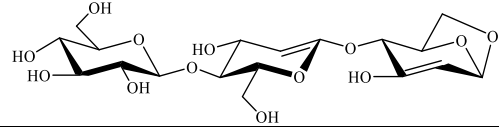
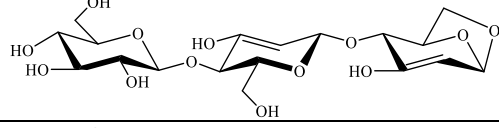
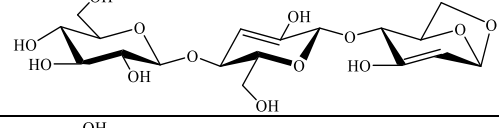
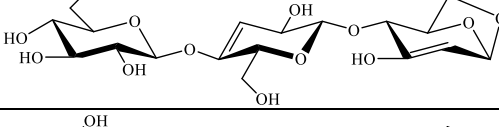
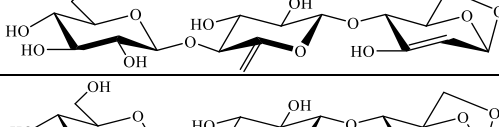
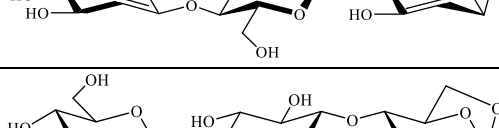
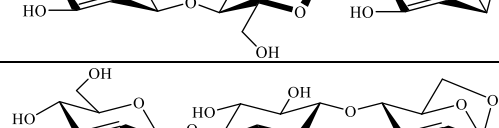
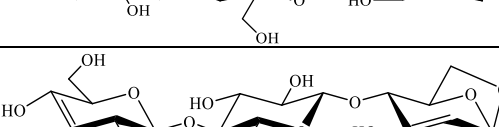
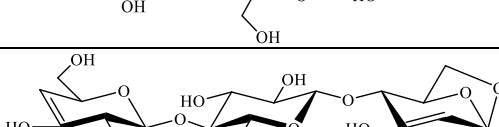
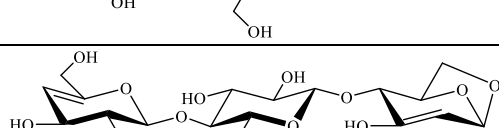
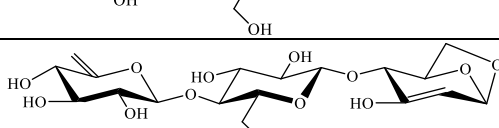
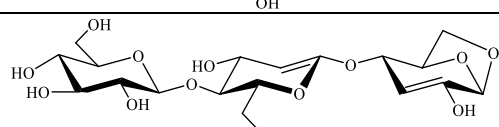
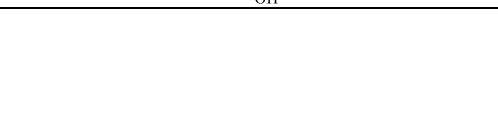
Table S6. Product structure and relative energetics of the singly dehydrated cellotriosan

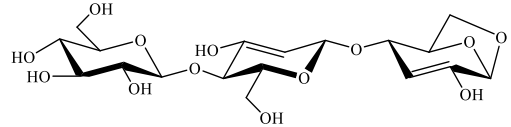
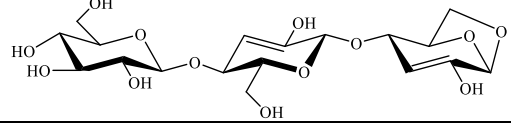
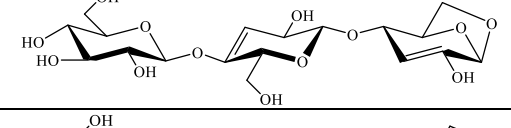
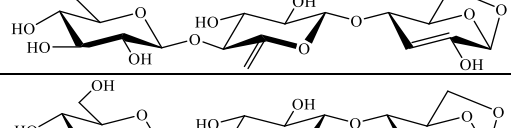
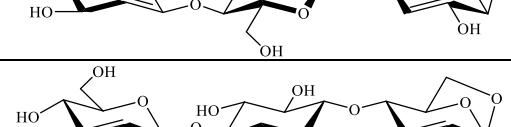
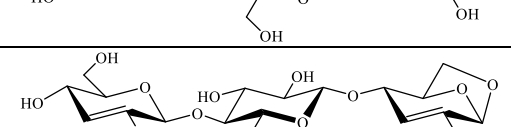
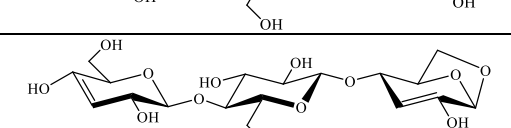
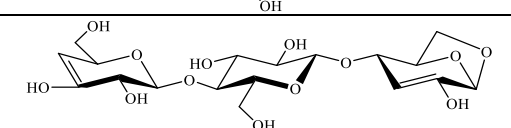
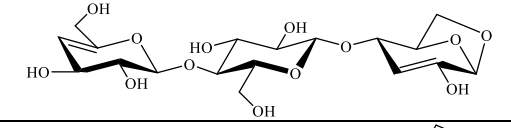
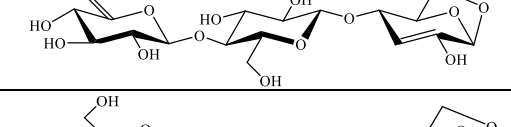
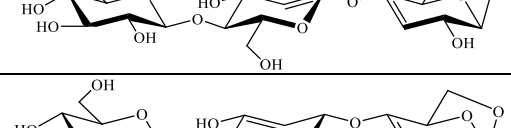
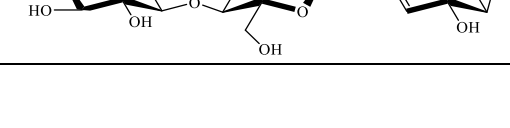

Reaction label	Product structure	ΔG_{rxn} kJ/mol	ΔH_{rxn} kJ/mol	ΔS_{rxn} J/mol.K
CTN21A		78.74	198.44	155
CTN23A		-79.23	47.99	165
CTN32A		-59.27	55.31	148
CTN34A		-2.95	53.25	180

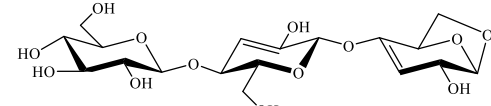
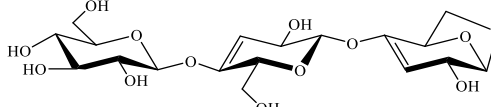
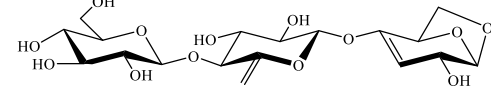
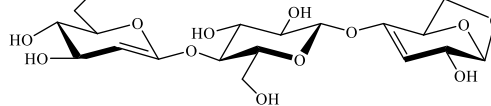
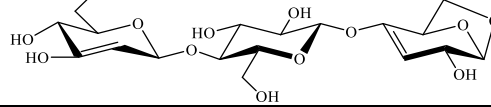
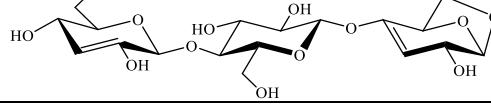
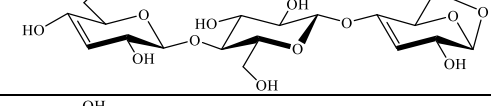
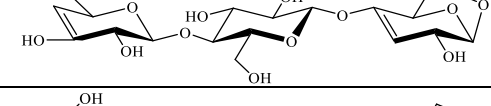
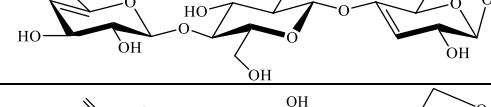
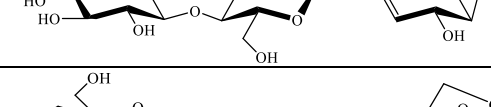
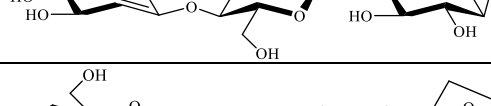
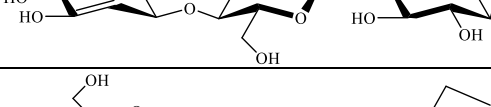
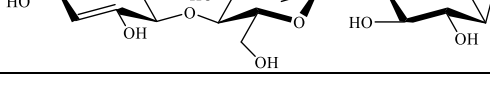
CTN21B		-64.89	62.82	165
CTN23B		-74.01	62.15	176
CTN32B		-54.79	86.01	182
CTN34B		-68.42	40.96	178
CTN65B		-67.81	59.79	165
CTN21C		-72.80	58.24	169
CTN23C		-75.11	52.03	164
CTN32C		-63.74	66.82	169
CTN34C		-82.33	53.25	184
CTN43C		-80.42	51.85	171
CTN45C		-72.70	54.76	165
CTN65C		-71.79	56.36	166

Table S7. Product structure and relative energetics of the doubly dehydrated cellotriosan

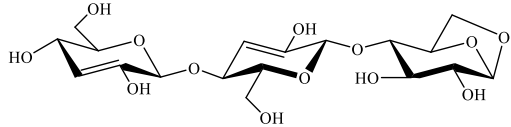
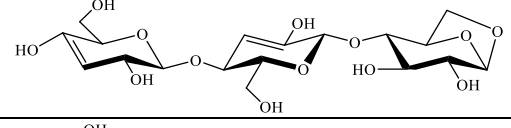
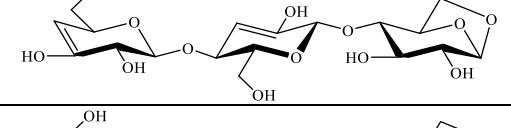
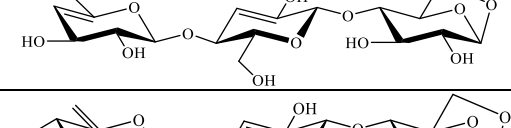
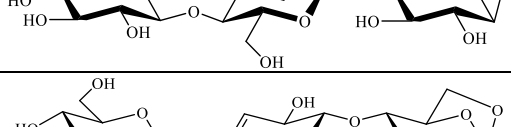
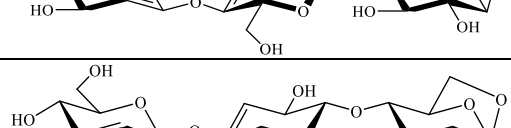
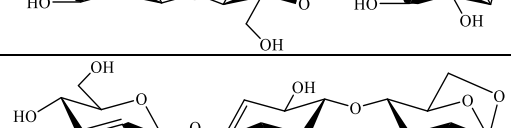
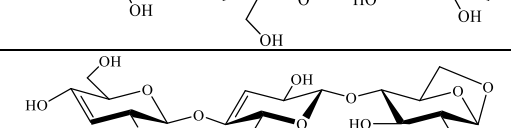
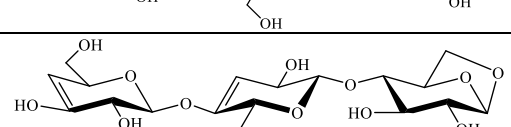
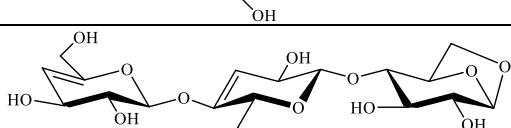
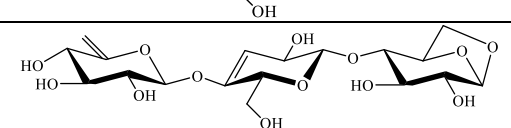
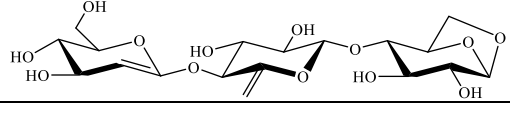

Reaction label	Product structure	ΔG_{rxn} kJ/mol	ΔH_{rxn} kJ/mol	ΔS_{rxn} J/mol.K
CTN21A-21B		12.69	261.66	322
CTN21A-23B		3.49	261.96	334
CTN21A-32B		19.81	285.27	343
CTN21A-34B		35.68	284.09	321
CTN21A-65B		9.36	260.51	325
CTN21A-21C		0.20	254.67	329
CTN21A-23C		2.94	250.45	320
CTN21A-32C		15.09	265.35	324
CTN21A-34C		1.18	251.86	324
CTN21A-43C		-1.17	250.21	325
CTN21A-45C		2.66	250.76	321
CTN21A-65C		7.13	254.41	320

CTN23A-21B		-146.17	103.63	323
CTN23A-23B		-156.85	109.34	344
CTN23A-32B		-138.40	130.23	347
CTN23A-34B		-145.79	111.10	332
CTN23A-65B		-148.23	102.17	324
CTN23A-21C		-155.21	104.75	336
CTN23A-23C		-152.55	99.63	326
CTN23A-32C		-145.92	114.57	337
CTN23A-34C		-154.74	101.14	331
CTN23A-43C		-157.58	99.90	333
CTN23A-45C		-152.70	102.94	331
CTN23A-65C		-153.49	104.39	334
CTN32A-21B		-130.04	108.83	309

CTN32A-23B		-142.24	121.89	342
CTN32A-32B		-125.52	147.46	353
CTN32A-34B		-140.34	130.87	351
CTN32A-65B		-158.80	85.87	316
CTN32A-21C		-143.14	125.39	347
CTN32A-23C		-137.66	121.58	335
CTN32A-32C		-125.74	146.66	352
CTN32A-34C		-139.25	105.68	317
CTN32A-43C		-141.14	107.17	321
CTN32A-45C		-134.91	110.30	317
CTN32A-65C		-135.79	111.27	320
CTN34A-21B		-136.86	101.23	308
CTN34A-23B		-163.61	101.44	343

CTN34A-32B		-108.91	130.89	310
CTN34A-34B		-113.88	111.44	339
CTN34A-65B		-157.85	98.09	331
CTN34A-21C		-161.64	109.50	351
CTN34A-23C		-163.83	104.95	348
CTN34A-32C		-152.49	107.15	336
CTN34A-34C		-165.75	92.00	333
CTN34A-43C		-164.81	93.00	333
CTN34A-45C		-160.12	96.11	331
CTN34A-65C		-154.40	110.05	342
CTN21B-21C		-137.94	117.90	331
CTN21B-23C		-139.35	115.38	329
CTN21B-32C		-127.17	130.32	333

CTN21B-34C		-141.66	124.55	344
CTN21B-43C		-139.95	114.13	329
CTN21B-45C		-142.59	117.40	336
CTN21B-65C		-137.90	120.00	334
CTN23B-21C		-148.63	112.67	338
CTN23B-23C		-150.87	113.05	341
CTN23B-32C		-140.42	116.46	350
CTN23B-34C		-152.10	129.58	337
CTN23B-43C		-146.82	131.95	336
CTN23B-45C		-149.44	128.80	339
CTN23B-65C		-140.98	112.03	327
CTN32B-21C		-142.43	130.59	353
CTN32B-23C		-134.28	137.85	352

CTN32B-32C		-126.83	154.08	363
CTN32B-34C		-135.35	133.84	348
CTN32B-43C		-129.25	135.64	343
CTN32B-45C		-135.96	140.42	357
CTN32B-65C		-44.62	132.42	229
CTN34B-21C		-133.72	127.22	338
CTN34B-23C		-129.64	139.17	348
CTN34B-32C		-119.30	155.88	356
CTN34B-34C		-122.74	136.11	335
CTN34B-43C		-140.72	128.29	348
CTN34B-45C		-142.53	122.87	343
CTN34B-65C		-133.97	128.86	340
CTN65B-21C		-146.38	113.16	336


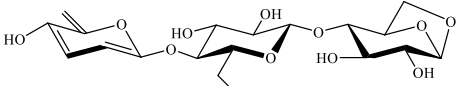
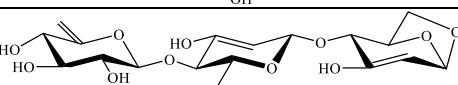
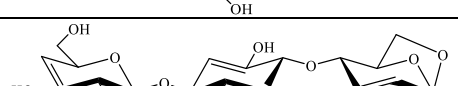
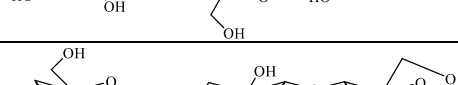
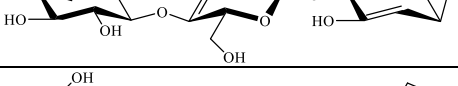
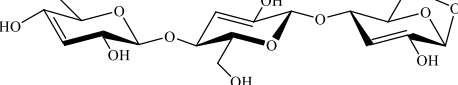
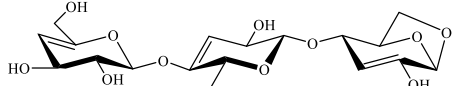
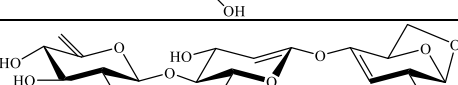
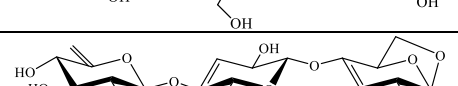
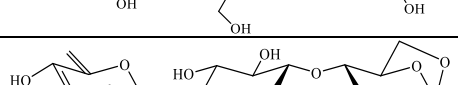
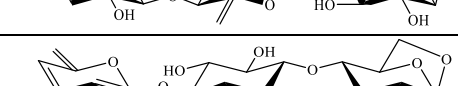
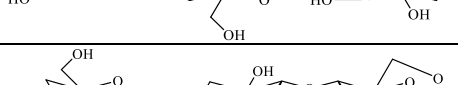
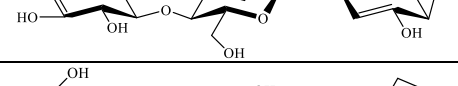
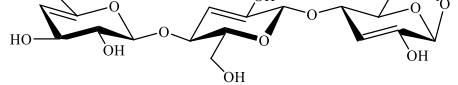
CTN65B-23C		-147.92	107.77	331
CTN65B-32C		-136.46	125.58	339
CTN65B-34C		-148.02	107.80	331
CTN65B-43C		-154.49	108.75	340
CTN65B-45C		-143.08	114.95	334
CTN65B-65C		-150.45	113.40	341
CTN21A-32A		141.44	407.27	344
CTN21A-34A		44.86	298.21	328
CTN23A-32A		113.45	369.89	332
CTN23A-34A		50.28	301.97	326
CTN21B-32B		24.72	294.39	349
CTN21B-34B		-144.48	128.13	353
CTN21B-65B		-137.73	123.80	338

CTN23B-32B		110.19	376.32	344
CTN23B-34B		41.29	313.98	353
CTN23B-65B		-151.26	118.64	349
CTN32B-65B		-132.43	146.49	361
CTN34B-65B		-134.61	124.92	336
CTN21C-32C		44.97	294.89	323
CTN21C-34C		-150.91	104.60	330
CTN21C-43C		-157.02	102.73	336
CTN21C-45C		-156.70	103.57	337
CTN21C-65C		-148.09	112.46	337
CTN23C-32C		104.17	364.51	337
CTN23C-34C		22.74	290.64	346
CTN23C-45C		-153.65	99.74	328

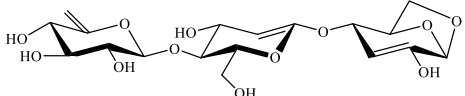

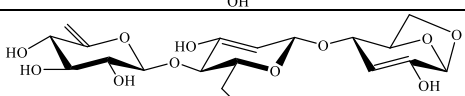
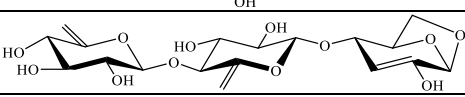
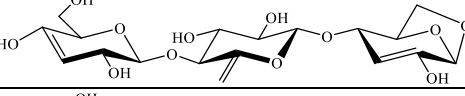
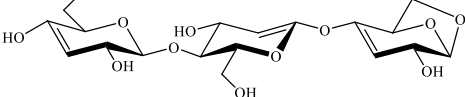
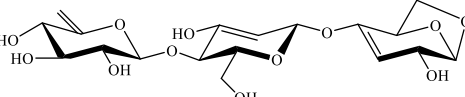

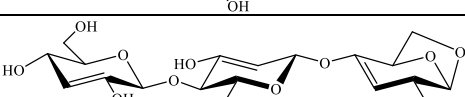
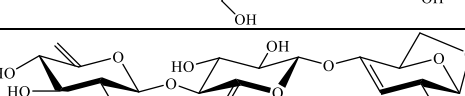
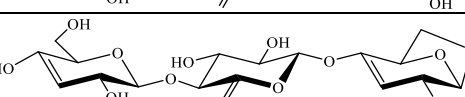
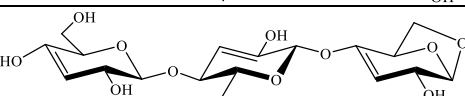
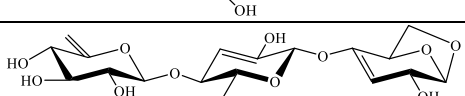
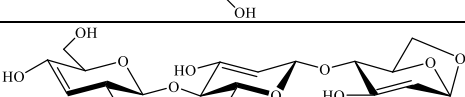
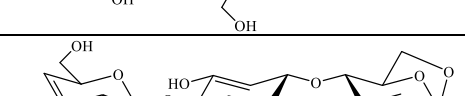
CTN23C-65C		-148.77	112.27	338
CTN32C-43C		38.49	300.53	339
CTN32C-45C		-167.16	96.938	342
CTN32C-65C		-138.34	125.53	341
CTN34C-43C		101.64	364.38	340
CTN34C-45C		47.89	315.37	346
CTN34C-65C		-168.23	88.60	332
CTN43C-65C		-177.84	79.97	333

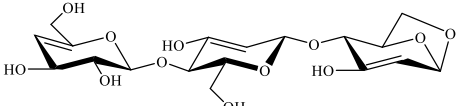
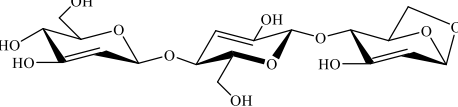
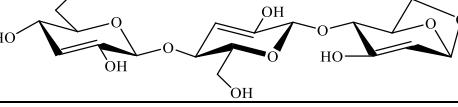
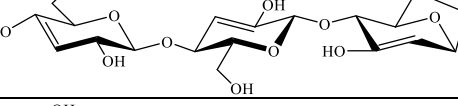
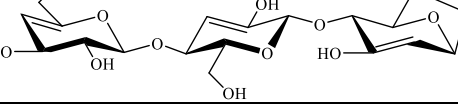
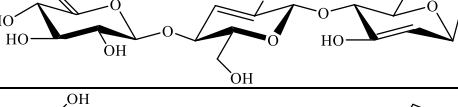
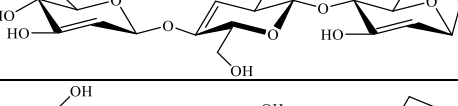
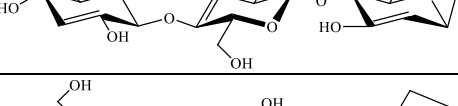
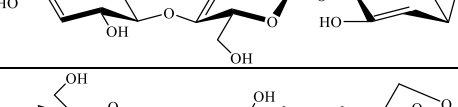
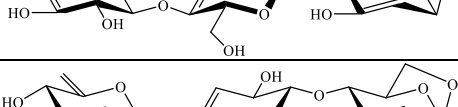
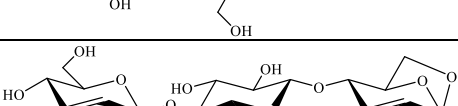
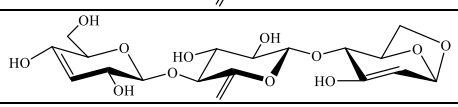
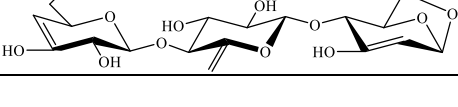

Table S8. Product structure and relative energetics of the triply dehydrated cellotriosan

Reaction label	Product structure	ΔG_{rxn} kJ/mol	ΔH_{rxn} kJ/mol	ΔS_{rxn} J/mol.K
CTN21A-21B-21C		-60.58	316.13	487
CTN23A-23B-23C		-239.04	159.33	515
CTN32A-32B-32C		-214.70	172.10	500
CTN34A-34B-34C		-190.73	223.63	536

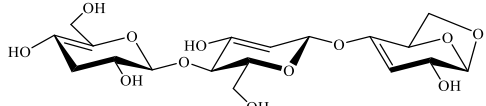
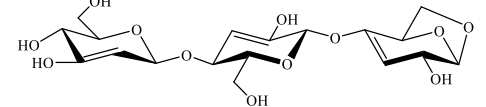
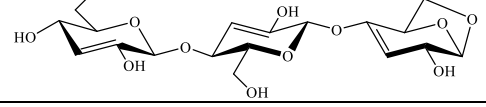
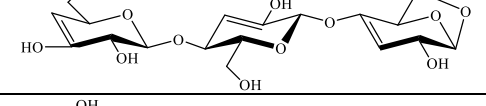
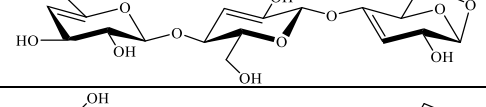
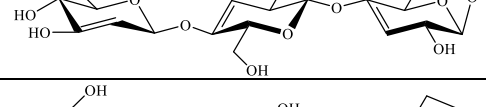
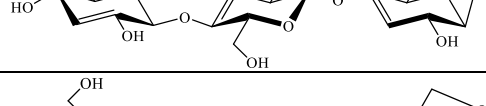
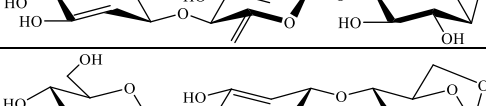
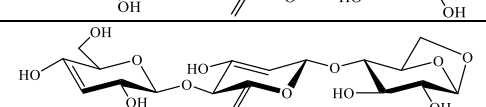
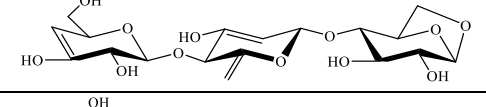
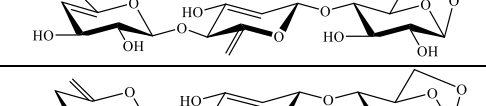
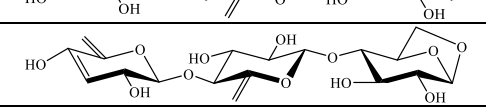
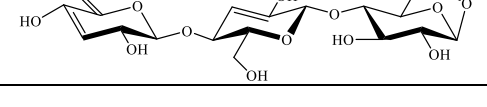

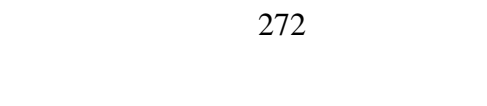
CTN21B-34B-65B		-240.02	161.70	520
CTN21C-34C-65C		27.50	413.13	499
CTN23A-23B-65C		-229.40	159.34	503
CTN23A-32B-43C		-219.33	185.17	523
CTN23A-34B-45C		-222.66	164.60	501
CTN32A-32B-34C		-190.73	223.63	536
CTN32A-34B-45C		-211.74	185.59	514
CTN34A-21B-65C		-212.91	174.70	501
CTN34A-34B-65C		-212.78	184.63	514
CTN65B-34C-65C		-244.35	146.20	505
CTN21C-43C-65C		-269.79	129.25	516
CTN32A-32B-43C		-202.26	204.61	526
CTN32A-32B-45C		-204.33	209.41	535
CTN32A-32B-65C		-200.06	200.86	519
CTN32A-34B-34C		-189.28	210.30	517

CTN32A-34B-43C		-212.24	181.46	509
CTN32A-34B-65C		-198.33	192.30	505
CTN34A-34B-43C		-224.32	174.65	516
CTN34A-34B-45C		-229.72	165.43	511
CTN21B-32B-45C		-29.66	364.67	510
CTN21B-32B-65C		-21.45	369.04	505
CTN21B-34B-34C		-218.60	188.36	526
CTN21B-34B-45C		-219.39	180.33	517
CTN21B-34B-65C		-229.13	177.02	525
CTN21B-65B-32C		-205.84	190.39	512
CTN21B-65B-45C		-212.91	178.87	507
CTN21B-65B-65C		-220.21	177.94	515
CTN23A-65B-65C		-227.84	155.89	496
CTN23A-65B-32C		-219.94	167.88	502
CTN32A-23B-23C		-219.50	180.83	518

CTN32A-21B-65C		-218.28	177.44	512
CTN32A-23B-45C		-220.04	179.44	517
CTN32A-23B-65C		-212.35	179.66	507
CTN32A-65B-65C		-217.24	171.17	502
CTN32A-65B-34C		-222.48	165.78	502
CTN34A-21B-34C		-218.37	170.33	503
CTN34A-23B-65C		-228.69	162.46	506
CTN34A-23B-43C		-237.62	149.64	501
CTN34A-23B-32C		-223.71	180.23	522
CTN34A-65B-65C		-229.53	155.49	498
CTN34A-65B-34C		-233.23	149.72	495
CTN34A-32B-34C		-218.68	184.63	522
CTN34A-32B-65C		-210.97	184.90	512
CTN23A-23B-34C		-236.04	154.82	506
CTN23A-23B-43C		-234.37	159.39	509

CTN23A-23B-45C		-236.16	160.12	513
CTN23A-32B-23C		-218.33	186.95	524
CTN23A-32B-32C		-208.07	203.85	533
CTN23A-32B-34C		-216.84	183.13	517
CTN23A-32B-45C		-218.88	190.42	529
CTN23A-32B-65C		-216.32	182.27	516
CTN23A-34B-23C		-210.91	182.51	509
CTN23A-34B-32C		-199.85	199.25	516
CTN23A-34B-34C		-213.22	185.76	516
CTN23A-34B-43C		-224.29	160.63	498
CTN23A-34B-65C		-217.29	169.93	501
CTN23A-65B-23C		-228.75	150.45	490
CTN23A-65B-34C		-228.75	150.69	491
CTN23A-65B-43C		-229.28	151.28	492

CTN23A-65B-45C		-227.84	155.89	496
CTN32A-23B-32C		-219.50	180.83	518
CTN32A-23B-34C		-222.36	175.66	515
CTN32A-23B-43C		-222.94	180.56	522
CTN32A-32B-23C		-200.20	206.92	527
CTN32A-34B-23C		-199.60	205.71	524
CTN32A-34B-32C		-189.43	222.31	533
CTN32A-65B-21C		-217.05	170.91	502
CTN32A-65B-23C		-219.81	166.45	500
CTN32A-65B-32C		-205.98	184.14	505
CTN32A-65B-43C		-222.40	167.06	504
CTN32A-65B-45C		-213.93	173.08	501
CTN34A-23B-23C		-242.80	150.19	508
CTN34A-23B-34C		-238.65	157.28	512

CTN34A-23B-45C		-238.70	152.81	506
CTN34A-32B-23C		-217.91	189.02	526
CTN34A-32B-32C		-205.29	206.46	533
CTN34A-32B-43C		-213.29	187.67	519
CTN34A-32B-45C		-215.47	193.10	528
CTN34A-34B-23C		-224.93	172.01	513
CTN34A-34B-32C		-203.55	209.14	534
CTN23B-65B-23C		-227.46	168.87	513
CTN23B-65B-32C		-216.95	185.11	520
CTN23B-65B-34C		-229.83	166.54	513
CTN23B-65B-43C		-222.41	166.33	503
CTN23B-65B-45C		-224.97	169.11	510
CTN23B-65B-65C		-219.48	168.26	501
CTN65B-34C-65C		-244.38	145.93	505
CTN32B-34C-65C		-227.86	161.86	504

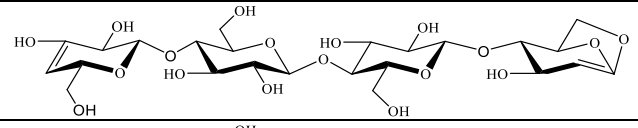
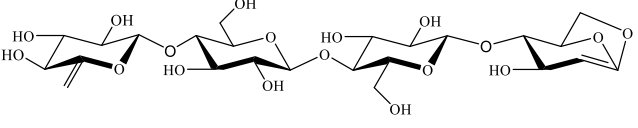
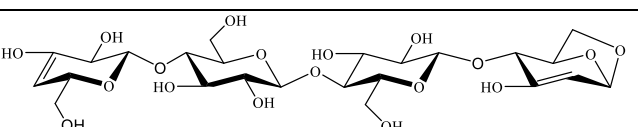
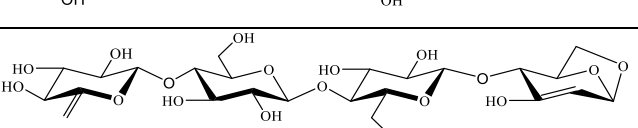
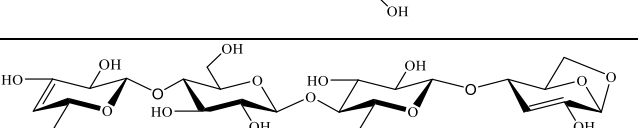
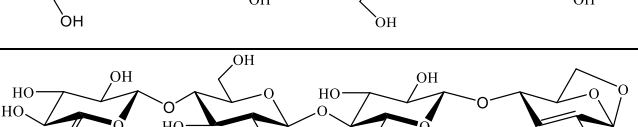
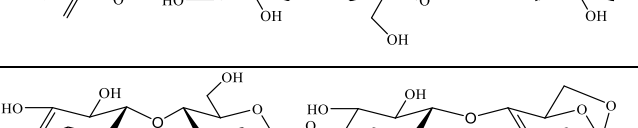
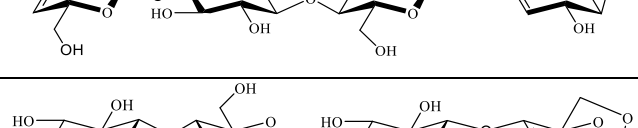
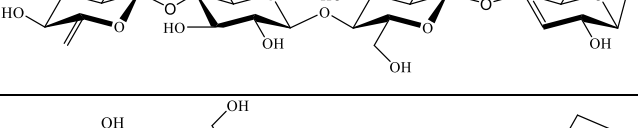
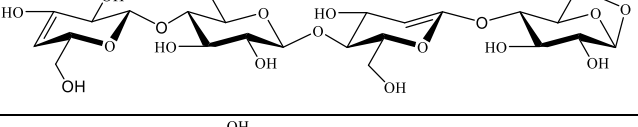
CTN65B-23C-45C		-229.85	156.84	500
CTN21C-34C-65C		27.50	413.13	499
CTN21C-32C-45C		-93.17	295.80	503
CTN34B-32C-45C		-235.59	157.40	508
CTN34B-32C-65C		-200.51	197.60	515
CTN34B-34C-65C		-225.37	160.32	499
CTN34B-43C-65C		-236.83	152.02	503
CTN23A-43C-65C		-256.38	127.98	497
CTN23B-43C-65C		-244.99	134.48	491
CTN32A-43C-65C		-249.86	147.99	515
CTN32B-43C-65C		-237.17	155.85	508
CTN21B-65B-65C		-220.16	177.94	515
CTN21A-43C-65C		-98.57	278.21	487
CTN21B-43B-65C		-246.94	143.58	505

Table S9. Product structure and relative energetics of the singly dehydrated celloquatrosan

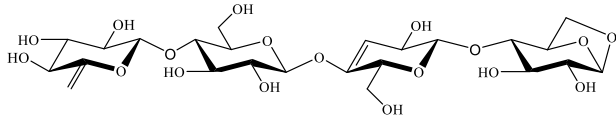
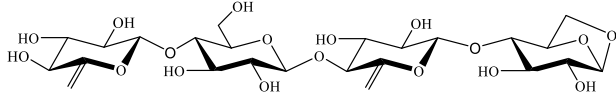
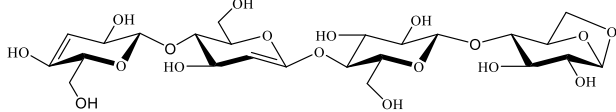
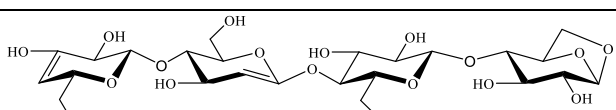
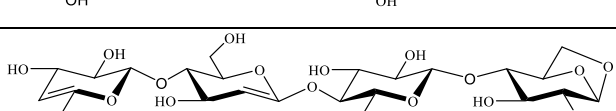
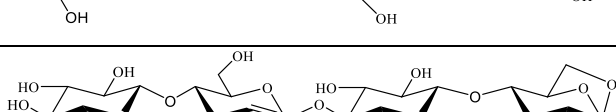
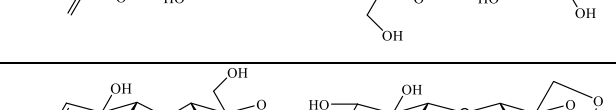
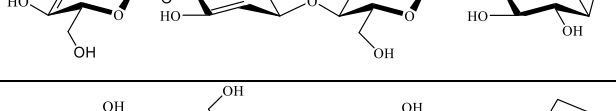
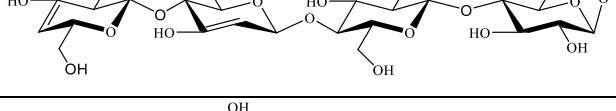
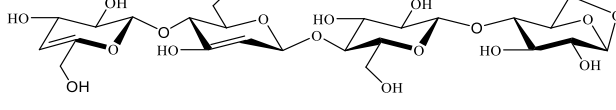
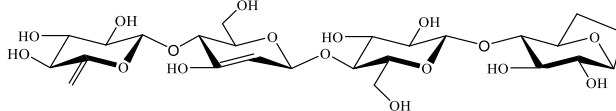
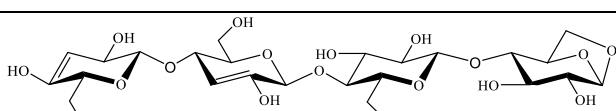
Reaction label	Product structure	ΔG_{rxn} kJ/mol	ΔH_{rxn} kJ/mol	ΔS_{rxn} J/mol.K
CQN21A		92.38	212.14	155
CQN23A		-77.20	48.05	162
CQN32A		-65.79	69.64	175
CQN34A		-79.07	53.91	172
CQN21B		-47.40	77.17	161
CQN23B		-72.49	61.31	173
CQN32B		-58.33	87.29	188
CQN34B		-64.19	65.80	168
CQN65B		-55.67	73.50	167
CQN21C		-58.37	67.02	162

CQN23C		-72.70	63.18	175
CQN32C		-57.15	85.27	184
CQN34C		-53.82	84.08	178
CQN65C		-57.97	70.87	167
CQN21D		-56.73	74.85	170
CQN23D		-60.81	65.42	163
CQN32D		-54.31	73.40	165
CQN34D		-64.07	67.14	170
CQN43D		-68.42	59.22	165
CQN45D		-64.42	63.07	165
CQN65D		-56.61	70.21	164

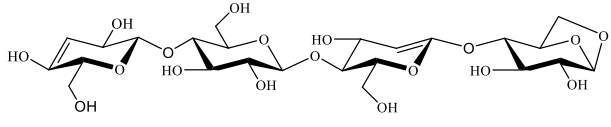
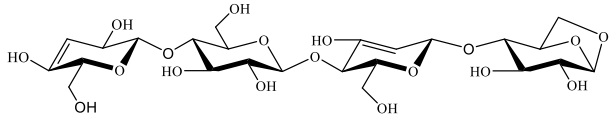
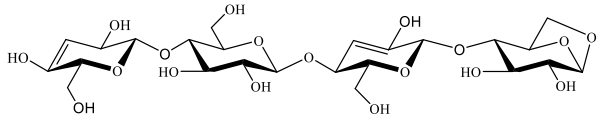
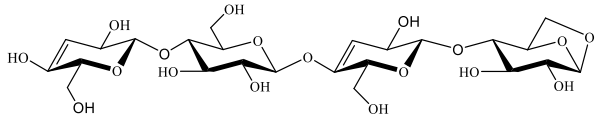
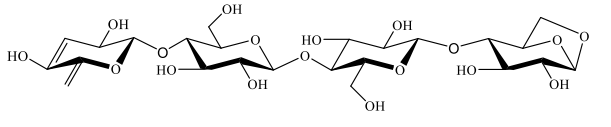
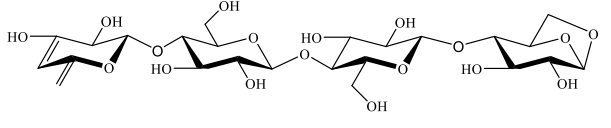
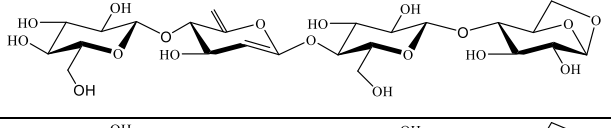
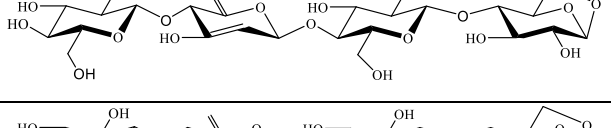
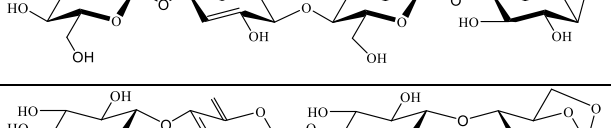
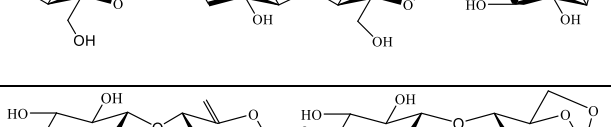
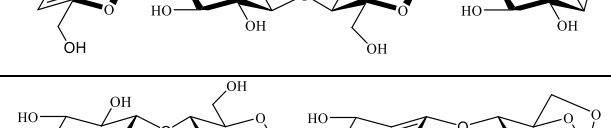
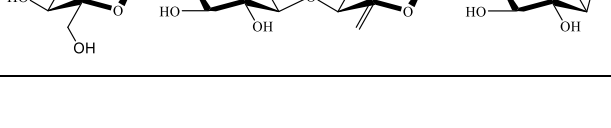
Table S10. Product structure and relative energetics of the doubly dehydrated celloquatrosan

Reaction label	Product structure	ΔG_{rxn} kJ/mol	ΔH_{rxn} kJ/mol	ΔS_{rxn} J/mol.K
CQN21A-43D		17.69	263.96	319
CQN21A-65D		20.46	268.81	321
CQN23A-43D		-139.88	113.30	327
CQN23A-65D		-134.44	118.33	327
CQN32A-43D		-125.18	134.91	336
CQN32A-65D		-120.20	139.97	336
CQN34A-43D		-143.58	119.15	340
CQN34A-65D		-139.98	124.04	341
CQN21B-43D		-124.37	128.84	328
CQN21B-45D		-123.41	131.89	330

CQN21B-65D		-119.86	133.71	328
CQN23B-43D		-134.44	126.81	338
CQN23B-45D		-132.09	130.12	339
CQN23B-65D		-133.40	131.62	343
CQN32B-43D		-115.51	152.32	346
CQN32B-45D		-114.06	155.73	349
CQN32B-65D		-112.39	156.64	348
CQN34B-43D		-106.87	153.35	337
CQN65B_43D		-134.81	125.15	336
CQN34B-45D		-113.21	150.03	340
CQN65B-45D		-128.06	128.12	331

CQN34B-65D		-104.81	155.42	337
CQN65B-65D		-125.51	130.40	331
CQN21C-34D		-123.34	142.16	343
CQN21C-43D		-122.74	132.50	330
CQN21C-45D		-122.24	135.49	333
CQN21C-65D		-120.36	138.59	335
CQN23C-34D		-137.06	124.91	339
CQN23C-43D		-132.41	129.23	338
CQN23C-45D		-138.19	136.16	355
CQN23C-65D		-127.67	128.56	331
CQN32C-34D		-115.31	148.52	341
CQN32C-43D		-116.27	150.19	345

CQN32C-45D		-119.07	154.92	354
CQN32C-65D		-112.82	147.36	337
CQN34C-34D		-109.61	149.79	336
CQN34C-43D		-126.38	143.72	349
CQN34C-45D		-116.84	156.89	354
CQN65C-45D		-130.32	126.34	332
CQN34C-65D		-110.91	155.26	344
CQN65C-65D		-133.95	125.02	335
CQN21A-34D		9.63	272.05	339
CQN23A-34D		-141.25	121.20	339
CQN32A-34D		-127.16	143.23	350
CQN34A-34D		-151.29	127.15	360

CQN21B_34D		-130.36	137.06	346
CQN23B_34D		-134.50	118.65	327
CQN32B_34D		-115.94	160.91	358
CQN34B_34D		-109.63	152.50	339
CQN34D-65D		-150.27	103.0	328
CQN43D-65D		-164.53	93.48	334
CQN21C-65C		-118.57	138.68	333
CQN23C-65C		-129.44	133.99	341
CQN32C-65C		-108.57	159.54	347
CQN34C-65C		-124.83	135.97	337
CQN43D-65C		-139.85	121.96	339
CQN21B_65B		-126.21	141.64	346

CQN23B_65B		-142.38	131.20	354
CQN32B_65B		-111.07	161.67	353
CQN34B_65B		-118.36	137.51	331

Table S11. Product structure and relative energetics of the triply dehydrated celloquatrosan

Reaction label	Product structure	ΔG_{rxn} kJ/mol	ΔH_{rxn} kJ/mol	ΔS_{rxn} J/mol.K
CQN65D_43D_23A		- 241.86	141.55	496
CQN65D_43D_34A		- 245.68	147.34	508
CQN65D_43D_32A		- 227.84	163.32	506
CQN45D_32D_34A		- 214.44	168.51	495
CQN45D_32D_32A		- 204.24	184.33	503
CQN43D_21D_34A		- 223.33	170.62	509
CQN65D_43D_21A		-87.33	292.08	491
CQN65D_43D_65B		- 232.18	153.67	499

CQN65D_43D_32B		- 217.39	180.07	514
CQN65D_43D_23B		- 234.73	154.75	504
CQN65D_43D_34B		- 210.69	178.41	503
CQN45D_32D_34B		- 182.21	199.22	493
CQN45D_32D_23B		- 209.93	176.13	499
CQN65D_43D_21B		- 225.82	157.21	495
CQN65D_43D_65C		- 238.52	147.86	500
CQN65D_43D_34C		- 217.79	177.30	511
CQN65D_43D_23C		- 232.43	150.82	496
CQN65D_43D_32C		- 217.61	170.56	502
CQN65D_43D_21C		- 224.18	165.63	504
CQN65C_34C_65B		- 201.68	191.79	509
CQN65C_34C_34B		- 176.34	207.88	497

CQN65C_34C_32B		- 188.38	217.25	525
CQN65C_34C_34A		- 203.86	188.97	508
CQN65C_34C_32A		- 189.36	204.52	509
CQN65C_34C_23A		- 202.34	183.61	499
CQN34C_21C_34A		- 212.00	200.87	534
CQN65C_23C_34A		- 216.67	186.94	522
CQN65B_34B_34A		- 201.54	178.24	491
CQN34B_21B_34A		- 195.54	197.08	508
CQN65B_34B_23A		- 190.31	195.52	499
CQN65B_34B_32A		- 190.32	195.52	499
CQN65D_65C_65B		- 207.82	182.26	505
CQN23D_65C_65B		- 213.36	176.50	504
CQN32D_65C_65B		- 197.36	193.86	506
CQN45D_65C_65B		- 206.05	183.46	504

CQN21D_65C_65B		-52.92	328.59	493
CQN34D_65C_65B		-216.69	176.82	509
CQN43D_65C_65B		-211.83	177.58	504
CQN65D_32C_34B		-169.38	240.77	531
CQN65D_65C_34A		-217.38	178.67	512
CQN65D_65C_32A		-201.81	193.58	511
CQN65D_34C_34A		-202.36	187.23	504
CQN65D_65C_23A		-217.05	173.25	505
CQN65D_65B_34A		-215.77	172.81	503
CQN45D_65B_34A		-212.18	180.02	507
CQN43D_65B_34A		-220.33	173.81	510
CQN65D_65B_32A		-196.41	189.10	499
CQN65D_65B_23A		-208.45	172.79	493
CQN34D_34C_34B		-179.18	221.57	518

CQN43D_34C_34B		- 165.11	234.31	517
CQN45D_34C_34B		- 169.99	225.37	511
CQN65D_34C_34B		- 169.62	240.77	531
CQN65D_65C_34B		- 192.40	197.87	505
CQN65C_65B_34A		- 214.89	170.30	498
CQN65C_34B_34A		- 187.14	209.67	513
CQN34C_34B_34A		- 162.41	235.78	515
CQN34C_34B_32A		- 173.80	240.38	536
CQN65C_34B_32A		- 182.44	207.54	504
CQN65C_34B_23A		- 196.70	185.09	494
CQN34C_34B_23A		- 177.18	206.54	496
CQN65C_32B_34A		- 193.75	202.06	512
CQN65C_23B_34A		- 208.52	177.54	499

CQN65C_65B_21A		-52.92	328.59	493
CQN65C_65B_23A		-211.97	170.32	494
CQN65C_65B_32A		-200.53	186.44	501
CQN65C_34C_21C		-221.78	175.64	514
CQN65B_34B_21B		-220.12	175.78	512
CQN65D_43D_21D		-255.00	131.13	499
CQN65D_43D_32D		-41.20	334.83	486

Table S12. Number of atomic groups in each compound for Joback¹, Perez-Ponce⁴, and Lydersen et al.⁵ estimation methods

Reaction label	--OH (alcohol)	--O-- (ring)	--O-- (non-ring)	--CH ₂ -- (ring)	--CH ₂ -- (non-ring)	=CH-- (ring)	>CH-- (ring)	=C< (ring)	=CH ₂ (non-ring)
LG23	2	2	0	1	0	1	3	1	0
LG32-45	1	2	0	1	0	2	1	2	0
CBN65B	5	3	1	1	0	0	9	1	1
CBN43B-65B	4	3	1	1	0	0	7	2	1
CBN23A-43B-65B	3	3	1	1	0	2	5	3	1
CTN34A	8	4	2	1	2	1	13	1	0
CTN43C-65C	7	4	2	1	1	1	12	2	1
CTN21C-43C-65C	6	4	2	1	1	2	10	3	1
CQN34A	11	5	3	1	3	1	18	1	0
CQN43D-65D	10	5	3	1	2	1	17	2	1
CQN21D-43D-65D	9	5	3	1	2	2	15	3	1

Table 13. Number of atomic groups in each compound for Chueh & Swanson⁶ estimation method

Reaction label	--OH	--O-- (ring)	--O-- (non-ring)	-- CH ₂ -- (ring)	-- CH ₂ -- (non-ring)	=CH-- (ring)	=C< (ring)	=CH ₂ (non-ring)	>CH-- (ring)
LG23	2	2	0	1	0	1	1	0	3
LG32-45	1	2	0	1	0	2	2	0	1
CBN65 B	5	3	1	1	0	0	1	1	9
CBN43 B-65B	4	3	1	1	0	1	2	1	7
CBN23A-43B-65B	3	3	1	1	0	2	3	1	5
CTN34A	8	4	2	1	2	1	1	0	13
CTN43C-65C	7	4	2	1	1	1	2	1	12
CTN21C-43C-65C	6	4	2	1	1	2	3	1	10
CQN34A	11	5	3	1	3	1	1	0	18
CQN43D-65D	10	5	3	1	2	1	2	1	17
CQN21D-43D-65D	9	2	5	2	2	2	2	1	15

Table S14. Number of atomic groups in each compound for Stein & Brown² estimation method

Reaction label	--OH (sec)	--OH (pri)	--O-- (ring)	--O-- (ring)	-- CH ₂ -- (ring)	-- CH ₂ -- (non-ring)	=CH-- (ring)	=C< (ring)	=CH ₂ (non-ring)	>CH-- (ring)
LG23	2	0	2	0	0	1	1	1	0	3
LG32-45	1	0	2	0	0	1	2	2	0	1
CBN65 B	5	0	3	1	0	1	0	1	1	9
CBN43 B-65B	4	0	1	1	0	1	1	2	1	7
CBN23A-43B-65B	3	0	3	1	0	1	2	3	1	5
CTN34A	6	2	4	2	1	1	1	1	0	13
CTN43C-65C	6	1	4	2	1	1	1	2	1	12
CTN21C-43C-65C	5	1	4	2	1	1	2	3	1	10
CQN34A	8	3	5	3	1	3	1	1	0	18
CQN43D-65D	8	2	5	3	1	2	1	2	1	17
CQN21D-43D-65D	7	2	2	5	2	2	2	2	1	15

Table S15. Number of atomic groups in each compound for Stefanis and Panayiotou³ estimation method

Reaction label	--OH	--CHO--	--CH ₂ O--	--CH=C<	--CH<	CH ₂ O=C<	--CH ₂ - -	CH ₂ =C<	--O--
LG23	2	1	1	1	2	0	0	0	0
LG32-45	1	1	1	2	0	0	0	0	0
CBN65 B	5	3	1	0	6	1	0	0	0
CBN43 B-65B	4	3	1	1	4	1	0	0	0
CBN23A-43B-65B	3	3	1	2	2	1	0	0	0
CTN34A	8	5	1	1	8	0	2	0	0
CTN43C-65C	7	5	1	1	7	0	1	1	0
CTN21C-43C-65C	6	4	1	2	6	0	1	1	1
CQN34A	11	7	1	1	11	0	3	0	0
CQN43D-65D	10	7	1	1	10	0	2	1	0
CQN21D-43D-65D	9	6	1	2	9	0	2	1	1

Scheme S1. Sample input file for DFT calculations

```
%NProcShared=20
%mem=20gb
%Chk=LG21_deh
#M062X/6-311++G(d,p) Scf(Maxcycle=999) opt(maxcycle=160) Temperature=773.15 freq ginput iop(6/7=3)
```

LG21_deh

```
0 1
O
O      1      B1
O      1      B2  2      A1
O      3      B3  1      A2  2      D1  0
C      1      B4  2      A3  4      D2  0
C      3      B5  1      A4  5      D3  0
C      4      B6  3      A5  1      D4  0
C      7      B7  4      A6  3      D5  0
C      8      B8  7      A7  4      D6  0
C      2      B9  1      A8  9      D7  0
H      5      B10 1      A9  9      D8  0
H      6      B11 3      A10 1      D9  0
H      7      B12 4      A11 3      D10 0
H      8      B13 7      A12 4      D11 0
H      10     B14 2      A13 1      D12 0
H      10     B15 2      A14 1      D13 0
H      3      B16 1      A15 9      D14 0
H      4      B17 3      A16 1      D15 0
```

```
B1      2.20524360
B2      3.24502918
B3      3.02232503
B4      1.44666219
B5      1.41433506
B6      1.40553728
B7      1.50720170
B8      1.33021370
B9      1.46538264
B10     1.08924129
B11     1.09224234
B12     1.09566416
B13     1.08063173
B14     1.08708396
B15     1.09132770
B16     0.96304023
B17     0.96266890
A1      115.53396389
A2      76.57655979
A3      78.86613202
A4      40.84582854
A5      53.22944987
A6      109.88000392
A7      110.51443183
A8      74.66906294
A9      110.01563458
A10     105.45486163
A11     110.89159426
A12     120.88252317
A13     108.03702531
A14     108.30534393
A15     69.20347202
A16     58.90042694
D1      -70.34799136
D2      73.99274780
D3      -62.31483710
D4      -5.82835853
D5      147.18728850
D6      -165.84498646
D7      -125.52991314
D8      162.94136296
D9      161.54726762
D10     -87.28371257
D11     -11.60123332
D12     -106.35252467
D13     131.75349537
D14     -147.64084164
D15     -159.20165735
```

APPENDIX A: REFERENCES

1. Joback KG. A unified approach to physical property estimation using multivariate statistical techniques. Published online 1984. <http://dspace.mit.edu/handle/1721.1/15374>
2. Stein SE, Brown RL. Estimation of normal boiling points from group contributions. *J Chem Inf Comput Sci*. 2002;34(3):581-587. doi:10.1021/CI00019A016
3. Stefanis E, Panayiotou C. Prediction of Hansen Solubility Parameters with a New Group-Contribution Method. *Int J Thermophys*. 2008;29:568-585. doi:10.1007/s10765-008-0415-z
4. Pérez Ponce, A. A.; Salfate, I.; Pulgar-Villaruel, G.; PalmaChilla, L.; Lazzus, J. A. New group contribution method for the prediction of normal melting points. *J. Eng. Thermophys*. 2013, 22 (3), 226–235.
5. Lydersen, A. L.; Greenkorn, R. A.; Hougen, O. A. Estimation of Critical Properties of Organic Compounds. Engineering Experiment Station Report 3; College of Engineering, University of Wisconsin: Madison, WI, 1955; pp 1–22
6. Chueh, C. F.; Swanson, A. C. Estimation of liquid heat capacity. *Can. J. Chem. Eng.* 1973, 51 (5), 596–600.

APPENDIX B: SUPPLEMENTAL INFORMATION FOR CHAPTER FOUR

Table S16. Product structure and relative energetics of the proposed sugar oligomer fragments where hydroxyacetaldehyde was removed.

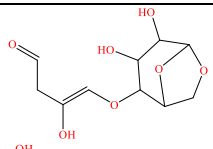
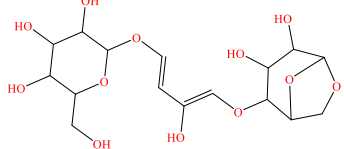
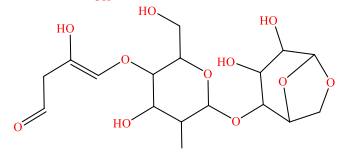
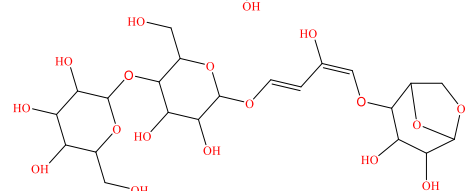
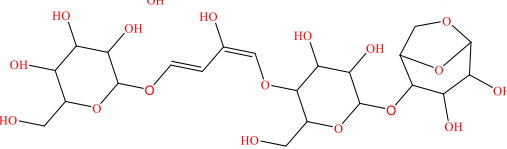
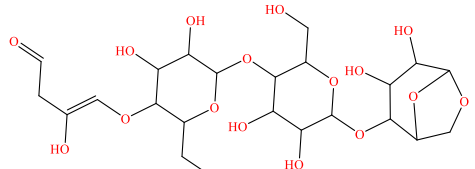
Reaction Label	Product Structure	ΔG_{rxn} (kJ/mol)	ΔH_{rxn} (kJ/mol)	ΔS_{rxn} (J/mol. K)
CBN-HAAb		-108.60	40.91	415
CTN-HAAb		-80.21	85.83	437
CTN-HAAc		-103.37	42.75	411
CQN-HAAb		-76.26	80.80	425
CQN-HAAc		-65.09	84.75	416
CQN-HAAd		-84.00	51.94	398

Table S17. Product structure and relative energetics of the proposed sugar oligomer fragments where hydroxyacetone was removed.

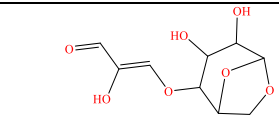
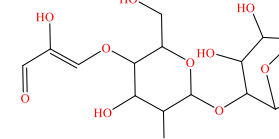
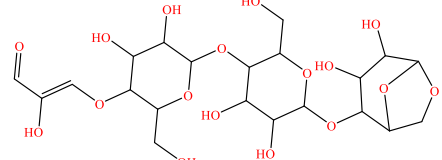
Reaction Label	Product Structure	ΔG_{rxn} (kJ/mol)	ΔH_{rxn} (kJ/mol)	ΔS_{rxn} (J/mol.K)
CBN-HAb		-170.94	147.22	411
CTN-HAc		-202.92	107.44	401
CQN-HAd		-162.49	152.11	407

Table S18. Cartesian Coordinates of the Optimized Product Structures

a. Hydroxyacetone fragmentation											
CBN-HAb				CTN-HAc				CQN-HAd			
O	0	0	0	O	0.800355	0.396538	-0.2829	O	-3.62369	-0.61586	0.290329
O	0	0	3.364388	O	-2.48693	1.823213	0.395203	O	-0.164	-0.65031	-0.69665
O	2.230425	0	-0.34321	O	2.871341	1.293442	-0.48605	O	-5.16155	0.982722	0.755826
O	-1.75649	-2.88527	3.609674	O	-3.91825	-1.51877	-1.67562	O	1.411862	0.961789	-0.89543
O	0.871449	-2.72664	2.73104	O	5.246478	-0.62952	-1.39802	O	-8.0752	0.104738	1.6785
O	0.622877	-3.14819	-0.19225	O	-0.93661	4.067415	-0.42434	O	-0.5863	2.047777	0.759389
O	-1.84477	-0.36081	5.380008	O	1.819304	3.837428	0.142632	O	-3.19187	2.963643	0.418362
O	-0.86487	-1.30631	7.761993	O	2.438079	-1.24358	1.351331	O	-5.86005	-1.34281	-1.29485
O	-3.01614	-2.98904	6.907756	O	-5.05255	1.765015	1.503191	O	1.833412	-2.53943	-0.11852
C	0.836886	-0.3456	2.252585	O	-6.99947	0.713015	-0.04242	O	4.431888	-1.78296	-0.96555
C	0.592444	0.665465	1.112419	O	-5.34528	-3.63624	0.730865	O	-8.23248	-2.56758	-0.32206
C	0.502546	-1.75708	1.777452	O	4.193115	-3.26133	0.367741	O	-3.48252	-3.0424	-0.92882
C	1.208772	-2.04213	0.454842	O	-0.34003	-1.89518	0.611509	O	-9.63102	0.572744	0.151005
C	1.063166	-0.80923	-0.45273	O	6.754863	-0.92389	0.21883	O	1.685045	3.603944	-0.41702
C	1.900099	1.121161	0.471095	C	-1.2043	1.660053	-0.20524	C	-1.25428	-0.23404	0.115739
C	0.391951	-0.44067	4.570858	C	-0.39402	2.896268	0.147256	C	-1.52938	1.269432	0.046544
C	-0.51445	-0.5709	5.553603	C	1.040213	2.780354	-0.35723	C	-2.8868	1.613069	0.665036
C	-0.09476	-1.02867	6.869104	C	-0.46914	0.432451	0.333039	C	-2.46589	-0.99222	-0.42391
C	-2.23303	-3.48664	5.861903	C	1.649548	1.467582	0.117062	C	-3.98529	0.741151	0.0835

C	-2.58091	-2.8995	4.503211	C	3.799861	0.461908	0.205625	C	-6.36129	0.658851	0.061544
C	-3.98559	-2.41028	4.309757	C	-3.53998	1.315917	-0.26673	C	1.098082	-0.28541	-0.28857
H	1.879782	-0.31135	2.59	C	3.351503	-1.00302	0.296163	C	-6.54851	-0.8493	-0.16127
H	-0.06758	1.467226	1.437043	C	5.114731	0.537131	-0.59134	C	-7.51177	1.184212	0.938948
H	-0.57499	-1.79695	1.5922	C	-4.77332	1.306436	0.263729	C	2.102597	-1.32264	-0.76751
H	2.275837	-2.21627	0.636431	C	-5.88298	0.768141	-0.51741	C	3.516108	-0.84575	-0.44373
H	0.883795	-1.09324	-1.48833	C	-5.24347	-2.39382	0.073278	C	3.749898	0.549456	-1.01444
H	-4.68346	-3.22067	4.536944	C	4.557529	-1.90846	0.536686	C	-8.02596	-1.17252	-0.37559
H	1.740735	2.00556	-0.15034	C	-4.05735	-2.41347	-0.87451	C	2.663174	1.483172	-0.49359
H	2.707367	1.30313	1.181125	C	-1.14679	-0.88387	0.026128	C	-2.33912	-2.49158	-0.28527
H	1.442046	-0.66549	4.723289	C	5.694275	-1.571	-0.45037	C	-8.89546	-0.49766	0.704756
H	0.996963	-1.12834	7.001399	C	6.381846	0.449906	0.289699	C	-8.73437	1.680321	0.132679
H	-1.15765	-3.35965	6.02614	C	-3.07772	-3.54487	-0.7304	C	2.742036	2.890451	-1.03799
H	0.072243	-2.97018	3.223451	H	-1.30836	1.583658	-1.29439	H	-1.06881	-0.52132	1.159859
H	-4.12363	-2.06345	3.287461	H	-0.36829	2.986012	1.24288	H	-1.54607	1.561966	-1.01214
H	-4.19099	-1.61925	5.032944	H	1.037762	2.768617	-1.45543	H	-2.84737	1.407443	1.743373
H	0.633768	-3.88478	0.427848	H	-0.36118	0.523046	1.425604	H	-2.58615	-0.75018	-1.49188
H	-1.99094	-0.1184	4.45607	H	1.743136	1.46016	1.215391	H	-4.10389	0.924231	-0.99776
H	-2.42117	-4.56477	5.779398	H	3.933871	0.85993	1.219803	H	-6.35024	1.166082	-0.91222
H	-2.56628	-2.21567	7.277904	H	-2.73717	-3.60327	0.307866	H	1.144509	-0.17877	0.806748
				H	2.912532	-1.275	-0.66777	H	-6.21903	-1.35978	0.748173
				H	5.093587	1.410854	-1.23895	H	-7.12191	1.921525	1.637226
				H	-3.37651	0.9016	-1.25733	H	1.988505	-1.41983	-1.85613
				H	-5.65088	0.40587	-1.52986	H	3.62707	-0.78784	0.647007
				H	-6.13975	-2.14636	-0.5054	H	3.718693	0.517722	-2.11142
				H	4.925707	-1.74265	1.557512	H	-8.33143	-0.78534	-1.35659
				H	-1.22645	-1.01325	-1.05899	H	2.719844	1.530308	0.604849
				H	-2.15325	-0.8882	0.461097	H	-2.32877	-2.74811	0.779901
				H	6.060987	-2.46187	-0.95566	H	-1.41167	-2.8277	-0.75467
				H	6.19352	0.742717	1.325918	H	-9.571	-1.20884	1.175229
				H	7.19631	1.050757	-0.11557	H	-8.47683	1.947779	-0.89565
				H	-1.79105	4.239419	-0.01639	H	-9.22116	2.526978	0.617378
				H	1.37625	4.658656	-0.09527	H	0.126096	2.335292	0.171326
				H	-2.25204	-3.40213	-1.42682	H	-2.43549	3.471606	0.731689
				H	-3.58328	-4.4922	-0.93044	H	2.61228	2.861664	-2.12621
				H	1.544907	-1.32919	0.989827	H	3.717027	3.321502	-0.79265
				H	-6.00807	1.657511	1.624296	H	-5.03943	-1.77364	-1.01555
				H	-5.06031	-1.57053	0.779752	H	2.569666	-3.12957	-0.31449
				H	-6.07329	-3.6061	1.355433	H	5.145472	-1.89087	-0.3179
				H	3.454671	-3.42118	0.965253	H	-7.61486	-2.95614	-0.95136
				H	-0.54136	-2.74322	0.209489	H	-3.52442	-3.98694	-0.76624
								H	1.64061	4.496576	-0.76631
								O	5.015922	1.046035	-0.58494

O	6.016792	-1.56936	1.299945
O	7.572794	1.209755	0.456518
O	9.573947	0.21341	-1.16918
O	9.405579	-0.73374	1.534294
C	6.08003	0.650877	-1.28483
C	7.329893	0.754555	-0.7935
C	8.437893	0.283235	-1.60287
C	8.377787	-1.63759	1.185057
C	7.058892	-1.23621	1.823885
C	7.114538	-0.5041	3.129838
H	7.544044	0.484581	2.960599
H	5.914601	0.251575	-2.28073
H	8.193208	-0.03618	-2.62928
H	8.224519	-1.70391	0.105061
H	6.113161	-0.41489	3.544578
H	7.780139	-1.02762	3.820444
H	8.50523	1.04051	0.66591
H	8.607704	-2.64722	1.553629
H	10.00069	-0.64817	0.780215

b. Hydroxyacetaldehyde fragmentation

CBN-HAAb			CTN-HAAc			CQN-HAAd					
O	-2.85943	0.205054	-1.28245	O	1.415319	0.761378	0.537598	O	-3.66666	-0.58739	0.393469
O	-0.52202	-1.84434	-0.87192	O	-1.99531	1.807767	0.021631	O	-0.15835	-0.74939	-0.38409
O	-4.38515	0.192394	0.343831	O	2.549133	-1.18998	0.328669	O	-5.20886	1.060378	0.598716
O	2.848193	4.505993	-0.54492	O	-4.8158	-1.15454	-0.44819	O	1.440512	0.827471	-0.65913
O	-0.08956	0.091673	1.569203	O	5.60307	-1.29681	1.209767	O	-8.18871	0.298769	1.423663
O	-1.74352	2.359666	0.995531	O	-2.15248	-1.18766	0.388105	O	-0.63007	2.095969	0.753533
O	1.704206	-0.80398	-1.97415	O	0.174303	-2.47276	-0.47756	O	-3.19777	2.983332	0.177234
O	3.687817	-3.06724	1.600379	O	3.725637	1.463858	-0.95631	O	-5.81175	-1.46024	-1.24042
O	2.110076	1.085621	0.0911	O	-4.22047	2.737007	-1.27857	O	1.788297	-2.5818	0.478579
C	-1.46598	-1.25629	0.029304	O	-7.51251	0.389514	-0.03888	O	4.417684	-1.94692	-0.30309
C	-2.7804	-1.11406	-0.75064	O	6.336279	1.777999	0.126223	O	-8.25754	-2.55928	-0.30465
C	-0.99576	0.131851	0.487115	O	1.821534	3.418447	0.152934	O	-3.48551	-3.12882	-0.55366
C	-2.17014	1.017546	0.893958	O	6.98101	-1.56939	-0.52229	O	-9.63586	0.625939	-0.24163
C	-3.2983	0.934623	-0.15651	O	-6.77349	-3.92553	0.345231	O	1.723301	3.500615	-0.44571
C	-4.04036	-1.17504	0.144389	C	-0.96962	0.960114	0.512904	C	-1.2845	-0.24056	0.317341
C	0.699814	-2.14062	-0.31881	C	-1.05199	-0.44098	-0.09115	C	-1.53784	1.249125	0.074946
C	1.79515	-1.65424	-0.89711	C	0.190973	-1.26466	0.241496	C	-2.92371	1.662928	0.576877
C	3.197607	-1.91561	-0.44582	C	0.358403	1.589299	0.099873	C	-2.47362	-1.04328	-0.20823

C	3.256368	-2.09008	1.056088	C	1.450712	-0.49629	-0.12294	C	-3.99793	0.742741	0.025915
C	2.936313	3.31961	-0.41428	C	3.779715	-0.92466	-0.33731	C	-6.369	0.674565	-0.12969
C	1.831779	2.469747	0.188385	C	-3.24311	1.595744	0.521478	C	1.086343	-0.35029	0.049592
H	-1.58169	-1.91543	0.898329	C	4.30513	0.498432	-0.09894	C	-6.56242	-0.84709	-0.20954
H	-2.79713	-1.82542	-1.57407	C	4.79293	-1.9362	0.227719	C	-7.56291	1.294477	0.619036
H	-0.53063	0.609487	-0.38418	C	-4.32728	2.090401	-0.07162	C	2.102055	-1.43504	-0.27295
H	-2.56592	0.671071	1.856528	C	-5.71077	1.883317	0.461197	C	3.502112	-0.93663	0.07123
H	-3.63055	1.92424	-0.46227	C	-6.5622	1.007705	-0.44123	C	3.788323	0.391567	-0.62151
H	0.721479	-2.79835	0.543872	C	5.812948	0.551907	-0.33686	C	-8.02785	-1.17845	-0.48509
H	-4.87087	-1.67082	-0.3576	C	-5.2499	-2.17488	0.029872	C	2.681305	1.375434	-0.25386
H	-3.84842	-1.66601	1.102507	C	0.596579	2.953432	0.703803	C	-2.37319	-2.52042	0.093203
H	3.636123	-2.78514	-0.93907	C	6.522702	-0.60304	0.398935	C	-8.95405	-0.39034	0.463065
H	2.861957	-1.23407	1.638092	C	5.8535	-2.39598	-0.79915	C	-8.72592	1.72118	-0.30569
H	3.844936	2.759873	-0.71924	C	-6.69903	-2.57276	-0.04379	C	2.802429	2.717962	-0.93519
H	0.803481	0.194758	1.209562	H	-1.02462	0.893331	1.608611	H	-1.16125	-0.41648	1.394971
H	0.872907	2.73971	-0.26897	H	-1.11202	-0.33172	-1.18337	H	-1.49243	1.427645	-1.0081
H	1.768819	2.712294	1.252779	H	0.220151	-1.44729	1.324411	H	-2.94673	1.568871	1.671149
H	-1.08394	2.39267	1.696407	H	0.381159	1.686905	-0.99697	H	-2.52954	-0.91419	-1.30084
H	0.785041	-0.8213	-2.27882	H	1.506148	-0.33151	-1.21188	H	-4.05139	0.813107	-1.07354
H	3.796438	-1.03334	-0.6989	H	3.63414	-1.07769	-1.41468	H	-6.29429	1.079568	-1.14758
H	2.01642	0.782389	-0.82415	H	-3.32095	1.007623	1.429344	H	1.077849	-0.13787	1.130668
				H	4.119651	0.746886	0.949889	H	-6.29834	-1.26444	0.766356
				H	4.256198	-2.7577	0.697066	H	-7.20452	2.092654	1.265305
				H	-6.2341	2.848283	0.543446	H	2.040131	-1.63955	-1.35071
				H	-6.26994	0.980372	-1.50593	H	3.558906	-0.77139	1.155219
				H	6.003127	0.444848	-1.41288	H	3.798479	0.247183	-1.71051
				H	-4.59164	-2.88165	0.568179	H	-8.26471	-0.89049	-1.51784
				H	0.670144	2.852529	1.792539	H	2.684718	1.53591	0.835437
				H	-0.23365	3.615789	0.445952	H	-2.42623	-2.66393	1.178178
				H	7.352394	-0.24147	1.002546	H	-1.42498	-2.90944	-0.28479
				H	5.52274	-2.25966	-1.83221	H	-9.66956	-1.04451	0.956659
				H	6.14115	-3.43607	-0.64388	H	-8.40149	1.889856	-1.33593
				H	-2.96756	-0.9552	-0.08314	H	-9.23122	2.612588	0.067048
				H	-0.68142	-2.88185	-0.3101	H	0.126564	2.302163	0.186132
				H	-7.06177	-2.39573	-1.06224	H	-2.44461	3.511046	0.465208
				H	-7.25645	-1.90439	0.62428	H	2.725663	2.577259	-2.01956
				H	3.036236	1.948803	-0.48091	H	3.769058	3.164364	-0.68689
				H	-4.79617	3.50753	-1.28518	H	-5.01432	-1.86302	-0.86737
				H	-5.70189	1.447466	1.461425	H	2.533747	-3.18524	0.384227
				H	5.821799	2.470764	-0.30239	H	5.152359	-1.9191	0.323149
				H	2.091648	4.228225	0.590841	H	-7.60336	-3.01398	-0.84674
				H	-7.69241	-4.17722	0.454683	H	-3.54325	-4.05267	-0.30188
								H	1.699354	4.345547	-0.8996

O	5.02372	0.939217	-0.19145
O	5.964377	-1.24778	1.956508
O	7.512287	1.446494	0.773163
O	8.645186	-0.72276	-3.28788
O	9.292168	-0.17306	2.104478
C	6.129852	0.517091	-0.86179
C	7.358287	0.773098	-0.40886
C	8.600535	0.414438	-1.17711
C	8.382362	-0.74809	-2.11892
C	6.964579	-0.71397	2.355517
C	8.340062	-1.2116	1.959278
H	5.97104	0.016665	-1.81092
H	8.997132	1.263485	-1.73956
H	7.955217	-1.65971	-1.65242
H	6.938763	0.130625	3.063468
H	8.293047	-1.57666	0.927658
H	8.567656	-2.06076	2.613603
H	8.4163	1.343331	1.096036
H	9.373458	0.097318	-0.46146
H	10.11928	-0.51494	2.449102

Table S19. Number of atomic groups in each compound for Joback¹, Perez-Ponce⁴, and Lydersen et al.⁵ estimation methods

Reaction label	--OH (alcohol)	--O-- (ring)	--O-- (non-ring)	--CH ₂ -- (ring)	=CH-- (non-ring)	>CH-- (ring)	=C< (non-ring)	O=CH-- (aldehyde)	--CH ₂ -- (non-ring)
Hydroxyacetone fragmentation									
CBN-HAb	3	2	1	1	1	5	1	1	0
CTN-Hac	6	3	2	1	1	10	1	1	1
CQN-Had	9	4	3	1	1	15	1	1	2
Hydroxyacetaldehyde fragmentation									
CBN-HAAb	3	3	2	2	1	5	2	1	1
CTN-HAAc	6	3	2	1	1	10	1	1	2
CQN-HAAd	9	4	3	1	1	15	1	1	3

Table S20. Number of atomic groups in each compound for Chueh & Swanson⁶ estimation method

Reaction label	--OH	--O-- (ring)	--O-- (non-ring)	--CH ₂ -- (ring)	>CH-- (ring)	=CH-- (non-ring)	=C< (non-ring)	--CH ₂ -- (non-ring)	O=CH-- (aldehyde)
Hydroxyacetone fragmentation									
CBN-HAb	3	2	1	1	5	1	1	0	1
CTN-HAc	6	3	2	1	10	1	1	1	1
CQN-HAd	9	4	3	1	15	1	1	1	2
Hydroxyacetaldehyde fragmentation									
CBN-HAAb	3	2	1	1	5	1	1	1	1
CTN-HAAc	6	3	2	1	10	2	1	1	1
CQN-HAAd	9	4	3	1	15	1	1	3	1

Table S21. Number of atomic groups in each compound for Stein & Brown² estimation method

Reaction label	--OH (sec)	--OH (pri)	--O-- (ring)	--O-- (non-ring)	--CH ₂ -- (ring)	- CH ₂ - (non-ring)	=CH-- (non-ring)	=C< (non-ring)	O=CH-- (aldehyde)	>CH-- - (ring)
Hydroxyacetone fragmentation										
CBN-HAb	3	0	2	1	1	0	1	1	1	5
CTN-HAc	5	1	3	2	1	1	1	1	1	10
CQN-HAd	7	2	4	3	1	2	1	1	1	15
Hydroxyacetaldehyde fragmentation										
CBN-HAAb	3	0	2	1	1	1	1	1	1	5
CTN-HAAc	5	1	3	2	1	1	1	1	1	10
CQN-HAAd	7	2	4	3	1	3	1	1	1	15

Table S22. Number of atomic groups in each compound for Stefanis and Panayiotou³ estimation method

Reaction label	--OH	--CHO-- (ethers)	--CHO-- (aldehyde)	--CH ₂ O--	--CH=C<	--CH<	--CH ₂ --
Hydroxyacetone fragmentation							
CBN-HAb	3	2	1	1	1	3	
CTN-HAc	6	4	1	1	1	6	1
CQN-HAd	9	6	1	1	1	9	2
Hydroxyacetaldehyde fragmentation							
CBN-HAAb	3	2	1	1	1	3	1
CTN-HAAc	6	4	1	1	1	6	2
CQN-HAAd	9	6	1	1	1	9	3

APPENDIX B: REFERENCES

1. Joback KG. A unified approach to physical property estimation using multivariate statistical techniques. Published online 1984. <http://dspace.mit.edu/handle/1721.1/15374>
2. Stein SE, Brown RL. Estimation of normal boiling points from group contributions. *J Chem Inf Comput Sci*. 2002;34(3):581-587. doi:10.1021/CI00019A016
3. Stefanis E, Panayiotou C. Prediction of Hansen Solubility Parameters with a New Group-Contribution Method. *Int J Thermophys*. 2008;29:568-585. doi:10.1007/s10765-008-0415-z
4. Pérez Ponce, A. A.; Salfate, I.; Pulgar-Villaruel, G.; PalmaChilla, L.; Lazzus, J. A. New group contribution method for the prediction of normal melting points. *J. Eng. Thermophys*. 2013, 22 (3), 226–235.
5. Lydersen, A. L.; Greenkorn, R. A.; Hougen, O. A. Estimation of Critical Properties of Organic Compounds. Engineering Experiment Station Report 3; College of Engineering, University of Wisconsin: Madison, WI, 1955; pp 1–22
6. Chueh, C. F.; Swanson, A. C. Estimation of liquid heat capacity. *Can. J. Chem. Eng.* 1973, 51 (5), 596–600.

APPENDIX C: SUPPLEMENTAL INFORMATION FOR CHAPTER SIX

Analysis of the light-oxygenated compounds removed from the bio-oil

1. FTIR. The same procedure described in the main paper was employed for the FTIR analysis on the light-oxygenated compounds removed from the bio-oil. The result (Figure S1) shows a major peak between 3000 to 3800 cm^{-1} that is traced back to the OH groups and is mostly associated with water evolution. The peak seen between 1600 to 1800 cm^{-1} originated from the C=O stretch of aldehydes, ketones, and carboxylic acid likely related to acetol, glycolaldehyde, and ketones. The smaller peak at 1304 cm^{-1} is assigned to the C-O bond stretch associated with the presence of carboxylic groups. The assignment of peaks was based on previous papers that studied the same raw material (BTG bio-oil).^{1,2}

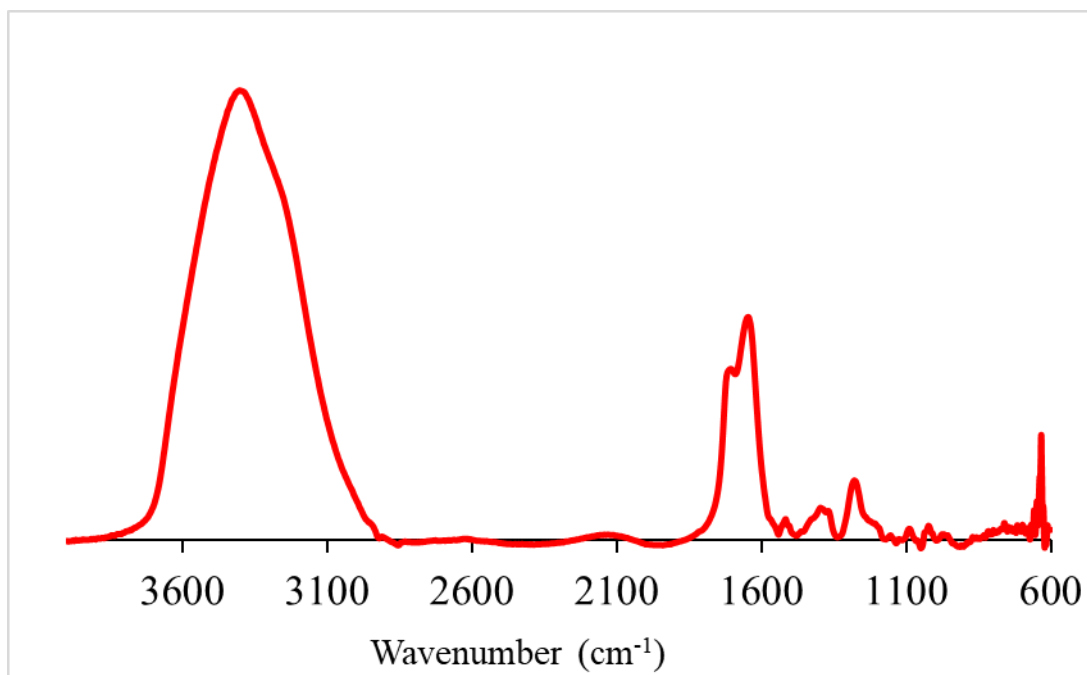


Figure S2: FTIR analysis on the light oxygenates.

2. UV-Fluorescence. The procedure for the UV-Fluorescence analysis is described in the main paper. The result (Figure S2) clearly shows a big peak at 289 nm which is attributed to monomer compounds.² A small peak was also seen around 307 nm which could be attributed to small dimeric compounds.³

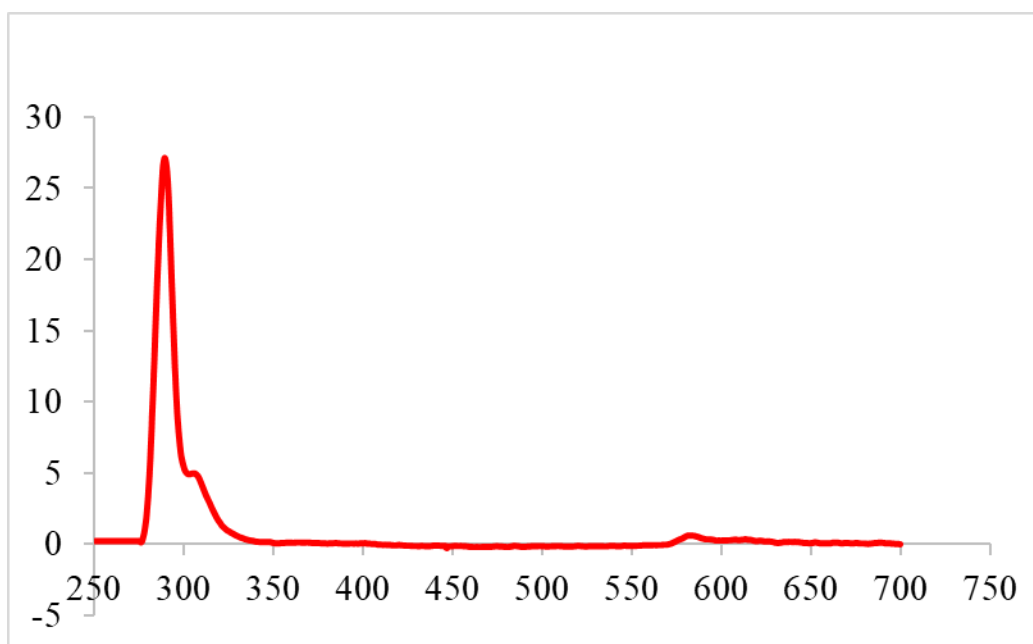


Figure S3: UV-Fluorescence analysis on the light oxygenates.

3. NMR. The ^{13}C and ^1H NMR analyses of the light oxygenates was done on a Bruker 500 Neo spectrometer, equipped with a 5mm Prodigy broadband cryoprobe with Z-axis gradients. An amount of 30 mg samples was dissolved in 0.7 mL dimethyl sulfoxide-d6 (DMSO-d6) (99.9 %, Cambridge Isotope Laboratories, Inc.). The ^{13}C -NMR spectra were obtained at 125.77 MHz with 90° pulse angle (10.0 ms), 1.08 s acquisition time, relaxation delay d1 of 2 s, and inverse-gated ^1H composite pulse decoupling using 4000 scans, a spectral width of 30120.5 Hz and 32768 points. The ^1H NMR spectra were obtained at 500.13 MHz, 30°C with 16 scans, 90° pulse (12.0 ms), 3 s relaxation delay, an acquisition time of 4.4 s, 32768 points, and a spectral width of 7463 Hz.

Apodization with 8 Hz and 1.3 Hz of line broadening was performed for the ^{13}C and ^1H data, respectively.

Result of the ^{13}C NMR analysis (Figure S3, top) showed a big peak at 39.5 ppm which is associated with the solvent. The peaks at 68 to 80 ppm are assigned to protons from alcohol groups, the peaks between 160 to 175 integration regions originated from carboxylic acids, and peaks between 200 to 210 are assigned to protons linked to aldehydes and carbonyls/ketones. For ^1H -NMR (bottom), the big peak at 3.5 ppm comes from the protons from alcohol groups and usually evolution from water. The spectral region at 4.5 to 5.1 ppm is assigned to olefinic protons. Protons that belong to the aromatic and aldehyde groups are also observed at 8.14 ppm and 9.6 ppm, respectively.⁴

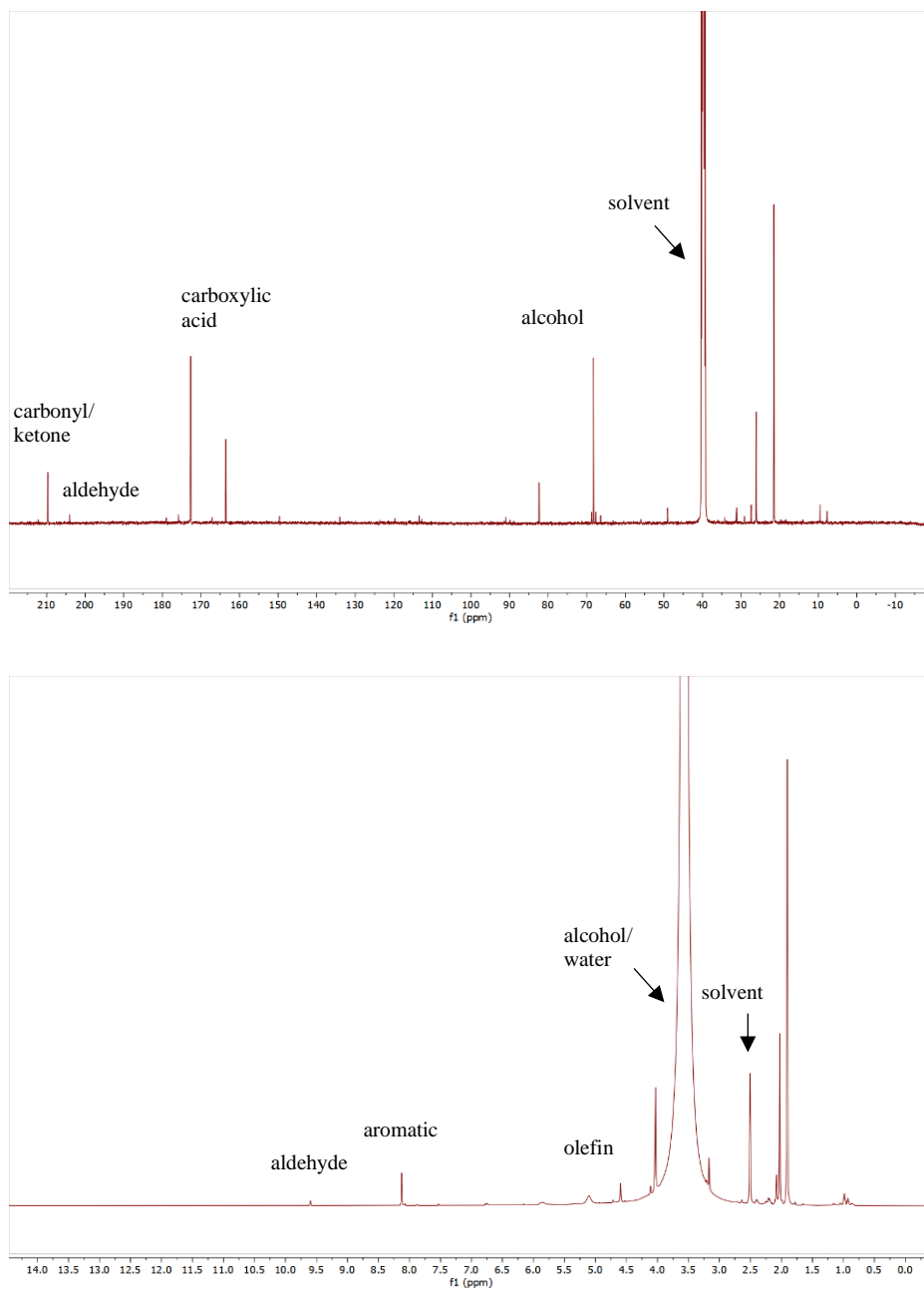


Figure S4: ^{13}C NMR (top) and ^1H NMR (bottom) analysis on the light oxygenates.

APPENDIX C: REFERENCES

- (1) Stankovikj, F.; Garcia-Perez, M. TG-FTIR Method for the Characterization of Bio-Oils in Chemical Families. *Energy and Fuels* **2017**, *31* (2), 1689–1701. <https://doi.org/10.1021/acs.energyfuels.6b03132>.
- (2) Han, Y.; Pinheiro Pires, A. P.; Denson, M.; McDonald, A. G.; Garcia-Perez, M. Ternary Phase Diagram of Water/Bio-Oil/Organic Solvent for Bio-Oil Fractionation. *Energy and Fuels* **2020**, *34* (12), 16250–16264. <https://doi.org/10.1021/acs.energyfuels.0c03100>.
- (3) Stankovikj, F.; McDonald, A. G.; Helms, G. L.; Olarte, M. V.; Garcia-Perez, M. Characterization of the Water-Soluble Fraction of Woody Biomass Pyrolysis Oils. *Energy and Fuels* **2017**, *31* (2), 1650–1664. <https://doi.org/10.1021/acs.energyfuels.6b02950>.
- (4) Stankovikj, F.; McDonald, A. G.; Helms, G. L.; Garcia-Perez, M. Quantification of Bio-Oil Functional Groups and Evidences of the Presence of Pyrolytic Humins. *Energy and Fuels* **2016**, *30* (8), 6505–6524. <https://doi.org/10.1021/acs.energyfuels.6b01242>.

APPENDIX D: SUPPLEMENTAL INFORMATION FOR CHAPTER SEVEN

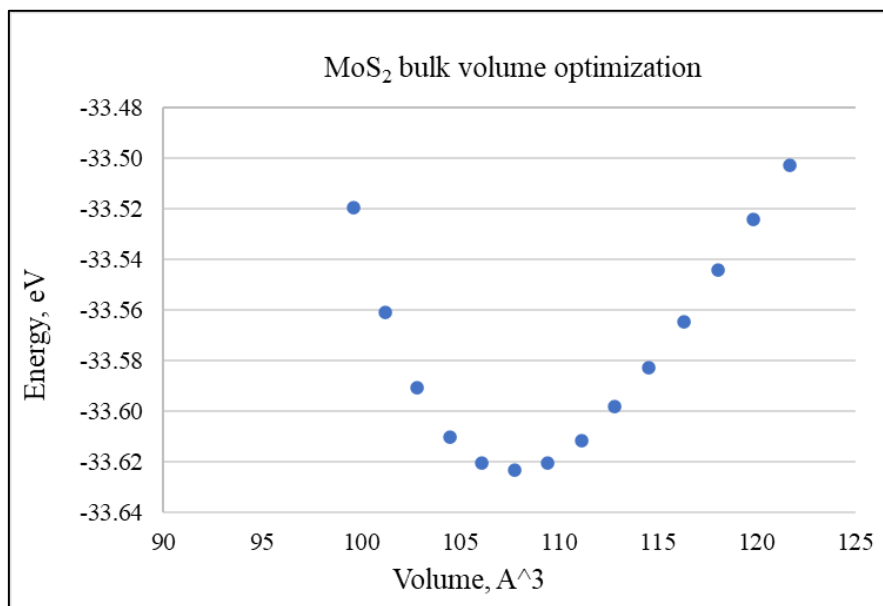


Figure S9: Energy plot of the MoS₂ bulk structure volume optimization.

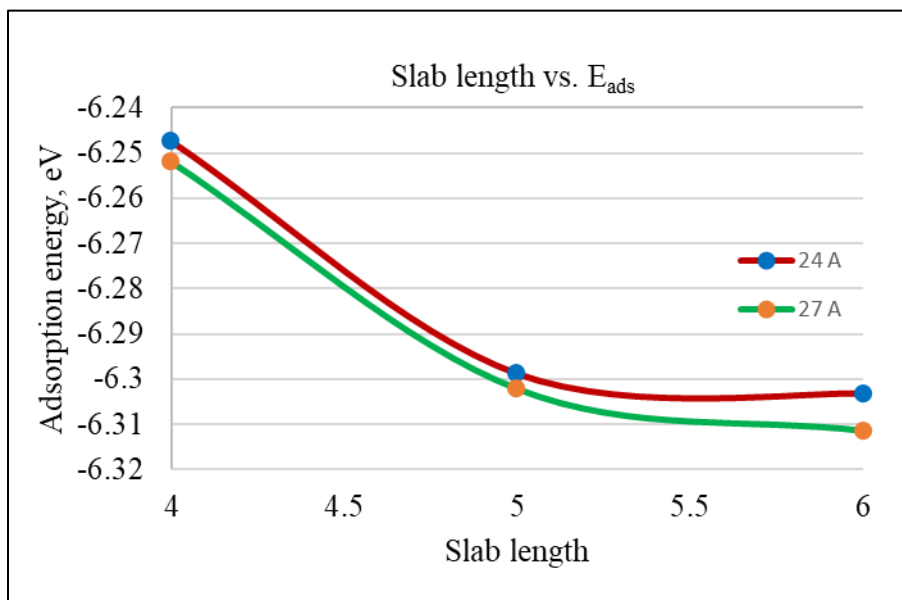


Figure S10: Oxygen atom adsorption energy plot vs. slab length.

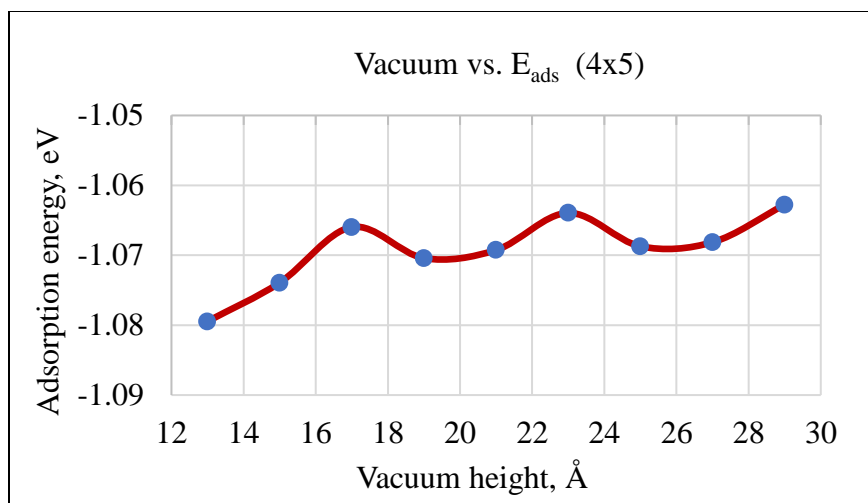


Figure S11: Hydroxyacetone adsorption energy plot vs. vacuum height.